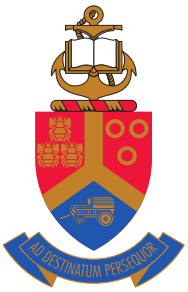

UNIVERSITEIT VAN PRETORIA
UNIVERSITY OF PRETORIA
YUNIBESITHI YA PRETORIA

Experimental Investigation of Factors that Influence Bevameter Terrain Characterisation

by

Ray Kruger

Submitted in partial fulfilment of the requirement for the degree

Master of Engineering (Mechanical Engineering)

in the Faculty of

Mechanical and Aeronautical Engineering

at the

The University of Pretoria

7 October 2022

Abstract

Title: Experimental Investigation of Factors that Influence Bevameter Terrain Characterisation
Author: Ray Kruger
Supervisor: Prof. P.S. Els
Co-Supervisor: Dr. H.A. Hamersma
Department: Mechanical and Aeronautical Engineering
Degree: Master of Engineering (Mechanical Engineering)

The Bekker-Wong soil-wheel interaction model has been widely adopted in the terramechanics field. This model traditionally requires the soil to be characterised using a Bevameter, which entails performing in situ plate sinkage and shear stress tests. Bevameter soil characterisation is not a standardised test procedure, and the test setup may influence the identified soil model parameters. This study investigates the influence of the following five factors for partially saturated sandy soil: i) soil preparation on pressure-sinkage, ii) soil preparation on shear stress, iii) torsional vs. translational shear mechanism, iv) shear contact area, and v) shear velocity. Literature indicates in situ soil mechanical properties exhibit stochastic behaviour; however, the uncertainty of the identified soil parameters is rarely taken into consideration. This study employs the Bayesian statistical framework for probabilistic parameter estimation and formal hypothesis testing. The results indicated that the influence of soil preparation on pressure-sinkage response is substantial, exhibiting an order of magnitude influence. The influence of soil preparation on shear tests is notable, but less significant. The shear mechanism, shear contact area and shear velocity all exhibited a statistically significant influence (Bayes Factor >10) with a maximum absolute shear stress difference of 18%, 20% and 10%, respectively. Moreover, depending on the test setup configuration and data processing decisions, the estimated internal soil friction angles ranged from 16.5 to 37.5 degrees for the same soil. The findings are expected to have significant implications for the prediction of vehicle drawbar pull using the Bekker-Wong model. Further investigation into which Bevameter test configuration is more representative of the shear stress-displacement curve of an actual wheel is recommended.

Keywords: Bevameter, soil characterisation, pressure-sinkage, soil shear stress, shear mechanism, shear velocity, parameter estimation, Bayesian statistical framework, hypothesis test.

Acknowledgements

First and foremost, I would like to thank and praise my Heavenly Father, who bestowed untold blessings upon me. All glory and honour to Him. Furthermore, I would like to thank the following individuals who have played a part in this study:

- I would like to thank my supervisor, Prof. P.S. Els. His advice has helped me focus on the research aspect of this study and not the engineering aspect. I would also like to thank him for financial assistance and the opportunity to be part of the Vehicle Dynamics Group (VDG).

- Thank you to my co-supervisor, Dr. H.A. Hamersma, for guidance and feedback on my thesis. Funding provided by Dr. Hamersma also helped source critical components required for the manufacture of a new Bevameter.

- A special thanks to the engineering staff at VDG solutions, Mr. G. Guthrie and Mr. W.C.W. Penny. Without their assistance, this project could not be possible. They offered their time to help transport the Bevameter on a daily basis during experimental testing. Also, thank you to Mr. Guthrie for acting as a springboard for ideas and recommendations on the design of the Bevameter and to Mr. Penny for his help with the custom strain gauge amplifier circuits.

- I would like to extend my appreciation to the technicians of the heavy machine laboratory, Mr. E. Mohale and Mr. P. Kruger, for all their assistance in the manufacturing aspect of the Bevameter. Mr. Mohale's technical advice and words of encouragement were appreciated. Mr. Kruger was also always eager to assist with anything manufacturing-related.

- Thank you to fellow students R. Lategan for assistance with Computer Numerical Control (CNC) machining and welding on this project and to N. Muire for assistance in general fabrication.

- I would also like to thank Dr. R. He for proofreading and reviewing parts of this thesis.

- Lastly, I would like to express my heartfelt appreciation to my Mother for language corrections and proofreading.

Table of Contents

List of Figures

List of Tables

List of Algorithms

List of Appendices

List of Symbols

Symbol	Description	Units (SI)
a	Parameter lower bound	[Base unit]
A	Intersection point (Bekker drag shear correction method)	[-]
A'	Corrected intersection point (Bekker drag shear correction method)	[-]
α	a. Angular displacement	[Rad]
	b. Significance level	[-]
α_i	Categorical offset coefficient (i^{th} category)	[N/m^2]
b	a. Parameter upper bound	[Base unit]
	b. Ground engagement tool width	[m]
b	a. Smallest dimension of sinkage plate	[m]
	b. Strength exponent (Coffin-Manson strain-life model)	[-]
B	Maximum point on shear stress line (Bekker drag shear correction method)	[-]
B'	Maximum point on corrected line (Bekker drag shear correction method)	[-]
b_s	Corrected fatigue strength exponent (Coffin Manson strain-life model)	[-]
β	Prior standard deviation	[Base unit]
β_i	Moisture dependant coefficient (i^{th} category)	[N/m^2]
$[B]$	Offset matrix (load cell regression model)	[V]
c	a. Soil cohesion	[N/m^2]
	b. Ductility exponent (Coffin Manson strain-life model)	[-]
	c. Calibration intercept (S-type load cell)	[V]
c'	Effective cohesion	[N/m^2]
C	Cauchy distribution	[-]
C_u	Soil coefficient of uniformity	[-]
CV	Coefficient of variation	[Base unit]
$[C]$	Calibration matrix (load cell regression model)	[V/N],[V/Nm]
$[C']$	Strain compliance matrix (load cell regression model)	[$\mu\epsilon$/N], [$\mu\epsilon$/ Nm]
D	Shear ring outside diameter	[m]
D1-D9	Load cell critical dimensions	[m]
df	Degree of freedom	[-]
D_{10}	Soil particle diameter (10th Percentile)	[m]
D_{50}	Soil particle diameter (50th Percentile)	[m]
D_{60}	Soil particle diameter (60th Percentile)	[m]
D_d	Relative density	[-]
D_i	a. Shear ring inside diameter	[m]
	b. Category indicator variable (i^{th} category)	[-]
D_0	Shear ring outside diameter	[m]
$\boldsymbol{D}$	Data vector	[Base unit]
$\boldsymbol{D_1}$	Data vector (Mohr-Coulomb model)	[Base unit]
$\boldsymbol{D_2}$	Data vector (Shear stress-displacement model)	[Base unit]
$\widetilde{\boldsymbol{D}}$	Unobserved data vector (Posterior Predictive Distribution)	[Base unit]
E	Elastic modulus (Romberg-Osgood stress-strain model)	[N/m^2]
e_{max}	Maximum void ratio	[-]
e_{max}	Minimum void ratio	[-]

ϵ	b. Pooled error	[N/m^2]
	c. Strain	[-]
ϵ_{1-16}	Strains corresponding to strain gauges 1-16	[-]
ϵ_a	Strain amplitude (Romberg-Osgood stress-strain model)	[-]
$\epsilon_f{}'$	Material property coefficient (Coffin-Manson strain life model)	[N/m^2]
ϵ_w	Wong's goodness of fit	[-]
$[\epsilon_{eff}]$	Mean effective strain matrix	[-]
F_x	a. Horizontal reaction force	[N]
	b. Shear force	[N]
F_z	a. Vertical load	[N]
	b. Vertical reaction force	[N]
$[F]$	Applied load matrix (load cell regression model)	[N],[Nm]
$[\hat{F}]$	Estimated load matrix (load cell regression model)	[N],[Nm]
G_a	Amplifier gain vector	[-]
h	b. Grouser height	[m]
	c. Annular ring width	[m]
h	Bandwidth parameter of Gaussian kernel density estimate	[Base unit]
H_0	Null hypothesis	[-]
H_1	Alternative hypothesis	[-]
H	Height	[m]
H'	Material strength coefficient (Romberg-Osgood stress-strain model)	[N/m^2]
i	a. Wheel slip	[-]
	b. Category index	[-]
	c. Parameter index	[-]
j	a. Shear displacement	[m]
	b. Data point number index	[-]
	c. Sample index	[-]
$\boldsymbol{j}$	Shear displacement vector	[m]
K	a. Shear deformation modulus (Janosi-Hanamoto model)	[m]
	b. Shear deformation modulus (new shear stress-displacement model)	[m]
	c. Kernel density function	[-]
	d. Parameter index	[-]
k_c	Cohesion coefficient (Bekker pressure-sinkage model)	[N/m$^{(n+1)}$]
k_ϕ	Friction angle coefficient (Bekker pressure-sinkage model)	[N/m$^{(n+2)}$]
K_s	Wheatstone bridge gauge factor	[-]
k	a. Sinkage modulus (Bernstein pressure-sinkage model)	[N/m$^{(n+2)}$]
	b. Load cell degree of freedom (load cell regression model)	[-]
	c. Parameter index	[-]
	d. Gauge factor	[-]
L	Length	[m]
l	Length (literature)	[m]
m	a. Gradient parameter (proposed shear stress-displacement model)	[m^{-1}]
	b. Gradient (S-type load cell calibration)	[V/N]
$\mathcal{M}$	General nonlinear model (Bayesian parameter estimation)	[-]

$\mathcal{M}_0$	Model one (Bayes Factor)	[-]
$\mathcal{M}_1$	a. Model two (Bayes Factor)	[-]
	b. Model one (Mohr-coulomb model)	[-]
$\mathcal{M}_2$	Model two(shear stress-displacement model)	[-]
M_z	Torque about z-axis	[Nm]
My	Bending moment about y-axis	[Nm]
n	a. Pressure-sinkage exponent (Bekker pressure-sinkage model)	[-]
	b. Number of samples (Kernel Density Estimation)	[-]
	c. Strain hardening exponent (Romberg-Osgood stress-strain model)	[-]
N	Number of data points (general nonlinear function)	[-]
n_0	Number of posterior samples (model one, Bayes Factor sampling)	[-]
n_1	Number of posterior samples (model two, Bayes Factor sampling)	[-]
N_e	Endurance life	[-]
N_f	Cycles to failure	[-]
$N_{samples}$	Number of samples (Gibbs sampling)	[-]
$\mathcal{N}$	Gaussian distribution	[-]
η	Tractive efficiency	[-]
$[O]$	Wheatstone bridge output matrix	[V]
$[O']$	Output matrix with offset removed	[V]
P	Pressure (literature)	[N/m^2]
P	Pressure	[N/m^2]
p	Probability	[-]
Φ	Objective function	[-]
ϕ	Soil angle of internal shearing resistance	[Rad]
ϕ'	Soil effective friction angle	[Rad]
$\emptyset$	Shear annulus outside diameter	[m]
r	Wheel radius	[m]
R^2	Coefficient of determination	[-]
R_c	Relative soil compaction	[-]
r_i	Shear ring inside radius	[m]
r_m	Mean radius	[m]
r_o	Shear ring outside radius	[m]
R1-R16	Resistors corresponding to strain gauges 1 to 16	[Ohm]
ρ_{dmin}	Minimum dry density	[kg/m^3]
ρ_d	Dry density	[kg/m^3]
ρ_{dmax}	Maximum dry density	[kg/m^3]
s	Grouser spacing	[m]
σ	a. Normal stress	[N/m^2]
	b. Standard deviation (coefficient of variation)	[Base unit]
σ_1	Standard deviation (group one, standardised difference)	[Base unit]
σ_2	Standard deviation (group two, standardised difference)	[Base unit]
σ_a	Stress amplitude	[N/m^2]
σ_ϵ	Standard deviation (Gaussian likelihood function)	[N/m^2]
σ_{max}	Maximum stress	[N/m^2]
σ_{min}	Minimum stress	[N/m^2]

σ_{res}	Standard error (S-type load cell linear regression)	[V]
σ_u	Ultimate tensile stress	[N/m^2]
$\boldsymbol{\sigma}$	Normal stress vector	[N/m^2]
$\sigma_f{}'$	Fatigue strength coefficient (Coffin-Manson stress-strain model)	[N/m^2]
S_{rmax}	Degree of saturation at max density	[-]
S_{rmax}	Degree of saturation at min density	[-]
T	Shear ring torque	[Nm]
τ	Shear stress	[N/m^2]
$\boldsymbol{\tau}$	Shear stress vector	[N/m^2]
τ_x	Shear stress distribution along wheel soil interface	[N/m^2]
τ_{max}	Maximum shear stress	[N/m^2]
$\boldsymbol{\tau_{max}}$	Maximum shear stress vector	[N/m^2]
$\tau_{max,ij}$	Maximum shear stress (i^{th} category, j^{th} data point)	[N/m^2]
θ	a. Wheel angle	[rad]
	b. Model parameter	[Base unit]
θ_i	Parameter (i^{th} parameter, KDE estimation)	[Base unit]
θ_1	Soil entry angle (Rigid soil-wheel interaction model)	[rad]
$\boldsymbol{\theta}_{0,j}^{s}$	Parameter sample vector (model one, j^{th} sample, Bayes Factor sampling)	[Base unit]
$\boldsymbol{\theta}_{1,j}^{s}$	Parameter sample vector (model two, j^{th} sample, Bayes Factor sampling)	[Base unit]
$\boldsymbol{\theta}_{0,i}^{s}$	Parameter sample (Mohr-Coulomb model, i^{th} sample, Gibbs sampling)	[Base unit]
$\boldsymbol{\theta}_{1,i}^{s}$	Parameter sample (Stress-displacement, i^{th} sample, Gibbs sampling)	[Base unit]
$\theta_{i,j}^{s}$	Parameter sample (i^{th} parameter, j^{th} sample, KDE estimation)	[Base unit]
$\boldsymbol{\theta}$	Parameters vector	[Base unit]
$\boldsymbol{\theta}^{s}$	Parameter sample vector	[Base unit]
$\boldsymbol{\theta}^{*}$	Parameter vector before concatenating likelihood standard deviation	[Base unit]
$\boldsymbol{\theta_1^*}$	Parameter vector before likelihood std. dev. (Mohr-Coulomb model)	[Base unit]
$\boldsymbol{\theta_2^*}$	Parameter vector before likelihood std. dev. (Stress-displacement model)	[Base unit]
$\boldsymbol{\theta_0}$	Parameter vector (model one, Bayes Factor)	[Base unit]
$\boldsymbol{\theta_1}$	a. Parameter vector (model two, Bayes Factor)	[Base unit]
	b. Parameters vector (group one, Bayesian Hypothesis testing)	[Base unit]
$\boldsymbol{\theta_2}$	Parameters vector (group two, Bayesian Hypothesis testing)	[Base unit]
$\boldsymbol{\theta_{MAP}}$	Maximum a Posterior parameter vector	[Base unit]
$\boldsymbol{t}$	Dependent value vector (general nonlinear function)	[Base unit]
μ	Mean (coefficient of variation)	[Base unit]
μ_1	Mean (group one, standardised difference)	[Base unit]
μ_2	Mean (group two, standardised difference)	[Base unit]
V_{ex}	Excitation voltage (Wheatstone bridge)	[V]
W	Applied vertical load	[N]
W	Width	[m]
$\boldsymbol{w}$	Moisture content vector	[-]
w	Moisture content (by mass)	[-]
w_{ij}	Observed extraneous variable (i^{th} category, j^{th} data point)	[-]
ω_0	Proposal distributions (model one, Bayes Factor sampling)	[-]
ω_1	Proposal distributions (model two, Bayes Factor sampling)	[-]

$\boldsymbol{x}$	Independent variable vector (general nonlinear function)	[Base unit]
$\boldsymbol{X}$	Independent data vector	[Base unit]
$\boldsymbol{X_1}$	Independent data vector (Mohr-Coulomb model)	[Base unit]
$\boldsymbol{X_2}$	Independent data vector (Stress-displacement model)	[Base unit]
χ^2	Chi-squared distribution	[-]
$\boldsymbol{y}$	Dependant data vector	[Base unit]
Y	Scaling parameter (proposed shear stress-displacement model)	[-]
y_{model}	General nonlinear function	[-]
λ	Soil specific gravity	[kg/m^3]
γ_{Ff}	Safety factor for damage tolerance	[-]
z	Sinkage	[m]
z_0	Sinkage at a specific soil depth	[m]
$\boldsymbol{z}_{1-3}$	Random variable vector (Gibbs sampling)	[Base unit]
$\boldsymbol{z}^s_{1-3,i}$	Random variable sample vector (i^{th} sample, Gibbs sampling)	[Base unit]
δ_i	Standardised difference (i^{th} parameter)	[Base unit]
$\boldsymbol{\delta}^{\boldsymbol{s}}_{ij}$	Standardised difference sample (i^{th} parameter, j^{th} sample)	[Base unit]

List of Abbreviations

Abbreviation	Expansion
2D	Two Dimensional
3D	Three Dimensional
ADC	Analogue to Digital Conversion
ANCOVA	Analysis of Covariance
ANOVA	Analysis of Variance
AVDL	Advanced Vehicle Dynamics Laboratory
BF	Bayes Factor
CDF	Continues Distribution Function
CI	a. Credible Interval
	b. Confidence Interval
	c. Cone Index
CNC	Computer Numerical Control
COBYLA	Constrained Optimisation By Linear Approximation
DAG	Directed Acyclic Graph
DOF	Degree Of Freedom
DP	Drawbar Pull
ECDF	Empirical Continues Distribution Function
FEM	Finite Element Method
FF	Feed Forward
FFT	Fast Fourier Transform
GHG	Global Greenhouse Gas
GPS	Global Positioning System
GUI	Graphical User Interface
GW	Goodman and Weare
HPD	Highest Probability Density
IQR	Interquartile Range
ISTVS	International Society for Terrain Vehicle Systems
IV	Independent Variable
KDE	Kernel Density Estimate
MAP	Maximum a Posterior
MC	Moisture Content
NA	Not Applicable
NATO	North Atlantic Treaty Organization
NHST	Null Hypothesis Significance Testing
NLLSQ	Nonlinear Least Squares
NP	Nondeterministic Polynomial time
PC	Personal Computer
PDF	Probability Distribution Function
PI	Proportional Integral
PPD	Posterior Predictive Distribution
PPF	Percent Point Function
PSA	Penetro-Shear Apparatus

RMSE	Root Means Square Error
RPM	Revolutions Per Minute
SBF	Sequential Bayes Factor
SD	Standard Deviation
SG	Strain Gauge
SI	International System of Units
SUV	Sports Utility Vehicle
SWT	Smith Weston and Topper
VDG	Vehicle Dynamics Group

CHAPTER 1

Introduction

"When something is important enough, you do it even if the odds aren't in your favour."

-Elon Musk[1]

[1] AZ Quotes (2022), *Elon Musk Inspirational Quotes*. Available at: https://www.azquotes.com/author/10617-Elon_Musk/tag/inspirational (Accesed: 5 Jan 2022).

1. Introduction

1.1 Background

Global warming is a major problem and scientific evidence for its occurrence is unequivocal (Stocker *et al.*, 2013). A study by Lynas *et al.* (2021) of 3000 peer-reviewed papers on climate change indicated that greater than 99% consensus had been reached that humans are the direct cause of the observed climate change. A major contributor to climate change is the agricultural sector, with an estimated 24% of Global Greenhouse Gas (GHG) emissions attributed to this sector (Intergovernmental Panel on Climate Change, 2015).

One aspect in the agricultural sector that has potential for improvement is the tractive efficiency of agricultural vehicles. Tractive efficiencies of agricultural vehicles barely reach 50% in typical field conditions (Zoz, 1970, cited in Lyasko, 2010a; Renius *et al.*, 1985, cited in Osinenko *et al.*, 2015). The motion resistance due to plastic failure of the terrain during vehicle locomotion on soft soils results in non-recoverable energy loss (He *et al.*, 2020). Wheel slip is a major contributor to power loss that affects the operational efficiency of agricultural vehicles (Wong, 2010). The shearing action of the running gear causes the soil to deform plastically and the wheel to slip, reducing a vehicle's actual forward speed in relation to the theoretical speed if no wheel slip occurred. Figure 1 illustrates the tractive efficiency and wheel slip for a typical agricultural vehicle and how it can vary depending on the terrain and drawbar load.

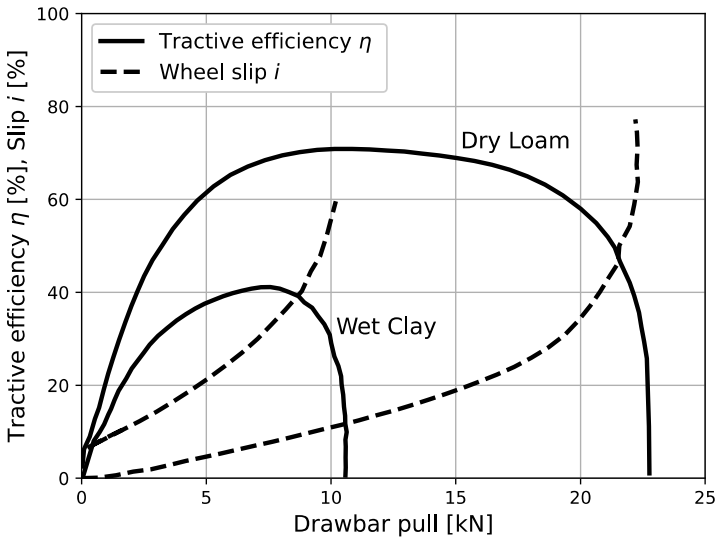

Figure 1-Tractive efficiency of a tractor on different terrain. Experimental data from Sohne (1968).

The design and optimisation of vehicle and mobility systems for improved tractive efficiency require accurate tyre-terrain-vehicle interface models. Traditional on-road tyre models are not able to adequately capture the tyre-soil interaction as they do not account for the deformable terrain (Taheri *et al.*, 2015a). The deformable terrain modelling problem is highly complex and can be split into a number of fundamental components: terrain behaviour modelling, tyre modelling, vehicle modelling and finally, complete terrain-tyre-vehicle system modelling (Sandu *et al.*, 2019a). An overview of the typical modelling process is indicated in Figure 2.

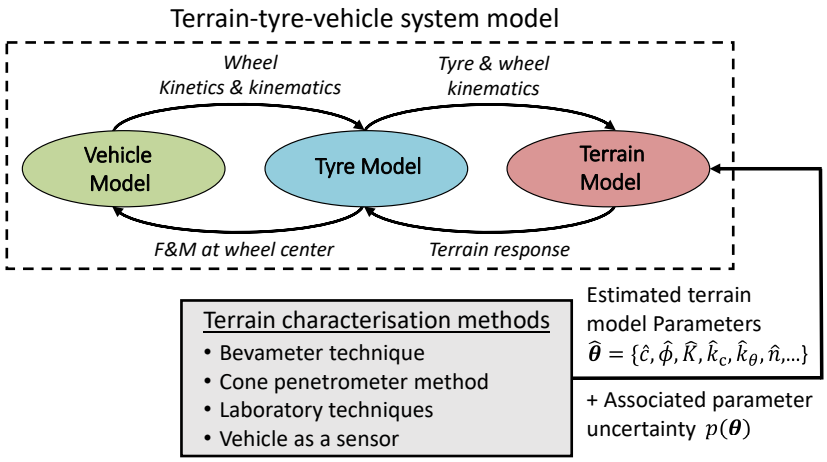

Figure 2-Modelling vehicle traction on soft soil. Adapted from Sandu et al. (2019a). *The indicated terrain model parameters are parameters required for the Bekker terrain model* (Bekker, 1964).

Figure 2 illustrates that the characterisation of the terrain's mechanical behaviour forms the basis for all further vehicle mobility modelling. Characterisation of the terrain's mechanical behaviour is a major consideration, if not the most important consideration, for predicting vehicle traction on soft soil (Shoop, 1993b; Lyasko, 2010a). However, in the terramechanics field, relatively limited studies focus on the terrain characterisation aspect, while a large body of literature focuses on the theoretical modelling of tyre-terrain interaction. Error at the terrain characterisation level may propagate and cause significant inaccuracies further in the terrain-tyre-vehicle modelling process.

The Bevameter soil characterisation technique is a popular and widely employed terrain characterisation method in the terramechanics field (Wong, 2010). The most prominent terrain-tyre interaction model employed today is the Bekker-Wong model (Lyasko, 2010a; Harnisch *et al.*, 2011; Gallina *et al.*, 2014; Taheri *et al.*, 2015b). This model is based on and traditionally requires Bevameter soil characterisation (Bekker, 1969; Gallina *et al.*, 2014; Shamrao *et al.*, 2018). Although Bevameter soil characterisation is a popular method used for vehicle mobility modelling, outdated practices exist for terrain characterisation using this method (He *et al.*, 2020). Currently, there is no fixed test equipment specification, and test equipment is tailored to the need of the researcher (He *et al.*, 2020).

It has long been recognised that the test equipment and experimental test setup factors influence the soil properties obtained using the Bevameter technique (Reece, 1964; Bekker, 1969). Although decades of research exist on the topic, a number of factors have been identified that have not been thoroughly investigated. One prominent but scarcely investigated factor is how the in situ shear mechanism affects the identified mechanical soil properties. Specifically, how the in situ longitudinal translational shear apparatus differs from in situ torsional shear apparatus. Another factor includes the influence of the shear tool contact area. It is said that tests should be conducted at contact areas and loads comparable to the intended running gear of the target vehicle (He *et al.*, 2020). However, tests are often done at smaller loads and contact areas to keep tests within practical limits. Shear velocity is another scarcely investigated factor that may be important. A vehicle's dynamic nature dictates that shear at the tyre-terrain interface occurs at a certain speed.

Furthermore, early soil characterisation methods did not attempt to quantify the uncertainty of the estimated soil parameters (Apfelbeck *et al.*, 2011). Soil mechanical behaviour is inherently a stochastic process (Bekker, 1969; Apfelbeck *et al.*, 2011; Gallina *et al.*, 2016). The identification of soil properties should therefore be viewed from a probabilistic perspective (Bekker, 1969). Recently, nonlinear parameter estimation with uncertainty quantification has been applied for Bevameter soil characterisation (Apfelbeck *et al.*, 2011). However, the inference method, based on a weighted covariance estimator, is only an approximate method that relies on large sample theory, linearisation and assumes the parameters are Gaussian distributed (Hougaard, 1988; Seber and Wild, 2003). This method may not be accurate for soil parameter estimation for Bevameter testing, which typically relies on a small number of tests. Bayesian parameter estimation via the Monte Carlo Markov Chain (MCMC) sampling approach is proposed as an alternative method that can account for non-Gaussian parameter distributions and achieve asymptotically exact inference at small sample sizes (Bishop, 2006).

Finally, investigating the mentioned test setup factors itself raises technical challenges. Typical Bevameters in literature are tailored to specific use cases and not to the study of a wide range of experimental setup factors. As part of this study, it is required to develop a device to enable fundamental research to be conducted on a wide range of factors that affect Bevameter soil characterisation. The development of a new Bevameter and associated soil bin infrastructure forms part of spearheading terramechanics research at the University of Pretoria, which previously did not have access to a Bevameter and a soil bin.

1.2 Problem statement

Bevameter soil characterisation is not a standardised procedure, and experimental test setup factors may influence the identified soil parameters. Furthermore, in situ soil mechanical properties exhibit stochastic behaviour, but the uncertainty of the identified soil parameters is rarely considered or estimated using approximate methods. Finally, a Bevameter device is required to study factors that affect Bevameter soil characterisation.

1.3 Aim and objectives

Research aim:

The main aim of the study is to determine if, and to what extent, intrinsic experimental test setup factors influence Bevameter soil characterisation.

Specific research objectives:

In order to accomplish the overall aim, the research is divided into three specific research objectives,

(1) Develop a new Bevameter device and accompanying infrastructure to enable the study of factors that affect Bevameter soil characterisation.
(2) Use the developed Bevameter to experimentally investigate test setup factors that may affect Bevameter soil characterisation.
(3) Use a probabilistic approach to estimate the soil model parameters and determine if the factors under investigation in objective two (2) are statistically significant.

1.4 Thesis outline

The thesis is divided into six chapters. An outline of the thesis structure is indicated in Table 1.

Table 1-Thesis outline.

Chapter	Chapter Overview
Chapter 1: Introduction	The first chapter presents the background of the problem and formulates the study's aim and objectives.
Chapter 2: Literature Study	The literature study covers essential information required to perform Bevameter soil characterisation. Furthermore, it scrutinises the state of the art and highlights gaps in the literature. Based on the identified gaps, specific factors to be investigated in this study are narrowed down.
Chapter 3: Bevameter Hardware and Soil Bin Setup	The Bevameter hardware and soil bin developed for this study are presented in this chapter. This chapter also includes matching the Bevameter hardware to the target vehicle running gear and loading conditions. This chapter primarily serves to address **research objective one (1)**.
Chapter 4: Experimental and Data Analysis Methods	This chapter presents the methods used to gather experimental data and methods used to analyse the data. Herein a new methodology to quantify the uncertainty of the identified soil model parameters and a method to determine the statistical significance of nonlinear Bevameter data is presented. This chapter contributes toward addressing **research objective three (3)**.
Chapter 5: Results & Discussion	The results of the experimental investigation are presented and discussed in this chapter. The data analysis methods presented in chapter four are extensively applied in this chapter to analyse data. This chapter addresses **research objectives two (2) and three (3)**.
Chapter 6: Conclusion & Recommendations	The final chapter summarises the results and draws an overall conclusion about the outcome of this investigation. Recommendations are also made for future work.

Chapter 6 is followed by the **References** used in this study. Finally, the **Appendices** contain additional information and are presented in the order they appear in this thesis.

CHAPTER 2

Literature Study

"Research is what I'm doing when I don't know what I'm doing."

-Wernher von Braun[2]

[2] Brainy Quote (2022) *Wernher von Braun Quotes*. Available at: https://www.brainyquote.com/authors/wernher-von-braun-quotes. (Accesed: 5 Jan 2022).

2. Literature Study

2.1 Preamble

The goal of this chapter is to cover the essential background necessary for conducting experimental Bevameter tests and investigate the state of the art to identify areas that are lacking in existing research regarding Bevameter soil characterisation. More specifically, this chapter will cover:

2.2 Soil characterisation methods for vehicle mobility modelling on soft soils

In order to demonstrate the relevance and motivation for investigating the Bevameter technique, a high-level overview of different soil characterisation methods and their ***applicability*** for modelling terrain-vehicle interaction is covered in this section.

2.2.1 The applicability of the Bevameter method

Today, the majority of terrain-tyre-vehicle interaction models follow the semi-empirical approach by Bekker-Wong (Lyasko, 2010a; Harnisch *et al.*, 2011; Gallina *et al.*, 2014; Taheri *et al.*, 2015b). The Bekker-Wong modelling approach traditionally requires the terrain to be characterised with a Bevameter, which entails performing in situ plate sinkage tests and in situ shear tests (Gallina *et al.*, 2014; Shamrao *et al.*, 2018). The wide adoption of the Bekker-Wong modelling approach, and by extension, Bevameter soil characterisation, is attributed to the fact that it has been used for many years and has given satisfactory results in solving off-road vehicle mobility problems (Lyasko, 2010b).

Figure 3 indicates the spectrum of modern vehicle-terrain interaction modelling approaches (NATO, 2021). The domain where Bevameter soil characterisation is applicable is indicated in red. This category, labelled “simple terramechanics”, has historically been the main focus area of off-road vehicle mobility research (Gallina *et al.*, 2014). Only recently has literature started to move towards

higher fidelity macro-scale physics-based terrain models as computing power and model complexity continue to increase. However, macro-scale physics-based methods have not shown adequate maturity and effectiveness in predicting vehicle traction (Lyasko, 2010b; Wong, 2010).

	Quantum Mechanics	Molecular Dynamics	Micro-scale Model Complex Terramechanics	Macro-Scale Model Complex Terramechanics	Height Field Model Simple Terramechanics	Height Model Simple Terramechanics	Vehicle Cone-Index Empirical Model
Fidelity	Very high						Very low
Description	Sub-atomic to atomic scale models	Molecular scale model	Soil grains individually modeled	Soil particles lumped to form a virtual particle or a finite element (e.g. DEM or FEM)	Terrain is divided into vertical cells. For each cell height and state of stress are stored. A Bekker-Wong-Janosi type pressure-sinkage-traction-slip model is used for each cell.	Normal stress and slip are used to calculate sinkage and tractive force using a Bekker-Wong-Janosi type model.	Vehicle-scale empirical steady-state model based on the Cone Index (implemented in NRMM / NRMM-II)
Terrain discretisation	3D	3D	3D	3D	2D or 1D	0D	0D
Discretisation scale	Sub-atomic scale	Molecular scale	Soil grain	Tread-block	Tread-block or Running gear	Running gear	Vehicle scale
Deformation/flow directions	3D	3D	3D	3D	1D - Vertical or 2D - Vertical + Horizontal	1D - Vertical	1D - Vertical
Number of Soil DOFs for vehicle mobility applications	$>10^{20}$	$\sim10^{18}$	$10^{14} - 10^{11}$	$10^{7} - 10^{6}$	$10^{4} - 10^{3}$	1	0
Current Computational Cost	Prohibitive	Prohibitive	Years of HPC time.	6 hours to 1 week	Minutes/ real time	Faster than real time	Faster than real time
Current state of development	Unknown how to take the model to the macro-scale	Taking the model to the macro-scale requires more research because the soil consists of many materials	More research is needed to understand the micro-mechanical soil interaction forces	More research is needed to improve, calibrate, and validate the soil models	More research is needed to improve, calibrate, and validate the soil models	More research is needed to improve, calibrate, and validate the soil models	Implemented in NRMM/NRMM-II

Figure 3-Approaches to modern vehicle-terrain interaction modelling based on fidelity and scale (NATO, 2021).

Although the Bevameter soil characterisation method is a popular method for vehicle mobility modelling, literature indicates that it tends to over-predict the drawbar pull of vehicles (Chang and Baker, 1973; Shoop, 1993b). Figure 4 (a) indicates a case where the drawbar pull of a tracked vehicle is over-predicted by 30-40%. Figure 4 (b) indicates a case where the in situ shear annulus over-predicts the shear stress of a Sports Utility Vehicle (SUV) by 11-19% in the 92-150kPa normal stress range.

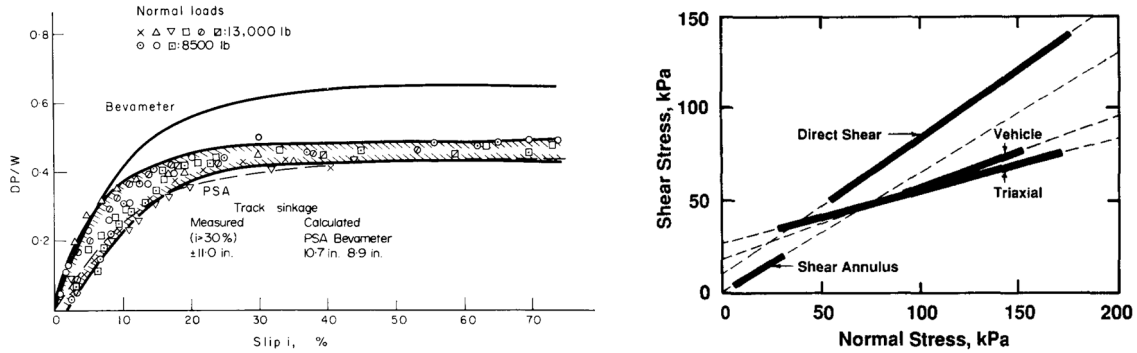

(a) (b)

Figure 4-Examples of over-prediction of vehicle traction using the Bevameter method. (a) Predicted drawbar pull vs. actual drawbar pull (Chang and Baker, 1973). *(b) Measured shear stress of different soil characterisation methods* (Shoop, 1993b).

2.2.2 The cone penetrometer and other in situ methods

The cone penetrometer method

A contemporary soil characterisation method that is widely employed is the cone penetrometer method (Shoop, 1993a). However, a number of studies have shown that the cone penetrometer shows poor correlation in predicting vehicle traction (Reece, 1981; Upadhyaya *et al.*, 1989; Okello, 1991; Shoop, 1993a; Wong, 2010; NATO, 2021). The consensus in literature is that this method of soil characterisation is limited to "GO, NO-GO" vehicle mobility prediction. This is likely attributed to the cone penetrometer lumping the soil's complex nonlinear normal stress-strain and shear stress-strain behaviour into a single parameter known as the Cone Index (CI). The CI is then used to predict vehicle

traction. It can be concluded that this single parameter is not sufficient to calibrate a unique set of soil model parameters to predict vehicle traction under varying wheel shear stress and normal stress loads.

Vehicle as a sensor

New methods are emerging in the terramechanics field that characterises the soil directly from soil wheel interaction tests without the need to explicitly perform traditional soil characterisation tests. Gallina *et al.* (2014) and Shamrao *et al.* (2018) used the Bayesian framework to infer both the soil model parameters and the soil-wheel interaction model parameters simultaneously. This approach significantly improved vehicle drawbar pull prediction compared to predictions made purely from traditional soil characterisation methods (Shamrao *et al.*, 2018).

However, soil parameters identified using this approach only apply to the current vehicle configuration and specific test conditions. Therefore, this method is not suitable for the predictive modelling of different vehicle configurations or parametric wheel-soil interaction studies. Gallina *et al*. (2014) state that the method is considered an augmentation to improve experimental correlation in the presence of model and soil parameter uncertainty. Gallina *et al*. (2014) still advocate the use of Bevameter soil characterisation to determine the prior parameter probability distributions for the Bayesian approach.

Other in situ methods

Other less popular in situ methods include the in situ direct shear box (Baladi, 1987), in situ shear vane (Baladi, 1987) and penetrating cone shear apparatus (Chang and Baker, 1973). These methods have not seen widespread application in the terramechanics field, and therefore their usefulness is limited.

2.2.3 Laboratory methods

Basic laboratory methods

A number of laboratory soil characterisation techniques exist. The triaxle test, direct box shear test, shear graph, simple shear device and enclosed annular ring are some typical examples (Muro and O'Brien, 2005). However, depending on the soil-wheel interaction model employed, certain terrain parameters, such as the pressure-sinkage and shear stress-displacement parameters, cannot be determined using standard laboratory techniques as they depend on the in situ soil response.

However, some soil parameters, like the Mohr-Coulomb maximum shear stress parameters, may be obtained using standard methods in the laboratory. However, Bekker (1956, 1969) states that the Mohr-Coulomb parameters identified in the laboratory rarely apply to predicting traction in field conditions. For the Mohr-Coulomb parameters, literature strongly recommends the use of in situ methods over laboratory measurements (Bekker, 1956, 1969; Okello, 1991; Shoop, 1993a; Wong, 2010).

Advanced laboratory methods

The laboratory methods investigated by Bekker (1969), Okello (1991) and Shoop (1993a) in the terramechanics field are standard laboratory soil characterisation techniques used for basic civil engineering purposes. Only simple parameters like the Mohr-Coulomb failure criteria parameters were investigated. These parameters do not account for the soil's nonlinear stress-strain evolution or take soil conditions like compaction level, moisture content and loading condition into account.

In order to characterise soil for any soil condition and under general loading conditions requires constitutive soil models (Karstunen and Amavasai, 2017). Parameterisation of these soil models requires specialised soil characterisation procedures that, even today, are not included in standard

engineering practice due to their complexity (Seyedan and Sołowski, 2019). Soil models characterised in this way are able to capture a soil's nonlinear stress-strain evolution with hardening and softening laws, including dilation effects and the effect of the soil compaction level. Examples of constitutive soil models are the empirical NorSand and Cam Clay soil models (Jefferies, 1993). However, evidence for these models applied in the terramechanics field is limited. Therefore, the practical application thereof is limited. However, constitutive soil models are noted as a promising avenue for future studies.

2.2.4 Summary of characterisation methods for vehicle mobility modelling on soft soils

It can be concluded that, for the time being, the Bevameter soil characterisation method is the most applicable method for vehicle mobility modelling on soft soil. Its close ties with the Bekker-Wong model and modern height field soil-wheel interaction models make it a soil characterisation method that other approaches cannot readily replace. Now that it is established that the Bevameter method is the most applicable method, a more in-depth review of the method can be conducted.

2.3 The Bevameter in situ soil strength characterisation technique

2.3.1 A brief history of the method

The Bevameter soil characterisation technique was pioneered by Bekker (1956, 1960, 1969) and is based on the premise that the soil strength for predicting vehicle traction is best measured in situ under similar loading conditions expected by a vehicle's running gear (Wong, 2010). The instrument used to perform the characterisation is called a Bevameter (short for **Be**kker **Va**lue **Meter**) (Shoop, 1993a). The Bekker values refer to two sets of terrain model parameters; one set that describes the in situ pressure-sinkage (or bearing capacity) relationship (n, k_c, k_ϕ) and another set that describes the in situ shear stress-displacement behaviour (c, ϕ, K), (Shoop, 1993a). Today, the Bevameter soil characterisation method is used to estimate the parameters for a wide range of terrain models that describe the in situ pressure-sinkage and soil shear stress-displacement response (He *et al.*, 2019a).

2.3.2 Equipment and test procedures

Figure 5 indicates the equipment required to perform Bevameter tests. Figure 5 (a) indicates the typical equipment used to perform the pressure-sinkage tests, and Figure 5 (b) indicates the typical equipment used to perform shear stress tests. Besides the torsional shear device depicted in Figure 5 (b), an in situ translational shear device may also be used, like the instrument developed by Upadhyaya *et al.* (1993).

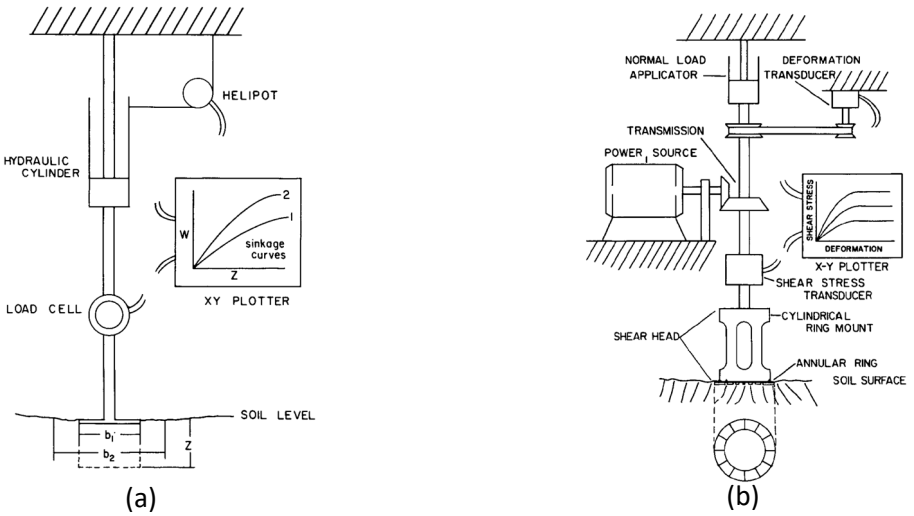

Figure 5-Schematic of Bevameter equipment. (a) Pressure-sinkage test. (b) Shear-displacement test (SAE, 1967).

The Bevameter pressure-sinkage test, depicted in Figure 5 (a), seeks to determine an empirical relationship between the soil's vertical bearing capacity and plate sinkage depth. The tests are to be performed with at least two different plate sizes (SAE, 1967; He *et al.*, 2020). This allows for interpolation and extrapolation at other contact areas (Tsitouridis, 2019). This is important because the wheel-soil contact area is not fixed and varies continually with wheel slip and sinkage. In order to eliminate uncertainty in the application of pressure-sinkage tests to wheel soil interaction, the plate contact area should be the same as the running gear contact area (Bekker, 1956, 1969; Wong, 2010).

The Bevameter shear stress-displacement test, depicted in Figure 5 (b), seeks to determine the relationship between shear stress τ (the response variable) and two input variables, namely, normal stress σ and shear displacement j (Muro and O'Brien, 2005). Practically the Bevameter soil shear tests consist of applying a fixed vertical load to a rotating annular ring or translational shear device and enforcing a relative angular or linear horizontal displacement. The normal loads should include expected ground vehicle pressures (SAE, 1967). The test device should incorporate grousers (SAE, 1967). This ensures that the soil fails in the soil plane and not at the soil plate surface interface. The grouser size should be comparable to the grouser or track tread length of the running gear (SAE, 1967). For torsional shear tests, the shear displacement should be expressed in terms of equivalent linear shear j at the mean shear ring radius r_m given by (Reece, 1964),

$$j = r_m \alpha = \frac{r_o + r_i}{2} \alpha \tag{1}$$

Where α is the angular rotation, r_o is the outside radius and r_i is the inside radius of the annular ring.

2.3.3 Standards and recommended practices

In 1969 Bekker (1969) already indicated the need to standardise Bevameter tests, and more recently, the International Society for Terrain Vehicle Systems (ISTVS). To this day, this has not been truly realised (Kim *et al.*, 2022). However, recommended practices do exist. The SAE 939 (SAE, 1967) off-road vehicle mobility evaluation standard does prescribe guidelines for Bevameter soil characterisation. However, the standards have not been updated since 1967 and are likely outdated (He *et al.*, 2020). More recently, the North Atlantic Treaty Organization (NATO) has issued the AMSP-06 standard for guidance on drafting new standards for next-generation vehicle mobility modelling (NATO, 2021). Herein they also provide recommended practices for performing Bevameter tests. It should be emphasised that both the SAE 939 and AMSP-06 standards are only considered rough guidelines with equipment specifications and detailed procedures lacking compared to traditional laboratory soil characterisation techniques. The experience gained in this study ultimately aims to benefit the ISTVS in drafting new standards for Bevameter soil characterisation.

2.3.4 Typical pressure-sinkage and shear stress-displacement response

Figure 6 indicates typical pressure-sinkage and shear responses observed for Bevameter tests.

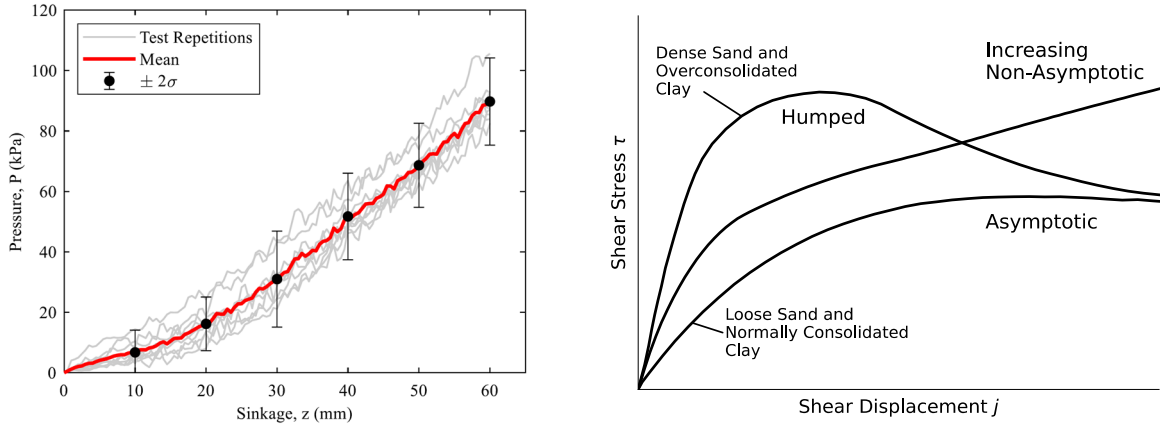

(a) (b)

Figure 6-Typical Bevameter results found in literature. (a) Pressure-sinkage for dry sandy soil for a 60mm by 30 mm rectangular plate (Tsitouridis, 2019). *(b) Typical shear stress test responses after* Upadhyaya (1994) and Bekker (1969).

Pressure-sinkage tests typically exhibit one of two trends (Bekker, 1969). The first is the exponentially increasing trend observed in Figure 6 (a), which is representative of ”weak soils” on a “strong base”. Examples include loose soils such as sand, ploughed fields and fresh snow on a rigid base (Bekker, 1969). The second is the increasing but concave-down trend, which is representative of “strong soils” on a “weak base”. Examples include muskeg or peat moss on mud or fluid substratum (Bekker, 1969).

Shear stress-displacement tests typically exhibit one of three forms. The hump type curve in Figure 6 (b) is representative of firm soils such as densely compacted sands and overconsolidated clays (Upadhyaya *et al.*, 1994). The asymptotic type of curve is representative of loose sands and normally consolidated clay (Upadhyaya *et al.*, 1994). A third type is the continuously increasing non-asymptotic type curve (Bekker, 1969). The non-asymptotic type curve is only observed for Bevameter tests, with no evidence indicating this form exists for laboratory shear tests. Reece (1964) and Bekker (1969) attribute the non-asymptotic form to “drag shear” that artificially increases the measured shear strength.

2.3.5 Empirical soil models

It is standard practice to fit an empirical regression model to the Bevameter experimental pressure-sinkage and shear-displacement data (Wong, 2010; He *et al.*, 2019a). Although the use of a model prevents the data from being presented exactly, it provides a standard means to exchange soil parameters, smoothes the data variability and allows predictive capability (Upadhyaya *et al.*, 1994).

Pressure-sinkage models

The oldest and simplest pressure-sinkage model is the Bernstein (1913, cited in He *et al.* 2019a) model,

$$P(\mathrm{z}) = kz^n \tag{2}$$

Where P is the pressure exerted on the plate, z is the plate sinkage, k is the sinkage modulus, and n is the sinkage exponent. Although simple, the model can accommodate a wide range of soil behaviour, from exponentially increasing soil behaviour to concave-down soil hardening behaviour.

The Bekker (1960) pressure-sinkage model, indicated in equation (3), is arguably the most popular empirical pressure-sinkage model in use today. The Bekker model incorporates plate size as an input parameter in an attempt to predict the pressure for any given plate size.

$$P(z) = (\frac{k_c}{b} + k_\phi)z^n \quad (3)$$

Where b is the smallest dimension of the sinkage plate, k_c is an empirical parameter influenced by soil cohesion and k_ϕ is an empirical parameter influenced by the soil's friction angle (Wong, 2010).

He *et al.* (2019a) provide a comprehensive review of an additional 34 pressure-sinkage models. He *et al.* (2019a) notes that although many attempts have been made at more sophisticated pressure-sinkage models, most models do not have truly invariant soil parameters and extrapolate poorly. Therefore, Bevameter tests should strive to match the running gear soil contact patch area as closely as possible.

Maximum shear stress models

The basis for the majority of soil shear stress models in the terramechanics field is the Mohr-Coulomb soil failure theory (He *et al.*, 2019a). The Mohr-Coulomb failure criteria is given by,

$$\tau_{max}(\sigma) = c + \sigma\tan(\phi) \quad (4)$$

Where τ_{max} is the maximum shear stress, σ the normal stress, c is the soil cohesion, and ϕ is the soil internal friction angle. The Mohr-Coulomb model does not describe shear behaviour at any point other than at the peak shear stress. For modelling wheel tractive effort when maximum soil strength is not developed, additional parameters are required that describe the shear stress evolution (Bekker, 1956).

Shear stress-displacement models

The shear stress-displacement model describes the evolution of shear stress in terms of absolute displacement j. These models typically employ a hierarchical modelling approach that takes the maximum shear stress from the Mohr-Coulomb model as input (He *et al.*, 2019a). The most common shear stress response encountered is the asymptotic type curve, for which the Janosi-Hanamoto model is recommended (Upadhyaya *et al.*, 1994). The Janosi-Hanamoto (1961) model is given by,

$$\tau(\tau_{max}, j) = \tau_{max}(1 - e^{-\frac{j}{K}}) \quad (5)$$

Where τ is the shear stress, τ_{max} is the maximum stress from the Mohr-Coulomb failure model, and K is the bulk deformation modulus. The parameter K is proportional to the gradient of the curve at the origin. This is made clear by evaluating the derivative of equation (5) with respect to j at the origin,

$$\left.\frac{d\tau}{dj}\right|_{j=0} = \left.\frac{\tau_{max}}{K}e^{-\frac{j}{K}}\right|_{j=0} = \frac{\tau_{max}}{K} \quad (6)$$

On a plot of shear stress τ vs. displacement j, the parameter K also indicates the distance from the τ-axis to the intercept of the tangent line of the model at the origin and the horizontal line $\tau = \tau_{max}$.

He *et al.* (2019a) provide a review of eight additional shear stress-displacement models. For information on these alternative models and scenarios where each might be applicable, see He *et al.* (2019a).

2.3.6 Application of Bevameter tests

In order to fully comprehend the Bevameter soil characterisation technique, it is important to understand, if only on a high level, how Bevameter test data is applied in terrain-wheel interaction modelling. In the original Bekker rigid wheel terrain interaction modelling approach, the pressure acting on the wheel rim perpendicular to the circumference of the wheel is assumed to be equal to the pressure underneath a flat plate at the same depth as the pressure-sinkage test (Bekker, 1956). Figure 7 indicates how the normal stress from the sinkage tests is mapped to the soil wheel interface.

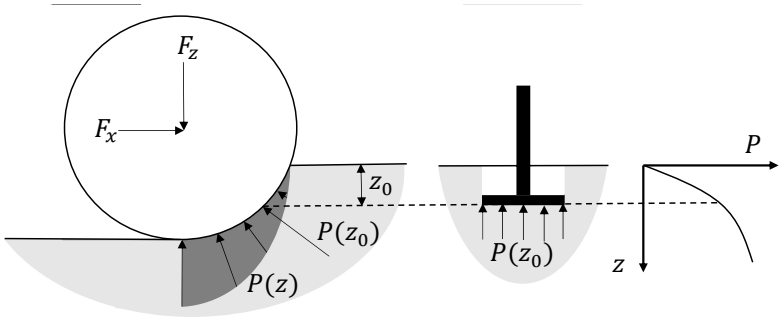

Figure 7-Principles of the pressure-sinkage analogy. After Bekker (1956) *and Harnisch et al.* (2011).

It should be noted that the analogy in Figure 7 is dated. In 1967 Wong and Reece (1967) pointed out that Bekker's approach is not entirely correct, with empirical evidence indicating the peak pressure occurs more toward the front of the wheel. Wong and Reece (1967) extended Bekker's approach to incorporate additional parameters to alter the pressure distribution to match empirical test data. Integration of the normal pressure (and shear stress) over the wheel surface is then used to determine the horizontal and vertical forces on the wheel. Through discretisation of the soil-wheel interface, the same approach can also be applied to flexible pneumatic tyres (Senatore and Sandu, 2011).

Similar to the pressure-sinkage tests, the Bevameter shear stress-displacement results are mapped to the soil-wheel interface through geometric relations. For a rigid wheel, it can be shown that the equivalent linear shear displacement j along the soil-wheel interface is dependent on wheel slip i and the current angular position on the wheel θ (Wong and Reece, 1967),

$$j(\theta, i) = r[\theta_1 - \theta - (1 - i)(sin\theta_1 - \sin\theta)] \tag{7}$$

Where r is the wheel radius and θ_1 is the soil entry angle. Substituting the equivalent linear displacement into a soil shear stress-displacement model, for example, in the Janosi-Hanamoto model from equation (5), the shear stress distribution τ_x along the wheel-soil interface can be found,

$$\tau_x(\theta, i) = (c + \tan(\phi))(1 - e^{-\frac{r[\theta_1 - \theta - (1-i)(sin\theta_1 - \sin\theta)]}{K}}) \tag{8}$$

Again, the same approach can be applied to flexible pneumatic tyres through discretisation of the soil-wheel interface in the angular domain (Senatore and Sandu, 2011).

2.3.7 Correction measures for drag shear

In situ Bevameter shear tests are said to include a physical phenomenon that artificially increases the measured shear strength called "drag shear" (Reece, 1964; Bekker, 1969). Drag shear consists of a number of contributing factors that vary depending on the specific shear mechanism employed. Reece (1964) states that for in situ translational shear tests, the main contributors are,

- Bulldozing of the first grouser.
- Grouser lateral drag (from the peripheral grouser shear area).
- Soil fallback drag (from soil collapsing and impacting the side and top of the shear tool).

Reece (1964) and Bekker (1969) suggested using experimental methods to measure and compensate for drag shear. These experimental correction methods are said to fully correct the data from the non-asymptotic form observed in Figure 6 to an asymptotic form (Bekker, 1969). Figure 8 indicates two methods presented by Bekker for correcting drag shear. It should be noted that more modern literature that accounts for drag shear could not be found.

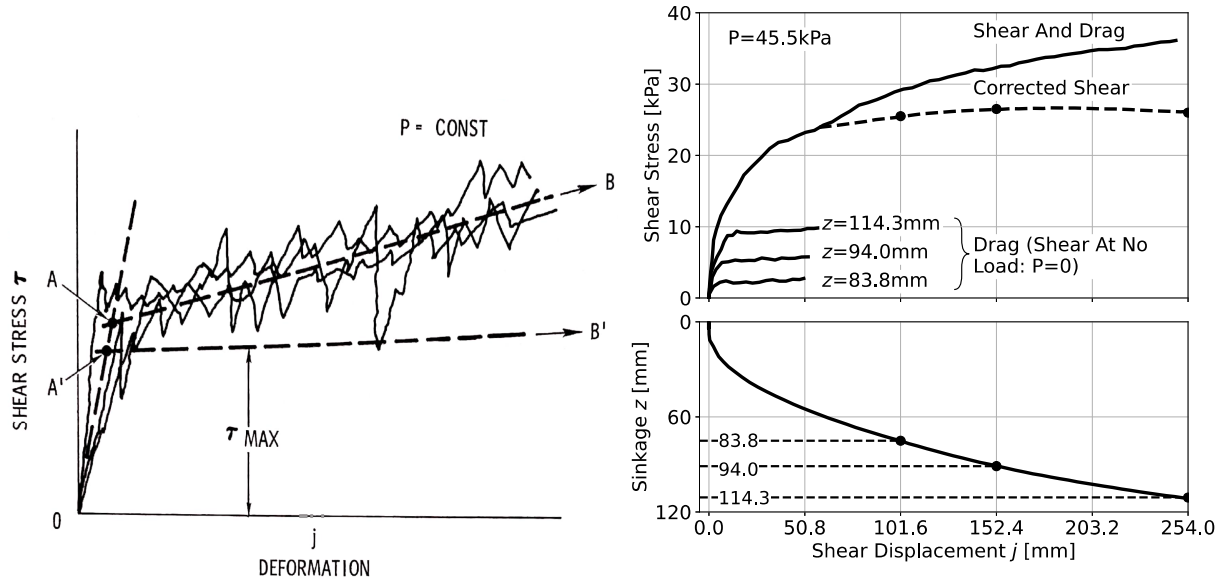

Figure 8-Methods for correcting Bevameter shear data of non-asymptotic form. (a) Method one (Bekker, 1969). (b) Method two (reproduced from Bekker (1969)).

Bekker's (1969) first method, indicated in Figure 8 (a), consists of fitting two piecewise linear regression lines. The intersection of two lines, Point A, forms the yield point of the soil. After the main test, a drag shear test is performed by removing the load and performing another shear test. The maximum drag shear is then subtracted from point A to form point A′. A horizontal line is then extended from A′ to B' to form the elastic, fully plastic curve OA′B′. The reason for extensively altering the measured physical soil behaviour using this approach was not justified.

Bekker's (1969) second method, indicated in Figure 8 (b), also performs drag shear tests after the standard test has been conducted. However, in this method, the shear instrument is lifted in increments, and the drag shear at specified sinkage is mapped through the nonlinear sinkage function and subtracted from the standard shear measurement. A criticism of this method is that at maximum sinkage, the bottom surface is still in contact with the soil. This may artificially increase measured drag shear. It is argued that lifting the shear tool a few millimetres is a better representation of drag shear.

2.3.8 Soil preparation methods for repeated tests

For any experimental soil-machine interaction study that plans to do repeated tests, soil preparation is a curial aspect. The soil preparation procedure itself is said to induce variance in the soil's mechanical behaviour, and this needs to be controlled as much as possible to lower inter tests variance (Apfelbeck *et al.*, 2011). Inadequate control of the soil state (compaction level, moisture content, etc.) will make isolating the effect of intrinsic Bevameter test setup factors, such as contact area, difficult.

Only a few studies have performed repeated Bevameter tests in a laboratory setting. Examples of such studies are those done by Reece (1964), Bekker(1969), Apfelbeck *et al.*(2011), Shamrao *et al.*(2018), and Tsitouridis (2019). In the wider soil-machine interaction field, many laboratories perform soil preparation for repeated testing. The soil preparation strategies range from highly professional, fully mechanised soil preparation methods (Godwin *et al.*, 2006; He *et al.*, 2018; Kumar *et al.*, 2019; Lisowski *et al.*, 2022) to partially mechanised (Reece, 1964; Bekker, 1969; Godwin *et al.*, 1980; He *et al.*, 2019a) and lastly, manual soil preparation methods for small soil boxes (Apfelbeck *et al.*, 2011; Shamrao *et al.*, 2018; Tsitouridis, 2019).

Given the resource and time constraints, a partially mechanised soil preparation strategy similar to that employed by the Advanced Vehicle Dynamics Laboratory (AVDL) at Virginia Polytechnic University is considered the most viable approach for this study (Pinto, 2012; He *et al.*, 2019b). Figure 9 indicates the soil preparation procedure at AVDL (Pinto, 2012). The preparation procedure consists of (i) disturbing the soil with a hand-operated rotary tiller, (ii) hand raking, (iii) machine levelling, (iv) hand tampering and (V) machine roller compaction. He *et al.* (2019b) from ADVL employed a similar strategy but omitted the hand tampering step and added a hand shovelling step prior to rotary tilling. He *et al.* (2019b) altered the soil compaction state by changing the number of roller passes. The soil compaction state was quantified with the Cone Index (CI) from cone penetrometer tests and Relative Compaction (RC) from in situ piston sample tests (see He *et al.* (2020) for applicable standards). CI values and RC values ranged from 345kPa and 90.8% for a low soil compaction state to 779kPa and 91.2% for a medium soil compaction state and finally, 1071kPa and 93.5% for a high soil compaction state.

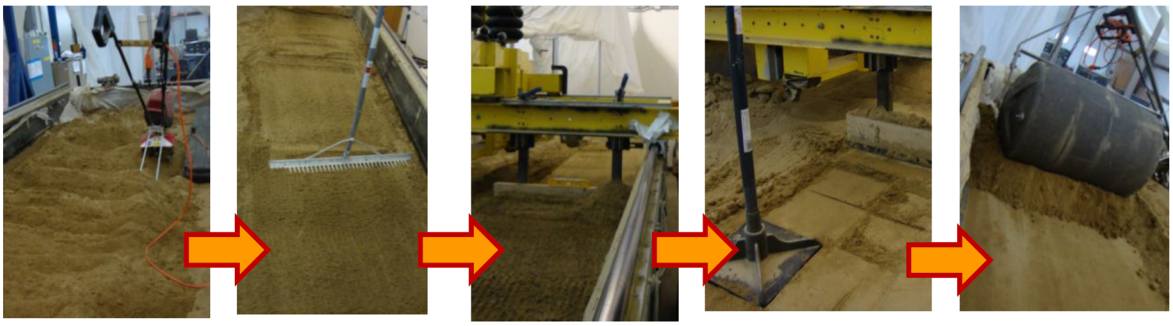

Figure 9-Soil preparation procedure at Virginia Polytechnic Institute and State University (Pinto, 2012)

Measuring the repeatability of Bevameter tests

To measure the repeatability of Bevameter tests, Bekker (1969) analysed the mean value for a pressure-sinkage test and reported a 95% confidence level on the mean. Wong (1989) suggests fitting a model to pressure-sinkage data and using a modified version of the normalised root mean square error ϵ_w to evaluate the repeatability. Wong's (1989) goodness of fit is given by,

$$\epsilon_w = 1 - \frac{\sqrt{\sum \frac{\left(\boldsymbol{t}(\boldsymbol{x}) - y_{model}(\boldsymbol{x}, \widehat{\boldsymbol{\theta}})\right)^2}{N-2}}}{\sum \frac{\boldsymbol{t}(\boldsymbol{x})}{N}} \tag{9}$$

Where $\boldsymbol{t}(\boldsymbol{x})$ is the dependent data given by independent variable $\boldsymbol{x}$, y_{model} is a general nonlinear model, $\widehat{\boldsymbol{\theta}}$ is the estimated model parameters, and N is the number of data points. Apfelbeck *et al.* (2011) used Wong's approach to quantify the repeatability of different soil preparation procedures. However, an immediate drawback to this approach is that it partially measures the ability of the model to fit the data and partially measures the repeatability of the test.

Tsitouridis (2019) used the coefficient of variation CV to determine repeatability of Bevameter tests and soil preparation. The coefficient of variation is defined as,

$$CV(x) = \frac{\hat{\sigma}(x)}{\hat{\mu}(x)} = \frac{\sqrt{\frac{\sum(\boldsymbol{t}(x) - (\boldsymbol{t}(x))^2}{N-1}}}{\mathbb{E}(\boldsymbol{t}(x))} \tag{10}$$

Where $\hat{\sigma}(x)$ is the estimated standard deviation of the dependant values $\boldsymbol{t}(x)$, evaluated at discrete points of the independent variable x, $\hat{\mu}(x)$ is the mean of repeated tests, $\mathbb{E}$ is the expected value

operator, and N is the number of data points. An advantage of this metric is that it provides a way to universally compare data from different researchers without requiring a specific model to fit the data.

2.3.9 Summary of the Bevameter in situ soil characterisation technique

A detailed description of the Bevameter soil strength characterisation technique was given. It covered the test equipment required, test procedures, the expected results, standard empirical soil models, how Bevameter results are applied in soil-wheel interaction models, special correction measures, and soil preparation methods. With the basics of the technique covered, the state of the art on experimental Bevameter tests can be investigated.

2.4 State of the art on experimental investigations

2.4.1 Overview of the state of the art

Table 2 indicates an overview of critical literature regarding experimental Bevameter soil characterisation. The literature is limited to original experimental investigations and excludes purely theoretical work and review papers. Figure 2 lists a number of factors of interest that might affect Bevameter soil characterisation, and the studies have addressed these factors. The factors of interest consist mainly of those highlighted by Bekker (1969) that may influence Bevameter tests but also include aspects judged by the author to be important for Bevameter testing.

Table 2-Overview of the state of the art on Bevameter soil characterisation.

Category	Hardware & Standard Tests			Factors Influencing Pressure Sinkage			Factors Influencing Shear Stress					Uncertainty Quantifi-cation			Other		
Factor of Interest / Study	Match loads to vehicle	Present new hardware	Soil parameter estimation	Sinkage velocity	Plate size/contact area	Plate shape	Shear mechanism (in situ)	Contact area	Tool geometry	Shear velocity	Grouser/surface interface	95% CI on raw data	95% CI on soil parameters	Test for statistical sig.	Effect of soil density	New theoretical models	Other objectives
(Kim *et al.*, 2022)			■		■						■						■
(Kim *et al.*, 2021)		■	■		■												
(Mähönen *et al.*, 2021)	■	■	■		■												
(Salman *et al.*, 2020)		■	■		■												■
(Tsitouridis, 2019)		■	■		■	■						■				■	■
(Shamrao *et al.*, 2018)		■	■									■	■				■
(Edwards *et al.*, 2017)	■	■	■		■										■		
(Apfelbeck *et al.*, 2011)	■		■	■		■			■	■	■	■	■				
(Meirion-Griffith and Spenko, 2011)		■	■		■	■										■	
(Massah & Noorolahi, 2010)		■	■		■	■								■			
(Apfelbeck *et al.*, 2009)		■	■		■												■
(Shoop, 1993b)			■														■
(Upadhyaya *et al.*, 1993)		■	■		■	■			■						■		
(Bilanski and L'Esperance, 1990)			■														■
(Stafford & Tanner, 1982)		■	■											■			■
(Wong *et al.*, 1979)			■		■	■					■					■	
(Wells & Treesuwan, 1978)			■		■										■	■	■
(Chang & Baker, 1973)		■	■														■
(Bekker, 1969)	■	■	■	■	■	■			■	■	■		■	■		■	■
(Reece, 1964)		■	■	■	■	■	■		■		■						■
Total (out of 20)	4	14	20	3	14	8	1	0	4	2	5	3	3	3	3	5	12

From Table 2, it is observed that a large number of experimental studies present new hardware (14/20) and perform soil parameter estimation (20/20). However, most studies do not indicate how the Bevameter equipment matches the target vehicle, with only four out of twenty studies (4/20) doing so. Matching the Bevameter equipment to a target vehicle's running gear is an essential aspect of Bevameter soil characterisation for vehicle traction prediction (Bekker, 1969).

Many authors find fault with Bevameter pressure-sinkage tests, with many studies investigating the effect of plate size (14/20) and plate shape (8/20). Sinkage velocity is the least investigated factor, with only three studies doing so (3/20). However, in general, pressure-sinkage tests are well-studied.

Factors that influence the shear stress test are investigated significantly less than factors that influence the pressure-sinkage test. To the best of the author's knowledge, no study directly investigated the influence of shear contact area (0/20). Similarly, the in situ shear mechanism (linear vs. torsional shear) has only been investigated by a single author (1/20). The tool geometry (e.g. solid disk vs. annular ring) has been investigated by four studies (4/20), and five studies (5/20) investigated the influence of grousers. Overall a clear gap is identified regarding factors that influence Bevameter shear stress tests.

The inclusion of uncertainty quantification in Bevameter soil characterisation has also been scarce. Few studies perform repeated testing and uncertainty quantification. Given the well-known stochastic nature of in situ soil characterisation, the disregard for uncertainty quantification is alarming. More specifically, only three studies (3/20) indicate confidence intervals on the raw data, and only three (3/20) indicate confidence intervals on identified soil parameters. Only three (3/20) performed formal tests for statistical significance. None of the studies indicated confidence intervals on shear stress data.

Another scarcely investigated factor is related to soil density. Although it is not an intrinsic experimental test setup factor, soil density is an important factor that influences the soil's mechanical response. Only three studies (3/20) considered the influence of soil density on soil strength.

Finally, it should be noted that approximately 50% of studies also investigate other objectives regarding Bevameter tests than the listed factors. These objectives are typically related to the application of Bevameter test data to predict vehicle mobility. Examples are predicting wheel traction (Tsitouridis, 2019) or predicting a soil engagement tool draft force (Bilanski and L'Esperance, 1990).

From reviewing the state of the art on experimental Bevameter tests, it is clear that limited focus has been placed on certain aspects. The gap in the literature is summarised below,

1) **Factors that influence shear stress tests:** Factors regarding shear tests have been investigated less compared to pressure-sinkage, with few studies performing a detailed investigation of factors that affect soil shear strength. The factors identified as most important are: 1) shear mechanism, 2) shear contact area, and 3) shear velocity.
2) **Uncertainty quantification:** Very few studies include confidence intervals for the identified soil model parameters or confidence intervals on the raw data. Two important factors that should be included in this study are: 1) probabilistic parameter estimation with uncertainty quantification and 2) formal tests for statistical significance of factors that influence Bevameter tests.
3) **Other shortcomings worthwhile addressing:** Literature is eager to present new hardware and perform basic tests, but few studies show how the Bevameter test equipment matches the target vehicle. Furthermore, the influence of soil density is important but rarely studied.

Now that the gap in the literature has been identified, a more detailed review of the specific factors of interest can be conducted.

2.4.2 A detailed review of selected factors that influence Bevameter shear tests

Influence of shear mechanism

Two types of instruments exist for Bevameter shear tests. The first is the classic rotational shear annulus indicated in Figure 5 (b). The second is the linear shear device, such as the one developed by Upadhyaya *et al.* (1993). Disagreement exists about which method is more representative and how the identified soil properties are affected by the different shear mechanisms. Bekker (1956) originally advocated the use of a linear in situ shear test device. However, he later advocated using a rotational shear device over the linear shear device due to concerns caused by bulldozing of the first grouser for linear shear (Bekker, 1969). In opposition, Upadhyaya *et al.* (1993) are of the opinion that a tyre or track undergoes linear shear motion, and the linear shear device is a better analogue of a vehicle's running gear.

Stafford and Tanner (1982) published a comprehensive study on the effect of different shear test mechanisms. They compared an in situ Bevameter torsional shear device to a shear box test, enclosed shear annulus and triaxle tests. The results indicated significantly different peak shear stress for the different methods. Stafford and Tanner (1982) concluded that the shear mechanism is highly influential.

Reece (1964) presents the only study that performed both in situ linear and in situ torsional shear tests. He investigated a range of linear shear test configurations and a single torsional shear test setup. The results from the study are indicated in Figure 10. Reece (1964) made no comments about the difference between linear vs. torsional shear other than that both methods differ significantly from the shear box test. Given the scatter of the data in Figure 10, both methods appear to be equivalent.

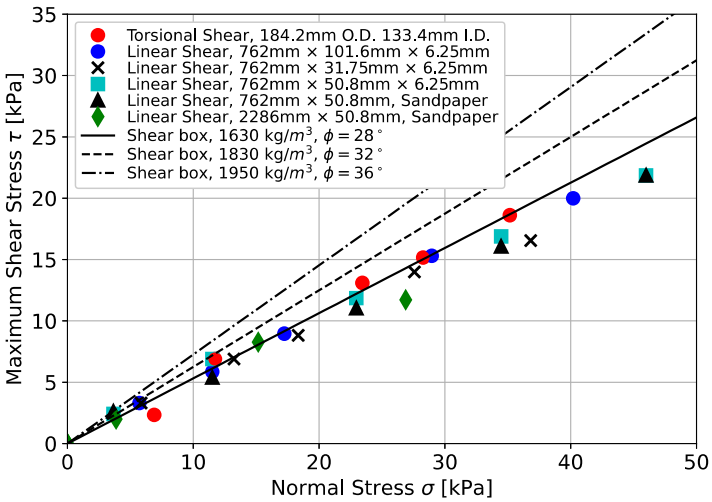

Figure 10-Influence of shear test configuration on maximum shear stress for dry sand. Data from Reece (1964).

From reviewing the state of the art, it is concluded that limited and conflicting information exists about the influence of the shear mechanism. This warrants further investigation in this study.

Influence shear contact area

Wong (1989) states that to prevent uncertainty in the extrapolation of performance in full-scale vehicles, the size of the Bevameter contact area should be the same as the contact area of the tyre or track link. However, no distinction is made between pressure-sinkage and shear tests. Similar vague statements about representative contact areas were found by other researchers (Okello, 1991; Shoop, 1993; He *et al.*, 2020). However, Bekker (1956, 1969) states explicitly that the ***shear*** test contact area should be comparable to the vehicle running gear. This is typically not the case with most authors

utilizing Bevameter shear contact areas smaller than the running gear areas. Even the SAE J939 (SAE, 1967) standard recommends a relatively small shear ring with an area of only $129cm^2$.

Apfelbeck *et al.* (2011) indirectly compared the influence of contact area by comparing two different rotational shear instruments, one with an annular ring and one with a solid disk. However, by changing both the contact area and geometry, the effect of the area cannot readily be isolated. Furthermore, they tested at small vertical loads and contact areas that are not representative of large SUV-size vehicles. Reece (1964) also perturbed both the shear instrument geometry and contact area.

No research could be found that directly investigated the effect of the contact area. Furthermore, shear tests are typically not performed at areas representative of the contact patch area of large SUV-size vehicles. This warrants further investigation in this study.

Influence of shear velocity

Many publications exist relating to soil shear strength under quasi-static conditions. However, off-road vehicles and tillage implements work at a certain speed. Bekker (1969) states that the shear rate in vehicle applications is in the range of 25-254mm/s, which is significantly higher than quasi-static test conditions typically used. Wong (1989) and He *et al.* (2019a) state that the shear rate should preferably match the slip velocity of the vehicles running gear.

Bekker (1956) states that for saturated soil, loads exerted by a vehicle's running gear carry a considerable part of stress through the hydrostatic pressure of the enclosed pores. The influence of shear rate is then determined by the loading rate and permeability of the soil (Bekker, 1956). However, experimental testing by Bekker (1969) found the shear rate had practically no effect for three different types of saturated soils for Bevameter tests done at shear rates of 51deg/s and 1.2deg/s.

Apfelbeck *et al.* (2011) studied the effect of shear rate on shear strength using the Bevameter soil characterisation technique. Their results indicated that the shear rate has no significant effect. However, their research was in application to planetary rover mobility, where the expected shear rate is very low. Shear tests were done at 0.1, 0.2, and 0.3 RPM, corresponding to average linear velocities of 1.3mm/s to 3.9mm/s. This shear rate is very slow and is not representative of large SUV-size vehicles.

Dechao and Yuso (1991) investigated the effect of shear rate specifically in application to vehicle-terrain interaction modelling. Their results showed that the shear rate significantly influenced shear stress. Furthermore, the results indicated that at high shear rates, the results did not fit the classic straight line of the Mohr-Coulomb failure criterion. However, the study used a laboratory shear box test, which may not be representative of in situ soil behaviour.

In the field of landslide modelling, a number of studies have shown shear rate to have a significant influence on identified soil properties (Wang *et al.*, 2010; Jiang *et al.*, 2017; Li *et al.*, 2017; Wang and Cong, 2019). Depending on soil type and saturation state, the soil may exhibit rate-weakening or rate strengthening (Scaringi *et al.*, 2018). The studies mentioned all used enclosed annular ring-type shear devices that may not be applicable to in situ conditions.

The results from previous studies suggest that consensus has not been reached on the influence of shear rate on shear strength in terramechanics applications. Limited studies investigated the shear rate for Bevameter tests in the range expected for larger vehicles (25-254mm/s). The soil type and soil saturation state may also have a significant influence. This warrants further investigation in this study.

2.4.3 A detailed review of soil parameter estimation and statistical analysis methods

Several authors have mentioned the importance of the inclusion of uncertainty quantification and statistical analysis in Bevameter testing (Bekker, 1969; Stafford and Tanner, 1982; Apfelbeck *et al.*, 2009, 2011; NATO, 2021). However, as indicated in Table 2, most studies present no attempt to include uncertainty quantification. Bekker (1969) states that even in controlled laboratory conditions, soil model parameters are said to exhibit significant variation. Soil model parameters should therefore be expressed probabilistically instead of being expressed deterministically (Bekker, 1969).

Soil parameter estimation

When the Bevameter soil characterisation technique first appeared in the 1950s, simple point parameter estimation was performed. This was achieved by establishing a soil model, transferring the data and model to the log-log domain, and performing regression by eye (Bekker, 1956, 1969). Wong (1984) improved early works by introducing a weighted linear least squares approach with closed-form analytical solutions. However, Wong (1984) was still limited to linear soil models in the log domain.

More recently, Nonlinear Least-Squares (NLLSQ) regression with numeric algorithms has been applied to determine pressure-sinkage and shear stress model parameters (Apfelbeck *et al.*, 2011). The advantage of the NLLSQ approach is that it can accommodate nonlinear soil models. Statistically, the NLLSQ estimate is the minimum variance estimator for data under the assumption of a Gaussian residual distribution (Seber and Wild, 2003). The more general Maximum Likelihood (ML) regression of Fisher (1922) can accommodate other residual distributions, which in some cases can provide a better fit than NLLSQ. However, both the NLLSQ and ML methods are only point estimate approaches.

In the frequentist approach to uncertainty analysis, the benchmark for estimating parameter uncertainty for nonlinear models is the Cramer-Rao Lower Bound (CRLB) (Lin *et al.*, 2005). The CRLB, which is proportional to the inverse of the Fisher information, provides a theoretical lower bound of a minimum variance for any unbiased point estimator (Lin *et al.*, 2005). Apfelbeck *et al.* (2011) implemented a weighted nonlinear covariance estimator that follows closely from CRLB theory to estimate confidence intervals of soil parameters for Bevameter testing (Basu and Bresler, 2000). The shortcomings of this technique are that it is only an approximate inference method that is asymptotically consistent as the number of samples tends to infinity ($N \rightarrow \infty$), it linearises the model around the point estimate and assumes a Gaussian parameter distribution (Hougaard, 1988; Seber and Wild, 2003). The method cannot be guaranteed to be accurate for parameters or residuals that are not Gaussian distributed, which is typically the case for small sample sizes. Small sample sizes can always be expected for Bevameter tests, with the number of tests typically in the range of 1-10.

The Bayesian framework provides an alternative method for parameter estimation. The Bayesian parameter estimation approach expresses parameters as a probability distribution instead of point estimates. However, the multidimensional integrals required for nonlinear Bayesian regression are notoriously difficult to evaluate. The advent of increased computing power has recently made nonlinear Bayesian regression tractable through MCMC sampling methods. A significant advantage of the Bayesian sampling approach is that it can determine arbitrary and asymptotically exact parameter probability distributions (Bishop, 2006). The Bayesian MCMC approach is widely considered the "gold standard" for performing nonlinear parameter estimation (Nemeth and Fearnhead, 2019). In small sample size settings, literature frequently advocates Bayesian parameter estimation methods over frequentist methods (Rupp *et al.*, 2004; Kruschke *et al.*, 2012; He *et al.*, 2021). Furthermore, it can also

incorporate prior beliefs about parameters and allow recursive parameter updating. Recently Bayesian parameter estimation has been applied in the terramechanics field by Gallina *et al.* (2014) and Shamrao *et al.* (2018) in using the vehicle as a sensor to simultaneously estimate the soil and soil-wheel interaction model parameters. However, to the best of the author's knowledge, the approach has not been applied to estimate soil parameters purely obtained from Bevameter tests.

Other than the classic frequentist approach and the Bayesian approach, other methods exist for performing inference on nonlinear models. These methods include variational inference (popular in machine learning), the bootstrap method, Laplace's method, as well as different nonlinear covariance estimators for the frequentist approach (Azevedo-Filho and Shachter, 1994; Bishop, 2006; Reece and Nicholson, 2007). However, these methods are not considered as they are not asymptotically exact.

Formal test for statistical significance of factors that influence Bevameter tests

Bekker (1969) presented the first inclusion of formal hypothesis testing to determine if experimental factors influence Bevameter soil characterisation. He applied the statistical framework of Analysis of Covariance (ANCOVA) to determine whether plate size has a statistically significant influence on the pressure-sinkage response. ANCOVA has a distinct advantage over other statistical methods as it takes into consideration the influence of covariates and increases the statistical power (Van Breukelen, 2006). Both the Bevameter pressure-sinkage and shear stress tests vary longitudinally as a function of covariates (sinkage z and shear displacement j). A significant drawback of the ANCOVA framework, amongst other assumptions, is that the response variable must be a linear function of the covariates. Bekker (1969) was able to employ ANCOVA for pressure-sinkage tests as his data was linear in the log domain. For shear tests, Bekker presented no formal means of assessing statistical significance.

Massah and Noorolahi (2010) used the more basic Analysis of Variance framework (ANOVA) for testing the statistical significance of plate sizes for Bevameter pressure-sinkage tests. In doing so, they neglected the longitudinal variation of pressure-sinkage data, reducing the 2D data to univariate distributions. This is said to reduce statistical power (Van Breukelen, 2006). Furthermore, their results are considered doubtful as their sample size consisted of a single Bevameter test per group.

An alternative method for testing the statistical significance of longitudinal data is the repeated measures ANOVA. However, the repeated measures ANOVA in itself is considered a forerunner to more versatile regression modelling (Fitzmaurice *et al.*, 2008). Today hypothesis tests based on regression modelling have largely replaced ANOVA and ANCOVA for longitudinally varying data (Fitzmaurice *et al.*, 2008). However, in the frequentist setting, hypothesis tests are still primarily based on linear models since nonlinear and hierarchical models can be very challenging (Kruschke, 2013).

Bayesian hypothesis testing based on Bayesian regression provides an alternative solution for performing hypothesis tests for nonlinear longitudinally varying data. Recent literature indicates that the Bayesian hypothesis testing approach holds significant advantages over traditional p-value Null Hypothesis Significance Testing (NHST) (Gelman *et al.*, 2012; Kruschke, 2013; Schönbrodt *et al.*, 2017; Kruschke and Liddell, 2018; Kelter, 2020). The paper by Krushke (2013) titled "*Bayesian estimation supersedes the t-test*" indicates the current trend in literature. One of the advantages of the Bayesian approach is that, unlike the dichotomous p-value, which provides no indication of the uncertainty of a hypothesis, the Bayesian approach provides a complete probability distribution in support of either the null or alternative hypothesis (Kruschke and Liddell, 2018). Another advantage of the Bayesian approach is that hypothesis tests on multiple parameters do not require special correction measures, such as the Bonferroni correction required for the frequentist approach (Gelman *et al.*, 2012).

Sources of uncertainty in soil characterisation

Parameter estimation and Hypothesis tests deal with determining model parameters and making formal decisions in the presence of uncertainty. It is important to understand where the different sources of uncertainty arises. Figure 11 indicates the taxonomy of uncertainty in a physical system.

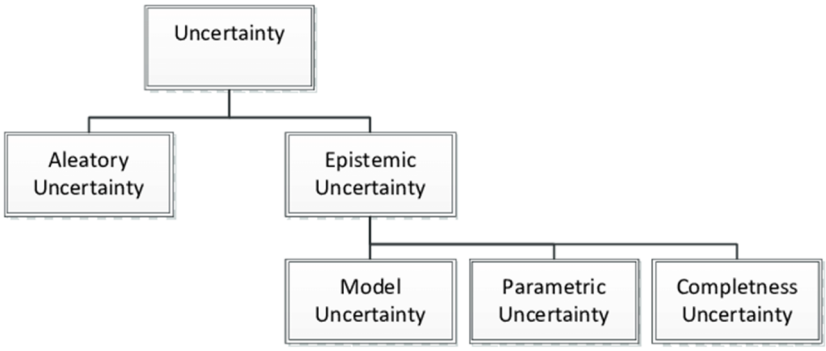

Figure 11-Taxonomy of uncertainty (Dantan *et al.*, 2013).

The total observed uncertainty of a system comes from two primary sources: Aleatory uncertainty and Epistemic uncertainty. Aleatory uncertainty is the inherent variance of the physical processes (Dantan *et al.*, 2013). It is irreducible and is represented by random variables in the modelling process. In application to Bevameter tests, aleatory uncertainty arises due to the natural variation of soil strength properties. Soil is a complex multiphase material made up of solids, liquids and gases, with the solid part made up of an ensemble of granular particles. The random distribution of solid particles, liquids and gases gives rise to variations in soil strength properties. In situ soil strength is even more complex, with the soil composition, density, and moisture varying spatially between locations and depths. This non-homogeneity gives rise to random variation in soil strength even under ideal conditions.

On the other hand, epistemic uncertainty arises due to a lack of knowledge of the physical system (Dantan *et al.*, 2013). There are three contributors to epistemic uncertainty. The first is model uncertainty, which arises due to assumptions on the form of the model and simplifications of the physical system. The second is parametric uncertainty, which arises due to a lack of data (we only have a limited number of data points and assume the form of the parameter distribution). Finally, completeness uncertainty is caused by the uncertainty of the analysis completion (e.g. have all possible solutions been considered?). Epistemic uncertainties can be reduced by an increased understanding of the problem and by collecting more data (Dantan *et al.*, 2013).

Bevameter soil characterisation has both large aleatory uncertainty (e.g. natural variation in situ soil strength properties, as pointed out by Bekker (1969)) and epistemic uncertainty (e.g. models based on Bevameter data perform poorly in predicting vehicle traction, as pointed out by Chang and Baker (1973)). These uncertainties cannot be neglected and need to be quantified using probabilistic methods.

Summary of parameter estimation and statistical analysis methods

Literature indicates that Bevameter soil parameter estimation has long indicated a need to move away from simple point estimates and towards a probabilistic approach. Existing methods only provide approximate inference and may be inaccurate for small sample sizes associated with Bevameter tests. Bayesian parameter estimation via MCMC presents the next logical step toward moving to a more rigorous and robust uncertainty analysis approach for the small sample sizes associated with Bevameter tests. Regarding tests for statistical significance, formal hypothesis testing has been applied in Bevameter soil characterisation using the ANCOVA framework and the ANOVA framework;

however, these methods require restrictive assumptions. For data with covariates, literature has moved away from these methods and towards a regression-based approach. Bayesian regression combined with Bayesian hypothesis testing is proposed as a means for formal statistical significance testing for nonlinear data with covariates. This approach makes no assumptions about the form of the model or the parameter probability distributions.

2.5 Chapter summary

The literature study confirmed that the Bevameter soil characterisation is the most applicable soil characterisation method in the terramechanics field, with the majority of terrain-vehicle models specifically requiring Bevameter soil characterisation. The literature study also covered the necessary background on fundamental aspects required to perform Bevameter soil characterisation. The fundamental aspects ranged from the equipment required, to empirical soil models employed, to special drag shear corrections methods and finally, soil preparation procedures for repeated testing.

From reviewing the state of the art on experimental Bevameter investigations, it is clear that limited emphasis has been placed on two specific aspects of Bevameter testing. They are ***factors that influence Bevameter shear stress tests*** and the inclusion of ***uncertainty quantification.***

More specifically, the following three factors that influence shear stress were identified as the most prominent and least investigated: 1) shear mechanism, 2) shear contact area, and 3) shear velocity. All three factors present novel research opportunities that have not been explicitly investigated by previous studies. Differences in the measured shear stress at the soil characterisation level may have a profound effect on terramechanics models that rely on the equilibrium of shear and normal stress.

Given the known stochastic nature of in situ soil strength characterisation, the widespread disregard for uncertainty quantification is concerning. Although literature has long indicated a need to move away from simple point parameter estimation and towards a probabilistic approach, this has not been realised or only in a limited capacity. Bayesian parameter estimation presents the next logical step toward moving to a more robust parameter estimation approach. Nonlinear regression-based hypothesis testing was identified as the most appropriate method for statistical significance testing.

The literature study presented a refinement of the original research question: ”If and to what extent do experimental test setup factors influence Bevameter soil characterisation”. This has been refined to factors that affect Bevameter shear tests. In order to answer this question in a rational manner for a stochastic process like in situ soil characterisation requires probabilistic data analysis.

CHAPTER 3

Bevameter Hardware and Soil Bin Setup

"Give me six hours to chop down a tree I will spend the first four sharpening the axe."

-Abraham Lincoln[3]

[3] Brainy Quote (2022), *Abraham Lincoln Quotes*. Available at: https://www.brainyquote.com/authors/abraham-lincoln-quotes (Accessed: 5 Jan 2022).

3. Bevameter Hardware and Soil Bin Setup

3.1 Preamble

Research objective one (1) of this study is to develop a new Bevameter device and accompanying infrastructure to enable the study of factors that affect Bevameter soil characterisation. A description of the hardware developed to address this research objective is presented in this chapter.

3.2 Preliminary considerations-matching the Bevameter to target vehicle

From the literature study, it was established that Bevameter soil characterisation is tightly coupled to the specific vehicle application. Specifically, Bevameter tests should be conducted at contact areas and loads comparable to the running gear of the target vehicle (Bekker, 1969; He *et al.*, 2020). However, from Table 2 it was observed that most studies do not indicate how the Bevameter equipment matches the target vehicle. This study will provide clear information about how this was achieved.

3.2.1 Target vehicle platform

The target application of this research is agriculture vehicles. However, access to an agricultural test vehicle was not available at the Vehicle Dynamics Group (VDG) at the University of Pretoria. It is proposed to use a smaller SUV-size vehicle equipped with agricultural tyres as a surrogate for an agricultural vehicle. Previous collaboration between the VDG and the Advanced Vehicle Dynamics Laboratory (AVDL) at Virginia Polytechnic Institute and State University have agreed to use the instrumented vehicle at the VDG as the target vehicle platform for terramechanics research (Naranjo *et al.*, 2014). Therefore, the Bevameter was designed around this vehicle. The test vehicle and accompanying agricultural tyre are indicated in Figure 12.

Figure 12-Target vehicle platform fitted with Trelleborg TM700-280/70R16 agricultural tyres (Becker, 2022).

The test vehicle is a 1997 model Landrover Defender 110. The vehicle is equipped with the Trelleborg TM700-280/70R16 tyre. The tyre selection is justified by the following points: 1) it is a true agriculture tyre intended for agriculture harvesting machines and, therefore, applicable to the agricultural use case (Trelleborg, 2021), 2) prior research has been conducted on the ground pressure of this specific tyre.

3.2.2 Estimating the wheel ground pressures and contact area

Determining the ground pressure and contact area exerted by a tyre on soft terrain is a challenging problem. The problem is complicated by the fact that the tyre soil contact patch area varies with wheel sinkage. The tyre deformation and soil deformation form a coupled system that both need to be taken into account. Predicting the sinkage and tyre contact pressure requires a full 3-Dimensional flexible tyre model, such as the hybrid soft soil model developed by Sandu *et al.* (2019b). However, such a model requires extensive experimental verification that makes it unsuitable for a first-order estimate.

Wong (2010) suggests using the hard terrain ground contact area and pressure as a first-order estimate for average ground pressure on soft soil. Prior research at the VDG investigated the contact area and contact pressure of the target vehicle fitted with the Trelleborg TM700-280/70R16 tyre on hard terrain (Becker, 2022). Figure 13 indicates the contact area and average ground pressure for the Trelleborg TM700-280/70R16 tyre at different thread lengths. The contact area was determined with the paint transfer method and ground pressure with the Tekscan 8001 transducer (Tekscan, 2022).

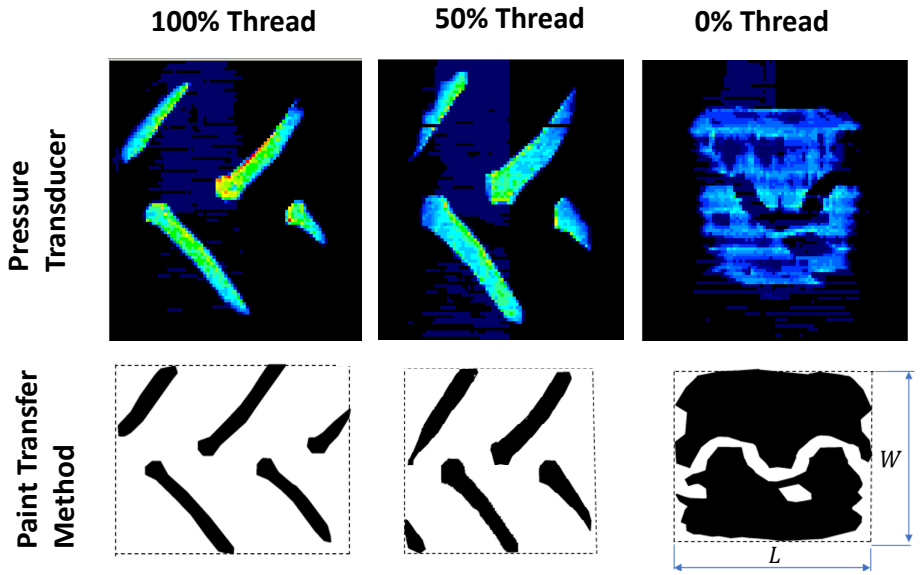

Figure 13-Methods used to determine the hard terrain contact pressure and area of the Trelleborg TM700 tyre (Becker, 2022).

The quantitative results of the contact area and pressures are indicated in Table 3.

Table 3-Trelleborg TM700 hard terrain contact area and pressures (Becker, 2022).

	Contact Area [cm²]		**Contact Pressure [kPa]**		**Nominal Contact Area [cm²]**		**Nominal Contact Pressure [kPa]**	
Tyre Inflation Pressure/ Thread	200 kPa	80 kPa	200 kPa	80 kPa	200 kPa	80 kPa	200 kPa	80 kPa
30mm (100%)	85	119	669	476	564	720	101	79
15mm (50%)	86	115	657	492	450	663	126	86
0mm (0%)	210	360	270	157	297	**583**	191	**97**

Note: The nominal contact area is calculated from length L and width W indicated in Figure 13. Vertical load is 5.68kN.

From Table 3, it is evident that even on hard surfaces, the ground contact area and ground pressure vary significantly based on inflation pressure, tread length and the definition of the contact area. The measured areas range from 85cm² to 720cm², and ground pressures from 79 to 669 kPa. The situation is complicated further when the soil deformation is taken into account. Current standards do not indicate how the ground contact area and pressure should be determined (SAE, 1967; He *et al.*, 2020).

It is proposed to use the nominal contact area of the 0mm tread condition to match the running gear contact area to the Bevameter contact area. The smooth tyre area is postulated to be the closest representation of the ground contact area on soft soil as the lugs are expected to sink into soft soil until the tyre carcass contacts the soil surface. The nominal area is used instead of the contact patch area because the contact patch area is influenced by small tyre deflections that are not expected to be consequential for soft soil application, for example, the S-shape curve in Figure 13. The 80kPa tyre inflation pressure is selected as it is the recommended inflation pressure for tyre loads of up to 680kg (Trelleborg, 2021). The following values are used for matching the Bevameter to the target vehicle,

- Nominal tyre contact area: 583cm^2
- Nominal vehicle ground pressure: 97kPa

The estimated ground pressure corresponds with the soil-tyre interface pressures of large agricultural vehicles. Raper *et al.* (1995) experimentally measured the soil-tyre interface pressure of a tractor tyre in tilled soil conditions to be in the range of 80-120kPa. For an SUV-size vehicle, Shoop (1993b) also experimentally determined the hard terrain ground pressures to be in the range of 92-152kPa.

3.2.3 Estimating Bevameter loads

Estimating the vertical load

The vertical load was estimated by matching the Bevameter vertical load to the target vehicle's maximum vertical wheel load. The estimated vertical load was selected to be 6.5kN for both pressure-sinkage and shear stress tests which is a conservative 30% higher than the maximum force exerted by a single wheel of the target vehicle under static conditions. 6.5kN also corresponds with the pressure-sinkage and shear stress test vertical load recommended by Golob (1981), in correspondence with Dr. M.G. Bekker, for use in the design of a Bevameter for SUV-size vehicles.

In retrospect, the estimation under-predicted the pressure-sinkage test requirements. It is known that horizontal loads reduce the ability of soils to support vertical loads (Reece, 1964). This implies that significantly larger pure vertical loads are required to reach the same depth as the dynamic wheel sinkage depth, which undergoes combined vertical and horizontal loads. Dynamic wheel sinkage may be up to 6 times more than static wheel sinkage (Ding *et al.*, 2014). The Bevameter was retrospectively modified to accommodate up to 15kN. This was still found to be inadequate for pressure-sinkage tests at the full contact patch area for intermediate-density soils. However, 15kN is still higher than the majority of Bevameter equipment from Table 2, with Bekker (1969) and Salman *et al.* (2020) being the exception. Future studies that develop new Bevameter equipment are advised to consider the effect of combined loading. Bevamters should be designed for much larger vertical loads than the target vehicle can exert.

Estimating the shear load

The Mohr-Coulomb failure criteria, indicated by equation (4), indicate that the maximum shear stress is dependent on three factors: the applied normal stress σ, the soil internal friction angle ϕ and the soil cohesion c. However, internal friction angles and cohesion are known to vary significantly and are dependent on many factors. Examples of factors that influence the Mohr-Coulomb parameters are: 1) soil grain size, 2) soil composition, 3) moisture content, 4) bulk density, and 5) particle shape/angularity. Due to the considerable variation of soil types and their associated shear strength, a probabilistic approach was used to estimate the upper bound for design purposes. In general, the peak shear stress for soils goes down as the clay content increases (Carter and Bentley, 2016). Therefore, primarily cohesionless (low or no clay content) soils were considered as they are expected

to result in the worst-case design load. A large sample of shear test data was found to be scarce for Bevameter tests; therefore, the more readily available data from the enclosed annular shear ring test was used. Figure 14 indicates the distribution of shear stress to normal stress for a range of 33 different soils and soil compaction states. The sources used to generate Figure 14 are indicated in Appendix A.

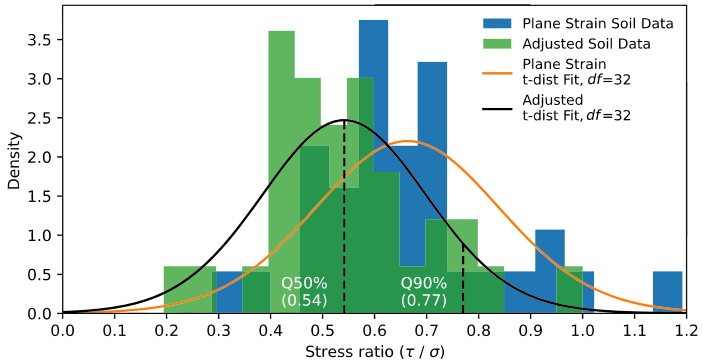

Figure 14-Distribution of soil shear stress ratio for a range of cohesionless soils.

Figure 14 indicates two shear stress ratio distributions: one is for the plane strain data, and one is for an adjusted distribution. It is known that the plane strain condition of the enclosed annular shear ring device results in a larger angle of internal friction ϕ than triaxle and in situ tests (Al-Khafaji, Amir Wadi; Andersland, 1992). This is because of the reduced freedom of movement of adjacent particles that results in greater interparticle locking. Al-Khafaji, Amir Wad and Andersland (1992) state that a friction angle increase of 2 to 4 degrees is expected in loose soils and 4 to 9 degrees in dense soils due to the plane strain condition. Therefore, the data is compensated by a median friction angle of 3 degrees for loose soils and 6.5 degrees for dense soils to account for the plain strain condition.

For the Bevameter structure and actuators, the 90th percentile ($\tau/\sigma = 0.77$) of the adjusted soil shear stress ratio was used as a reasonable estimate of the maximum expected shear load. For load cell design, the 50th percentile ($\tau/\sigma = 0.54$), or most probable value, was used. The maximum shear load F_x is then calculated according to equation (11). The result of the shear force calculation is indicated in Table 4 alongside other Bevameter specifications.

$$F_x = F_z(\tau/\sigma) \tag{11}$$

Estimating the torsion load

The torque of an annular shear ring in contact with soil is given by equation (12) (Okello, 1991; Apfelbeck *et al.*, 2011; Lin *et al.*, 2018).

$$T = \frac{2}{3}\pi\tau(\sigma)(r_o^3 - r_i^3) \tag{12}$$

Where r_o is the outside radius of the annular ring, r_i the inside radius and $\tau(\sigma)$ indicates the shear stress as a function of normal stress. For the $\tau(\sigma)$ term, the Mohr-Coulomb soil failure theory from equation (4) is employed. For cohesionless soils, the cohesion term c in the Mohr-Coulomb model is zero and the shear stress is only determined by the internal friction angle ϕ and normal stress.

The SAE J939 (SAE, 1967) standard recommends an annular ring with an outside diameter of 185.4mm and an inside diameter of 133.4mm for torsional Bevameter shear tests. This corresponds to an area of 129cm^2 with an aspect ratio of 0.719 (ID/OD). For this study, we would like to investigate areas up to the full tyre contact patch area of 583cm^2. At this area and aspect ratio, the outside diameter is 388mm. The resulting Bevameter torque, according to equation (12) , is indicated in Table 4.

3.3 Bevameter hardware

3.3.1 Mechanical design and operating principle

A new Bevameter was designed and commissioned for this study. The developed Bevameter aimed to address the shortcomings of equipment encountered in the literature. The most prominent shortcoming identified is that existing equipment is tailored to either performing translational or torsional shear tests, and is not capable of both. Furthermore, small-scale equipment is typically employed that is not capable of executing shear tests at the full tyre contact patch areas of full-size off-road vehicles. The developed Bevameter, depicted in Figure 15, aimed to address these shortcomings.

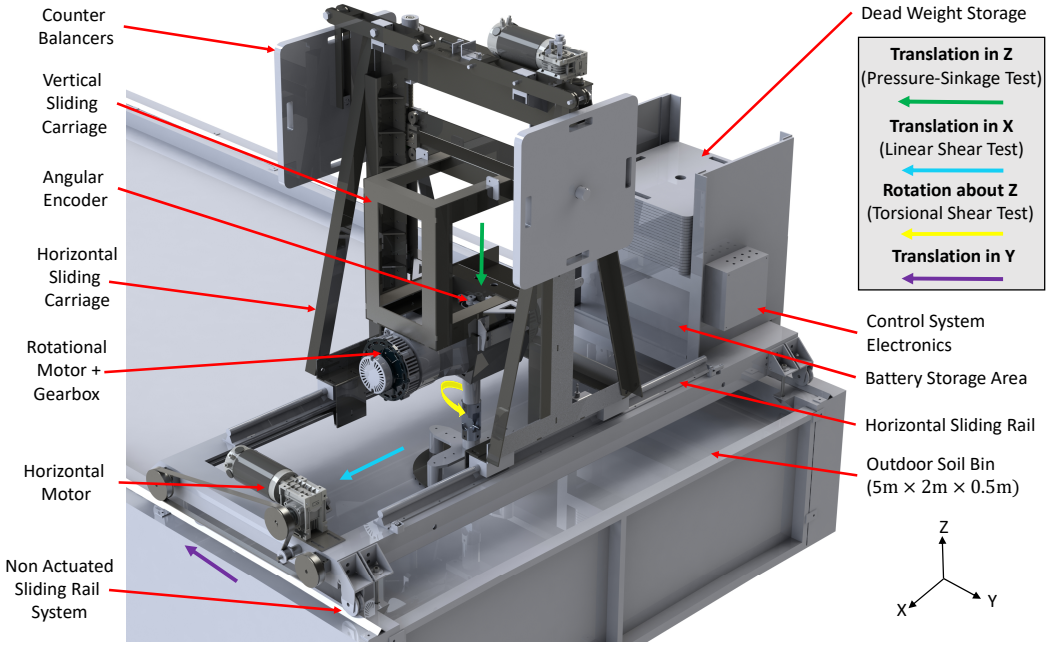

(a)

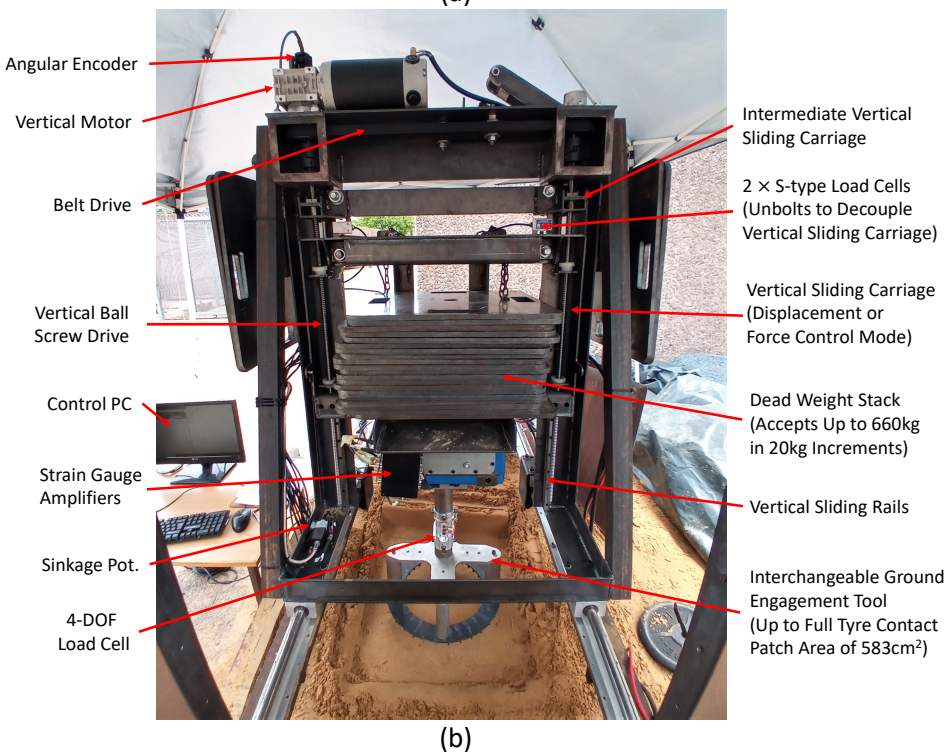

(b)

Figure 15-Bevameter hardware (a) Isometric view of computer-aided design. (b) Manufactured Bevameter on soil bin.

The developed Bevameter presents a self-contained in situ soil testing unit with onboard power sources, instrumentation and data recording equipment. For this study, the Bevameter is deployed on a dedicated outdoor soil bin for laboratory-style testing. However, field application is also possible. The Bevameter can perform three types of in situ soil characterisation tests. They are: 1) pressure-sinkage tests, 2) linear (longitudinal) shear tests, and 3) torsional shear tests. For pressure-sinkage tests, the Bevameter acts in displacement control mode with the vertical sliding carriage coupled to the displacement-actuated intermediate sliding carriage. For linear and torsional shear tests, the vertical sliding carriage is decoupled from the intermediate sliding carriage and can freely translate in the vertical direction. Vertical load control is then applied through the use of dead weights.

The Bevameter technical specifications are indicated in Table 4.

Table 4-Bevameter technical specifications.

Specification	Value
Normal force (displacement control) [kN]	15
Normal force (force control) [kN]	6.5
Shear force [kN]	3.5
Torque [Nm]	630
Vertical velocity [mm/s]	16
Horizontal velocity [mm/s]	20
Torsional shear velocity [mm/s, RPM]	600 (50)
Vertical travel [mm]	400
Horizontal travel [mm]	850
Overall dimensions (Height, Width, Length)[mm]	1200, 1480, 2230
Total gross mass [kg]	1020

3.3.2 Custom four degree of freedom (4 DOF) load cell

The Bevameter's primary means of force measurement is the custom 4 DOF load cell detailed in Figure 16. The load cell measures the vertical force F_z (for pressure-sinkage tests), shear force F_x (for linear shear tests) , Torsion M_z (for torsional shear tests) and bending M_y (for cross-coupling support). The unique design employs a shear web to directly measures shear strain. The strategic configuration of the strain gauges isolates the individual channels from cross-coupling with the remaining 5 DOF (except for channel M_y). The transducer shape was optimised through Finite Element (FE) modelling and numerical optimization to maximise strain sensitivity. The specifications of the load cell are listed in Table 5. For detail on the Strain Gauge (SG) configuration and load cell development, see Appendix B.

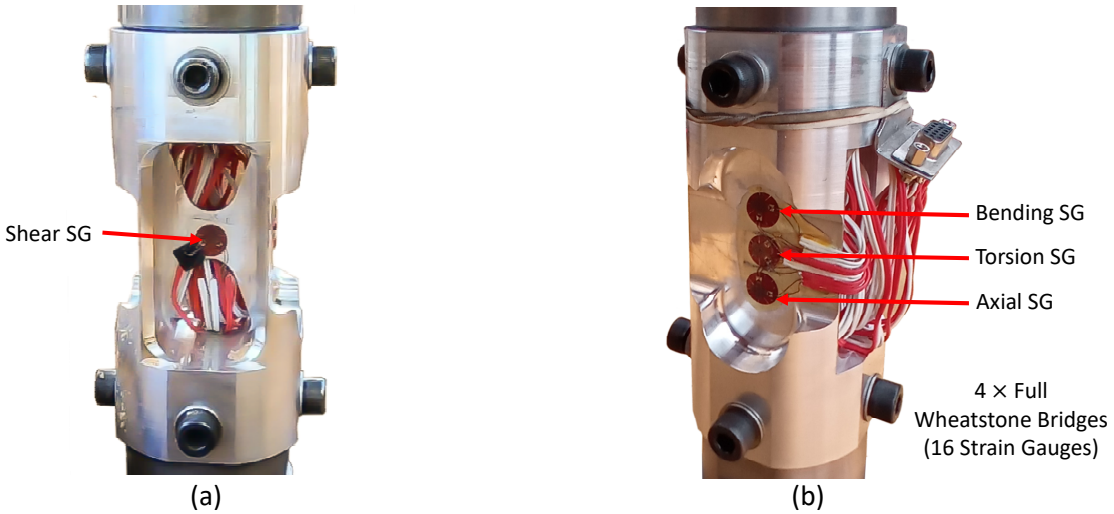

Figure 16-Custom 4 DOF load cell detail (a) Side view. (b) Isometric view.

3.3.3 Control system, data logging and signal processing

A high-level overview of the Bevameter control system and data logging scheme is indicated in Figure 17. The control system implements a Proportional Integral (PI) velocity control with an additional Feed Forward (FF) term to control the actuators. The closed-loop velocity control is implemented on a microcontroller (programmed in C++) which receives a velocity tracking signal from a control PC running a custom Graphical User Interface (GUI) (programmed in Python). The control system gains are tuned heuristically for each axis. A separate data logger records all sensor data (all analogue signals) at 1000Hz. For more detail on the control system and associated hardware, see Appendix C.

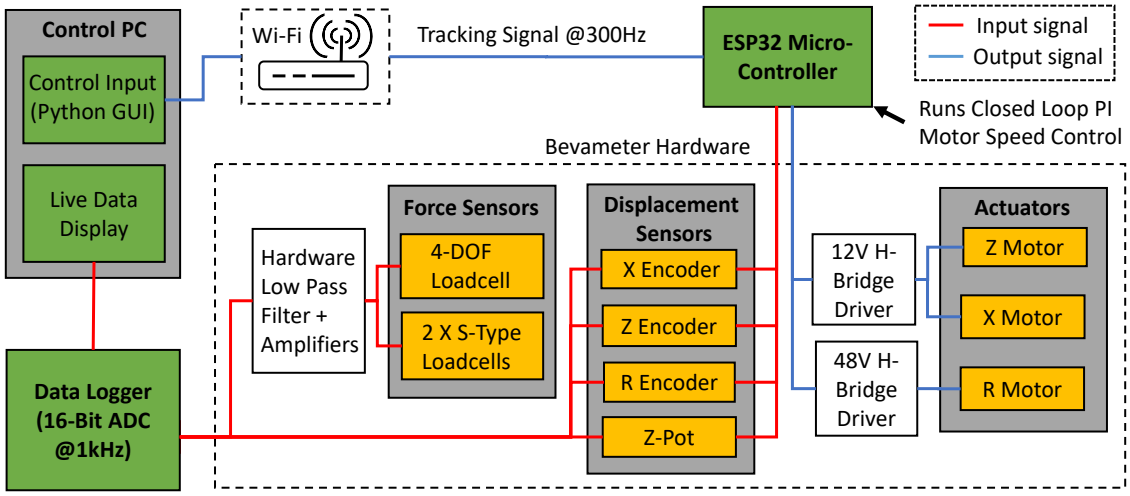

Figure 17-High-level overview of the Bevameter control system and data logging scheme.

The specifications of the sensors employed in Figure 17 are indicated in Table 5.

Table 5-Bevameter sensor specifications.

Sensor	Channel	Specifications	Application
4 DOF Load cell	1-4	F_x: 3500N, 5.41mV/V F_z: 15000N, 0.47mV/V M_y: 1332Nm, 2.01mV/V M_z: 630Nm, 7.56mV/V	-F_x: Linear shear force -F_z: Pressure-sinkage -M_y: Cross-coupling cancellation -M_z: Rotational shear torque
2 × S-type load cells	5-6	NS1-500kg, 2mV/V (Mavin, 2020)	-Weighing of Z-carriage for shear test -Pressure-sinkage tests
3× Rotary Encoders	7-8,11	AS5600, 12-bit (4096 increment) absolute rotary encoder (AMS, 2018)	-Rotational shear displacement -Vertical displacement(Pressure-sinkage) -Horizontal displacement -Actuator velocity control on X, Z, R axis's
Drawstring Potentiometer	9	SP1-25, 0-625mm travel Pot. (TE Connectivity, 2015)	-Shear sinkage measurement
Total	10		

The sensor data is filtered at both a hardware level and digitally during post-processing. Channels 1-6, corresponding to the force measurement channels, incorporate hardware-level active low pass filters set to 256Hz for anti-aliasing purposes. During post-processing, the data is filtered by transferring the data to the frequency domain using the Fast Fourier Transform (FFT), removing unwanted frequencies and is then converted back to the time domain. This ensures that the cut-off frequencies are exact and exhibit no phase shift. Channels 1-6 are low pass filtered at 256Hz and band-stop filtered in the range of 48-52Hz. Channels 7-11, corresponding to displacement encoders, are low pass filtered at 25Hz. The aggressive filtering on displacement is warranted, considering dynamics of

interest at higher frequencies are not of importance in this study. In order to calculate velocity, the absolute displacements of channels 7-11 require numerical derivation; this derivation significantly amplifies noise. Therefore, the velocity is further low pass filtered with a 3Hz cut-off.

3.3.4 Ground engagement tools

The Bevameter ground engagement tools used in this study are indicated in Figure 18. The detailed specifications of the ground engagement tools are indicated in Table 6.

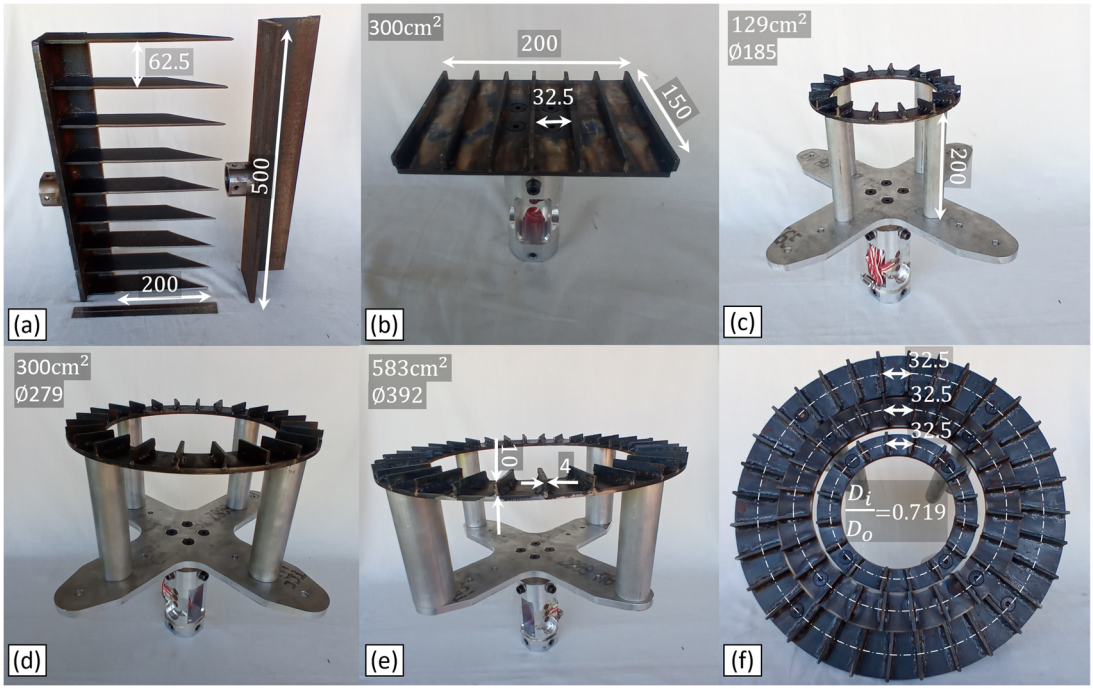

Figure 18-Bevameter ground engagement tools. (a) Left: Tool 01, Right: Tool 02. (b) Tool 03. (c) Tool 04. (d) Tool 05. (e) Tool 06. (f) Size comparison of Tools 04-06.

Table 6-Bevameter attachment tool specifications.

Tool	Area[cm²]	Dimensions [mm]	Mean Grouser/Tine spacing [mm]	Number of Grousers	Grouser /Tine height[mm]
01	-	$W = 500$	62.5	9	200
02	-	$H = 100, W = 500$	-	-	-
03	300	$L = 150 \times W = 200$	32.5	7	10
04[a]	129	$D_0 = 185, D_i/D_0$ =0.719	32.5	16	10
05	300	$D_0 = 279, D_0/D_i$ =0.719	32.5	24	10
06	583	$D_0 = 392, D_0/D_i$ =0.719	32.5	32	10
07[b]	176	D_0 =150	-	-	-

Note: [a]SAE J939 recommended rotational shear tool. [b]Pressure-sinkage tool is not indicated in Figure 18.

For all ground engagement tools, a grouser height of 10mm was selected to ensure the soil fails in the soil plane but is kept relatively small so that the grouser lateral drag and other grouser effects do not overwhelm other factors of interest, such as the contact area. All shear instruments, regardless of size or shear mechanism, employed a mean grouser spacing of 32.5mm. The grouser spacing was selected based on work by Rowland (1972, cited in Muro and O'Brien, 2005) that showed optimal grouser spacing for maximum traction occurs at a spacing-to-height ratio in the range of 3-4. The SAE J939 (SAE, 1967) recommendation of matching the grouser spacing to the tyre lug spacing was not practical and would result in excessive grouser spacing (see Figure 12). All the torsional shear instruments in Table 6 follow the aspect ratio of the shear annulus recommended by the SAE J939 standard.

3.3.5 Calibration of equipment

With the detail of Bevameter hardware covered, the next step is the calibration of said equipment. The calibration is necessary as all the force transducers employ empirical models that relate forces to measured voltages. The calibration also serves to instil confidence in the experimental equipment.

S-Type load cell calibration

The calibration of the single degree of freedom S-type load cells is straightforward and done with the application of calibrated weights. The results from the calibration are indicated in Appendix C.

4 DOF load cell calibration

In contrast to the single DOF load cells, the calibration of the 4 DOF load cell is not trivial. It is said that all multi-degree of freedom load cells suffer from cross-coupling to a certain extent (Chao and Chen, 1997). Intelligent mechanical design, such as employed in this case, may theoretically eliminate cross-coupling, but in reality, it is never zero. Using pure loads to calibrate the 4 DOF load cell is not a viable option as the effects of cross-coupling cannot be quantified. The calibration strategy employed is to apply combined loads (e.g. applying bending and shear force simultaneously) and make use of an empirical multi-input multi-output model with multivariate regression to isolate the individual forces.

The 4 DOF load cell is modelled as a linear multi-input multi-output system,

$$\underset{(n\times k)}{\begin{bmatrix} O_{11} & \dots & O_{1k} \\ \vdots & \ddots & \vdots \\ O_{nk} & \dots & O_{nk} \end{bmatrix}} = \underset{(n\times k)}{\begin{bmatrix} F_{11} & \cdots & F_{1k} \\ \vdots & \ddots & \vdots \\ F_{nk} & \dots & F_{nk} \end{bmatrix}} \underset{(k\times k)}{\begin{bmatrix} C_{11} & \dots & C_{1k} \\ \vdots & \ddots & \vdots \\ C_{nk} & \dots & C_{nk} \end{bmatrix}} + \underset{(n\times k)}{\begin{bmatrix} B_{11} & \dots & B_{1k} \\ \vdots & \ddots & \vdots \\ B_{nk} & \dots & B_{nk} \end{bmatrix}} \tag{13}$$

in matrix form, equation (14) becomes,

$$[O] = [\mathrm{C}][\mathrm{F}] + [\mathrm{B}] \tag{14}$$

Where:
$[O] - \text{Wheatstone Bridge Output matrix [mV]}$
$[C] - \text{Calibration matrix [mV/N] or [mV/Nm]}$
$[F] - \text{Applied load matrix [N or Nm]}$
$[B] - \text{Offest matrix } [mV]$
$n - \text{Number of measurements}$
$k - \text{Load cell degree of freedom}$

The diagonal terms C_{11} to C_{kk} of the calibration matrix account for the direct effect on corresponding input channels to corresponding output channels. The off-diagonal terms account for possible cross-coupling between channel inputs and outputs. The closed-form estimate of $[C]$ is given by $[\hat{C}]$,

$$[\hat{C}] = \left([O']^{\mathrm{T}}[O']\right)^{-1}[O']^{T}[F] \tag{15}$$

Where $[O']$ is the output voltage with the offset removed.

$$[O'] = [O] - [\hat{B}] \tag{16}$$

The offset matrix $[B]$ is excluded from the initial calibration. This is done because temperature and other factors may affect the Wheatstone bridge offset and drift over time. In order to compensate for these effects, the load cell offset voltage $[B]$ is removed before each and every measurement.

Finally, the inverse of equation (14) is used for force reconstruction. The forces $[\hat{F}]$ predicted by the load cell voltage matrix $[O']$ is then given by,

$$[\hat{F}] = [\hat{C}]^{-1}[O']^{T} \tag{17}$$

Experimental setup for the 4 DOF load cell calibration

The experimental setup used to calibrate the empirical model is indicated in Figure 19. The setup consisted of a calibrated reference load cell in line with a spring and a ratchet chain drive (not shown) to provide displacement control. In this case, the use of dead weights was impractical and would require the application of weights up to 500kg. The load application direction was measured with a precision digital level with conservative estimation placing the applied load direction accurate to 0.1 degrees.

(a) (b)

Figure 19-Experimental setup used for load cell calibration. (a) Torque calibration. (b) Vertical force calibration.

The calibration loads applied are indicated in Table 7. To accurately determine the diagonal terms, large loads were applied in the principal direction with small loads in other directions. In order to accurately determine the off-diagonal terms, combined loads of intermediate magnitude were applied.

Table 7-Load cell calibration load cases.

Load case	Load Description	F_x [N]	F_y [N]	M_y [Nm]	M_z [Nm]
1	Large shear + small bending	3000	0	300	0
2	Large bending + small shear	1000	0	600	0
3	Shear + bending + torsion	600	0	300	250
4	Pure torsion	0	0	0	425
5	Pure vertical	0	4800	0	0
6	Large vertical +small bending	0	1400	80	0

Note: Only maximum applied loads are indicated. A minimum of 6 load increments per load case was applied.

Calibration results

The calibration matrix from the theoretical FE model (detailed in Appendix B) and the experimentally determined empirical model are indicated in Figure 20 (a) and (b), respectively. As standard practice, the calibration matrix is indicated in mean effective strain per unit design load (Chao and Chen, 1997). For converting the units of the $[\hat{C}]$ from $[\mathrm{mv/N}, \mathrm{mv/Nm}]$ to $[\mu\epsilon/\mathrm{N}, \mu\epsilon/\mathrm{Nm}]$, see Appendix C.

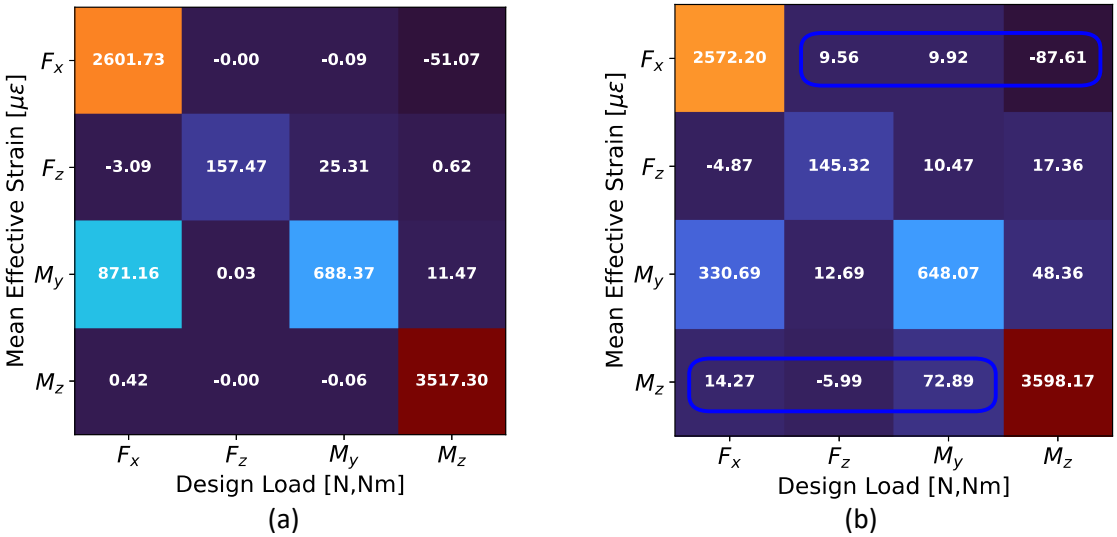

Figure 20-Load cell calibration matrix. (a) Finite Element model. (b) Empirical model.

Figure 20 indicates a strong agreement between the predicted strains from the theoretical FE model and experimental calibration. Note that the two primary channels of interest, channels F_x and M_z, which are used for the shear stress measurements, exhibit no significant cross-coupling with diagonal terms that are two orders of magnitude larger than the off-diagonal terms.

Figure 21 indicates the calibration data and the empirical model fit.

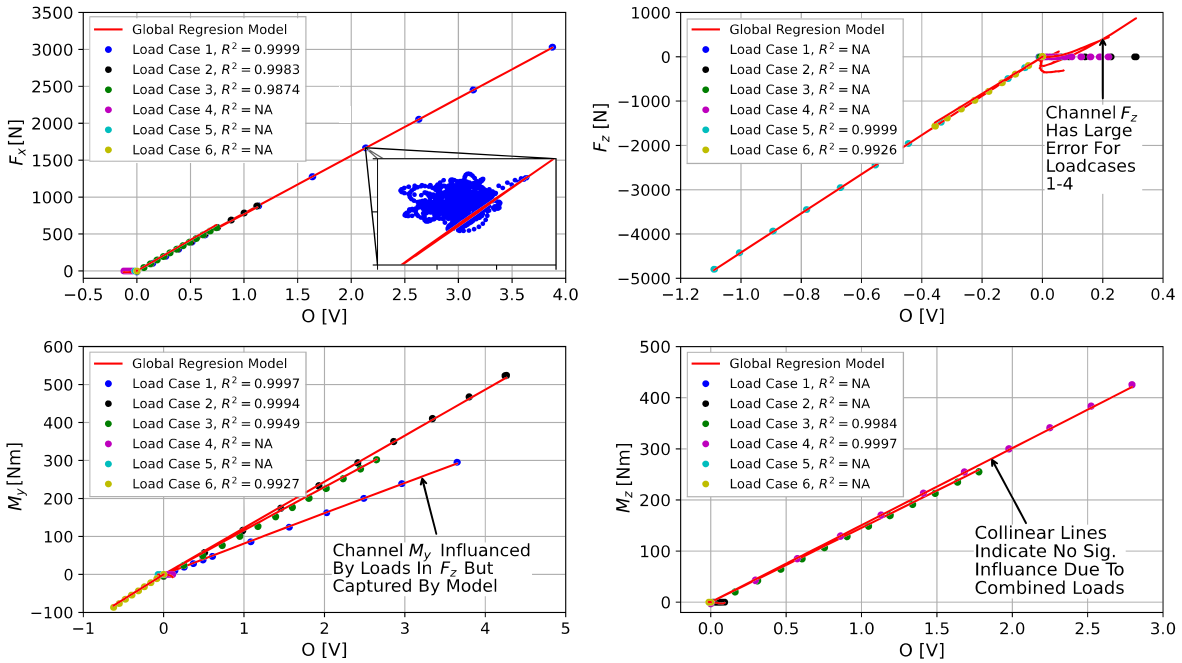

Note: NA indicates the coefficient of determination R^2 is not applicable. The denominator in the coefficient of determination is zero due to no applied loads for the specific direction and load case.

Figure 21-Load cell calibration data and empirical model fit.

Figure 22 indicates the error distribution of the model. The maximum error for all channels (except channel F_z) is less than 1.9%, even under severe combined loading conditions. Channel F_z exhibits up to 18.1% error under combined loads but less than 1.8% for pure loads. This was expected as the vertical force sensitivity is necessarily weak due to the cross-section area required to resist the large shear forces. For vertical force measurement (F_z), the S-type load cells from Figure 15 (b) are utilised.

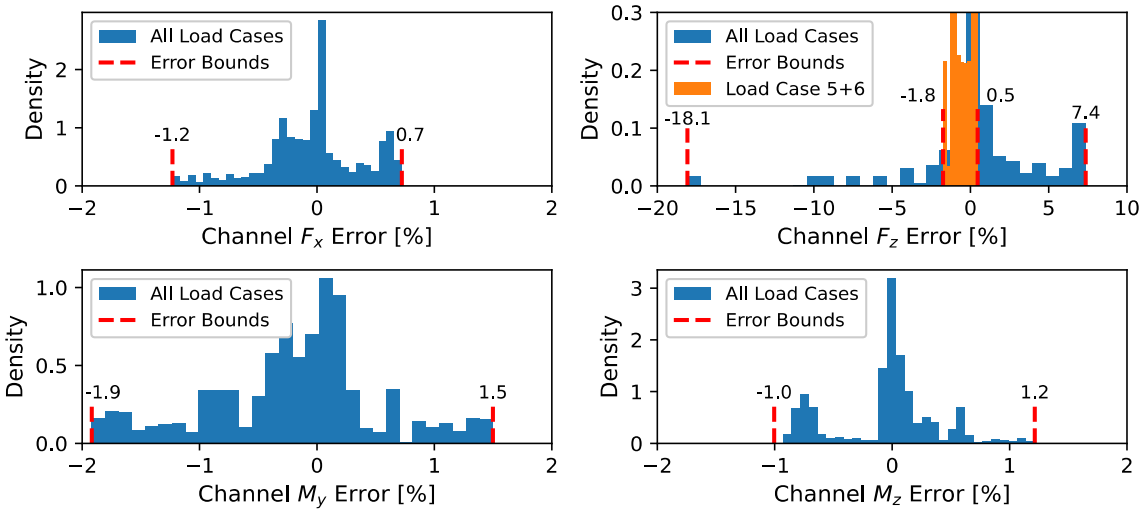

Figure 22-Residual plot for the 4 DOF load cell under combined loading conditions.

This section concludes the detail on all the Bevameter hardware. We may now proceed to the soil selection and soil bin setup.

3.4 Soil selection and soil bin setup

3.4.1 Soil selection

Considering the application of this study, it would be ideal to conduct the experimental investigation using soil with a texture classification that is representative of agricultural soil. It is generally agreed upon that loam soil (50% sand, 20% silt, 30% clay) is the best agricultural soil (Abdulazeez, 2017). Finding a source of a large homogenous quantity of soil of this composition is challenging. The difficulties include finding an excavation site, matching the desired composition, finding a method to sieve approximately 8000kg of excavated soil from larger particles and ensuring homogeneity. An alternative option is to engineer artificial soil using professionally graded materials with the desired composition and characteristics. However, the logistics of sourcing and mixing in large quantities of graded sand, silt and clay were not practical for a large outdoor soil bin. Finally, the inclusion of clay also makes it hard to control the moisture content because of the low water permeability.

For the reasons mentioned above, sandy soil was selected for this study. The selection of sandy soils is common practice for laboratory Bevameter investigations (Bekker, 1969; Van *et al.*, 2008). Van *et al.* (2008) state that this is because sandy soil produces repeatable soil conditions. This is corroborated by Bekker (1969), who states that dry cohesionless soils exhibit less variance for laboratory tests than other types of soil. Sandy soil is also said to be the easiest soil to prepare consistently (Bekker, 1969).

The specific soil selected is a fine sand with the colloquial name of Cullinan sand. This particular sand is selected to liaison with previous research done at the Civil Engineering department at the University of Pretoria. Cullinan sand is the standardised soil for engineering soil strength research and centrifuge testing at the University of Pretoria (Archer and Heymann, 2015). The sand originates from the

Cullinan area, a region located 45km east of the University of Pretoria. During preparation, the sand is washed, baked and graded by the supplier. The existing supply of Cullinan sand at the University of Pretoria was not available in adequate quantity for the construction of a large new soil bin; therefore, new soil was acquired from the supplier for this study.

It was decided to test the soil in a partially saturated state. It is expected that the inclusion of moisture is more representative of natural soils encountered by vehicles in the field than completely dry soil. It is also postulated that the inclusion of moisture will exhibit a shear rate effect through the activation of pore pressure. Furthermore, the inclusion of moisture has other benefits, such as facilitating compaction (Craig, 2002). However, a downside of the inclusion of moisture is that it adds complexity to the study as it introduces an additional variable that needs to be measured and controlled. The target moisture content was selected based on the SANS 3001-GR30:2015 (SANS, 2015) modified Proctor test for optimal compaction density (see Appendix E for more detail).

3.4.2 Soil characterisation

Due to a new batch of soil being sourced, thorough soil characterisation was performed using standardised test procedures. The selected soil's engineering characteristics and other important metrics essential to the study of mechanical soil strength are indicated in Table 8.

Table 8-Soil properties.

Soil Property	Value	Standard/Reference
Specific gravity λ [kg/m^3.]	2651	SANS 5844:2006 (SANS, 2006)
Maximum dry density ρ_{dmax} [kg/m^3]	1580.7	ASTM D4253-93-1B (ASTM, 1993a)
Minimum dry density ρ_{dmin} [kg/m^3]	1429.6	ASTM D4254-91-1A (ASTM, 1991)
Modified Procter (Mod. AASHTO) maximum dry density ρ_{dmax} [kg/m^3]	1784	SANS 3001-GR30:2015 (SANS, 2015)
Optimum moisture content w_{opt} (dry basis) [%]	6.5	
D_{50} [μm]	149	ASTM D6913-17 (ASTM, 2017)[2], SANS 3001-GR3:2014 (SANS, 2014)[3]
D_{60} [μm]	181.5	
D_{10} [μm]	73.5	
Coefficient of uniformity C_u	2.46	ASTM D2487-06 (ASTM, 2006)
Uniformity classification	Uniformly graded	
Sand [%]	96.2	USDA Soil Classification (USDA, 1987; He *et al.*, 2020)
Silt [%]	2.8	
Clay [%]	<1	
Textural classification	Fine sand	
Particle shape[1]	Sub Angular	
Effective friction angle ϕ' [Deg.]	36.1	ASTM 3080-72 (ASTM, 1972)[4]
Effective cohesion c' [kPa]	0	
Target moisture content w (dry basis) [%]	6.5	ASTM D4643-93 (ASTM, 1993b)
Maximum void ratio e_{max}	0.86	(Craig, 2002)
Minimum void ratio e_{min}	0.48	
Degree of saturation at max density S_{rmax} [%]	35.4	
Degree of saturation at min density S_{rmin} [%]	20.2	

Note: [1]Particle shape from electron microscope imaging on Cullinan sand by Archer (2014). [2]Sieve analysis. [3]Hydrometer analysis. [4] Direct shear box test under consolidated drained conditions, consolidated to 1784 kg/m^3 dry density at 6.5% moisture content.

The soil particle size distribution is indicated in Figure 23. For reference, the particle size distribution identified by Archer (2014) for Cullinan sand is also indicated.

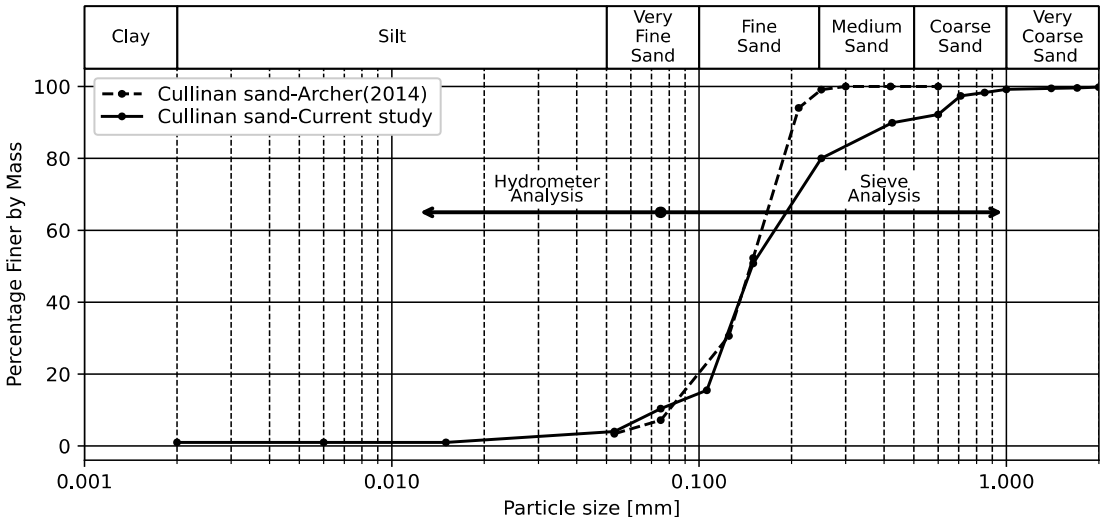

Figure 23-Soil particle size distribution (Particle size classes from USDA soil classification system (USDA, 1987)).

3.4.3 Soil bin setup

Figure 24 indicates the new soil bin commissioned at the University of Pretoria for this study. The soil bin is located outdoors and contains ±8000kg of soil. Although the outdoor location is not ideal, it was the only space available for this study. When not in use, the soil bin is covered to prevent moisture loss. A portable shade net (not depicted) provides shade and prevents moisture loss during testing.

Figure 24-Soil bin commissioned at University of Pretoria (Length:5m, Breadth:2m, Depth:0.5m)

Figure 25 indicates the boundary conditions of the soil bin during Bevameter testing. The soil bin is large enough to stay clear of the recommended distances to rigid boundaries specified by the SAE J939 (SAE, 1967) standard for Bevameter testing. However, in this study, special consideration should be

noted for the boundary formed between prepared soil and unprepared soil. The Bevameter's mechanical design from section 3.3.1 is limited to preparing an area of 800x500x200mm. In order to minimise the effect of density change at this interface boundary, both pressure-sinkage and shear stress tests are limited to 80mm sinkage depth.

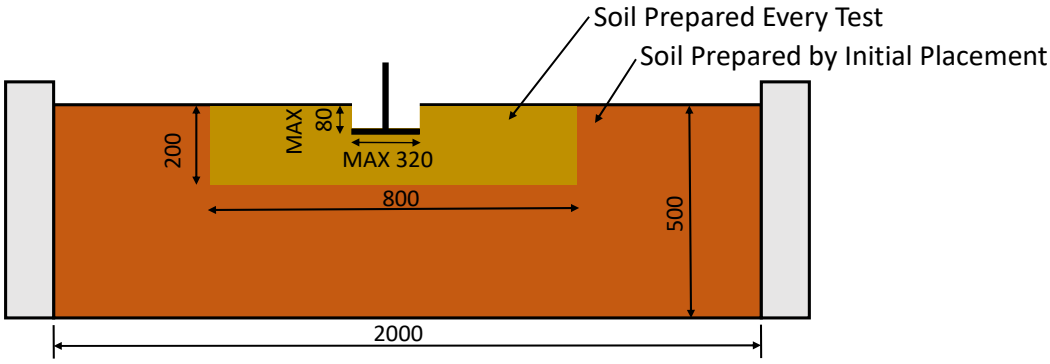

Figure 25-Soil bin boundary conditions.

Initial soil placement

Bekker (1969) indicated that a common problem for laboratory Bevameter testing in large soil bins is the compaction of deeper untilled layers over time, resulting in a change in the soil stiffness. In this case, the large mass of soil (+-8000kg) and the manual labour involved makes it impractical to repeat the initial soil placement step. In order to mitigate the soil compaction problem, the soil was initially placed in a high compaction state to prevent the lower soil layers (250mm-500mm) from compacting over time. The target soil compaction level was 95% Mod. AASHTO (86.2% realised). The soil compaction was achieved using a vibrating plate compactor by performing three passes at walking pace in 100mm layers as the filling of the soil bin progressed.

After the initial placement, the upper 200mm is loosened to below the ASTM D4254-91-1A (ASTM, 1991) minimum density and compacted to the desired soil density. More detail on the soil preparation procedure for repeated tests will be provided in section 4.3 when discussing the experimental methods.

3.5 Chapter summary

This chapter dealt with the Bevameter hardware and soil bin setup in preparation for the experimental study to follow. First, the running gear of the target vehicle was analyzed, where it was determined that the nominal vehicle ground pressure is 100kPa and the wheel contact area is 583cm^2. A new Bevameter device was developed to match said running gear loads and areas. Furthermore, the equipment was calibrated, and the error was quantified. Finally, a soil was selected, and the setup of a new soil bin was laid out. With the Bevameter hardware and soil bin setup established, we can move on to the experimental and data analysis methods.

CHAPTER 4

Experimental and Data Analysis Methods

"Probability is the mathematics of uncertainty…many modern theories have uncertainty built into their foundations. Thus learning to think in terms of probability is essential."

-Richard W. Hamming[4]

[4] Quotepark (2021) *Richard Hamming*. Available at: https://quotepark.com/quotes/1824310-richard-hamming-probability-is-the-mathematics-of-uncertainty-ma (Accessed: 25 April 2022).

4. Experimental and Data Analysis Methods

4.1 Preamble

This chapter aims to cover all the experimental and data analysis methods used in this study. Literature indicates that determining in situ soil mechanical behaviour is a stochastic process. Therefore, experiments should carefully consider the design of experiments and employ probabilistic data analysis. This is especially important for conducting experiments in an outdoor soil bin.

4.2 Design of experiment

Identification of variables

As established in section 2.5 of the literature study, this study primarily focuses on Bevameter shear tests. The important variables applicable to the shear test are indicated in Table 9.

Table 9-Identification of variables for Bevameter shear tests.

Independent variables	Response variables	Covariates	Extraneous variables	Confounding variables
• Soil preparation /soil density • Shear mechanism • Shear contact area • Shear Velocity	• Shear stress τ	• Shear displacement j •Normal stress σ	• Soil moisture content • Air temperature • Air humidity • Test protocols	• None

In Table 9, the independent variables are the variables that are purposely perturbed to study their influence on the response variable. In this case, the response variable is the measured shear stress τ. The covariates are variables that always vary during the experiments alongside the independent variables and influence the response variable. In this case, they are the shear displacement j and applied normal stress σ. The extraneous variables are variables that are not under investigation but may potentially influence the response variable and obscure the cause-and-effect relationship. Four potential extraneous variables are identified. Finally, the confounding variables are variables that are not under investigation that influence both the independent and response variables. No obvious confounding variables are identified.

The control strategy for limiting the influence of the extraneous variables is indicated in Table 10.

Table 10-Control strategy for extraneous variables.

Extraneous variable	Observability	Expected influence	Impact on	Control strategy
Soil MC	Observable (Observed)	Significant	Directly affects the soil shear strength.	• Physical control • Statistical control through regression analysis
Air temperature	Observable (Not observed)	Minor	Temperature drift may affect the load cell Wheatstone bridge lead wires & soil moisture loss rate.	• Physical control-remove load cell offset before tests.
Air humidity	Observable (Not observed)	Minor	Soil moisture loss rate.	• None
Test protocols	Not observable, Latent variable	Major	The reference point for sinkage and shear displacement. Soil loading sequence. Repeatability of soil preparation.	• Physical control-standardised procedures

Design of experiment

A high-level overview of the experimental design and data analysis strategy is indicated in Figure 26.

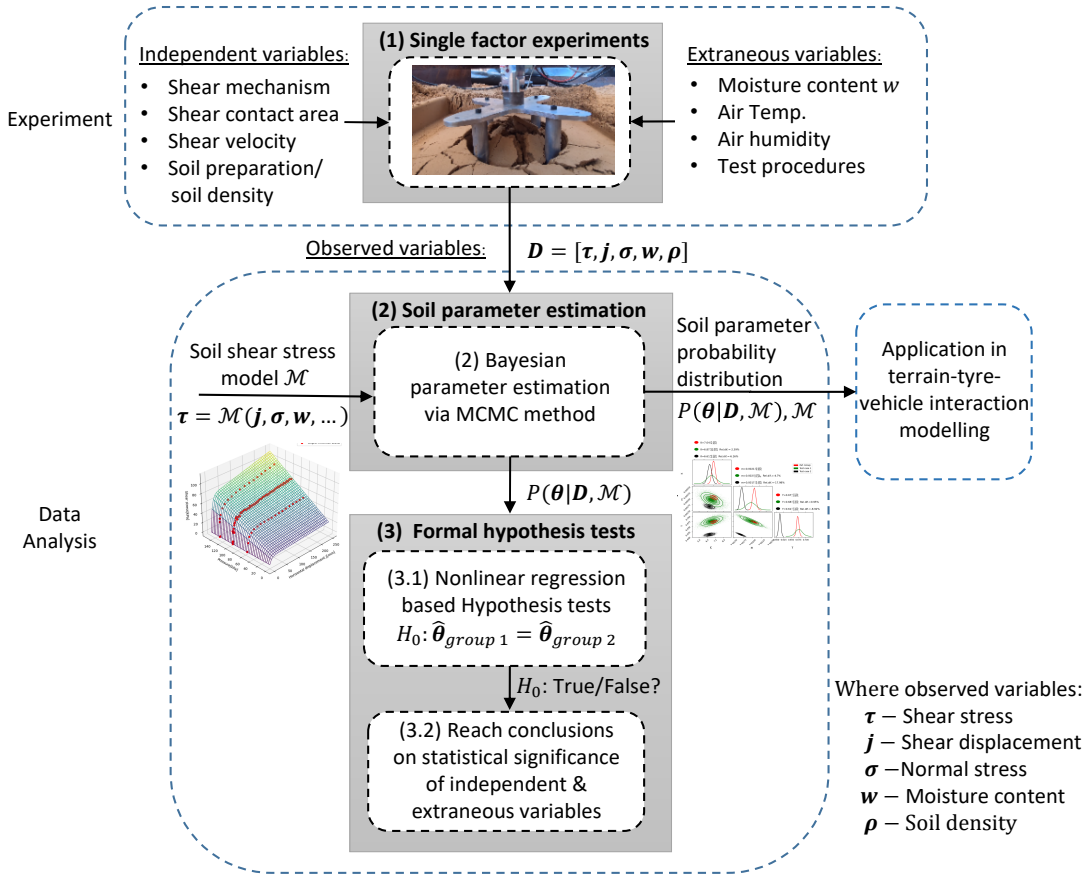

Figure 26-High level overview of experimental design and data analysis method.

Block (1) in Figure 26 indicates the physical experiment. The experiment is set up as a series of single-factor experiments where a single independent variable is perturbed at a time. The motivation for single-factor experimental design is the simplicity of the experimental design and the ability to make direct comparisons to determine the influence of a single variable without other independent variables simultaneously influencing the response. The observed variables from the experiment are shear stress τ, shear displacement j, normal stress σ, moisture content w and soil density ρ. The experimental methods used to gather the data for block (1) will be discussed in detail in section 4.3.

Block (2) in Figure 26 indicates the soil parameter estimation strategy. Soil parameter estimation is standard practice in Bevameter testing. However, early methods used point estimation methods with no uncertainty quantification. The literature study indicated that the soil parameters should rather be characterised in a probabilistic sense. From section 2.4.3, the Bayesian MCMC parameter estimation method was selected as the preferred strategy for soil parameter estimation as it is considered the "gold standard" for nonlinear parameter estimation and holds significant advantages over alternative methods. The Bayesian parameter estimation approach method will be detailed in section 4.4.

Block (3) in Figure 26 indicates the strategy to formally determine the influence of independent and extraneous variables on Bevameter soil characterisation. Formal hypothesis tests for factors that influence Bevameter tests have been done by Bekker (1969), Stafford and Tanner (1982) and Massah and Noorolahi (2010). However, their methods require linear soil models or disregard the influence of covariates. Literature indicated that for nonlinear data with covariates, regression-based methods are

the preferred method for statistical significance tests. Therefore, a nonlinear regression hypothesis testing strategy is implemented. The setup of the hypothesis tests will be discussed in section 4.5.

Experiment loads and levels

The experimental design loads and levels are indicated in Table 11.

Table 11-Experiment loads and levels.

Independent variable (IV)	Num. of IV levels	IV levels	Covariate levels per IV level (σ) [kPa]	Min. number of repeated tests per covariate level
Soil preparation method on pressure-sinkage[a]	5	Method-1,2,3,4,5	NA	1 (4 for selected method)
Soil preparation method on shear stress[b,c]	4	Method-2,3,4,5	93	1 (5 for selected method)
Shear mechanism[b]	2	Linear, Torsional	56, 93, 127	1,5,1[e]
Shear contact area [cm^2][b,d]	3	129, 300, 583	56, 93, 127	1,5,1[e]
Shear velocity [mm/s, RPM][b,d]	2	70 (6), 600 (48)	93	5

Note: [a]150mm diameter circular plate. [b]300cm^2 contact area. [c]Linear shear mechanism. [d]Torsional shear mechanism. [e]Number of repeated tests corresponding to 56kPa, 93kPa and 127kPa, respectively.

The first two independent variables (rows 1 to 2) of Table 11 investigate the soil preparation method. This presents a preliminary study to explore the soil in situ strength envelope to select an appropriate soil condition for the primary study to follow. The different soil preparation methods will be discussed in section 4.3.3. Independent variables three to five (rows 3 to 5) represent the main focus of the study. The shear test normal stress levels were centred around the nominal vehicle ground pressure of $\pm$100kPa. The initial number of tests per covariate level consisted of five tests at 93kPa and single tests at 56kPa and 127kPa. The total number of tests was allowed to vary and was determined by the hypothesis test evidence level (see the following sub-section on the data collection stopping criterion).

The shear rate was specified as 5mm/s for linear shear tests and 5.5 RPM for all torsional shear tests, which corresponds to linear shear velocities of 45, 70 and 97mm/s for the three (3) shear annuli. This represents the slowest speeds at which adequate motor speed control could be executed. Although the torsional shear was faster than linear shear, the results from perturbing IV five indicate that this difference is not consequential given the sensitivity of shear stress to shear rate for this soil.

Sample size and data collection stopping criteria

An open-ended Sequential Bayes Factor (SBF) data collection strategy is employed following the procedure laid out by Schönbrodt *et al.* (2017). Data is collected until the Bayes Factor (BF) of the hypothesis test in block (3) from Figure 26 reaches a specified evidence threshold and then terminated. The strategy allows flexible sampling with no strict prior power analysis and sample size specification (Schönbrodt *et al.*, 2017; Schönbrodt and Wagenmakers, 2018). Even if the BF does not reach the specified evidence threshold due to practical limits (e.g. data collection stops due to running out of time), one can interpret the evidence level in favour of the null or alternative hypothesis up to that point (Schönbrodt *et al.*, 2017). In this study, a conservative BF threshold of 10 is specified, which is the threshold for "strong evidence" (Wagenmakers *et al.*, 2018). As indicated in Table 11, an initial sample size of five tests is specified. Stafford and Tanner (1982) also used five Bevameter tests for hypothesis testing. Bekker (1969) and Massah and Noorolahi (2010) only used one test repetition.

With the high-level experimental design and data analysis strategy laid out, we can proceed to the detailed implementations of the methods used in blocks one (1) to three (3) of Figure 26.

4.3 Physical experimental methods

This section details the physical experimental methods used to collect the data for the single-factor experiments in ***block one (1)*** of Figure 26.

4.3.1 Measurement of the soil moisture content

The soil Moisture Content (MC) was determined using the ASTM D4643-93 (ASTM, 1993b) standard and is expressed in percentage dry mass (dry basis). Two moisture samples were taken per test day, one at the start and one at the end of the test day. Linear interpolation was used to determine the moisture for each individual Bevameter test. No intraday interpolation was performed as the conditions may change when left unobserved. Figure 27 indicates the soil bin moisture distribution vs. time for the duration of this study prior to performing any interpolation.

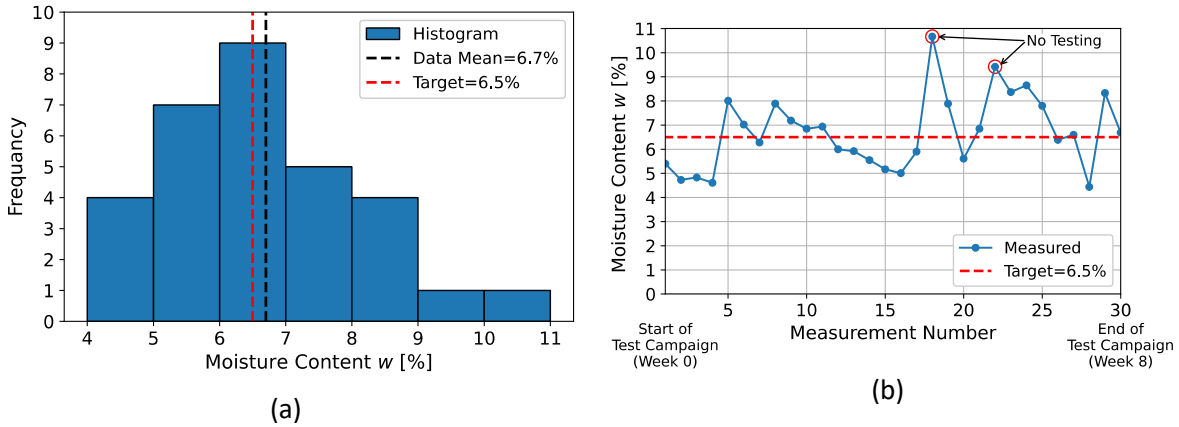

Figure 27-Soil Bin moisture content. (a) Soil moisture content histogram. (b) Temporal moisture content fluctuation.

The soil bin MC was controlled by leaving the soil bin in the sun to dry when oversaturated or adding moisture when the MC was below the target MC. Although the soil bin was covered to protect it from the elements, some moisture entered the soil bin during heavy rain events and caused the upward spikes in MC observed in Figure 27 (b). This made controlling the MC very difficult. However, the effect of forcefully applying physical MC control is illustrated by Figure 30 (a), where the MC exhibits an approximately Gaussian distribution with a mean that deviates 0.2% from the target MC.

4.3.2 Measurement of the in situ soil density and compaction level

The in situ soil compaction level is a critical factor that is expected to affect the soil's mechanical behaviour. In order to quantify the soil compaction level, the in situ density is expressed relative to two standard laboratory tests from Table 8. The first method utilised in this study is the relative compaction R_c, which express the in situ dry density ρ_d relative to the maximum dry density ρ_{dmax} from the SANS 3001-GR30:2015 (SANS, 2015) modified AASHTO Procter test,

$$R_c = \frac{\rho_d}{\rho_{dmax}} \times \ 100 \tag{18}$$

The second method is the relative density method, which compares in situ dry density relative to the maximum dry density from the ASTM D4253-93-1B (ASTM, 1993a) vibrating table compaction test and the minimum density ρ_{dmin} of the ASTM D4254-91-1A (ASTM, 1991) inverted cylinder test. The relative density D_d is then calculated according to equation (19).

$$D_d = \frac{\rho_{dmax}(\rho_d - \rho_{dmin})}{\rho_d(\rho_{dmax} - \rho_{dmin})} \times 100 \quad (19)$$

The in situ dry density ρ_d is typically measured using instruments like a nuclear soil density gauge AASHTO T-310-11 (AASHTO, 2011), sand cone method AASHTO T-191-02 (AASHTO, 2002) or balloon test device ASTM D2167-94 (ASTM, 1994). Unfortunately, these techniques require specialised test equipment that was not available. Berney *et al.* (2018) proposed using a photogrammetry technique to determine in situ soil density. For this study, a similar strategy is followed using the Meshroom (2021) open-source photogrammetry software. The procedure developed follows the guidelines by the AASHT0 T-191-02 (AASHTO, 2002) sand cone method for hole size specification and dry density calculation, but replaces the sand volume measurement with the photogrammetry measurement. Figure 28 (a) indicates a cross-section of a soil excavation determined using photogrammetry. Figure 28 (b) indicates the height map used for volume measurement by subtracting the two point clouds.

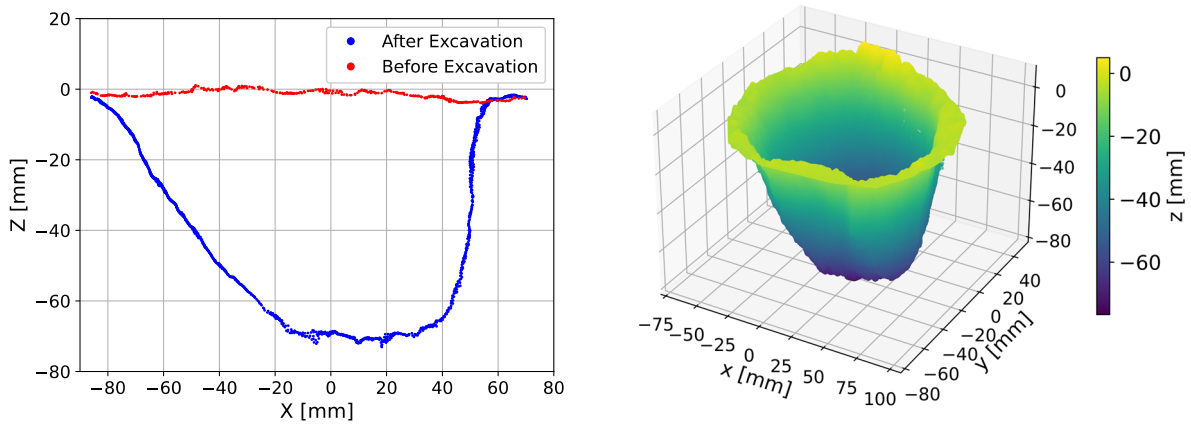

Figure 28-Photogrammetry in situ soil density measurement technique. (a) Cross-section profile. (b) Height map.

The repeatability of the soil density measurement and MC measurements was investigated by performing three density and three MC measurements after the initial soil placement took place. The results are indicated in Table 12. The density measurements indicate a realistic in situ dry density of 1538kg/m^3 that falls between the minimum (1430kg/m^3) and maximum (1784kg/m^3) soil densities from the laboratory tests in Table 8. The method exhibits repeatable results with an estimated standard deviation (SD) of 27kg/m^3 for dry density and 1.5% for relative compaction. In contrast, the relative density measurement is observed to be very sensitive to small density changes, with an SD of 19.3%. The difference between the minimum and maximum soil density for relative density in Table 8 is only 151.1kg/m^3, which explains the high sensitivity. Finally, the MC exhibits an estimated SD of 0.65% (note that this measurement includes spatial variation across the bin). For expressing soil compaction level in the results section, the Mod. AASHTO relative compaction method will be utilised. All soil densities in this study will be expressed in dry density unless specified otherwise.

Table 12-Repeatability of photogrammetry in situ density estimation method.

Test Number	Wet bulk density [kg/m^3]	Dry density [kg/m^3]	Moisture Content [%]	Relative compaction [%]	Relative density[%]
1	1603	1520	6.7	85.1	53.9
2	1681	1576	6.8	88.3	97.3
3	1618	1515	5.3	84.9	59.3
Mean	1634	1538	6.3	86.2	73.1
SD	32.0	27.7	0.65	1.5	19.3

4.3.3 Soil preparation method

As indicated in the experimental design in Table 11, five soil preparation methods that lead to five different soil densities were investigated. Figure 29 indicates the general procedure followed for all the soil preparation methods. Steps one (1), two (2), four (4), and five (5) remained the same for all the soil preparation methods investigated, with the only difference arising due to different compaction methods.

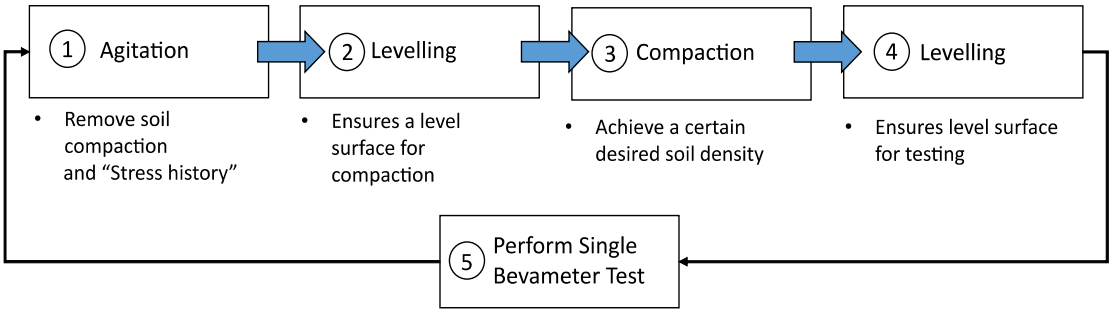

Figure 29-Soil preparation procedure diagram.

Figure 30 indicates the physical soil preparation procedure. A description of the procedures follows.

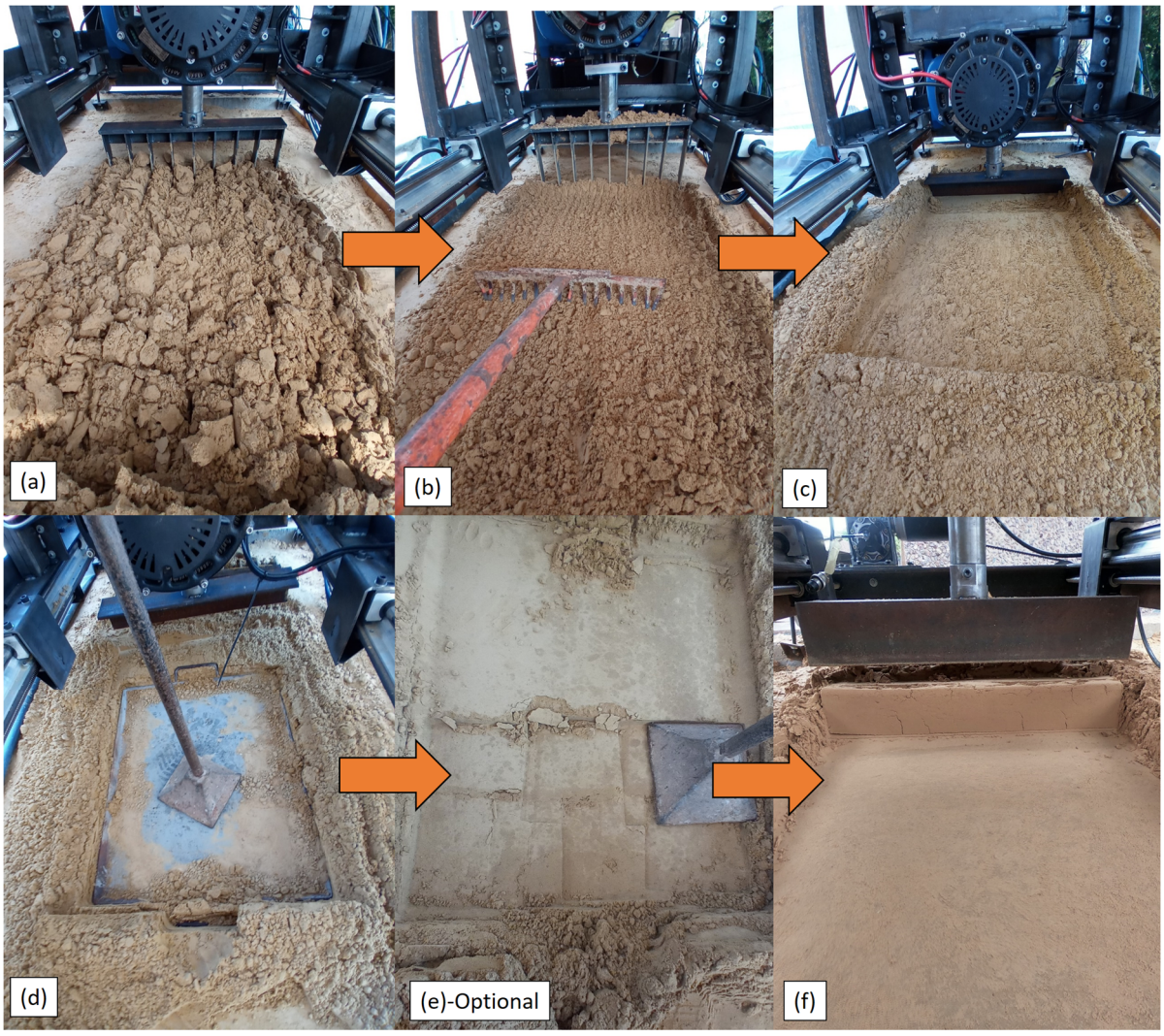

Figure 30-Physical soil preparation procedures. (a) Deep machine raking. (b) Hand raking. (c) First levelling. (d) Indirect tampering. (e) Optional direct tampering. (f) Final levelling.

Step (1): Agitation

The agitation procedure was kept constant throughout the soil preparation investigation. It consisted of the following two steps:

1. Machine raking with a rake attachment to a depth of 200mm as indicated in Figure 30 (a). The 200mm working depth is constrained by the 400mm vertical travel of the Bevameter. It consists of one forward pass and one reverse pass at a rate of 15mm/s.
2. Hand raking was performed, as indicated in Figure 30 (b), to roughly level the surface and further agitate and loosen the "clumps" that are present after the first agitation step. A procedure of three forward and three reverse passes was followed. The rake has a 50mm soil penetration depth.

Step (2 & 4): Levelling

A levelling tool attaches to the Bevameter, and levelling is performed as indicated in Figure 30 (c) and (f). This allows the surface to be levelled relative to the Bevameter ground engaging tool. In the final levelling step, $\pm$8mm of the compacted layer is removed. This is not ideal as it pre-shears and disturbs the surface from the compaction step; however, it is necessary to ensure a level test surface.

Step (3): Compaction

Five different compaction methods that lead to five different soil compaction levels were investigated. The primary compaction method used in this study consisted of impacting a tampering rod on a base plate, as indicated in Figure 30 (d). Optional further compaction is achieved by direct tampering, as indicated in Figure 30 (e). Lastly, to achieve even higher compaction, a vibrating plate compactor was utilised. Table 13 indicates the different soil compaction methods and the measured compaction state.

Table 13-Soil compaction procedure and resulting soil densities.

Method	Compaction method	Compaction energy $[kJ/m^2]$	Dry density $[kg/m^3]$	Relative compaction [%]	Relative density [%]	Density classification[1]
1	None	0	No data collected	-	-	-
2	20 indirect blows with tamper rod on base plate	1.1	No data collected	-	-	-
3	40 indirect blows with tamper rod on base plate	2.2	1390	77.4	-29	Very loose
4	20 indirect blows tamper rod on base plate + 20 direct blows with the tamper rod to the soil	2.2	1511	84.7	56.4	Medium Dense
5	Vibrating plate compactor (3 passes in 100mm layers)	48	1538	86.2	73.1	Dense

Note:[1]Soil density classification from Kaniraj (1988) based on relative density.

The results from Table 13 are in line with what is expected; an increase in compaction effort resulted in an increase in measured soil density. Note that method three exhibits negative relative density. This is explained by the inclusion of moisture which causes the soil particles to stick or clump together, as observed in Figure 30, leading to the formation of macroscopic and microscopic pockets of air which decrease soil density. The ASTM D4254-91-1A (ASTM, 1991) minimum density tests utilised completely dry soil. Although no density data were collected for methods one and two, these methods are expected to have even larger negative relative density. In contrast, method five exhibits a high compaction state and is classified as dense soil. Considering the large increase in compaction energy

of method five over method four, a more significant increase in density was expected. It may indicate that the soil is approaching the maximum compaction achievable in field conditions.

4.3.4 Experimental test procedures

In this study, three types of experimental tests were performed. The type of tests are: 1) in situ pressure-sinkage tests, 2) in situ rotational shear tests, and 3) in situ linear shear tests. An example of each type of test is indicated in Figure 31. A detailed description of the test procedure for each follows.

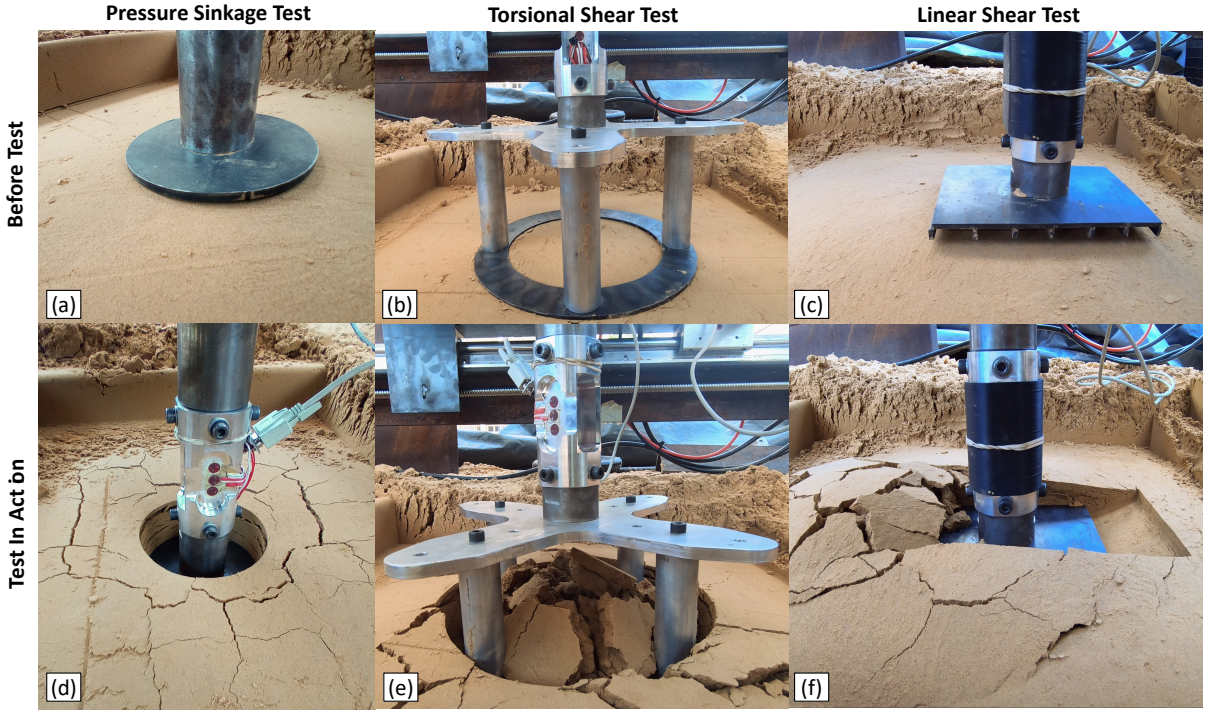

Figure 31-Examples of the three types of Bevameter tests in this study. (a) Pressure-sinkage test (before test), (b) Rotational shear (before test), (c) Linear shear (before test), (d) Pressure-sinkage (test in action), (e) Rotational shear (test in action), (f) Linear shear (test in action).

For the pressure-sinkage test, the Bevameter acts in displacement control mode in the vertical direction. First, the end effector is suspended approximately 10mm above the soil. Data recording of all 10 Bevameter channels is then started. In post-processing, this acts as the load offset removal for the six load cell channels. The penetrating plate is brought to the surface until it just touches the surface, as indicated in Figure 31 (a) and held for a period of time. This point is used in post-processing as the reference point for zero sinkage. The test is then run until the depth of 80mm is reached.

For the rotational shear test, the test procedure starts by removing the gearbox backlash by loading the effector opposite to the direction of motion. Data recording of all 10 Bevameter channels is then started with the Bevameter end effector suspended approximately 10mm above the soil. The effector is then slowly lowered in displacement control mode until the grousers are fully embedded in the soil, and the support plate just touches, as indicated by Figure 31 (b). This forms the tare position for the shear sinkage measurement. By continually monitoring the vertical force, the end effector is lowered further until the S-type load cells read zero force, indicating the soil has taken the full weight of the Z-carriage. The Z-carriage is then decoupled to allow the soil engagement tool to move freely in the vertical direction, with the vertical force now controlled by dead weight. The rotational shear test is then started, as indicated in Figure 31 (e), and the test continues until the shear sinkage reaches 80mm.

The procedure for the linear shear test is similar to the torsional shear test except for one additional consideration. For the linear shear test, it is critically important that the load cell is perfectly perpendicular to the direction of motion. Load cell alignment is achieved by using markings on the shaft indexed in two-degree increments. The shaft is then locked in place using a friction clamp mechanism.

This section concludes all the physical experimental methods used in this study. We may now proceed to the data analysis methods used to analyse the experiment.

4.4 Soil parameter estimation method

This section details the parameter estimation method of ***block two (2)*** in Figure 26.

The Bayesian parameter estimation approach

In the Bayesian parameter estimation approach, a model's parameter probability distribution is obtained from Bayes' rule for conditional probability, where Bayes' rule is given by,

$$p(\boldsymbol{\theta}|\boldsymbol{D},\mathcal{M}) = \frac{p(\boldsymbol{D}|\boldsymbol{\theta},\mathcal{M})p(\boldsymbol{\theta})}{p(\boldsymbol{D})} = \frac{p(\boldsymbol{D}|\boldsymbol{\theta},\mathcal{M})p(\boldsymbol{\theta})}{\int p(\boldsymbol{D}|\boldsymbol{\theta},\mathcal{M})d\theta} \tag{20}$$

where $p(\boldsymbol{\theta}|\boldsymbol{D},\mathcal{M})$ is the posterior distribution of parameter vector $\boldsymbol{\theta}$ given data vector $\boldsymbol{D}$ and model $\mathcal{M}$, $p(\boldsymbol{D}|\boldsymbol{\theta},\mathcal{M})$ is the likelihood of the data, $p(\boldsymbol{\theta})$ is the parameter prior probability distribution, and $p(\boldsymbol{D})$ is the marginal likelihood. The data $\boldsymbol{D}$ can be further expressed as $\boldsymbol{D} = \{\boldsymbol{X}, \boldsymbol{y}\}$ to distinguish between the dependent data vector $\boldsymbol{y}$ and the independent data vector $\boldsymbol{X}$ (Gelman *et al.*, 2013).

Setup of the probabilistic model for shear stress-displacement modelling

Figure 32 indicates the Directed Acyclic Graph (DAG) setup to infer the soil model parameters in plate notation form. The forward graph, or DAG, makes all the inference assumptions explicit. Note that the random variables in Figure 32 refer to stochastic variables with associated probability distributions.

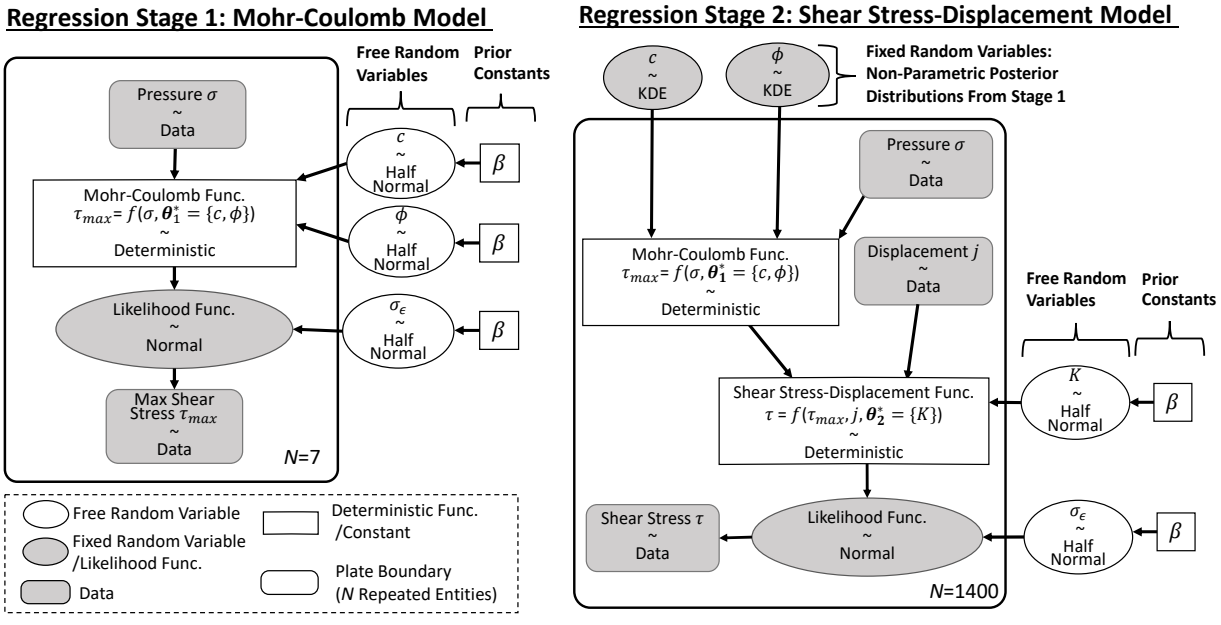

Figure 32-Probabilistic model used to infer the soil shear stress-displacement parameters (a) Regression stage 1: Inferring the maximum shear stress parameters (b) Regression stage 2: Inferring the shear stress-displacement model parameters.

In Figure 32, a hierarchical model with two-stage regression is implemented. Hierarchical modelling and two-stage regression is common practice for shear stress-displacement modelling. Eight of the nine state of the art stress-displacement models reviewed by He *et al.* (2019a) take the hierarchical

modelling approach, with the maximum shear stress from the Mohr-Coulomb model serving as input to the shear-displacement model. Separate (or two-stage) regression is required as the two models are fitted on different datasets. The Mohr-Coulomb model should only be fitted to the maximum shear stress data (i.e. $\boldsymbol{D} = \{\boldsymbol{X} = \boldsymbol{\sigma}, \boldsymbol{y} = \boldsymbol{\tau_{max}}\}$) (SAE, 1967). While the shear-displacement model should be fitted on the longitudinally varying shear stress data (i.e. $\boldsymbol{D} = \{\boldsymbol{X} = \{\boldsymbol{\tau_{max}}, \boldsymbol{j}\}, \boldsymbol{y} = \boldsymbol{\tau}\}$). An alternative approach is single-step regression, where all the parameters are inferred in one step (i.e. c and ϕ in Figure 32 (b) become free parameters). However, the latter approach compromises the Mohr-Coulomb envelope to satisfy the shear-displacement curve shape, and the Mohr-Coulomb model becomes dependent on the shear-displacement data (i.e. c and ϕ are influenced by $\boldsymbol{j}$ and $\boldsymbol{\tau}$ instead of only $\boldsymbol{\tau_{max}}$).

Intuitively, if the uncertainty of the parameters of the first model (Mohr-Coulomb) increases, the uncertainty in the parameters of the dependent model (shear-displacement) must increase. However, most literature is presented in the context of deterministic models and point estimation (e.g. least squares estimation), with no treatment of uncertainty and uncertainty propagation. Classic texts on terramechanics also do not deal with the uncertainty or uncertainty propagation between the Mohr-Coulomb and shear-displacement models (Bekker, 1969; Muro and O'Brien, 2005; Upadhyaya *et al.*, 2009; Wong, 2010). The ***conditional*** propagation of uncertainty from the first model to the second model is ***critically*** important for the accurate estimation of confidence intervals for parameters of the shear-displacement model. The remainder of this section will address how this can be achieved.

Form of the deterministic model

The form of the two deterministic models in Figure 32 is given by,

$$\tau_{max} = \mathcal{M}_1(\boldsymbol{X_1} = \{\sigma\}, \boldsymbol{\theta_1^*} = \{c, \phi\}) \tag{21}$$

$$\tau = \mathcal{M}_2(\boldsymbol{X_2} = \{\tau_{max}, j\}, \boldsymbol{\theta_2^*} = \{K\}) \tag{22}$$

where $\mathcal{M}_1$ is given by the linear Mohr-Coulomb model from equation (4) and $\mathcal{M}_2$ is any nonlinear model that is a function of maximum shear stress τ_{max}, shear displacement j and parameter vector $\boldsymbol{\theta_2^*}$. As an example, the parameters of the Janosi-Hanamoto model from equation (5) are indicated in Figure 32 and equation (22); however, other models of this form may also be used (as will be discussed later).

Form of the likelihood function

As indicated in Figure 32, a Gaussian likelihood is specified for both regression stages,

$$p(\boldsymbol{D}|\boldsymbol{\theta}) = \prod_{i=1}^{n} \mathcal{N}(\boldsymbol{y}, \mathcal{M}(\boldsymbol{X}, \boldsymbol{\theta}^*), \sigma_\epsilon) \tag{23}$$

where the standard error σ_ϵ is also a parameter inferred by the Bayesian parameter estimation with $\boldsymbol{\theta} = \{\boldsymbol{\theta}^*, \sigma_\epsilon\}$. A Gaussian likelihood is a common choice as it maximises the principle of entropy (Beck and Katafygiotis, 1998, cited in Gallina *et al.*, 2014). Not considering the influence of the prior, maximizing a Gaussian likelihood is equivalent to minimizing the least squares error (Seber and Wild, 2003).

Form of the prior probability distributions

For this study, it is desired to remain scientifically objective. Therefore, uninformative priors in the form of diffuse distributions are specified. For all free parameters in Figure 32, half-normal prior distributions are specified that are centred at zero with standard deviations of 10^3,

$$p(\boldsymbol{\theta}) \sim |\mathcal{N}(0, \beta = 10^3)| \tag{24}$$

The specified prior standard deviations are two orders of magnitude larger than the posterior standard deviations. This ensures that the priors have practically no influence on the posterior probability. Half-normal priors are selected as all soil model parameters are positive. Physically, negative cohesion c, friction angle ϕ, shear modulus K and likelihood standard error σ_ϵ do not exist.

Form of the posterior probability distributions

The posterior parameter distribution for the first regression stage in Figure 32 (a) becomes,

$$p(\boldsymbol{\theta_1}|\boldsymbol{D_1}, \mathcal{M}_1) = \frac{p(\boldsymbol{D_1}|\boldsymbol{\theta_1}, \mathcal{M}_1)p(\boldsymbol{\theta_1})}{\int p(\boldsymbol{D_1}|\boldsymbol{\theta_1}, \mathcal{M}_1)d\boldsymbol{\theta_1}} \tag{25}$$

The posterior distribution for the second regression stage in Figure 32 (b) is more complex as it has to account for the uncertainty of the parameters from the first regression stage. This requires marginalising (integrating) over all possible values of the posterior distribution $p(\boldsymbol{\theta_1}|\boldsymbol{D_1}, \mathcal{M}_1)$ from the first regression stage. The conditional posterior distribution of the second regression stage becomes,

$$p(\boldsymbol{\theta_2}|p(\boldsymbol{\theta_1}|\boldsymbol{D_1}, \mathcal{M}_1), \boldsymbol{D_2}, \mathcal{M}_2, \mathcal{M}_1) = \frac{\int p(\boldsymbol{D_2}|\mathcal{M}_2(\mathcal{M}_1(\boldsymbol{D_2}, p(\boldsymbol{\theta_1}|\boldsymbol{D_1}, \mathcal{M}_1)), \boldsymbol{\theta_2})p(\boldsymbol{\theta_2})\boldsymbol{d\theta_1}}{\int p(\boldsymbol{D_2}|\boldsymbol{\theta_2}, \mathcal{M}_2)\boldsymbol{d\theta_2}} \tag{26}$$

MCMC approximation of the posterior distributions

Evaluating equation (25) and (26) requires integration over $\boldsymbol{\theta_1}$ and $\boldsymbol{\theta_2}$. Closed form solutions are only available for a limited set of models and probability distributions. The MCMC method circumvents the need for integration of the denominator through sampling the density of the un-normalised posterior and allows the use of nonlinear models and arbitrary distributions (Bishop, 2006). However, due to the integral in the numerator in equation (26), naïve sampling of the un-normalised density is not possible.

Gibbs sampling is a well-known technique to sample from conditional distributions (Casella and George, 1992; Bishop, 2006). To illustrate how Gibbs sampling can help solve equation (26), consider the following example by Bishop (2006): Suppose we have the joint distribution $f(\boldsymbol{z}_1, \boldsymbol{z}_2, \boldsymbol{z}_3)$ of random variables and are interested in the marginal distribution $f(\boldsymbol{z}_1|\boldsymbol{z}_2, \boldsymbol{z}_3)$. The analytical solution would be,

$$f(\boldsymbol{z}_1|\boldsymbol{z}_2, \boldsymbol{z}_3) = \int\int f(\boldsymbol{z}_1, \boldsymbol{z}_2, \boldsymbol{z}_3)d\boldsymbol{z}_2\, d\boldsymbol{z}_3 \tag{27}$$

The integral in equation (27) may be difficult or intractable. In fact, the exact solutions of conditional probabilities are NP-hard (Nondeterministic Polynomial time) computational problems (Dagum and Luby, 1993). Gibbs sampling can obtain representative samples of the marginal distribution $f(\boldsymbol{z}_1|\boldsymbol{z}_2, \boldsymbol{z}_3)$ thereby avoiding direct integration. The Gibbs approximation of equation (27) is given by Algorithm 1.

Algorithm 1-Gibbs sampling-three variable case.

Algorithm 1: Gibbs sampling-three variable case
1: Initialise $\boldsymbol{z}^S_{1,0}, \boldsymbol{z}^S_{2,0}, \boldsymbol{z}^S_{3,0}$ at arbitrary starting values
2:For i in 1…$N_{samples}$ do:
2: $\boldsymbol{z}^S_{1,i} \sim p(\boldsymbol{z}_1|\boldsymbol{z}^S_{2,i-1}, \boldsymbol{z}^S_{3,i-1})$ //Fix $\boldsymbol{z}_2$, $\boldsymbol{z}_3$ to previous sample value & sample $\boldsymbol{z}_1$
3: $\boldsymbol{z}^S_{2,i} \sim p(\boldsymbol{z}_2|\boldsymbol{z}^S_{1,i}, \boldsymbol{z}^S_{3,i-1})$ //Fix $\boldsymbol{z}_1$, $\boldsymbol{z}_3$ to previous sample values & sample $\boldsymbol{z}_2$
4: $\boldsymbol{z}^S_{3,i} \sim p(\boldsymbol{z}_3|\boldsymbol{z}^S_{1,i}, \boldsymbol{z}^S_{2,i})$ //Fix $\boldsymbol{z}_1$, $\boldsymbol{z}_2$ to latest sample values & sample $\boldsymbol{z}_3$

Returning to the MCMC approximation of equations (25) and (26), the Gibbs sampling is started at the joint distribution of $\boldsymbol{\theta}_1$ and $\boldsymbol{\theta}_2$ conditioned on all constant values in Figure 32 (a) and (b),

$$p(\boldsymbol{\theta}_1, \boldsymbol{\theta}_2|\boldsymbol{D_2}, \boldsymbol{D_1}, \mathcal{M}_2, \mathcal{M}_1) \tag{28}$$

Following the Gibbs procedure, $\boldsymbol{\theta}_1$ is conditioned on the previous sample of $\boldsymbol{\theta}_2$ and other fixed values,

$$\boldsymbol{\theta}_{1,i}^{s} \sim p\left(\boldsymbol{\theta}_1 \middle| \boldsymbol{\theta}_{2,i-1}^{s}, \boldsymbol{D_2}, \boldsymbol{D_1}, \mathcal{M}_2, \mathcal{M}_1\right) \tag{29}$$

Since $\boldsymbol{\theta}_1$ is not a function of $\boldsymbol{\theta}_2$, equation (29) can be simplified to $\boldsymbol{\theta}_{1,i}^{s} \sim p(\boldsymbol{\theta_1}|\boldsymbol{D_1}, \mathcal{M}_1)$, which is equal to the left hand side of the posterior distribution in equation (25). Substituting the right-hand side of equation (25) and performing the standard MCMC simplifications (i.e. neglecting the denominator and taking the logarithm of the un-normalised posterior), samples from equation (25) are given by,

$$\boldsymbol{\theta}_{1,i}^{s} \sim \ln p(\boldsymbol{D_1}|\boldsymbol{\theta_1}, \mathcal{M}_1) + \ln p(\boldsymbol{\theta_1}) \tag{30}$$

For the the second Gibbs step, $\boldsymbol{\theta_2}$ is conditioned on the latest sample of $\boldsymbol{\theta_1}$ and other fixed values,

$$\boldsymbol{\theta}_{2,i}^{s} \sim p\left(\boldsymbol{\theta_2} \middle| \boldsymbol{\theta}_{1,i}^{s}, \boldsymbol{D_2}, \boldsymbol{D_1}, \mathcal{M}_2, \mathcal{M}_1\right) \tag{31}$$

Expanding equation (31) with Bayes' rule and performing the standard MCMC simplifications, samples from the posterior distribution of equation (26) is given by,

$$\boldsymbol{\theta}_{2,i}^{s} \sim \ln p(\boldsymbol{D_2}|\mathcal{M}_2\left(\boldsymbol{\theta}_2, \mathcal{M}_1\left(\boldsymbol{\theta}_{1,i}^{s}\right)\right)) + \ln p(\boldsymbol{\theta}_2) \tag{32}$$

It should be noted that Gibbs sampling requires the marginal distributions to be sampleable (Bishop, 2006). However, equations (30) and (32) are not simple distributions that are directly sampleable. Therefore, a nested sampling strategy is employed with another MCMC sampling method within Gibbs sampling. The complete algorithm for sampling equations (25) and (26) is given by Algorithm 2.

Algorithm 2-Procedure for sampling the conditional posterior distributions.

Algorithm 2: Procedure for sampling from the posterior distributions of equations (25) and (26)

1: Initialise starting values: $\boldsymbol{\theta}_{1,0}^{s} = \widehat{\boldsymbol{\theta}}_{\boldsymbol{1}}, \boldsymbol{\theta}_{2,0}^{s} = \widehat{\boldsymbol{\theta}}_{\boldsymbol{2}}$ //start at the maximum a posterior value

2: For i in $1 \ldots N_{samples}$ do:

3: $\boldsymbol{\theta}_{1,i}^{s} \sim \ln p(\boldsymbol{D}_1|\boldsymbol{\theta}_1, \mathcal{M}_1) + \ln p(\boldsymbol{\theta}_1)$ *//Draw one sample from model 1*

4: $\boldsymbol{\theta}_{2,i}^{s} \sim \ln p(\boldsymbol{D}_2|\mathcal{M}_2\left(\boldsymbol{\theta}_2, \mathcal{M}_1\left(\boldsymbol{\theta}_{1,i}^{s}\right)\right)) + \ln p(\boldsymbol{\theta}_2)$ *//Substitute the sample from model 1 (Mohr-Coulomb) into model 2 (shear-displacement) and draw one sample from the posterior of model 2*

Note: The samples $\boldsymbol{\theta}_{1,i}^{s}$ and $\boldsymbol{\theta}_{2,i}^{s}$ are drawn with the Goodman and Weare (2010) MCMC algorithm.

To execute the sampling of steps 3 and 4 in Algorithm 2, the Goodman and Weare (GW) (2010) MCMC sampling algorithm is utilised. The GW algorithm holds significant advantages over traditional MCMC methods, such as being affine (scale) invariant and requiring minimal manual tuning (Foreman-Mackey *et al.*, 2013). The GW MCMC sampling is implemented in Python using the *emcee* library (Foreman-Mackey *et al.*, 2013). A total of 5×10^5 posterior samples are drawn (after burn-in and thinning) with a burn-in set to one third of the chain length and thinning keeping one in five samples.

Finally, a Kernel Density Estimate (KDE) is fitted to the samples of the posterior of each parameter,

$$p(\theta_i|\boldsymbol{D}, \mathcal{M}) \approx \frac{1}{nh}\sum_{j}^{n} K\left(\frac{\theta_i - \boldsymbol{\theta}_{i,j}^{s}}{h}\right) \tag{33}$$

Where $K(\theta_i)$ is a kernel function, θ_i is the point where the KDE is evaluated, h is the bandwidth, $\boldsymbol{\theta}_{i,j}^{s}$ is the j^{th} sample of the i^{th} parameter, and n is the number of samples. This study uses a Gaussian kernel function and Scott's rule for bandwidth selection (Scott, 1979).

In layman's terms, the proposed method simply draws a parameter sample from the Mohr-Coulomb model, substitutes it into the shear-displacement model, draws a sample from this model and repeats the process, building up the density of all the parameters in the process. This allows the ***conditional*** propagation of uncertainty from the Mohr-Coulomb model to the stress-displacement model, which is ***critically*** important for the determination of the parameter probability distributions of the latter model.

Determining the Maximum a Posterior, credible intervals and Posterior Predictive Distribution

The determination of the Maximum a Posterior (MAP), parameter credible intervals and Posterior Predictive Distribution (PPD) is standard practice for Bayesian parameter estimation and not unique to this application; therefore, the reader is referred to standard textbooks on the matter (Bishop, 2006; Gelman *et al.*, 2013). For detail on the specific numerical methods employed, refer to Appendix F.

Evaluation criteria for model comparison

In this study, different shear stress-displacement models will be compared. Bayes Factor will be used as the primary performance metric. The Bayes Factor is considered the "gold standard" for comparing competing models ability to fit data (Dunstan *et al.*, 2022). The marginal likelihood used in calculating the Bayes Factor is theoretically equivalent to performing an exhaustive k-fold test-train split in the non-Bayesian framework (Fong and Holmes, 2020). Therefore it strongly discourages the use of meaningless parameters that result in overfitting (Dunstan *et al.*, 2022). The Bayes Factor is defined as,

$$\mathrm{BF}_{01} = \frac{\int p(\boldsymbol{D}|\boldsymbol{\theta}_0, \mathcal{M}_0) d\theta}{\int p(\boldsymbol{D}|\boldsymbol{\theta}_1, \mathcal{M}_1) d\theta} \tag{34}$$

Where $\mathcal{M}_0$ and $\mathcal{M}_1$ are the two models to be compared. The recommended method to evaluate the integrals of the Bayes Factor is the importance sampling method given by (Marin and Robert, 2009),

$$\mathrm{BF}_{01} = \frac{n_0^{-1} \sum_j^{n_0} p_0\left(\boldsymbol{D}\middle|\boldsymbol{\theta}_{0,j}^S\right) p_0(\boldsymbol{\theta}_{0,j}^S)/\omega_0(\boldsymbol{\theta}_{0,j}^S)}{n_1^{-1} \sum_j^{n_0} p_1\left(\boldsymbol{D}\middle|\boldsymbol{\theta}_{1,j}^S\right) p_1(\boldsymbol{\theta}_{1,j}^S)/\omega_1(\boldsymbol{\theta}_{1,j}^S)} \tag{35}$$

where $\boldsymbol{\theta}_0^S$ and $\boldsymbol{\theta}_1^S$ are samples drawn from the posterior of the two models and ω_0, ω_1 are proposal distributions. A natural choice for the proposal distributions is the KDE of the posterior.

A motivating example

Figure 33 indicates an example of applying Bayesian parameter estimation to real-world Bevameter data. In order to illustrate the core principles, the linear model from the first regression stage is indicated. For comparison, the nonlinear least squares estimate is also indicated. Note that the same point estimate is obtained. The advantage of the Bayesian approach is that the full parameter probability distributions are recovered, not just the point estimates. Furthermore, the approach has predictive capability and can determine the probability at any new unseen data point. Although closed-form solutions exist for linear models, they are not applicable to the nonlinear model of the second regression stage. Note that the probability distributions are non-parametric and can take any form (i.e. does not have to be Gaussian).

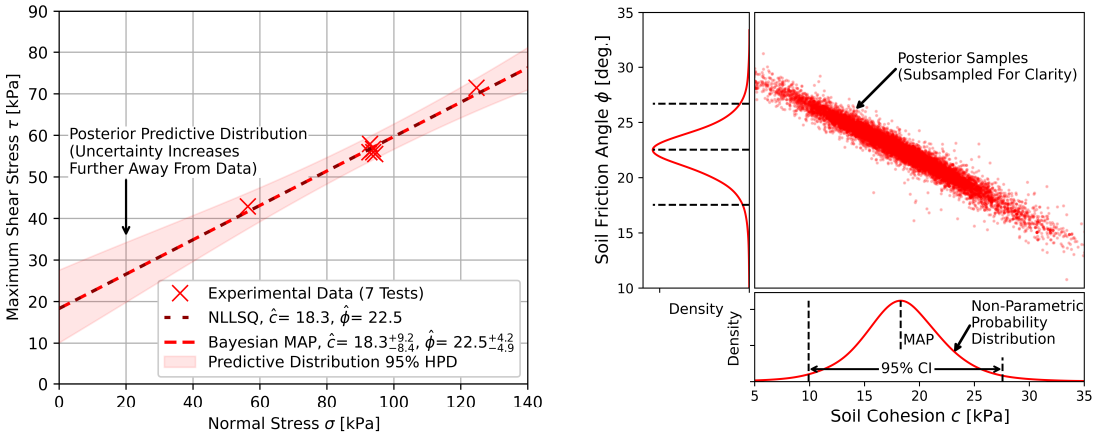

(a) (b)

Figure 33-Example of Bayesian parameter estimation. (a) Mohr-Coulomb plot. (b) Parameter probability distribution.

4.5 Formal Hypothesis tests for factors that influence Bevameter tests

This section details the methods for performing the hypothesis tests of ***block three (3)*** in Figure 26. Two types of hypothesis tests are performed, a hypothesis test for the influence of independent variables and a hypothesis test for the influence of extraneous variables.

4.5.1 Setup of the hypothesis tests for the influence of independent variables

The hypothesis test seeks to answer the simple question: Are the soil model parameters identified different if the independent variable is perturbed (e.g. shear mechanism changed)? In order to formally answer this question, the following hypothesis test is set up based on the soil parameters estimated from the ***nonlinear*** regression in section 4.4,

$$\begin{gathered} H_0: \widehat{\boldsymbol{\theta}}_{\mathbf{1}} = \widehat{\boldsymbol{\theta}}_{\mathbf{2}} \\ \{\widehat{\theta}_{11}, \widehat{\theta}_{1i}, .., \widehat{\theta}_{1k}\} = \{\widehat{\theta}_{21}, \widehat{\theta}_{2i}, \dots, \widehat{\theta}_{1k}\} \\ H_1: \widehat{\boldsymbol{\theta}}_{\mathbf{1}} \neq \widehat{\boldsymbol{\theta}}_{\mathbf{2}} \text{ for at least one parameter} \\ \{\widehat{\theta}_{11}, \widehat{\theta}_{1i}, .., \widehat{\theta}_{1k}\} \neq \{\widehat{\theta}_{21}, \widehat{\theta}_{2i}, \dots, \widehat{\theta}_{1k}\} \end{gathered} \tag{36}$$

Where $\widehat{\boldsymbol{\theta}}_{\mathbf{1}}$ is the estimate parameter vector of a first categorical group (e.g. torsional shear), $\widehat{\boldsymbol{\theta}}_{\mathbf{2}}$ is the estimated parameter vector of the second categorical group (e.g. linear shear). If the null hypothesis H_0 is false, with a certain degree of certainty, the independent variable has a statistically significant influence. Note that the hypothesis test is set up to determine the equivalence of categorical variables since the independent variables (e.g. shear mechanism) cannot be modelled as continuous variables.

4.5.2 Setup of the hypothesis tests for the influence of extraneous variables

To determine the influence of extraneous variables, the following linear regression model is set up,

$$\tau_{max,ij} = \sum_i^N [\alpha_i D_i + w_{ij} D_i \beta_i] + \epsilon \tag{37}$$

where $\tau_{max,ij}$ is the response variable of interest, w_{ij} is the observed extraneous variable (e.g. moisture content), β_i is the extraneous variable coefficient, i is the category number, j is the data point number, D_i is the category indicator variable (e.g. $D_0 = 0$ for torsional shear, $D_1 = 1$ for linear shear), α_i is the categorical variable coefficient, ϵ is the pooled error with $\epsilon \sim \mathcal{N}(0, \sigma_\epsilon)$ and N is the number of categories. The hypothesis test for the influence of the extraneous variable is then set up as,

$$\begin{gathered} H_0: \hat{\beta}_i = 0 \\ H_1: \hat{\beta}_i \neq 0 \end{gathered} \tag{38}$$

If $\hat{\beta}_i = 0$, in a probabilistic sense, w has no statistically significant influence on the response variable.

4.5.3 Evaluating the hypotheses

At least four methods exist to perform Bayesian hypothesis tests (Makowski *et al.*, 2019). Bayes Factor method, developed by Jeffrey (1961), is the preferred method (Rouder *et al.*, 2009; Van Ravenzwaaij *et al.*, 2019). Where the Bayes Factor is defined as the likelihood ratio of the competing hypotheses,

$$\text{BF}_{01} = \frac{p(\boldsymbol{D}|H_0)}{p(\boldsymbol{D}|H_1)} = \frac{\int p(\boldsymbol{D}|\theta, H_0) p(H_0) d\theta}{\int p(\boldsymbol{D}|\theta, H_1) p(H_1) d\theta} \tag{39}$$

The Bayes Factor is intuitively interpretable. For instance, if $\text{BF}_{01} = 10$, the data is ten times more likely for the null hypothesis H_0 than the alternative hypothesis H_1. If the priors are the same, as is the case for Jeffrey's hypothesis testing method, the Savage-Dickey Density Ratio (SDDR) method can be utilised instead of performing explicit integration of equation (39).

In the SDDR approach, the Bayes Factor is expressed as (Wagenmakers *et al.*, 2010),

$$\text{BF}_{01} = \frac{p(\boldsymbol{D}|H_0)}{p(\boldsymbol{D}|H_1)} = \frac{p(\theta=0|\boldsymbol{D},H_1)}{p(\theta=0|H_1)} \tag{40}$$

Prior to calculating the BF, the data is expressed in terms of standardised difference. This allows the BF to be evaluated in reference to standard priors (Rouder *et al.*, 2009; Kruschke, 2013). The standardised difference δ_i for the i^{th} parameter is given by (Kruschke, 2013),

$$\delta_i = \frac{\mu_1 - \mu_2}{\sqrt{\frac{\sigma_1^2 + \sigma_2^2}{2}}} \tag{41}$$

Where $\delta_i, \mu_1, \mu_2, \sigma_1$ and σ_2 are random variables, each with their own probability distribution and associated uncertainty. The procedure by Kruschke (2013) is followed to estimate δ_i using the Bayesian MCMC method. In this application, the data of the two groups in equation (41) is the samples of individual parameters $\boldsymbol{\theta}_{1i}^{S}$ and $\boldsymbol{\theta}_{2i}^{S}$. The parameters are resampled corresponding to the sample size of the number of Bevameter tests (e.g. 5 samples are drawn from $\boldsymbol{\theta}_1^S$ and $\boldsymbol{\theta}_2^S$) and δ_i estimated. For the MCMC estimation, 10^3 samples are drawn and the entire procedure repeated 10^3 times. For more detail on the MCMC estimation of δ_i, including priors and likelihood selection, see Kruschke (2013).

The hypothesis $H_0: \boldsymbol{\theta}_1 = \boldsymbol{\theta}_2$ and $H_1: \boldsymbol{\theta}_1 \neq \boldsymbol{\theta}_2$ are then reformulated in terms of standardised differences as $H_0: \boldsymbol{\delta} = 0$ and $H_1: \boldsymbol{\delta} \neq 0$. Following Wagenmakers *et al.* (2010), a non-parametric density estimate is fitted to the samples of the standardised difference. Similar to equation (33), a Gaussian KDE is fitted to the standardised difference δ_i of each individual parameter i,

$$p(\delta_i|\boldsymbol{D}, H_1) = \frac{1}{nh}\sum_j^n K\left(\frac{\delta_i - \boldsymbol{\delta}_{ij}^{\boldsymbol{S}}}{h}\right) \tag{42}$$

The prior on H_1 in equation (40) is specified as the standard Cauchy reference prior $p(H_1) \sim C(0, \sqrt{2}/2)$ (Wagenmakers *et al.*, 2018). Finally, once the BF is evaluated, the evidence level in support of either H_0 or H_1 is classified by Jeffrey's evidence scale. Jeffrey's evidence scale for BF_{10} is indicated in Table 14.

Table 14-Metrics used to interpret evidence level and effect size (Jeffreys 1961; Cited in Wagenmakers *et al.*, 2018).

Jeffrey's evidence scale	Cohen's d effect size
BF_{10}: 1-3 Anecdotal	0.2<d : small effect size
BF_{10}: 3-10 Substantial[a]	0.2≤ d<0.5 : Medium effect size
BF_{10}: 10-30 Strong	0.5≤d<0.8 : Large effect size
BF_{10}: 30-100 Very strong	0.8≤d: Very large effect size
BF_{10}: >100 Decisive	

Note: [a]$\text{BF}_{10} \geq 3$ is the threshold for statistical significance for this study

To help interpret the separation between two distributions, the point estimate of equation (41), known as Cohen's d, is also used. Cohen's d expresses the mean difference as a ratio of pooled standard deviations. The interpretation of Cohen's d, unrelated to Jeffrey's evidence, is also indicated in Table 14.

A motivating example

Figure 34 indicates a practical example of applying Bayesian hypothesis testing on real-world Bevameter data. Figure 34 (a) and (b) indicate the estimated Mohr-Coulomb parameters obtained from two different Bevameter experimental test configurations. The question posed in Figure 34 (a) highlights the need for formal hypothesis testing; without it, it would not be possible to answer this fundamental question on how the Bevameter test setup influences the identified soil parameters.

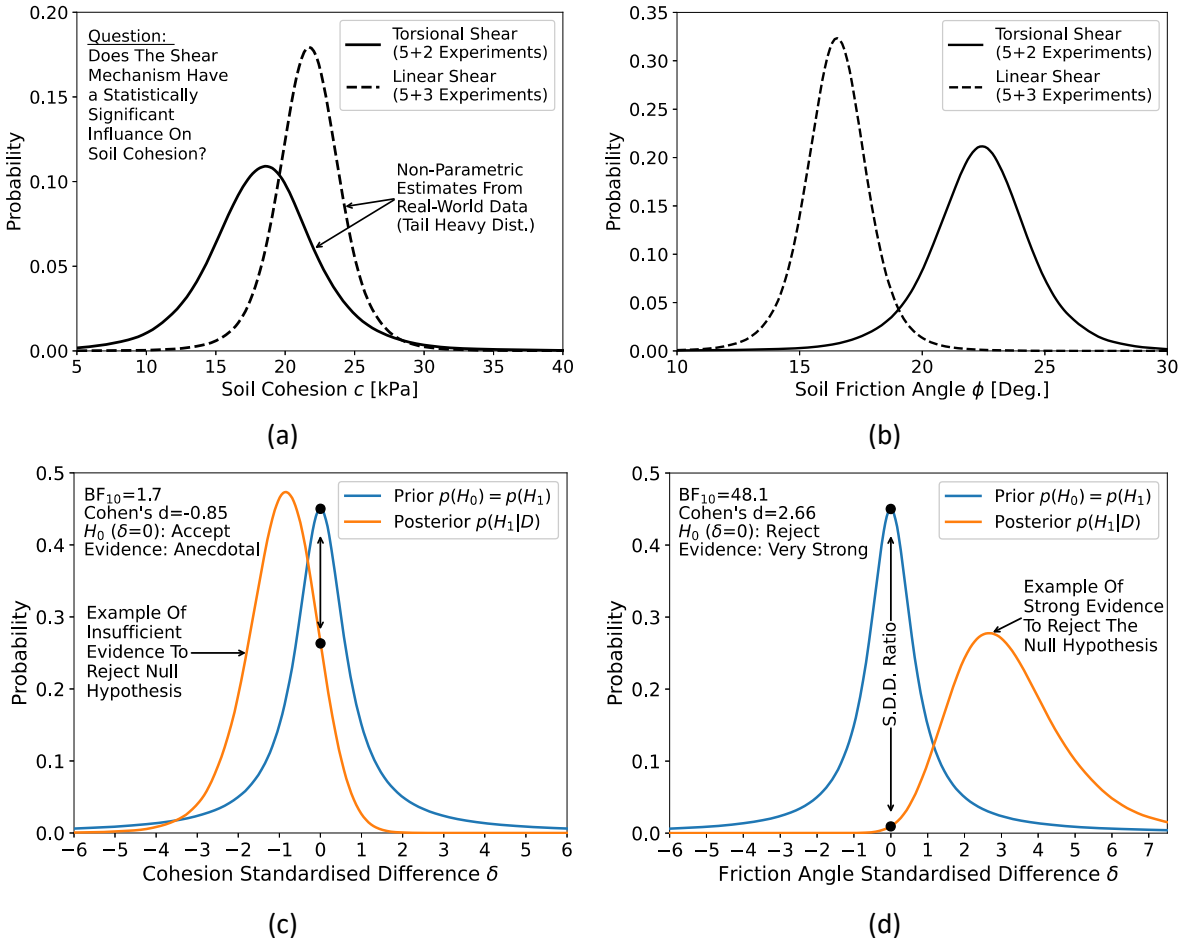

Figure 34-Example of Bayesian hypothesis testing using the Savage-Dicky density ratio method. (a) Estimated soil cohesion. (b) Estimated soil friction angle. (c) Cohesion standardised difference. (d) Friction angle standardised difference.

Figure 34 (c) indicates the standardised difference for soil cohesion c. In this case the distribution of the standardised difference is close to zero with a BF_{10} of 1.7; therefore, the hypothesis tests accept the null hypothesis. Figure 34 (d) indicates a standard difference for internal friction angle. In this case, the probability distribution is located far from zero with a BF_{10} of 48.1; therefore, the null hypothesis is rejected with strong evidence.

Note that for both cases in Figure 34, the standard difference δ is asymmetric and skewed towards zero. This is attributed to the distribution of the standard deviations σ_1 and σ_2 in the denominator of equation (41). By definition, the standard deviation is theoretically Chi-squared distributed (χ^2), which is a positively skewed distribution (Montgomery and Runger, 2014). To further verify the correct implementation of Kruschke's (2013) method to determine the standardised difference, δ was calculated for Kruschke's artificial datasets. The same results were obtained for all the test cases.

4.6 Chapter Summary

This chapter dealt with all the experimental and data analysis methods employed in this study. First, a high-level overview of experimental design and data analysis strategy was presented. This was followed by a detailed description of the physical experimental methods used to collect data. Furthermore, new methods for probabilistic soil parameter estimation and formal hypothesis tests for factors that influence Bevameter tests were presented. Now that the exact tests to be conducted and analysis procedures to be employed are established, we may proceed to view the experimental results.

CHAPTER 5

Results and Discussion

"Progress in science comes when experiments contradict theory."

-Richard P. Feynman[5]

[5] AZ Quotes (2022) *Richard P. Feynman*. Available at: https://www.azquotes.com/quote/530373 (Accessed: 7 August 2022).

5. Results and Discussion

5.1 Preamble

The presentation of the results follows the same order as the five independent variables listed in the experimental design in Table 11. More specifically, this chapter is organised as follows:

After performing the soil preparation investigation, an issue became apparent where the shear stress exhibited an increasing non-asymptotic form. The phenomenon has significant implications for all shear tests in this study. It is therefore treated separately in section 5.3 before analyzing the remainder of the test data. For each IV in sections 5.4 to 5.6, the raw data is first presented and discussed. This is followed by parameter estimation and hypothesis testing. Section 5.7 gives a holistic overview of parameters identified across the independent variables. Finally, section 5.8 discusses the limitations of this study.

5.2 The influence of soil preparation (Independent variables I & II)

The soil preparation method is not considered an intrinsic Bevameter test setup variable. However, it is an important aspect that will affect the in situ soil strength and the repeatability of the tests. The strategy employed is first to explore the terrains in situ vertical and horizontal stress response envelope. This is followed by selecting an appropriate soil state and investigating the repeatability of tests. This strategy maximises the number of soil states investigated while minimising the total number of tests.

5.2.1 Effect of soil preparation on pressure-sinkage (Independent variable I)

Figure 35 indicates the influence of the soil preparation method on the soil pressure-sinkage response. The soil preparation methods remained the same for all five steps in Figure 29 except for the compaction step; therefore, the soil preparation methods primarily reflect differences in soil density.

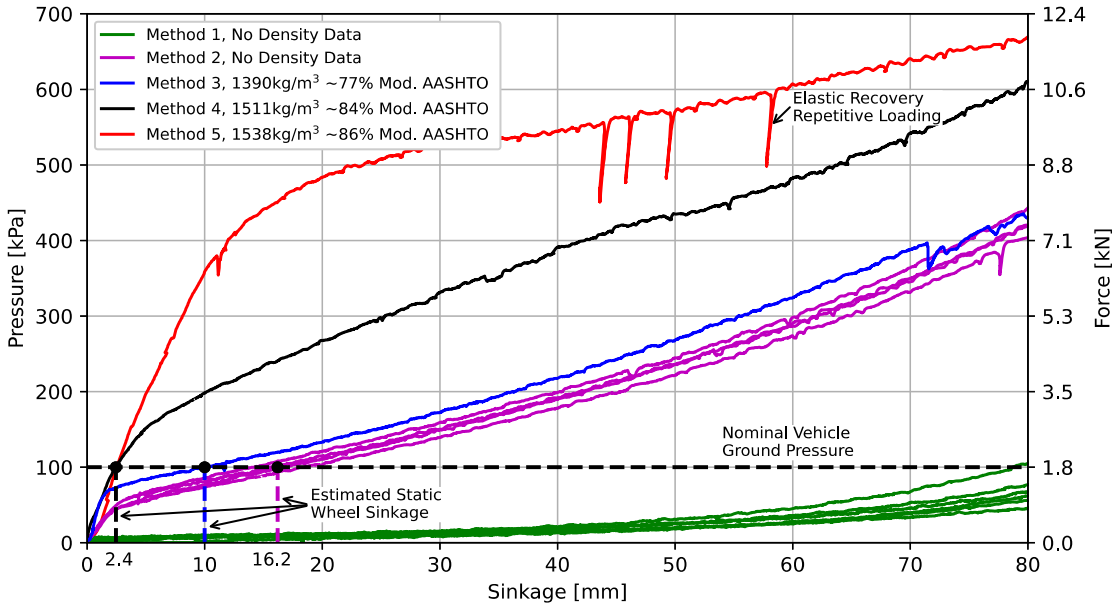

Figure 35-Influence of soil preparation methods on pressure-sinkage (150mm diameter circular plate).

From Figure 35, it is observed that the soil preparation method, and associated density, have a significant influence on the soil pressure-sinkage response. Method one (1) represents very loose soil, and Method five (5) represents dense soil near the maximum density achievable in field conditions using standard compaction methods. Method one (1) exhibits an exponentially increasing trend which is typical of Bevameter tests found in literature, such as the results indicated in Figure 6 (a). Method five (5) exhibits an initial linear increase that gradually transitions into a plastic flow. At the intermediate densities associated with methods 2-4, the soil exhibits a piecewise linear response with a sharp transition point between gradients. The results indicate that the soil's bearing capacity is highly sensitive to soil density, with small changes resulting in large changes in the bearing capacity.

Table 15 indicates the relative difference in soil bearing capacity for the different soil preparation methods. The results indicate an order magnitude difference exists in the soil bearing capacity.

Table 15-Relative soil bearing capacity for the different soil preparation methods.

Soil preparation method	Bearing capacity at 80mm sinkage [kPa]	Increase relative to method 1
1	64	-
2	418	653%
3	445	695%
4	611	954%
5	671	1048%

Note: See Table 13 for detail on the different soil preparation methods.

5.2.2 Effect of soil preparation on shear stress (Independent variable II)

Figure 36 indicates the influence of soil preparation methods and density on linear shear stress. Note that method one was not tested as the pressure-sinkage results from Figure 35 indicated that it would exceed the 80mm sinkage limit at 93kPa normal pressure even before applying lateral loads.

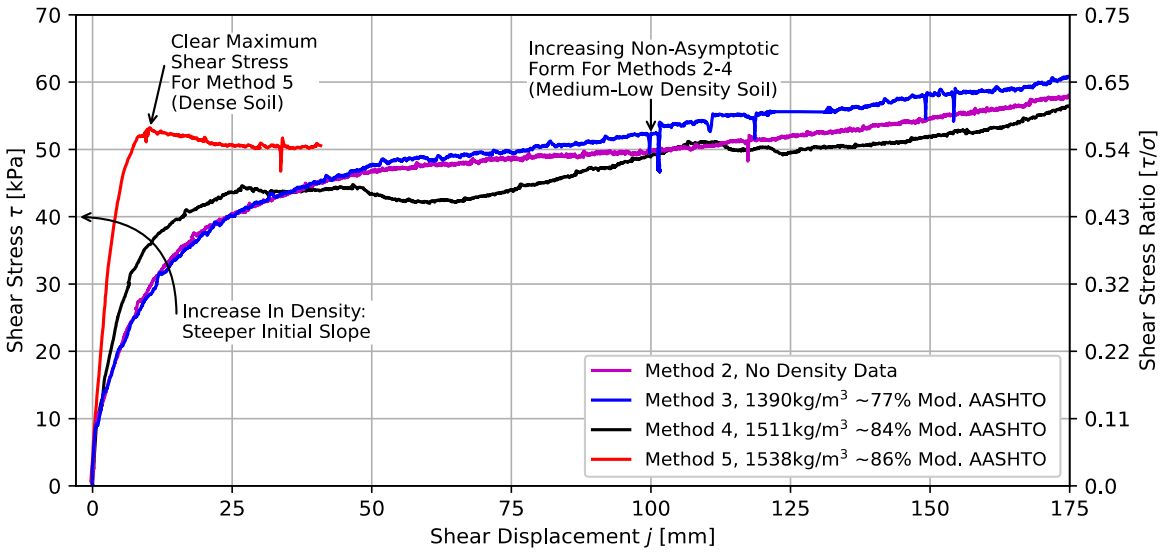

Figure 36-Influence of soil preparation methods on shear stress (linear shear, 93kPa normal pressure).

From Figure 36, it is observed that soil preparation has a less significant effect on shear stress compared to the influence it had on the pressure-sinkage. For method five, the soil exhibits a clear maximum shear stress. However, at lower soil densities associated with methods 2-4, the data exhibits no clear maximum shear stress with an increasing non-asymptotic form. This issue will be addressed in section 5.3. It is also observed that the soil density significantly affects the initial rate of stress increase.

5.2.3 Effect of soil preparation on identified soil parameters

Table 16 indicates the influence of soil preparation on the identified soil parameters. For the pressure-sinkage model, the Bernstein model from equation (2) is employed. In this case, the Bekker sinkage model is not advantageous since only a single plate size was used for the soil preparation investigation. The shear stress-displacement model employed the Janosi-Hanamoto model from equation (5). For this comparison, a 50mm displacement cut-off is selected. For visualization of the model fit, see Appendix G.

Table 16-Influence of soil preparation on the identified soil model parameter.

	Pressure-Sinkage model			**Shear stress-displacement model**	
Method	k [kN/m^{n+2}]	n [-]	R^2	K [mm]	R^2
1	485	1.75	0.812	-	-
2	419	0.94	0.973	11.8	0.994
3	339	0.83	0.978	11.1	0.959
4	235	0.56	0.993	6.1	0.994
5	157	0.33	0.934	2.9	0.836

Note: Determined using Bayesian parameter estimation. Parameter CI not indicated since no repeated tests were performed.

Table 16 indicates that as the soil compaction level increases, the sinkage coefficient k and sinkage exponent n both decrease significantly. Similarly, the shear deformation modulus decreases significantly as the soil compaction level increases. For the same soil but different soil compaction states, significantly different soil parameters are identified. This highlights that the Bekker soil characterisation approach is an empirical method that is highly dependent on the in situ soil conditions.

5.2.4 Selection of a soil preparation method

Based on the expected vehicle loads and soil response, soil preparation method three (3) is selected as the soil preparation method moving forward. Figure 35 indicates that this method lies halfway in the soil in situ bearing capacity envelope. Therefore, it represents a compromise in soil compaction

that is not too hard or too soft. At a nominal vehicle ground pressure of 100kPa, the static wheel sinkage is estimated to be 10mm. This is expected to be a realistic representation of "soft soil" likely encountered by agricultural vehicles. This represents the minimum sinkage under static conditions; dynamic shear slip sinkage is expected to contribute to further sinkage. Work by Ding *et al*. (2014) indicates that for a driven wheel, dynamic sinkage may increase up to 6-fold compared to static sinkage.

5.2.5 Repeatability of tests

The repeatability of pressure-sinkage and shear stress tests is indicated in Figure 37. Note that instead of the linear shear test used for exploration purposes in section 5.2.2, the repeatability is indicated for torsional shear as it forms the baseline for all further comparisons. Also, due to limited pressure-sinkage data, since it is not the main focus of this study, the repeatability is indicated for method two. Method two and three follow the same five soil preparation steps, except for the number of indirect tampering blows, and therefore is representative of the repeatability of the overall soil preparation procedure.

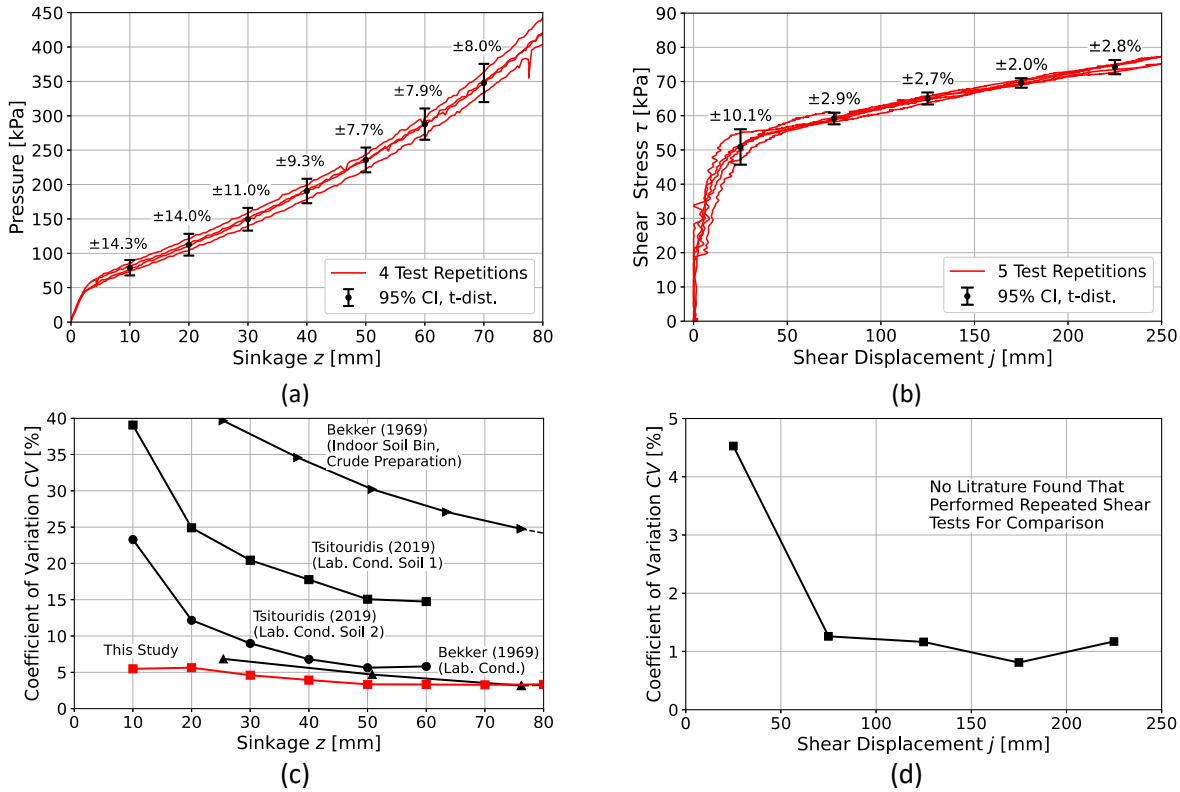

Figure 37-Repeatability of soil preparation. (a) Pressure-sinkage tests. (b) Shear tests (torsional shear, 300cm^2, 93kPa normal pressure). (c) Coefficient of variation of the pressure-sinkage test. (d) Coefficient variation of the torsional shear test.

From Figure 37, it is observed that the soil preparation method produces consistent and repeatable results for both pressure-sinkage and shear stress tests. Figure 37 (c) indicates that the pressure-sinkage coefficient of variation of 5.5% to 3.2% is on par with or exhibits a smaller variance than pressure-sinkage tests from literature with indoor laboratories. Figure 37 (d) indicates that the shear stress test coefficient of variation exhibits even lower variance with a range of 4.5% to 0.8%.

5.2.6 Summary of the soil preparation investigation

In summary, the soil's vertical and horizontal stress response envelope was explored, a soil preparation method was selected based on a realistic sinkage expected for the target vehicle on soft soil, and the repeatability investigated. With a repeatable soil preparation method established, we may proceed with the primary investigation on factors that influence Bevameter shear tests.

5.3 The non-asymptotic form of shear displacement data

5.3.1 Problems with the increasing non-asymptotic form

After collecting the data, an important issue became apparent where the shear stress-displacement curve exhibited a non-asymptotic and increasing form. Figure 38 indicates the typical shear stress-displacement form observed in this study. Other authors have noted similar observations (Reece, 1964; SAE, 1967; Bekker, 1969; Baladi, 1987; Okello, 1991). However, the phenomenon has scarcely been treated in detail by literature. As will become apparent, the phenomenon is highly problematic, and consensus has not been reached on how to address data of this form. This warrants a thorough investigation prior to performing further analysis with data of this form. For this investigation, the torsional shear test at 300cm^2 contact area and 70mm/s (5.5RPM) shear velocity will be used as an illustrative example. However, it should be noted that a similar increasing non-asymptotic form is also observed for all shear mechanisms, contact areas and shear velocities investigated in this study.

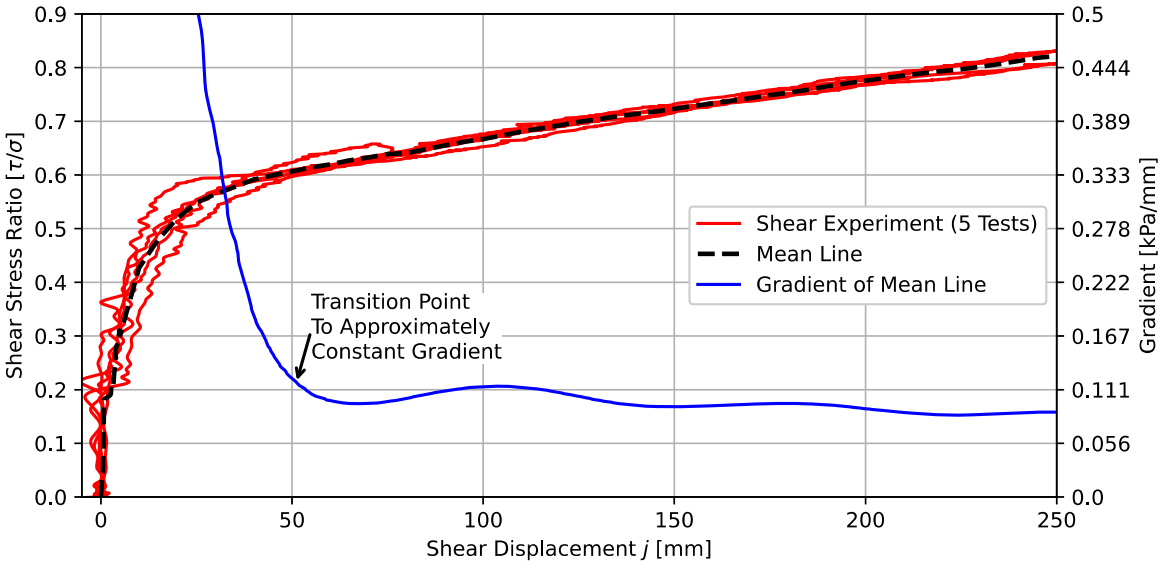

Figure 38-Example of the increasing non-asymptotic for shear stress (torsional shear, 93kPa normal stress, 300cm^2 area).

From Figure 38, it is observed that the shear stress tends to a linearly increasing non-asymptotic form. This is made clear by the gradient that appears to tend to a constant value instead of zero. Before 50mm, the gradient can be seen to change rapidly, after which it levels off and tends towards an approximately constant value. The non-asymptotic form immediately raises the following questions:

1. Why is the non-asymptotic behaviour problematic?
2. What is the cause of the non-asymptotic behaviour?
3. Do drag shear correction methods correct the non-asymptotic form?
4. Where should the shear displacement cut-off limit be for results of non-asymptotic form?

Question (1): Why is the non-asymptotic form problematic?

The first problem with the non-asymptotic form is that it never reaches a peak shear stress, making the determination of Mohr-Coulomb soil failure theory parameters arbitrary. Figure 39 illustrates the influence of the shear displacement cut-off selection on the identified Mohr-Coulomb parameters. Figure 39 was generated using the shear stress-displacement data from Figure 38 and single shear tests performed at 56kPa and 127kPa normal pressure (shear stress-displacement curves not indicated).

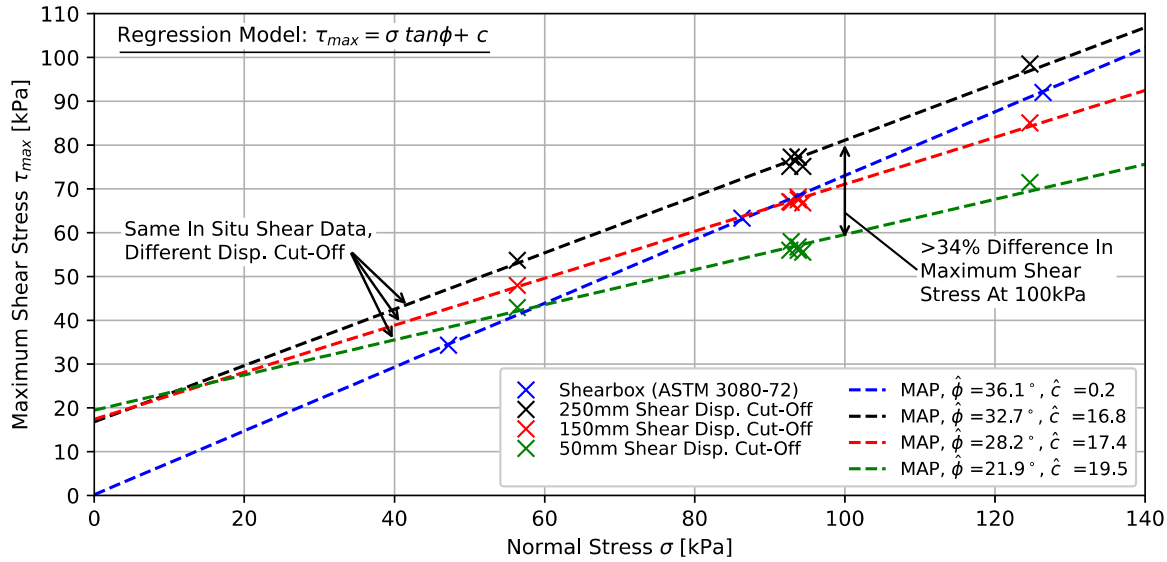

Figure 39-Effect of the Bevameter shear displacement cut-off on Mohr-Coulomb parameters (torsional shear, 300cm² area).

Figure 39 indicates that for the same experimental data, the soil's internal friction angle can range from 21.9° to 32.7° depending on the cut-off selection. This is considered a significant difference and leads to a large (>34%) shear stress difference at higher normal pressures (>100kPa). For each cut-off selection, a supporting argument can be made. The 250mm cut-off corresponds with the SAE J939 (SAE, 1967) recommendation to cut off the data for the non-asymptotic form at half a shear annulus rotation. This results in an internal friction angle in the range expected for fine sandy soil (30° to 35°) (Upadhyaya *et al.*, 1994). However, the SAE J939 recommended cut-off is also arbitrary as the shear stress continues to increase with the same trend past 250mm. It can also be argued to cut off the displacement once the gradient reaches an approximately constant value, e.g. at 50mm in Figure 38. However, this cut-off results in low friction angle of 21.9°, which is lower than expected for sandy soil.

A second problem with data of increasing non-asymptotic form is the high maximum shear stress to normal stress ratio of up to 0.81 observed in Figure 38 (with a further increase observed past 250mm displacement). This is considered unrealistically high for off-road vehicle traction prediction on soft soil and is on par with, or exceeds, the peak friction coefficient of agricultural tyres on a dry concrete road surface, which typically exhibits values in the range of 0.75-0.85 (Becker and Els, 2022).

The third problem is that a review of the state of the art shear stress-displacement models in He *et al.* (2019a) indicates that no models exist to accommodate the increasing non-asymptotic form. Furthermore, the basis for most shear displacement models is the maximum stress from the Mohr-Coulomb failure criterion (He *et al.*, 2019a). However, in this case, the maximum stress is arbitrary.

Question (2): What is the cause of the non-asymptotic behaviour (Applicable to all shear mechanisms)?

Postulate (1): The phenomenon is likely only observed because of the soil type. Highly cohesive soil is known to reach peak shear strength rapidly, after which it exhibits a weakening behaviour with an increase in shear displacement. In contrast, cohesion-less soils take longer to reach peak shear stress. However, asymptotic rather than increasing non-asymptotic behaviour is expected.

Postulate (2): Experimental evidence suggests the phenomenon is attributed to in situ boundary conditions of Bevameter testing. Laboratory tests conducted on the same soil indicated the soil reached failure in the expected asymptotic manner (see Appendix E). Therefore, the non-asymptotic phenomenon is not an inherent soil property and must be attributed to the in situ test conditions.

Postulate (3): Another postulate, with experimental evidence, is that the in situ soil density significantly influences the non-asymptotic behaviour. Figure 36 indicates that when the soil is highly compact, it behaves asymptotically. However, at intermediate and lower soil densities, it exhibits non-asymptotic behaviour. It is theorized that at intermediate and low densities, the shear displacement acts to compact the surrounding soil, resulting in an increase in strength as the surrounding soil increases in density. However, for the semi-infinite boundary condition, a large displacement is necessary to reach maximum compaction.

Postulate (4): Another postulate, with experimental evidence, is that the soil "fallback" artificially increases the measured shear strength. The phenomenon is indicated in Figure 40 for torsional shear. This occurs when the soil surrounding the shear plate collapses and falls back onto the shear plate, creating additional friction on the shear ring and shear ring posts. The soil fallback increase with sinkage as more soil falls back onto the shear plate, causing more drag and possibly contributing to the increasing non-asymptotic form. Figure 40 (a) indicates that the soil fallback initiates from the centre soil area while the surrounding soil tends to bow outwards and does not contribute to contact drag. The soil fallback mechanism is different for linear shear and will be discussed later in section 5.4.

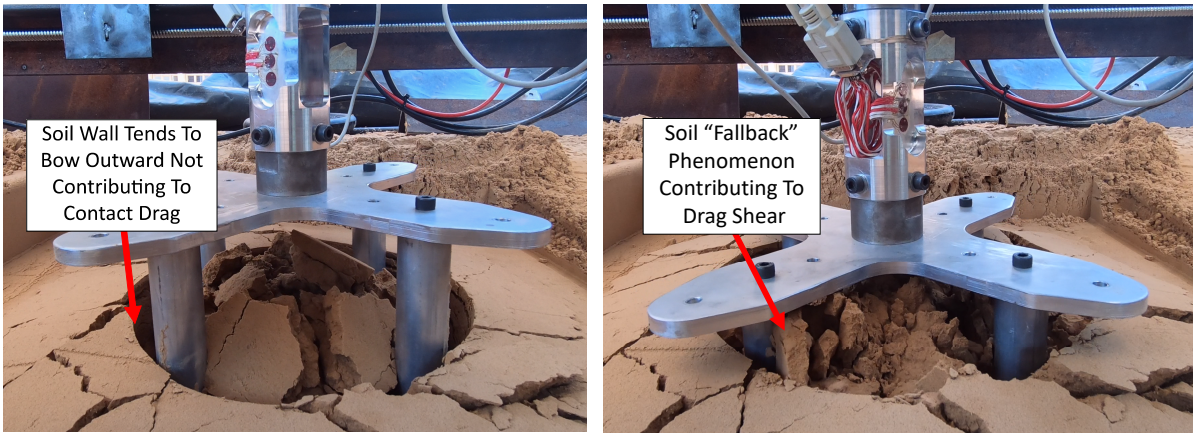

(a) (b)

Figure 40-Soil fallback phenomenon (torsional shear, 300cm² area). (a) j =70mm. (b) j =250mm.

Postulate (5): Grouser lateral drag is another known factor that contributes to increased measured shear stress for both linear and torsional shear. The areas $2\pi r_0 h$ and $2\pi r_i h$ in Figure 41 (a) indicates the additional shear surface area for the torsional shear mechanism. The area $2hl$ in Figure 41 (b) indicates the additional shear surface area for the linear shear mechanism. The grouser lateral drag may not be constant with sinkage. The pressure-sinkage analogy suggests that the elementary stresses, including lateral stresses, increase with sinkage, thereby possibly contributing to the non-asymptotic form.

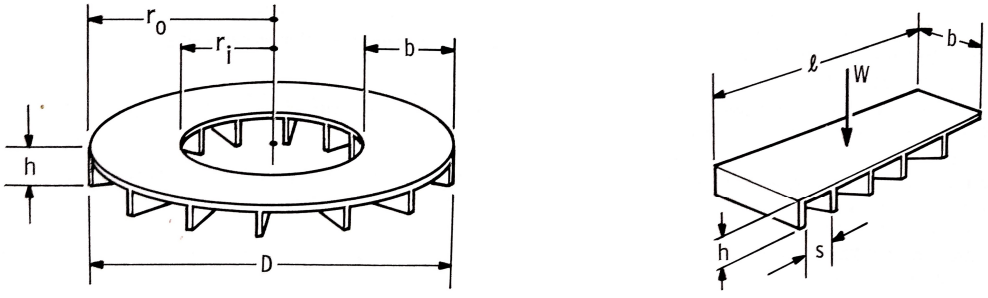

(a) (b)

Figure 41-Grouser lateral drag areas (Bekker, 1969). *(a) Rotational shear instrument. (b) Linear shear instrument.*

Postulate (6): Finally, the linear shear mechanism exhibits bulldozing of the leading edge of the first grouser, as indicated by area hb in Figure 41, which increases the measured shear strength. The bulldozing force may or may not be constant with shear sinkage and may also contribute to the increasing non-asymptotic form. This additional bulldozing force is not present for rotational shear. However, as will be discussed later in section 5.4, linear shear exhibits lower non-asymptotic behaviour. This indicates that other factors are more prominent than the bulldozing effect.

The analysis of the possible causes of the increasing non-asymptotic behaviour indicated it might be caused by a wide range of physical phenomena. The next section will investigate experimental methods used to compensate for some of these effects that artificially increase the measured shear strength.

Question (3): Do drag shear correction methods correct the non-asymptotic form?

Bekker's correction method two from section 2.3.7 is employed to determine the contribution of drag shear. The only configuration tested is at 5mm lift height ($z = -75$mm) and not multiple lift heights as suggested by Bekker (1969). The 5mm lift height ensures the bottom surface does not contribute twice to the shear measurement. Figure 42 indicates the results from the drag shear test.

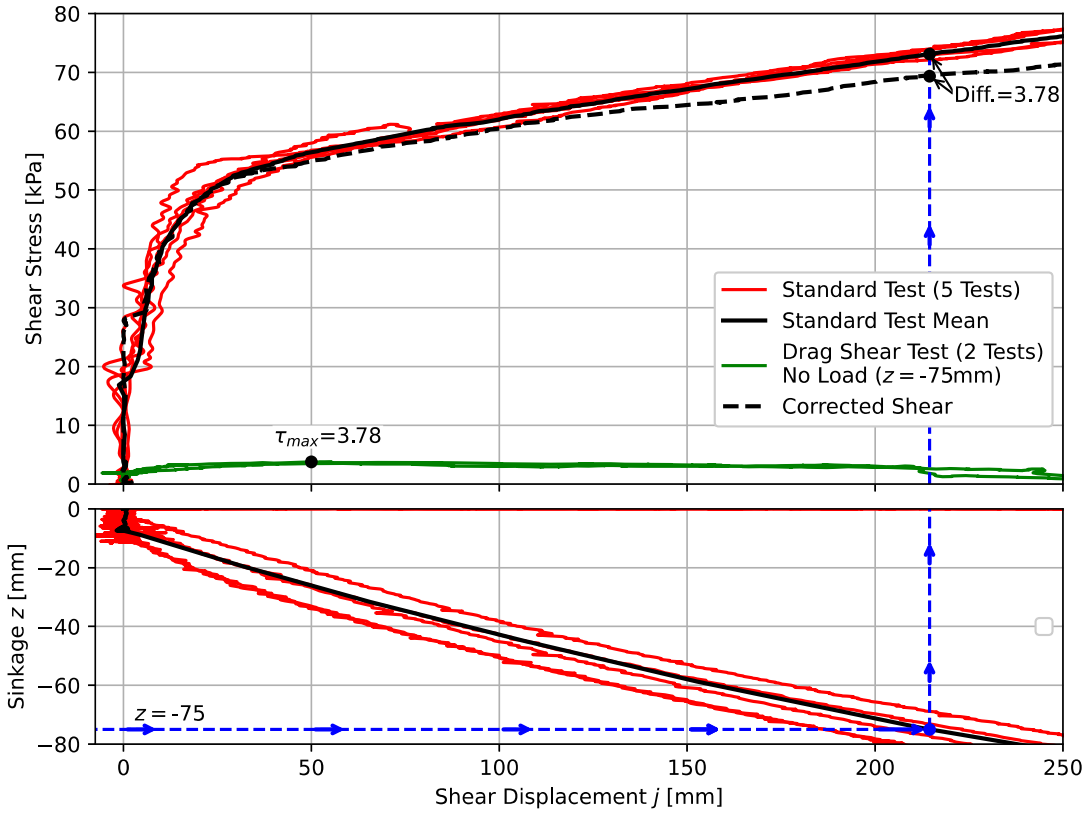

Figure 42-Drag shear correction using Bekker's method (torsional shear test, 93kPa normal pressure, 300cm² contact area).

From Figure 42, it is observed that drag shear has a small contribution relative to the total shear. At 75mm sinkage, the contribution is only 3.8kPa out of 73.1kPa (5.0%). At low shear displacement (<100mm), the effect has a negligible <1% difference. The evidence suggests that the non-asymptotic form cannot fundamentally be attributed to drag shear. The findings are in conflict with the findings by Reece (1964) and Bekker (1969). They claimed that drag shear correction methods fully corrects the non-asymptotic form to the asymptotic form for sandy soil.

Drag shear could only be measured for torsional shear. Measuring drag shear for linear shear is significantly more difficult. Reece (1964) and Bekker (1969) suggest digging a trench in front of the

linear shear plate and conducting a drag measurement. However, this practice is questionable as it disturbs the soil and alters the boundary conditions.

For further analysis and comparisons in this study, drag shear correction is not applied. This is for two reasons. Firstly, it is not very significant. Secondly, it should be applied to both torsional and linear shear mechanisms for a fair comparison. However, it is not practical to do so for linear shear.

Question (4): Where should the displacement cut-off limit be for results of non-asymptotic form?

The drag correction methods did not address the problem of displacement cut-off selection. Unless stated otherwise, the 250mm cut-off recommended by the SAE J939 standard is followed for data of non-asymptotic form. This leads to a more reasonable internal friction angle estimate than using an earlier cut-off. Bekker (1969) also frequently used a 250mm shear displacement cut-off.

5.3.2 Selection of a shear stress-displacement model

This section aims to find an empirical model that captures the non-asymptotic data. Without a model, data of this form cannot be applied in soil wheel interaction modelling. A representative model is also required to identify meaningful soil parameters and to enable regression-based hypothesis testing.

Evaluation of existing empirical models

Although non-asymptotic data has been reported by a number of authors (Reece, 1964; SAE, 1967; Bekker, 1969; Baladi, 1987; Okello, 1991), none of the nine (9) state of the art shear stress-displacement equations reviewed by He *et al.* (2019a), are catered to the increasing non-asymptotic form. Reece (1964) and Bekker (1969) recommended using correction methods to transform non-asymptotic data into an asymptotic form so that standard equations could be used. However, experimental evidence in section 5.3.1 indicates correction methods had negligible influence. The only literature that explicitly recommends a model for the increasing non-asymptotic form is the SAE J939 standard which recommends the Janosi-Hanamoto equation from equation (4) with a 250mm cut-off.

Figure 43 indicates equation (5) fitted to the torsional data using the Bayesian parameter estimation method detailed in section 4.4. From Figure 43, it is observed that the SAE J939 recommendation does not fit the data well with a coefficient of determination of $R^2 = 0.557$. The model is not representative of the data and the associated soil parameters are not meaningful. The model therefore exhibits large epistemic model uncertainty (lack of understanding of the physical process).

Proposal of a new shear stress-displacement model for data of increasing non-asymptotic form

A new model is proposed for data of the non-asymptotic form. The following reasons justify the need for a new model: 1) existing models and recommendations from literature represent the non-asymptotic data poorly (to the extent that standard models are not usable), 2) drag shear correction methods indicate negligible influence on the non-asymptotic form (therefore the non-asymptotic form is considered a physical phenomenon) and 3) no evidence indicates that the data is invalidated and should be cut-off before the onset of the increasing non-asymptotic trend. The proposed model takes inspiration from the Janosi-Hanamoto model. For reference, equation (5) is repeated,

$$\tau(\tau_{max}, j, \boldsymbol{\theta} = \{K\}) = \tau_{max}(1 - e^{-\frac{j}{K}})$$

The proposed model is indicated in equation (43),

$$\tau(\tau_{max}, j, \boldsymbol{\theta} = \{K, Y, m\}) = \tau_{max}\left[\left(1 - e^{-\frac{j}{K}}\right)Y + jm\right] \quad (43)$$

The model adds two additional physically interpretable parameters: a linear gradient term m and a scaling term Y. The linear term m allows the data to increase linearly with shear displacement j. The non-dimensional scaling term Y marks the maximum stress of the Janosi-Hanamoto portion of the model as a ratio of τ_{max}. The term $1-Y$ indicates the fraction (or %) of the maximum stress attributed to the non-asymptotic linear trend. The linear term m is multiplied by τ_{max} to scale the gradient with maximum shear stress, as it was observed that the non-asymptotic gradient tends to increase with τ_{max}. The units of m are partially non-dimensionalized and expressed in inverse meter [m^{-1}]. Multiplying m by τ_{max} at a specific normal pressure σ, expresses the units in [Pa/m]. The shear deformation modulus K retains the same practical meaning and indicates the distance from the τ-axis to the intercept of the tangent at the origin and the horizontal line $\tau = \tau_{max}Y$ (previously $\tau = \tau_{max}$).

In some cases, it is desirable to prevent linear extrapolation in the shear displacement direction. For these cases, equation (44) is proposed. Equation (44) should not be used for fitting and only to limit extrapolation to ensure the shear-displacement curve passes through the Mohr-Coulomb line.

$$\tau(\tau_{max}, j, \boldsymbol{\theta} = \{K, Y, m\}) = \min\left(\tau_{max}\left[\left(1 - e^{-\frac{j}{K}}\right)Y + jm\right], \tau_{max}\right) \tag{44}$$

What is objectionable about the proposed model is that it introduces two non-established empirical parameters. However, Bevameter soil characterisation and application thereof is fundamentally an empirical method. Literature indicated that the Bekker soil parameters are not considered invariant or "true" soil parameters (Reece, 1964; He *et al.*, 2019a). The empirical philosophy is supported by Bekker (1969), who states that using a Bevameter to identify "true" soil parameters, including Mohr-Coulomb parameters, is unreasonable. This is exemplified by Bekker's original shear-displacement model, which is modelled after the natural frequency curve of an overdamped spring-mass-damper system, whose parameters carry no strict quantifiable meaning for soil shear stress (Bekker, 1956).

Figure 43 compares the proposed model to the model recommended by the SAE J939 for data of non-asymptotic form. From Figure 43, it is observed that the proposed model fits the data significantly better than the SAE J939 recommendation. The likelihood ratio is 6.34 in favour of the proposed model, indicating the likelihood of observing the data is six times higher for the proposed model than the SAE J939 recommended model. However, the likelihood does not consider model complexity and will always favour models with more parameters. The Bayes Factor includes a penalty for more parameters. The Bayes Factor is 12.64 in favour of the proposed model (classified as strong evidence).

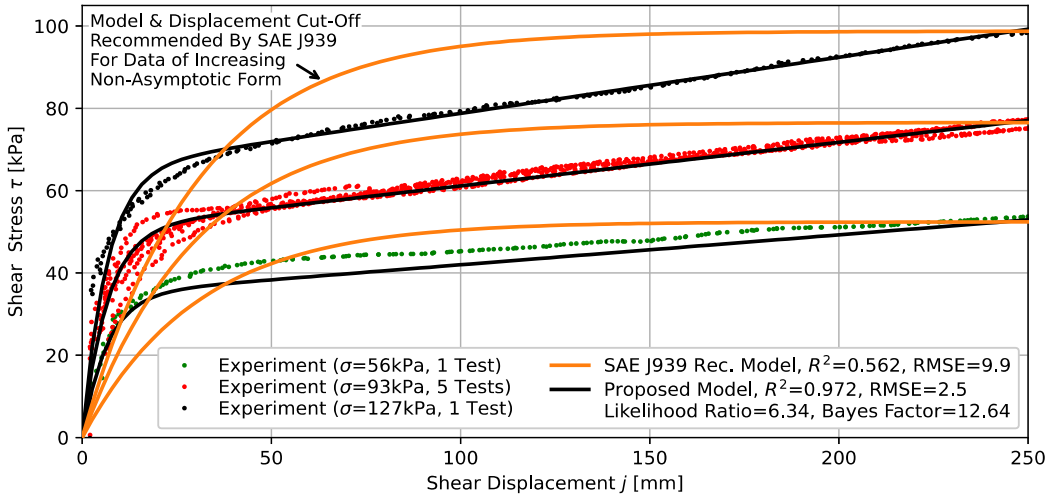

Figure 43-Proposed model vs. SAE J939 recommended model (torsional shear, 300cm², 250mm cut-off).

Figure 44, indicates that the proposed model can also accommodate data that appears asymptotic in shape. The data in Figure 44 is artificially cut off at 50mm and ignores the fact that it does not reach maximum shear stress. After fitting, equation (44) was used to prevent extrapolation in the shear displacement plane. In this case, the proposed model also gives a better fit. The likelihood ratio is 1.78, and Bayes Factor is 3.56 in favour of the proposed model. Even for this case, taking the penalty for more complex models into account, the data favours the more flexible model. This is confirmed with an RMSE of 4.7 vs. 3.8, respectively. Although it does not present a large improvement, it shows that the developed model can accommodate both non-asymptotic and asymptotic data. The proposed model is therefore "backwards compatible" with existing theory; if the regression deems it beneficial, the model can take on the form of the Janosi-Hanamoto model with $Y = 1$ and $m = 0$.

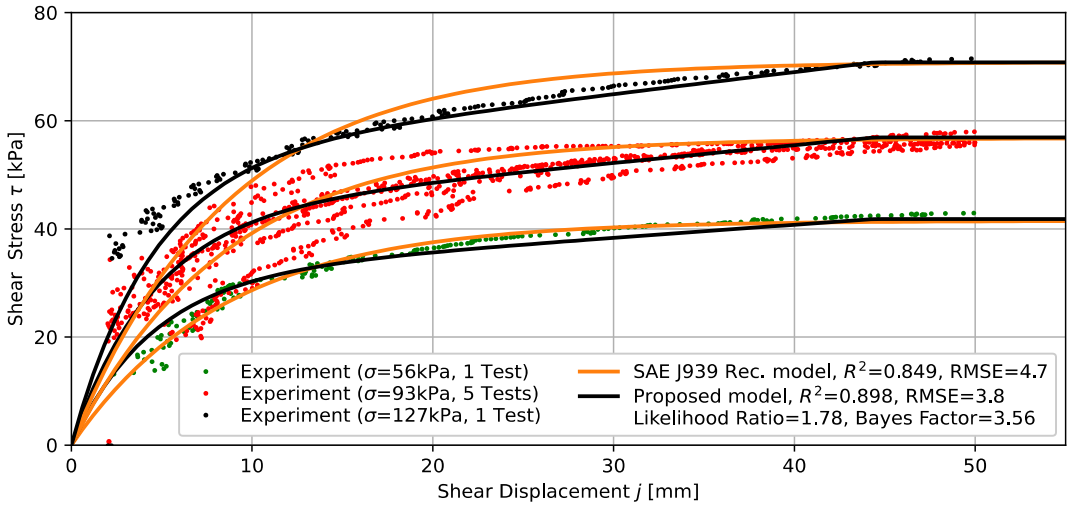

Figure 44-Proposed model vs. SAE J939 recommended model (torsional shear, 300cm², 50mm cut-off).

Figure 45 indicates the proposed model evaluated at out of sample pressures and shear displacements.

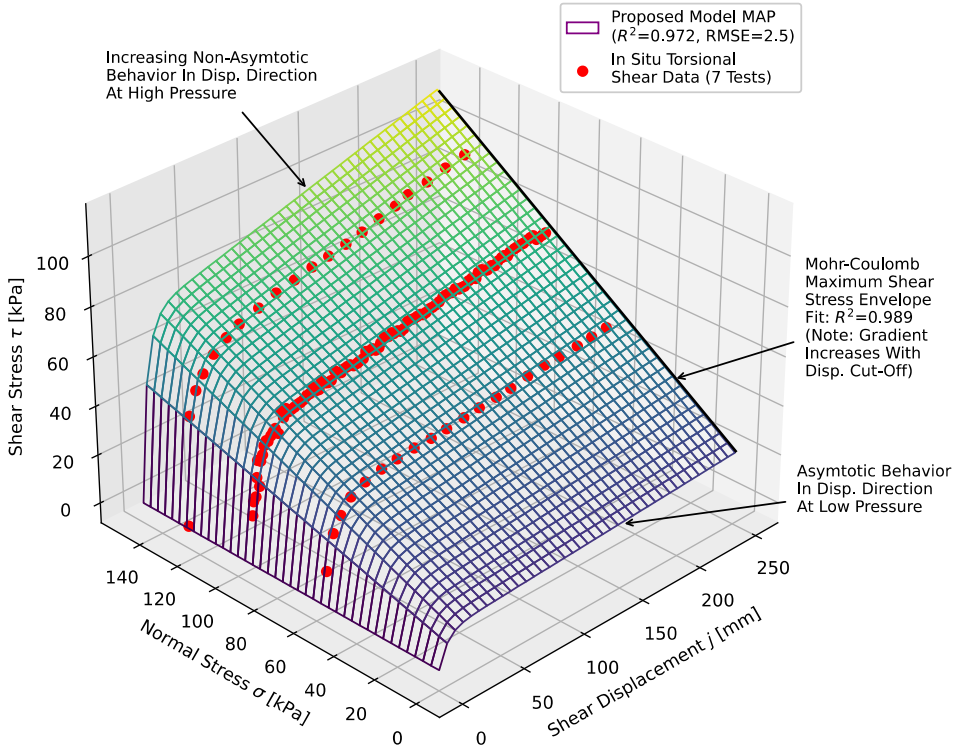

Figure 45-3D plot of Bevameter shear stress data and proposed model fit (torsional shear, 300cm², 250mm cut-off).

Figure 45 highlights that the soil shear stress response is a 3-Dimensional surface that varies both in the pressure direction and the shear displacement direction. Note that both shear sinkage and normal pressure result in an increase in the measured shear stress. At low pressures, the shear stress exhibits asymptotic behaviour in the displacement direction. This may explain why the increasing non-asymptotic behaviour has not been recently reported, as recent literature tends to test at very low normal pressures, often significantly lower than 40kPa (see Appendix H for typical normal pressures used by literature). However, at realistic vehicle ground pressures of $\pm$100kPa expected for the target vehicle and large agricultural vehicles, a significant non-asymptotic shear behaviour is observed.

5.3.3 Summary of critical findings regarding the non-asymptotic form

A) The non-asymptotic behaviour is a result of in situ nature of Bevameter testing; laboratory shear test of the same soil at equivalent normal loads does not exhibit this behaviour.

B) A number of different physical phenomena likely contribute to the non-asymptotic form. In order to isolate and determine the magnitude of the contributing factors requires further investigation.

C) Drag shear correction methods have a minor influence on non-asymptotic form. The non-asymptotic phenomenon cannot fundamentally be attributed to the effects of drag shear.

D) Soil density has a significant influence on non-asymptotic behaviour. Dense soil behaves in the expected asymptotic manner. Intermediate and low-density soil exhibits increasing non-asymptotic behaviour.

E) The applied normal pressure has a significant influence on non-asymptotic behaviour. At low pressure, the shear stress tends towards asymptotic behaviour, while at higher pressures ($\geq$93kPa) exhibits significant increasing non-asymptotic behaviour.

F) The observed maximum shear stress to normal stress ratio is very high, with a shear stress ratio of up to 0.81. This is likely attributed to a number of factors that cause additional shear stress for in situ Bevameter tests (e.g. lateral grouser drag, bulldozing, etc.).

G) The shear cut-off choice significantly affects the identified Mohr-Coulomb failure criteria parameters. For the non-asymptotic form, the parameters are considered arbitrary as it never reaches peak shear stress, with the shear strength continually increasing with shear displacement.

H) Current terramechanics shear-displacement theory breaks down for data of increasing non-asymptotic form. The model recommended by current standards for data of non-asymptotic form leads to a poor model fit that is not representative of the data with an R^2 of 0.56. A new model is proposed for data of this form. The model evidence for the proposed model is significantly higher than existing model recommendations, with a BF of 12.6 and $R^2 > 0.97$. The proposed model can also accommodate data of asymptotic form and incorporates physically meaningful parameters.

5.4 The influence of shear mechanism (Independent variable III)

5.4.1 Experimental results

Before quantitatively comparing linear and torsional shear, it is beneficial to compare the physical processes side by side. Figure 46 indicates the shear evolution at equivalent linear displacement.

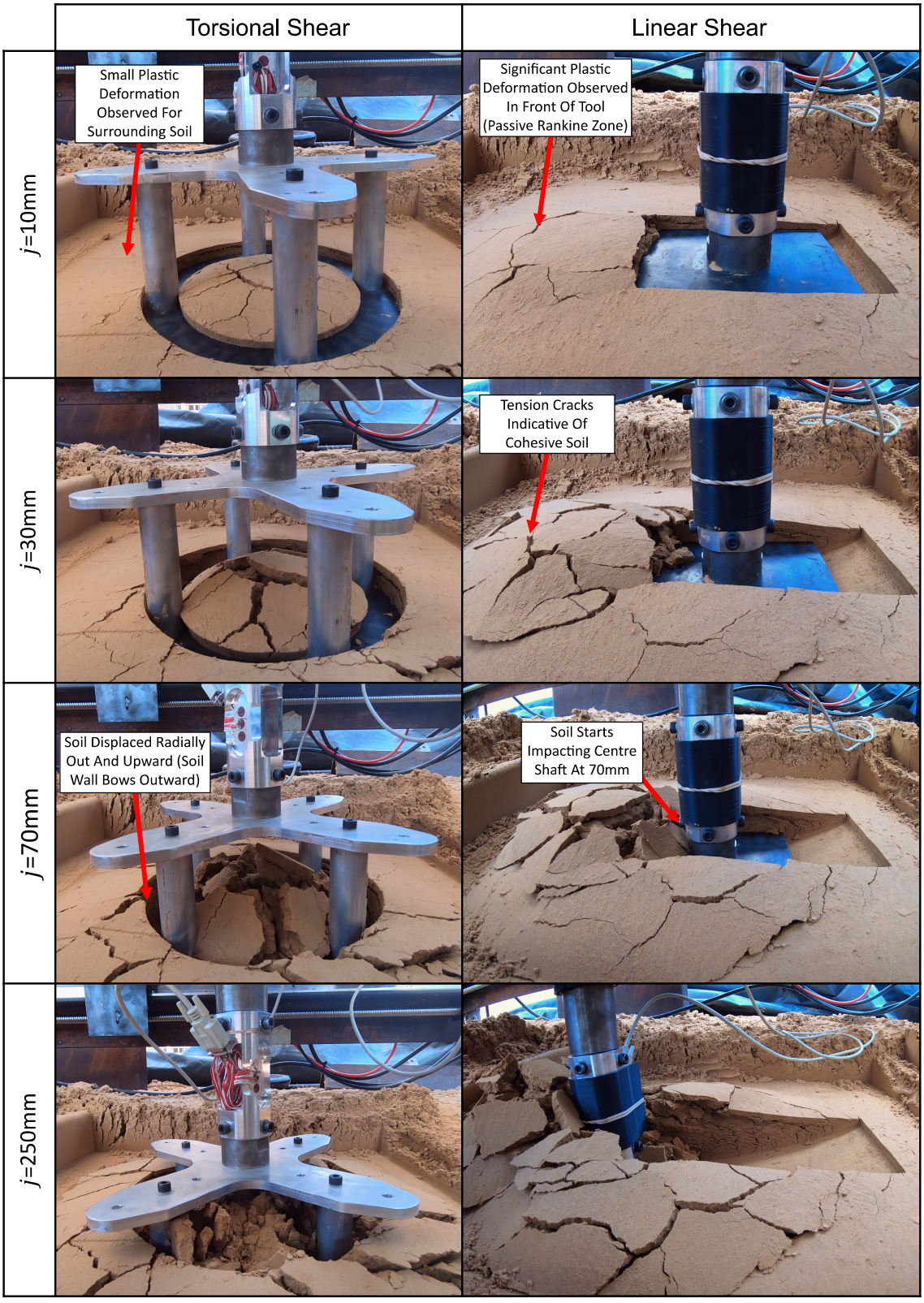

Figure 46-Torsional vs. linear shear displacement evolution (93kPa normal pressure, 300cm^2 contact area).

Figure 47 numerically quantifies the 3D soil displacement of the different shear mechanisms. The 3D scans were performed using the photogrammetry technique from section 4.3.2.

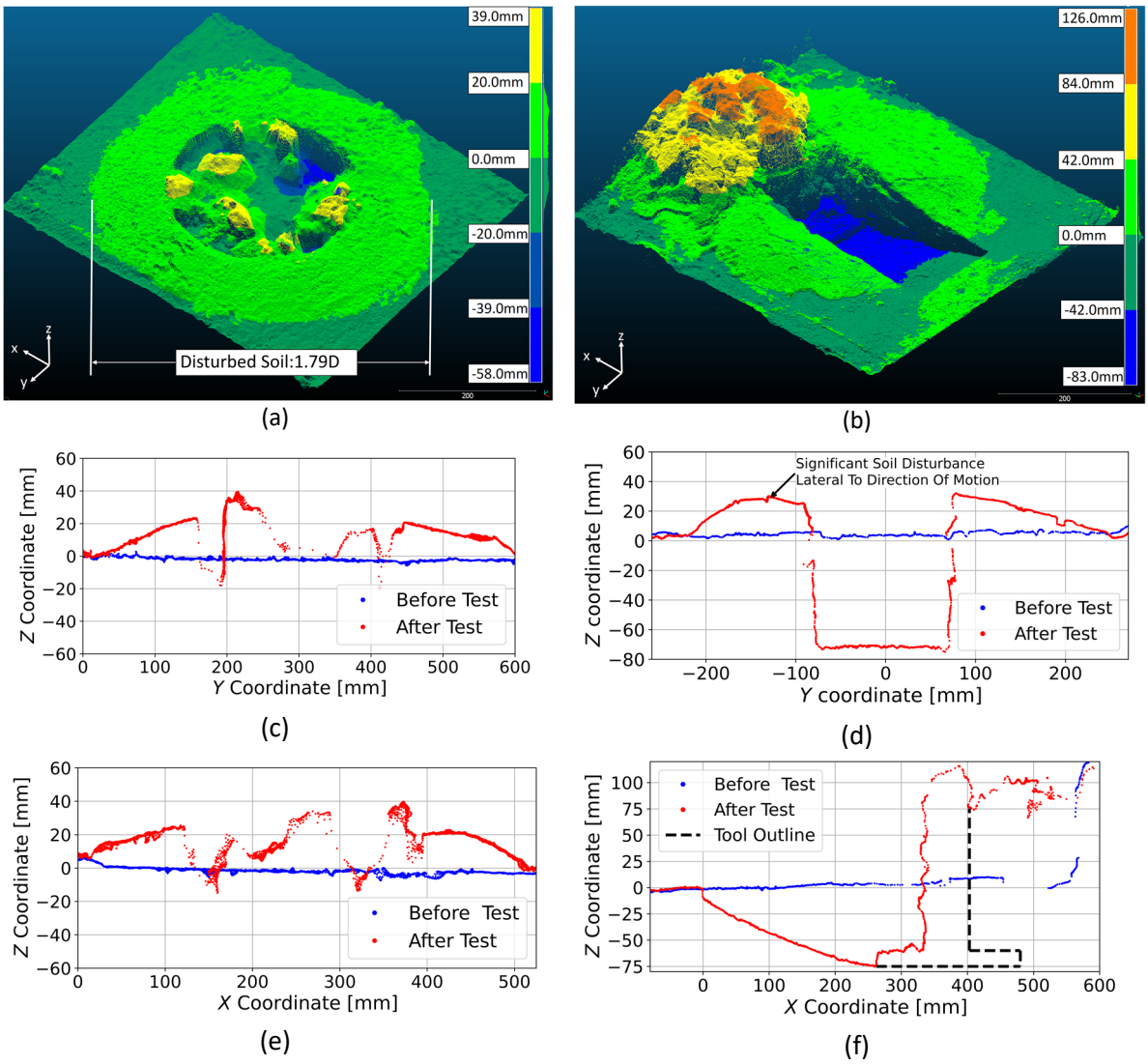

Figure 47-3D scan before and after Bevameter shear tests (93kPa normal pressure, 300cm^2). (a) Torsional shear test point cloud. (b) Linear shear test point cloud. (c) Torsional shear cross-section in Y. (d) Linear shear cross-section in Y. (e) Torsional shear cross-section in X. (f) Linear shear cross-section in X.

From Figure 46, it is observed that the physical shear mechanism is significantly different for linear and torsional shear. For linear shear, the soil tends to form a passive Rankine failure zone that extends in front of the shear tool in the direction of motion. The shear tool is observed to "plough" underneath the soil and experience significant bulldozing of the first grouser. At 70mm displacement, the centre shaft starts to engage the soil, arguably invalidating further shear measurements. Figure 47 (d) indicates linear shear exhibits a 3D soil failure pattern with significant soil disturbance (>30mm) lateral to the tool direction of motion.

Figure 46 and Figure 47 indicate that the torsional shear mechanism tends to push the soil radially out and upward transverse to the direction of the annular ring displacement. The soil failure beneath the torsional shear ring is complex and differs significantly from the linear shear mechanism. Unfortunately, the failure pattern beneath the soil surface is not observable. However, no evidence indicates torsional shear is invalidated at larger shear displacements, as is the case for linear shear.

Shear stress vs. displacement at nominal vehicle ground pressure

Figure 48 compares linear and torsional shear stress at nominal vehicle ground pressure.

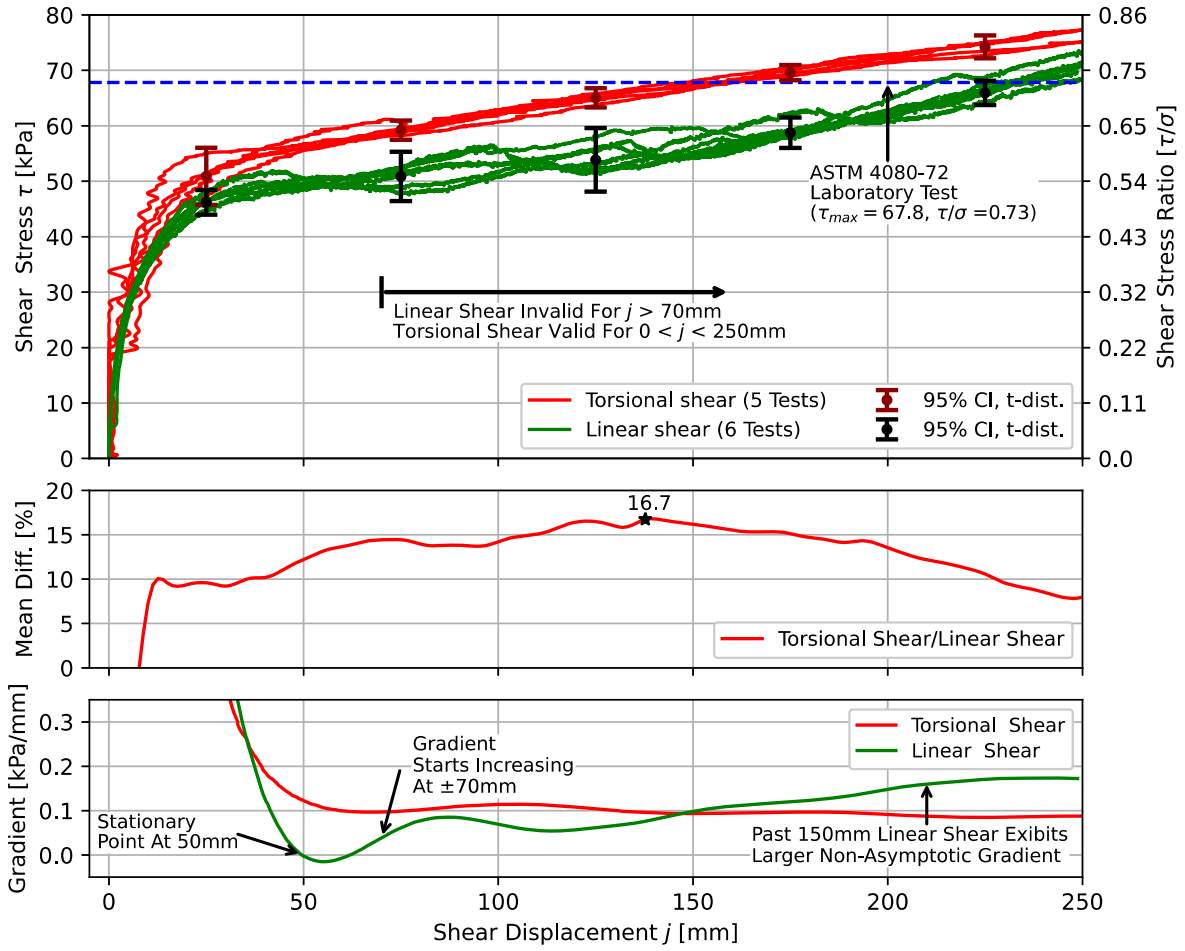

Figure 48-Torsional vs. linear shear stress (93kPa normal pressure, 300cm²).

Figure 48 indicates a significant difference is observed between linear and torsional shear with a clear separation between the 95% confidence intervals. Torsional shear exhibits greater shear across all shear displacements with a maximum difference of 16.7%. This is contrary to the expected result. Linear shear includes a bulldozing force due to the leading edge of the first grouser not being present for torsional shear. Furthermore, the centre shaft of the linear shear tool is in contact with the soil, artificially increasing the measured shear stress. Despite these factors, rotational shear still exhibits larger shear stress. One hypothesis for the difference is the larger perimeter, and therefore lateral grouser area, of the torsional shear mechanism. Another hypothesis is that linear shear forms a passive Rankine failure zone in front of the tool in the direction of motion, as indicated by the plastic failure far in front of the tool in Figure 46 at $j = 10$mm, weakening the soil in the direction of motion.

The gradient in Figure 48 indicates the linear shear exhibits less non-asymptotic behaviour than torsional shear up to 150mm displacement, with the gradient reaching a stationary point at 50mm. At 70mm, the centre shaft starts to touch the soil, after which the gradient increases monotonically until it exceeds torsional shear at 150mm. The stationary point at 50mm indicates linear shear might exhibit asymptotic behaviour at nominal vehicle ground pressures, not considering the centre shaft effects.

Shear stress vs. displacement at different normal pressures

Figure 49 compares linear vs. torsional shear stress at different normal pressures. For clarity, only the mean shear stress-displacement response at each pressure is indicated.

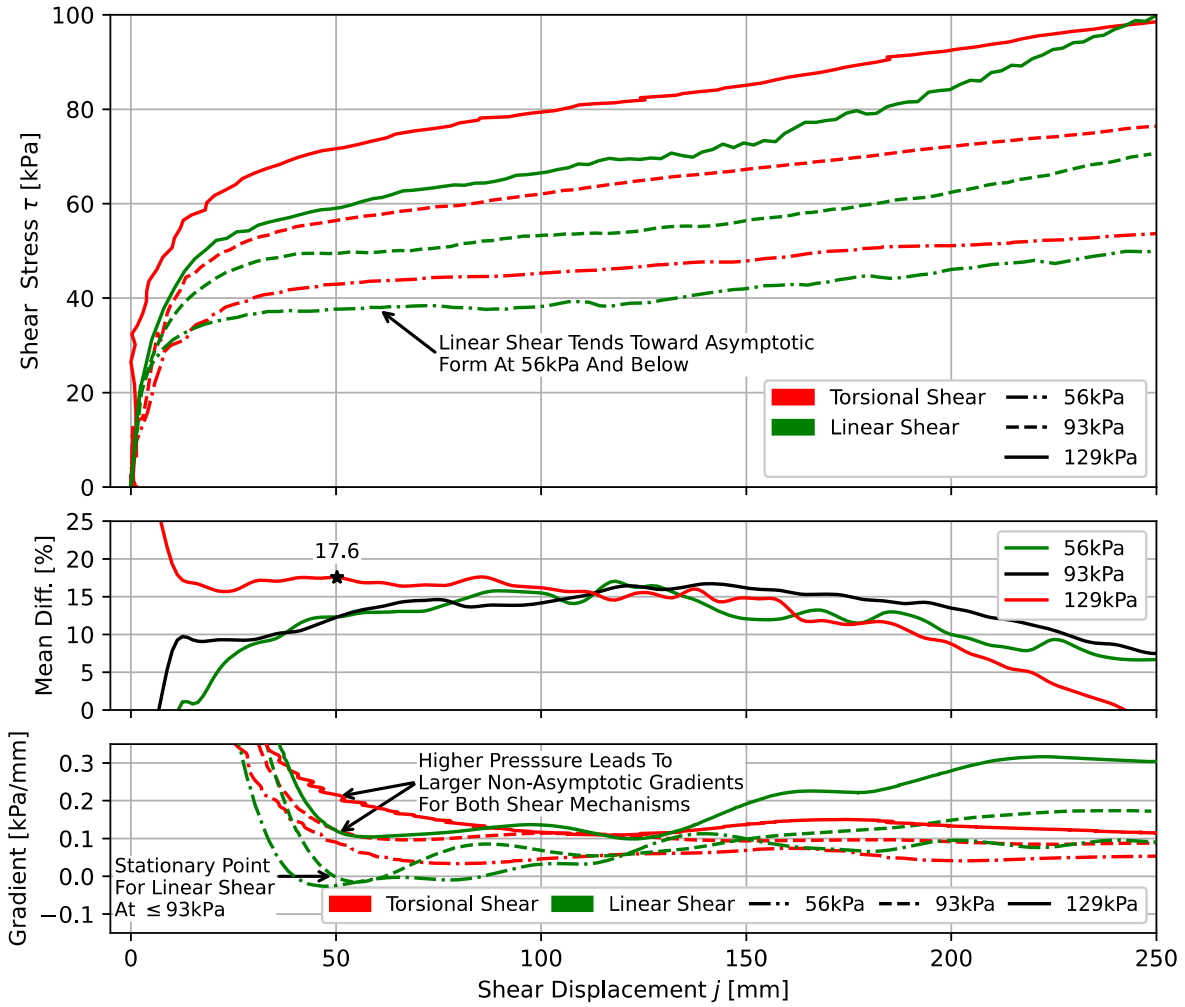

Figure 49-Torsional vs. linear shear stress at different normal pressures (300cm²).

Figure 49 indicates that torsional shear exhibits significantly larger shear stress across all normal pressures, with a maximum difference of 17.6%. Higher normal pressures lead to larger non-asymptotic gradients for both shear mechanisms, with significant non-asymptotic gradients observed at 129kPa. This confirms the observation from section 5.3.2 that the non-asymptotic behaviour is a pressure-dependent phenomenon. Linear shear is observed to exhibit a lower increasing non-asymptotic tendency than torsional shear, reaching temporary stationary points at 93kPa and lower pressures. After 70mm shear displacement, the linear shear gradients start to increase monotonically, while torsional shear gradients remain relatively constant at positive non-zero values for all pressures.

5.4.2 Soil parameter estimation

The best evidence from section 5.3.1 suggests torsional shear displacement should be cut-off at 250mm, as it corresponds with recommendations from literature and leads to the most reasonable internal friction angle estimate. However, evidence from Figure 46 indicates linear shear is invalidated past 70mm shear displacement. Furthermore, Figure 48 and Figure 49 indicate that the linear shear mechanism exhibits a stationary point at 50mm. Therefore, the best evidence for the linear shear cut-off is 50mm. This leads to conflicting evidence for cut-off selection for the different shear mechanisms.

For a fair ***comparative*** analysis of identified soil parameters and not necessarily the "best" estimates for each individual shear mechanism, a shear cut-off of 50mm is selected. The newly proposed shear stress-displacement model from equation (43) is utilised as section 5.3.2 indicated it had higher model evidence than existing model recommendations for data cut-off at 50mm. The model MAP, estimated using the Bayesian regression method detailed in section 4.4, is indicated in Figure 50.

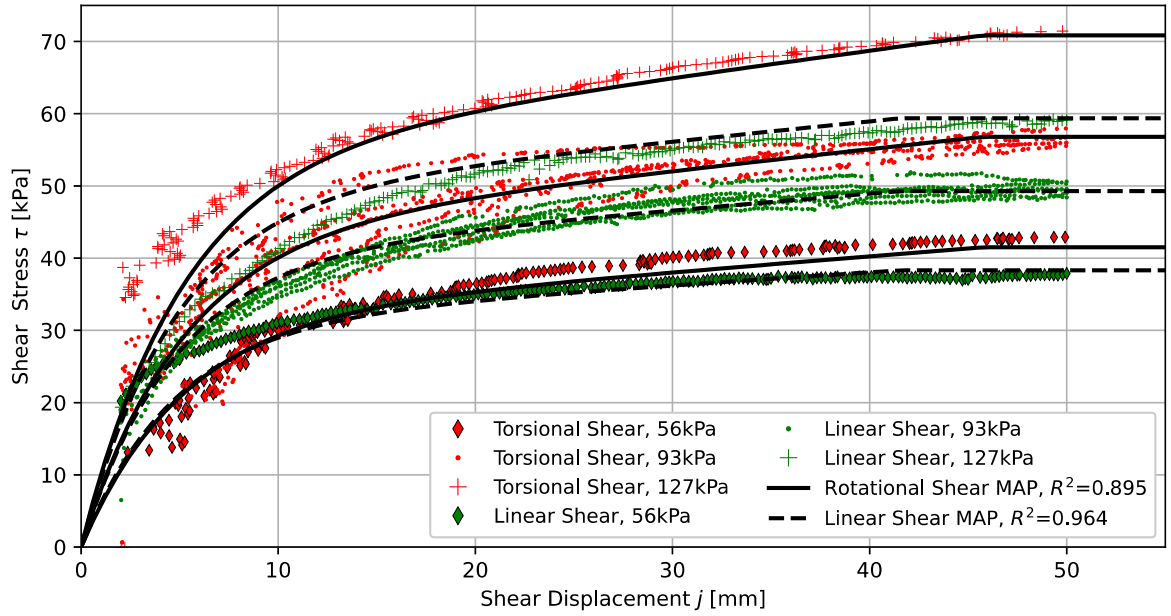

Figure 50-Torsional vs. linear shear regression model (50mm cut-off, 300cm²).

Figure 50 indicates that the proposed model represents the data well for both linear and torsional shear, with a coefficient of determination of 0.964 and 0.895, respectively. The corresponding Mohr-Coulomb failure envelope is indicated in Figure 51.

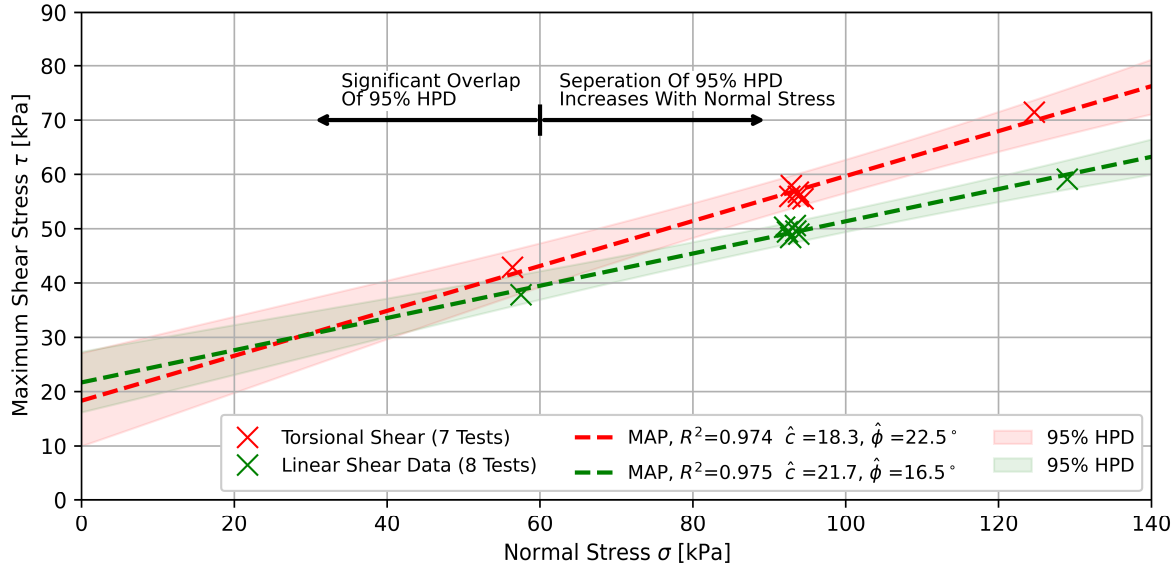

Figure 51-Torsional vs. linear shear Mohr-Coulomb failure envelope (50mm cut-off, 300cm²).

Figure 51 indicates that the Mohr-Coulomb assumption of a linear relationship between maximum shear stress and normal stress holds well for both shear mechanisms, exhibiting R^2 values greater than 0.974. Due to the high repeatability of the experiments and the strong linear relationship, the 95% Highest Probable Density (HPD) is relatively narrow, especially in the 56kPa to 127kPa normal stress range.

Figure 52 compares the soil model parameter probability distributions for the two shear mechanisms.

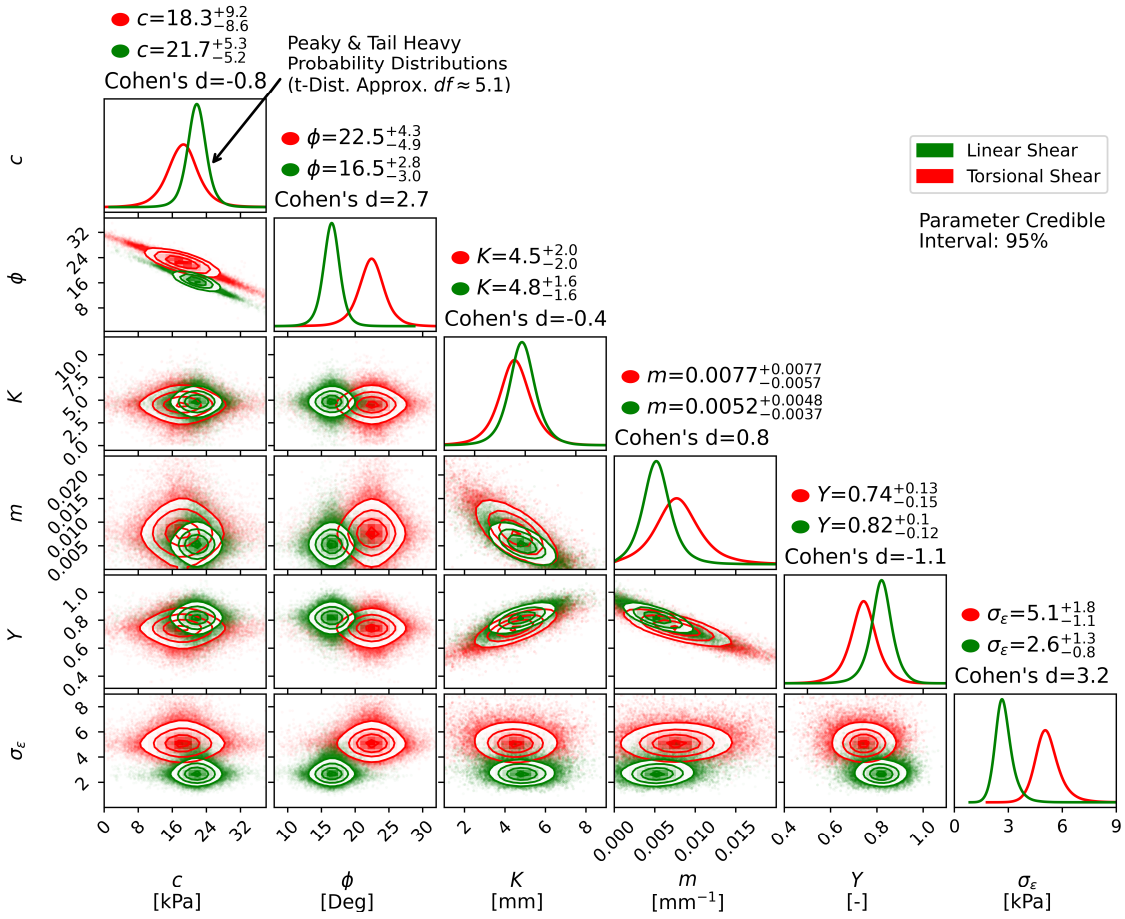

Figure 52-Influence of shear mechanism on soil parameter probability distributions.

From Figure 52 it is observed that the internal friction angle ϕ exhibits a significant difference, with $22.5°^{+4.3}_{-4.9}$ estimated for torsional shear and $16.5°^{+2.8}_{-3.0}$ for linear shear, indicating that shear stress increases more rapidly with an increase in normal pressure for torsional shear. The difference between the shear mechanisms observed in Figure 50 is mainly attributed to this difference in the friction angle.

The estimated soil cohesion exhibits a high 95% CI overlap, with linear and torsional shear exhibiting significant non-zero values of $21.7^{+5.3}_{-5.4}$kPa and $18.3^{+8.6}_{-8.2}$kPa, respectively. The cohesion contributes to 43% and 32% of total shear stress at 93kPa. The high cohesion is unusual for soil that is 96% sand but is supported by physical observations like the clumping and tension cracks observed in Figure 46. The high cohesion is attributed to the fine mean soil grain size and the inclusion of moisture.

The shear-displacement shape parameters K, m, Y all exhibit substantial probability distribution overlap. This is attributed to the uncertainty of the Mohr-Coulomb parameters that propagate to the shear-displacement model, increasing the overlap of the probability distributions. The parameters identified with and without uncertainty propagation will be compared in the following sub-section.

Finally, it should be noted that all parameters in Figure 52 exhibit peaky and tail-heavy probability distributions. Although non-parametric KDEs are employed, t-distribution approximations indicate ± 5.1 degrees of freedom, which is considered a highly non-Gaussian distribution. Since Bevameter tests are almost always associated with small sample sizes, the Bayesian MCMC parameter estimation method is recommended over alternative methods that make the Gaussian parameter distribution assumption.

Parameter estimation with and without uncertainty propagation

Figure 53 compares the parameters estimated with and without uncertainty propagation of the Mohr-Coulomb model to the shear stress-displacement model. For this comparison, the torsional shear data from Figure 50 is used. The method ***without*** uncertainty propagation uses the point estimates of the Mohr-Coulomb parameters (i.e. $\hat{c}$ and $\hat{\phi}$) as input to the hierarchical shear-displacement model in Figure 32 (b). In contrast, the method ***with*** uncertainty propagation, detailed by Algorithm 2, takes the full probability distribution of c and ϕ into account when estimating the shear-displacement parameters.

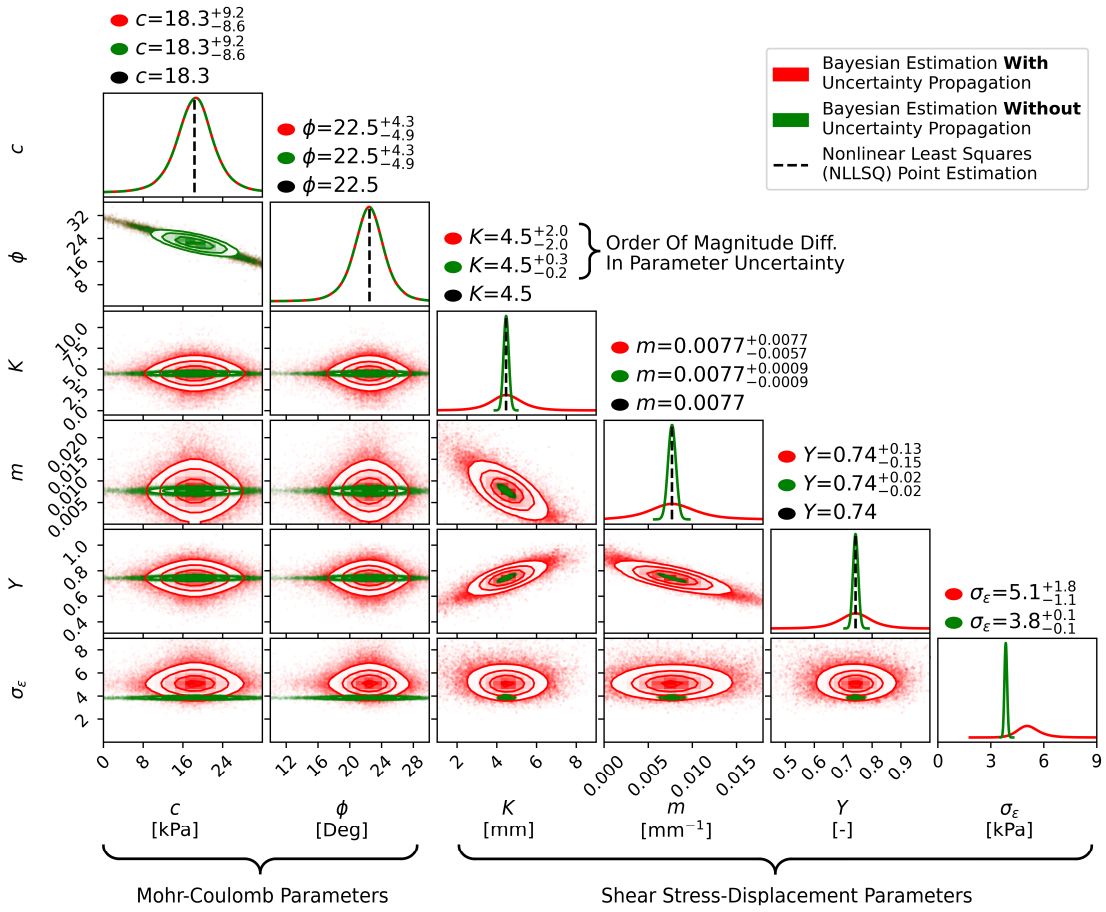

Figure 53-Parameter estimation with and without uncertainty propagation (torsional shear, 50mm cut-off).

From Figure 53 it is observed that the method ***without*** uncertainty propagation results in parameter credible intervals that are an order of magnitude smaller than that ***with*** uncertainty propagation. However, note that both methods identify the same point estimates. Similarly, the NLLSQ method identifies the same point estimates (for the indicated precision). Therefore, the point of contention is not the point estimates but rather the correct estimation of the parameter probability distributions. As discussed in section 4.4, the method with uncertainty propagation is argued to be the correct approach and is the method used throughout this study for parameter estimation and hypothesis tests.

The proposed method is not only applicable to the current model but to all shear-displacement models that take the maximum shear stress from the Mohr-Coulomb model as input, including the popular Janosi-Hanamoto (1961) model and eight out of the nine (8/9) models reviewed by He *et al.* (2019a).

It is unclear how frequentist parameter estimation methods, like the method proposed by Apfelbeck *et al.* (2011) for Bevameter soil parameter estimation, treat uncertainty for hierarchical models like those typically employed by state of the art shear stress-displacement models.

Assessing the integrity and robustness of the parameter estimation

The robustness and integrity of the parameter estimation can be compromised if the problem is ill-posed. It is important to establish if a problem is well or ill-posed to ensure the parameter estimates can be trusted. A problem is well-posed if it satisfies the following criteria (Latz, 2020),

- **Existence**-There exists a solution.
- **Uniqueness**-The solution is unique.
- **Stability**-The solution depends continuously on input data (marginal changes in the input result in marginal changes in the output).

Inverse problems, like parameter estimation, are often ill-posed, even if the forward model is well-posed (Latz, 2020). The degree of ill-posedness can be attributed to a number of factors, which include, but are not limited to: high measurement noise, high model complexity and lack of data (Latz, 2020). In practice, it is difficult to prove the well-posedness of a problem (Latz, 2020). Rigorous analytical proofs are highly complex and fall outside the scope of this thesis. However, several practical methods exist to evaluate the integrity of the parameter estimation process.

One practical approach employed in the machine learning field to determine if a problem is ill-posed is to plot and interpret the loss landscape (Sawicki *et al.*, 2018; Basir and Senocak, 2022). Typically parameter dimensionality reduction is first performed, or alternatively, random slices of parameter pairs are plotted. The loss function is then evaluated at a number of discrete points around the optimal solution, and a surrogate model is fitted for visualisation purposes (Sawicki *et al.*, 2018).

The Bayesian parameter estimation through the MCMC approach already evaluated the loss landscape for a large number of parameter combinations. In this case 5×10^5 parameter "combinations". Since our model only has six parameters, the loss can be plotted for all parameter combinations, where the loss is given by equation (20) and plotted in Figure 53. Theoretically, MCMC sampling will explore the entire parameter space given infinite computational resources (Bishop, 2006).

From Figure 53, the following observations are made regarding the robustness of parameter estimation,

- There exists at least one modal peak for each parameter. Therefore a solution ***exists***.
- The solution is uni-modal. Therefore, the solution is considered ***unique*** (Note: due to the use of non-parametric distributions, if a multi-modal solution existed, it would be observed).
- The loss landscape is continuous and convex across all parameters. The solution is ***stable*.**
- The three criteria for well-posedness are all ***weakly*** satisfied. Therefore the parameter estimation is considered ***well-posed*** and ***robust*** for both formulations indicated in Figure 53.

Alternative parameter estimation methods, like NLLSQ point estimation, are more challenging to assess the well-posedness since the loss landscape is not evaluated over a range of values. Furthermore, the Bayesian approach is inherently more stable than the NLLSQ approach, with the Bayesian prior adding stability to the inverse problem (Lanthaler *et al.*, 2022).

It can be concluded that, given the observed data and selected model, the parameter estimation is a well-posed problem with robust estimates. Bayesian parameter estimation through MCMC sampling is particularly well suited to assess the integrity and robustness of the parameter estimates compared to contemporary methods. However, it should be noted that the specific Bayesian posterior formulation used is critical; neglecting the hierarchical nature of the shear stress-displacement model results in the correct point estimates but incorrect uncertainty estimates of the parameters.

5.4.3 Formal hypothesis testing

Hypothesis tests for a difference in identified soil model parameters

Visual comparison in Figure 50 and Figure 52, indicate large separations between the raw data and the identified soil parameters, informally indicating a statistically significant difference exists due to the shear mechanism. Hypothesis tests are conducted to prove the previous observations formally and determine if a statistically significant difference exists for each of the individual soil model parameters. The test results are indicated in Table 17 and indicate that a significant difference exists between the shear mechanisms with a "very strong" level of evidence (largest BF_{10}>48). The parameters c, K and m are considered statistically equivalent (BF_{10}<3) and not significantly influenced by the shear mechanism.

Table 17-Hypothesis test for statistically significant difference between linear vs. torsional shear.

Null hypothesis $\mathbf{H_0}$	Effect size	BF_{10}	Evidence level	Accept or Reject $\mathbf{H_0}$
$\hat{c}_1 = \hat{c}_2$	0.8	1.7	Anecdotal	Accept
$\hat{\phi}_1 = \hat{\phi}_2$	-2.7	48.1	Very Strong	***Reject***
$\hat{K}_1 = \hat{K}_2$	-0.4	1.0	Anecdotal	Accept
$\hat{m}_1 = \hat{m}_2$	0.8	1.6	Anecdotal	Accept
$\hat{Y}_1 = \hat{Y}_2$	-1.1	3.0	Substantial	***Reject***
$\hat{\boldsymbol{\theta}}_1 = \hat{\boldsymbol{\theta}}_2$	NA	NA	Very Strong	***Reject***

Since at least one of the Bayes Factors is larger than the data collection threshold of BF_{10}=10 specified in the Sequential Bayes Factor experimental design from section 4.2, further data collection is terminated. The initial sample size is considered large enough, and more data is not required given the large evidence (Schönbrodt *et al.*, 2017). The large evidence is mainly driven by the large effect size.

Hypothesis tests for the influence of extraneous variables

Up to now, it was assumed that the observations were the result of perturbing the independent variable. However, extraneous variables could also have contributed to the observed effects. The most prominent extraneous variable in this study is the soil moisture content. The MC was placed under physical control, but due to the outdoor soil bin, the moisture could not be perfectly controlled. However, the MC is an observed variable, and further statistical control can be exerted through regression analysis. The MC is not an independent variable of interest, but we still would like to determine if it inadvertently influenced the experiment, possibly invalidating the results.

Figure 54 indicates the correlation between MC and maximum shear stress. Figure 54 (a) indicates a category dependant model, and Figure 54 (b) indicates a moisture dependant model.

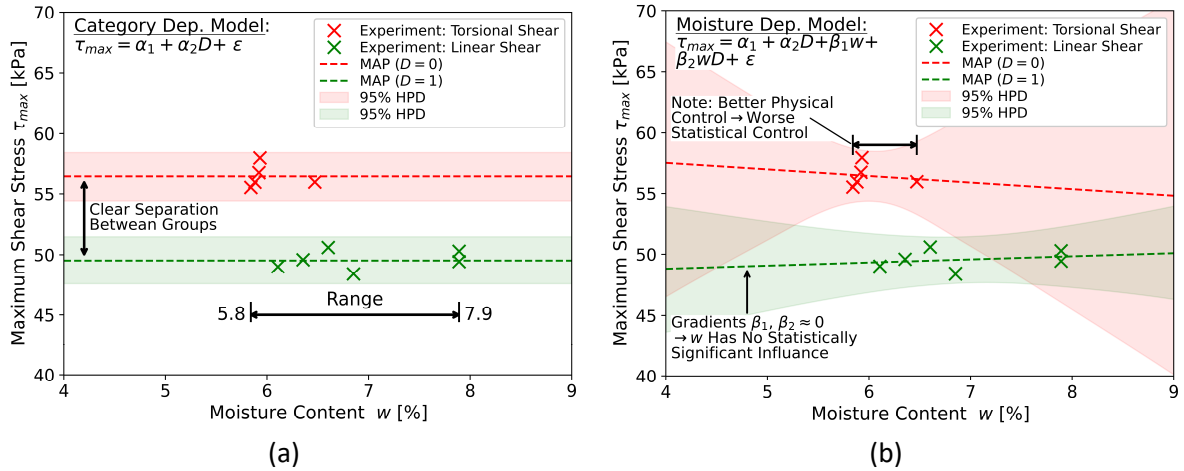

Figure 54-Influence of moisture content on maximum shear stress (93kPa normal pressure, 50mm cut-off). (a) Category dependant model. (b) Moisture dependant model.

Hypothesis tests for the significance of the model parameters in Figure 54 are indicated in Table 18.

Table 18-Hypothesis tests for the influence of soil moisture content on maximum shear stress.

Null Hypothesis H_0	Included Parameters	Lower Bound	MAP	Upper Bound	BF_{10}	Evidence level	Accept or Reject H_0
$\hat{\alpha}_1$=0	α_1, α_2	55.5	56.5	57.4	>10^3	Decisive	***Reject***
$\hat{\alpha}_2$=0	α_1, α_2	-8.1	-6.9	-5.5	>10^3	Decisive	***Reject***
$\hat{\beta}_1$=0	$\alpha_1, \alpha_2, \beta_1, \beta_2$	-5.4	-0.5	4.8	1.0	Anecdotal	Accept
$\hat{\beta}_2$=0	$\alpha_1, \alpha_2, \beta_1, \beta_2$	-4.8	0.8	5.9	1.1	Anecdotal	Accept

From Table 18 it is observed that the parameter α_2, which represents the offset between linear and torsional shear, is statistically significant with a decisive level of evidence (BF_{10}>100). This is supported by a clear separation of the credible intervals and a mean difference of $6.9^{+1.4}_{-1.2}$kPa between the groups.

The coefficients β_1 and β_2 of the moisture dependant model indicate that the MC fluctuation has no statistically significant influence on the maximum shear stress (BF_{10}<3). Furthermore, the MAP of β_1 and β_2 indicate low moisture sensitivity of 0.54kPa/% and 0.80kPa/%, which are statistically considered equal to zero. Relative to the large separation due to categorical groups, the influence of MC is minor (over the range of observed fluctuations) and did not significantly influence the experiment.

5.4.4 Summary of critical findings regarding the shear mechanism

A) Formal hypothesis testing found the influence of the shear mechanism to be significant with a decisive level of evidence (largest BF_{10}>48). This is supported by other observations, such as clear separation of the parameter credible intervals and confidence intervals in the data space.

B) Torsional shear exhibits a maximum mean increase of 17.6% over linear shear. An effect of this magnitude is expected to have significant implications for soil-wheel interaction models, like the Bekker-Wong model, which relies on the equilibrium of shear stress and normal stress.

C) Linear shear exhibits less non-asymptotic behaviour than torsional shear with lower non-asymptotic gradients. Linear shear also exhibits stationary points at low and intermediate pressures. At high pressures, both mechanisms exhibit significant non-asymptotic behaviour.

D) Linear shear becomes invalidated at higher shear displacement (>70mm) due to the soil impinging the centre shaft, while torsional shear remains unaffected. The best evidence suggests torsional shear displacement should be cut-off at 250mm and linear shear at 50mm.

E) The identified soil model parameters are significantly influenced by the shear mechanism. Most prominently, the internal friction angle was observed to vary from 16.5° for linear shear to 22.5° for torsional shear. A difference of this magnitude is considered highly significant.

F) The soil parameter probability distributions exhibit peaky and tail heavy distributions that are highly non-Gaussian. These findings support the use of the Bayesian MCMC parameter estimation method, which can determine the asymptotically exact parameter distributions.

G) The linear shear mechanism is expected to be the most representative method for predicting vehicle traction. Literature indicated that Bevameter soil characterisation tends to over-predict the shear stress of actual vehicles; therefore, linear shear tests are believed to be the more applicable method since it exhibits lower shear stress than torsional shear. However, neither of the methods resembles the physical shear process of a round wheel, which is expected to exhibit a significantly different shear stress-displacement curve.

5.5 The influence of shear contact area (Independent variable IV)

This section deals with the influence of perturbing the shear contact area. For this comparison, the torsional shear mechanism is used, as indicated in the experimental design in Table 11.

5.5.1 Experimental results

Shear stress vs. displacement at nominal vehicle ground pressure

Figure 55 indicates the influence of contact area on shear stress at nominal vehicle ground pressure. Note that tests at 583cm^2 were terminated early by the automatic load cell overload protection circuit. The load cell was designed for a shear stress ratio of 0.54 at 100kPa and 583cm^2; however, as observed in Figure 55, the realised shear stress ratio was significantly higher (0.65 to 0.92).

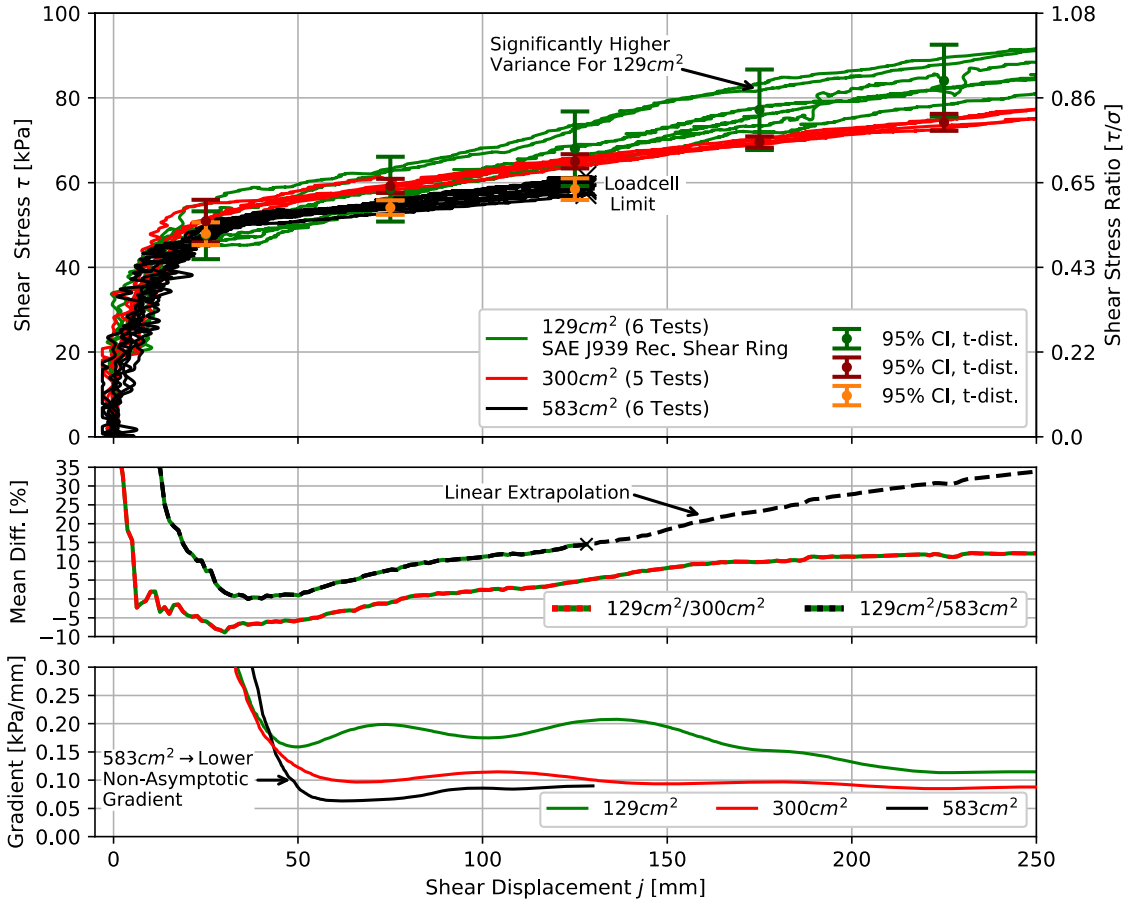

Figure 55-Influence of contact area on shear stress (torsional shear, 93kPa normal pressure).

Figure 55 indicates that the contact area significantly influences the measured shear stress, with a clear separation between the 95% confidence intervals and a maximum difference of 15% between the largest and smallest area. The results indicate that both the measured shear stress and non-asymptotic gradient decrease with an increase in the contact area. The mean difference is expected to be significantly larger (≈35%) had some tests not been terminated early. The result is contrary to the expected result. The large shear ring was expected to exhibit higher shear stress due to its larger perimeter and shear area. One hypothesis for the observed behaviour is that the grouser effects may be more significant for the smaller area since the grouser height was fixed for all tool configurations. Similarly, soil fallback may be more significant at the smaller absolute torque values. Another hypothesis is that the soil's vertical bearing capacity is higher for large areas, causing less slip-sinkage and, therefore, less lateral earth pressure (confining stress), resulting in lower principal stresses.

Shear stress vs. displacement at different normal pressures

Figure 56 compares the effects of the shear contact area at different normal pressures. For clarity, only the mean shear stress-displacement response at each pressure is indicated.

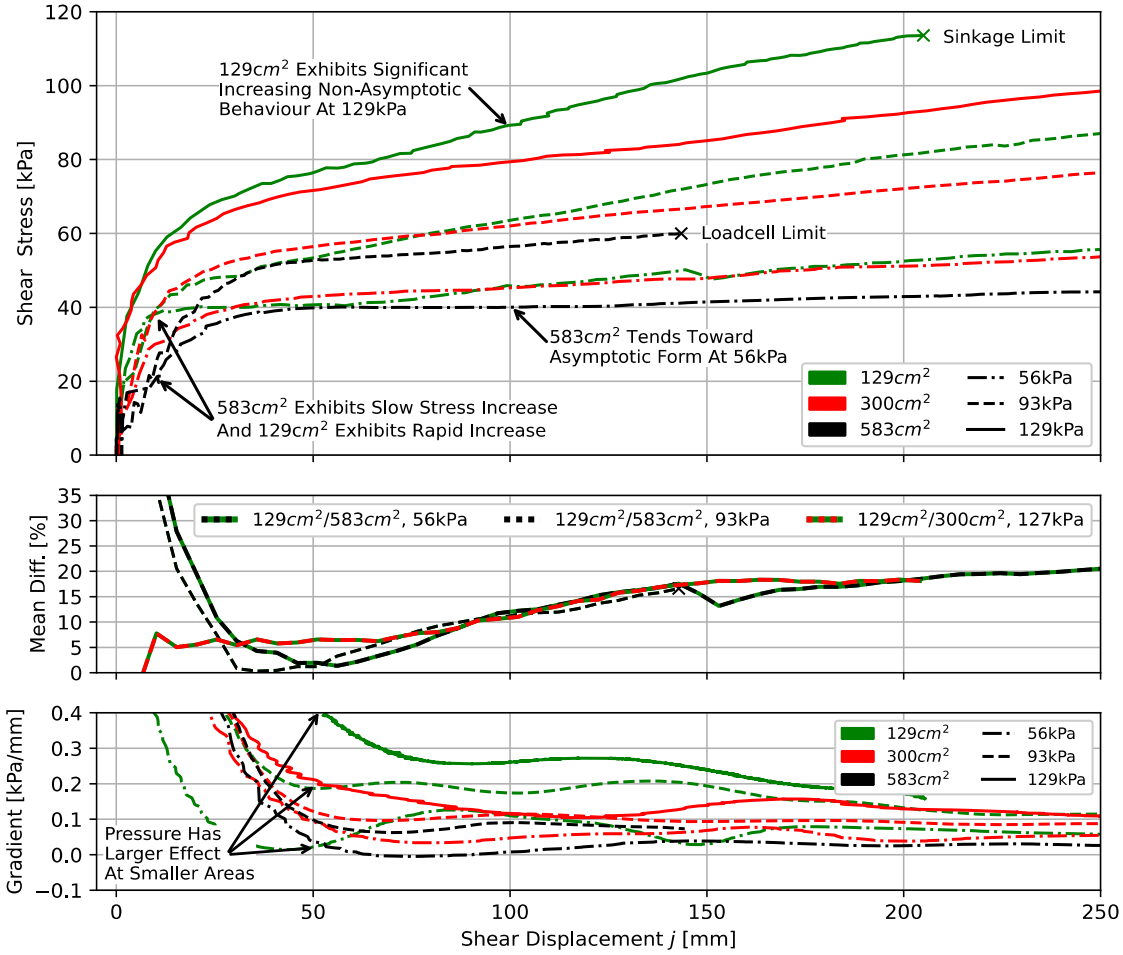

Figure 56-Influence of contact area on shear stress at different normal pressures (torsional shear).

From Figure 56 it is observed that the smallest area exhibits the largest shear stress across all normal pressures, with a maximum difference of 20% between the largest and smallest area. Again the difference is expected to be larger had some tests not been cut short. The shear curve shape at low shear displacement is observed to be significantly affected by the contact area, with the shear stress initially increasing more gradually for large areas while the small area exhibits a rapid initial shear stress increase. This effect is more pronounced at low pressures (≤56kPa). The normal pressure also had a more significant effect on the non-asymptotic behaviour for the small area, exhibiting a stationary point at 56kPa, but significant increasing non-asymptotic behaviour at 129kPa. The larger areas are proportionally less affected and exhibit lower non-asymptotic gradients.

The results from Figure 55 and Figure 56 indicate that the small 129cm^2 shear ring recommended by SAE J939 standard (SAE, 1967) exhibits significantly higher test variance, higher shear stress (with shear stress ratios up to 0.92) and larger non-asymptotic behaviour than the full tyre contact patch area of 583cm^2. Literature indicated that Bevameter tests tend to over-predict the shear stress of actual vehicles. Therefore, Bevameter shear tests are recommended to use the full tyre contact area as it leads to lower shear stress, lower variance, and lower non-asymptotic behaviour.

5.5.2 Soil parameter estimation

In order to investigate the influence of contact area on identified soil parameters and perform regression-based hypothesis tests, a displacement cut-off of 140mm is selected. Although it was established in section 5.3 that the best evidence indicates torsional shear should be cut-off at 250mm, the selected cut-off is necessary as some tests in section 5.5.1 were stopped early due to equipment limitations. Therefore, this section presents a ***comparative*** analysis of identified soil model parameters at an equivalent displacement cut-off. The model MAP for equation (43) is indicated in Figure 57.

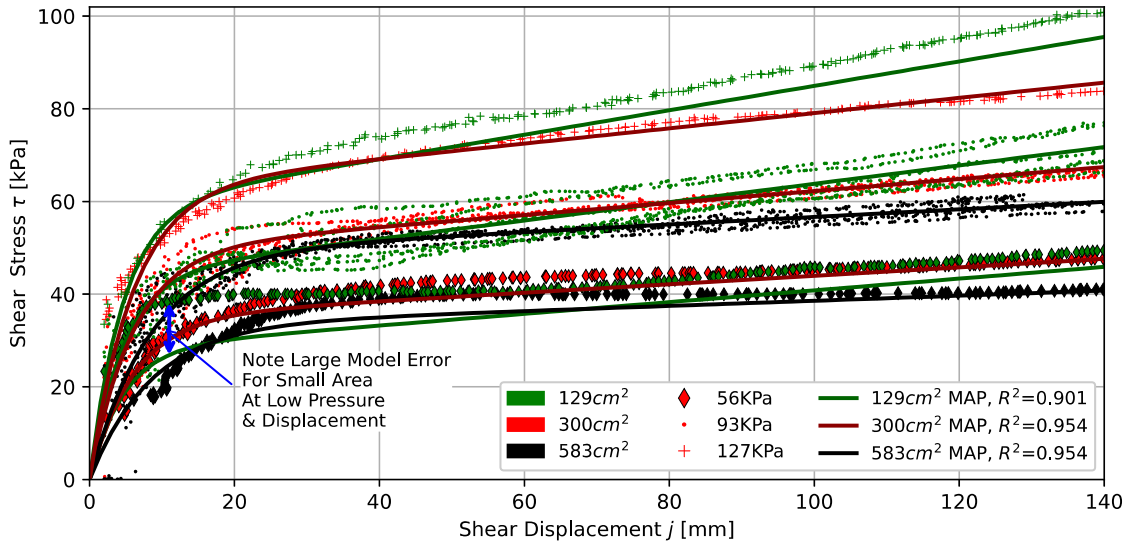

Figure 57-Regression model fit at different contact areas.

The associated Mohr-Coulomb failure envelope is indicated in Figure 58.

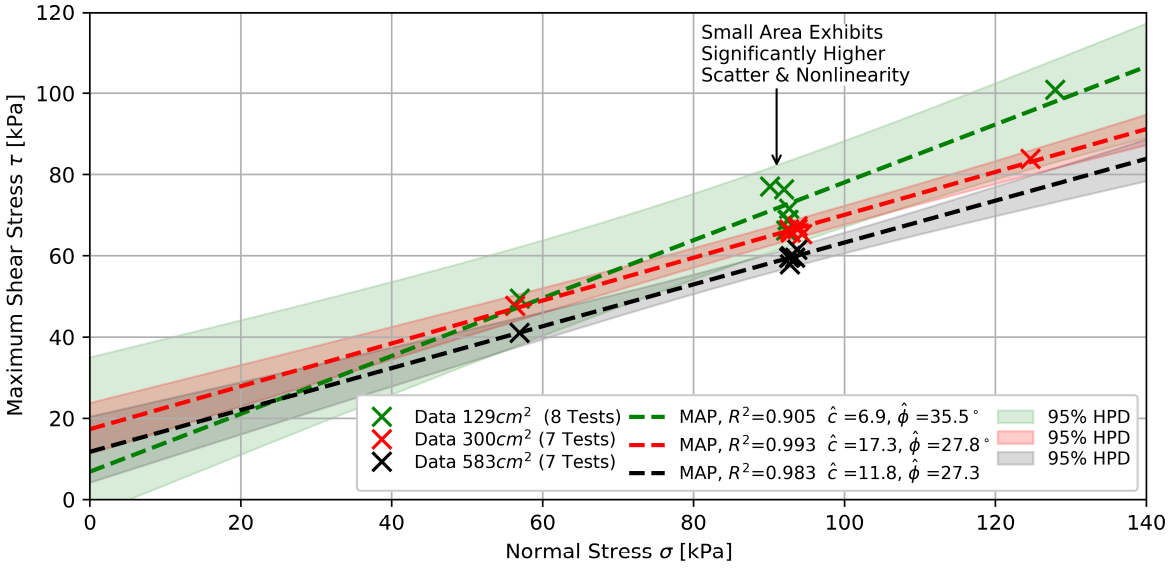

Figure 58-Mohr-Coulomb maximum shear stress envelope for different areas (140mm cut-off).

Figure 58 indicates that the 300cm^2 and 583cm^2 areas exhibit clear separation of the 95% HPD bands above 56kPa normal stress. Below 56kPa normal stress, the methods are considered equivalent due to the significant HPD overlap. The 129cm^2 area exhibits large data scatter and nonlinearity making clear separation from other areas difficult; however, it does exhibit a significantly steeper MAP.

Figure 59 indicates the estimated soil model parameter probability distributions.

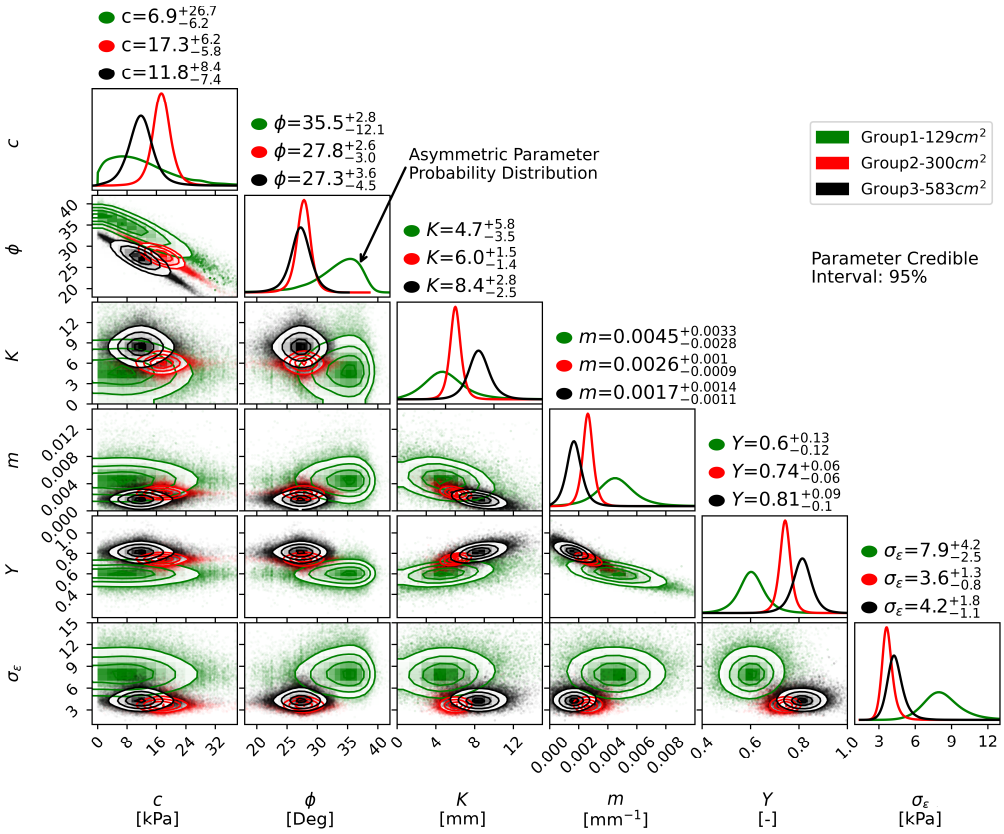

Figure 59-Influence of shear contact area on soil parameter probability distributions.

From Figure 59, it is observed that the friction angle ϕ exhibits significantly higher values for the small area, with an estimated value of $35.5°^{+2.8}_{-12.1}$ compared to $27.8°^{+2.6}_{-3.0}$ and $27.3°^{+3.6}_{-4.5}$ for the intermediate and large areas. The deformation modulus K shows a clear trend, with 4.7mm for the small area, 6.0mm for the intermediate area and 8.4 mm for the large area, indicating a slower initial shear stress increase for larger areas. The gradient term is also more than double for the smallest area compared to the largest area. This is reflected in the scaling parameter Y where 40% of the maximum stress is atributed to the increasing trend for the smallest area and 19% for the largest area. Finally, the small area exhibits skewed parameter distributions; this is attributed to the large data scatter and cohesion parameter that cannot be less than zero. This reinforces the importance of using non-parametric parameter estimation methods.

5.5.3 Formal hypothesis testing

Table 19 indicates the formal hypothesis tests for differences in the identified soil model parameters.

Table 19-Hypothesis test for the influence of contact area on shear stress.

Null hypothesis H_0	Effect size	BF_{10}	Evidence level	Accept or Reject H_0
$\hat{c}_1 = \hat{c}_2$	-1.0	2.1	Anecdotal	Accept
$\hat{\phi}_1 = \hat{\phi}_2$	1.5	6.1	Substantial	***Reject***
$\hat{K}_1 = \hat{K}_2$	-0.5	1.2	Anecdotal	Accept
$\hat{m}_1 = \hat{m}_2$	1.4	6.0	Substantial	***Reject***
$\hat{Y}_1 = \hat{Y}_2$	-2.4	36.3	Very Strong	***Reject***
$\hat{c}_1 = \hat{c}_3$	-0.1	0.9	Anecdotal	Accept
$\hat{\phi}_1 = \hat{\phi}_3$	1.6	8.4	Substantial	***Reject***
$\hat{K}_1 = \hat{K}_3$	-1.6	5.7	Substantial	***Reject***
$\hat{m}_1 = \hat{m}_3$	2.1	22.7	Strong	***Reject***
$\hat{Y}_1 = \hat{Y}_3$	-3.1	139.1	Decisive	***Reject***
$\hat{\boldsymbol{\theta}}_1 = \hat{\boldsymbol{\theta}}_2 = \hat{\boldsymbol{\theta}}_3$	NA	NA	Decisive	***Reject***

The hypothesis tests in Table 19 indicate a significant difference exists due to the contact area with a decisive level of evidence (largest BF_{10}>100). The findings are supported by other observations, such as a clear separation of the confidence intervals in the data and parameter space. At least one of the Bayes Factors exceeds the data collection threshold; therefore, further data collection is terminated.

Hypothesis test for the influence of extraneous variables

Figure 60 indicates the influence of moisture on maximum shear stress for the shear contact area experiment. Table 20 presents hypothesis tests for the influence of moisture content.

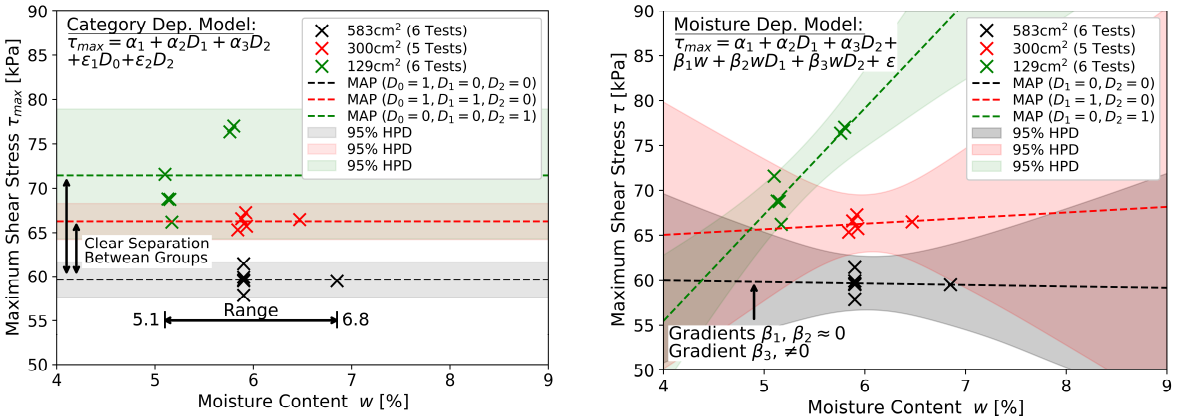

Figure 60-Influence of moisture content on the shear area experiment (93kPa normal pressure, 140mm shear cut-off). (a) Category dependant model. (b) Moisture dependant model.

Table 20-Hypothesis tests for the influence of contact area and moisture content.

Null Hypothesis H_0	Included Model Parameters	Lower Bound	MAP	Upper Bound	BF_{10}	Evidence Level	Accept or Reject H_0
$\hat{\alpha}_1$=0	$\alpha_1, \alpha_2, \alpha_3$	58.7	59.7	60.6	>10^3	Decisive	***Reject***
$\hat{\alpha}_2$=0	$\alpha_1, \alpha_2, \alpha_3$	5.2	6.4	8.1	>10^3	Decisive	***Reject***
$\hat{\alpha}_3$=0	$\alpha_1, \alpha_2, \alpha_3$	7.5	11.8	16.6	>10^3	Decisive	***Reject***
$\hat{\beta}_1$=0	$\alpha_1, \alpha_2, \alpha_3, \beta_1, \beta_2, \beta_3$	-4.5	-0.2	4.1	1.0	Anecdotal	Accept
$\hat{\beta}_2$=0	$\alpha_1, \alpha_2, \alpha_3, \beta_1, \beta_2, \beta_3$	-7.3	0.8	9.4	0.9	Anecdotal	Accept
$\hat{\beta}_3$=0	$\alpha_1, \alpha_2, \alpha_3, \beta_1, \beta_2, \beta_3$	5.7	12.0	18.6	225.3	Decisive	***Reject***

Hypothesis testing in Table 20 indicates that the category offset variables α_2 and α_3 are statistically significant with a decisive level of evidence (BF_{10}>100). For the $583cm^2$and $300cm^2$ areas the moisture-dependant coefficients β_1 and β_2 indicate no statistically significant influence (BF_{10}<3).

In contrast, the $129cm^2$ area indicates a significant influence (BF_{10}>100) due to moisture with an estimated gradient of 11.8kPa/%. Based on the evidence from the other two experimental test areas and hypothesis tests from Table 18, it is highly unlikely that moisture had a significant impact on this single experiment and not on the others. As discussed earlier, the $129cm^2$ area exhibits larger variance and is more sensitive to small fluctuations in torque and test conditions. Therefore, the results are attributed to the larger variance or other extraneous factors (e.g. applied normal load). Even by accepting the influence of the MC, the separation between the 95% HPD bands in Figure 60 (b) is significant; therefore, it does not alter the conclusion that the area influences the shear stress.

5.5.4 Summary of critical findings regarding the influence of contact area

A) Formal hypothesis tests indicate that the contact area has a statistically significant influence on shear stress with a decisive level of evidence (largest BF_{10}>100). This is supported by other observations, like clear separation of the confidence intervals in the data and parameter space.

B) The smallest area exhibits the largest shear stress for all normal pressures exhibiting a maximum difference of 20% between the largest and smallest area. An effect of this magnitude is expected to have significant implications for soil-wheel interaction models like the Bekker-Wong model that relies on an equilibrium of shear and normal stress. The difference is expected to be larger (~35%), had equipment limitations not been an issue.

C) The shear stress-displacement curve shape is significantly influenced by contact area, with a larger shear deformation modulus K identified for larger areas. This is indicative of a significantly slower initial shear stress increase for larger shear annuli than smaller ones.

D) The internal friction angle ϕ is significantly influenced by the contact area. At or above $300cm^2$ a similar friction angle is identified. However, the small area of 129 cm^2 identified a significantly higher friction angle, indicating larger normal pressure dependence for small areas.

E) The non-asymptotic shear stress behaviour is also significantly influenced by contact area, with a significantly higher non-asymptotic gradient parameter m identified for smaller areas.

F) The nominal tyre contact patch area of $583cm^2$ is expected to be the most representative shear stress area for vehicle traction prediction. However, testing at representative tyre contact areas for SUV-size vehicles is challenging and requires large equipment and applied loads. The next best evidence is in support of the 300cm^2 area, which exhibits higher repeatability, lower non-asymptotic gradients and lower shear stress than the 129 cm^2 shear ring recommended by the SAE 939 (SAE, 1967) standard.

5.6 The influence of shear velocity (Independent variable V)

This section deals with the influence of perturbing the shear velocity (independent variable V). For this comparison, the torsion shear mechanism is used, as indicated in the experiment design in Table 11.

5.6.1 Experimental results

Figure 61 indicates the influence of shear velocity on shear stress at nominal vehicle ground pressure.

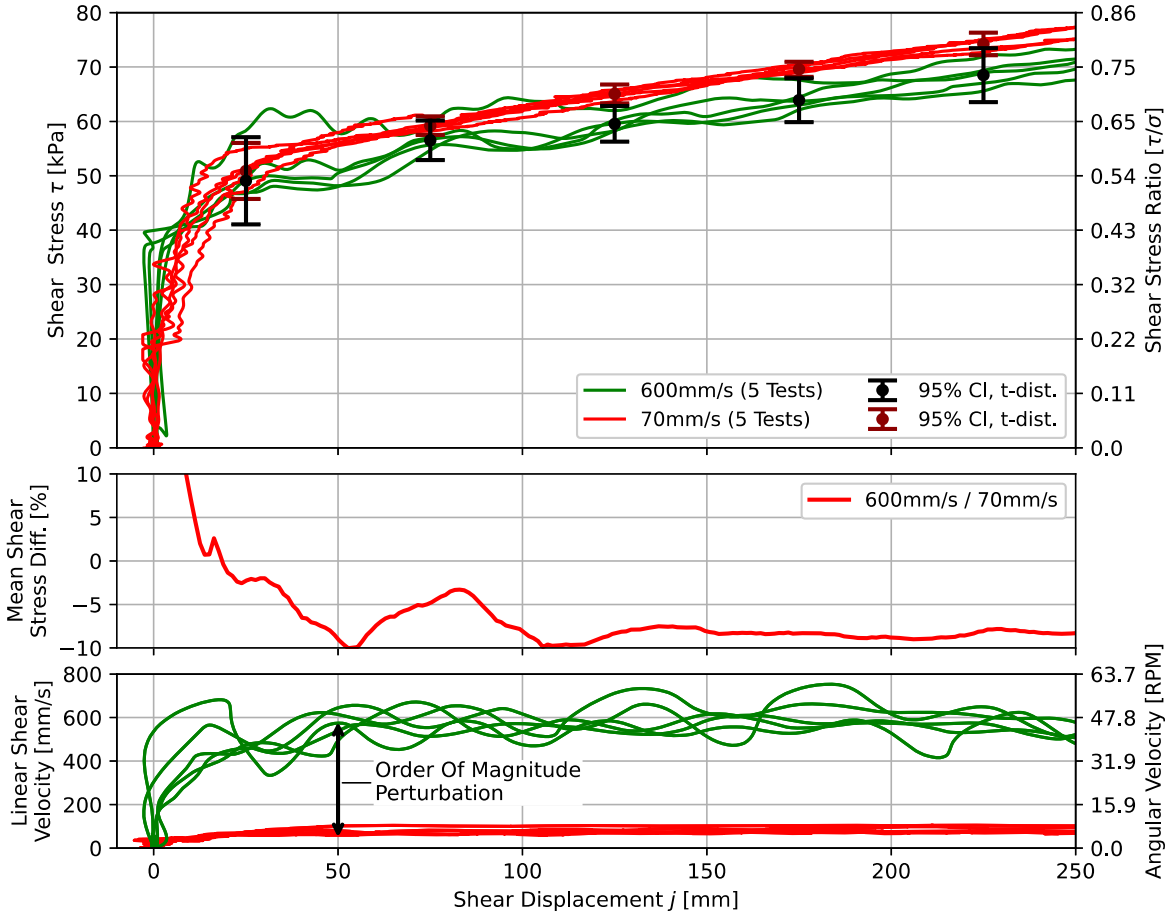

Figure 61-Influence of shear velocity on shear stress (torsional shear, 93kPa normal pressure, 300cm² shear ring).

Figure 61 indicates that the shear velocity had a relatively minor influence, with a shear rate weakening of 10% resulting from a shear rate increase of 850%. Considering the order of magnitude perturbation in shear rate, the sensitivity of shear stress to shear rate is very low. It was expected that rapid shearing of partially saturated soil would have resulted in an increased shear strength through activation of pore pressure. For Bevameter tests of a similar sandy soil, but under fully saturated conditions, Kim *et al.* (2022) observed a shear strength increase due to the influence of moisture even at a quasi-static shear rate. In this case, it is postulated that the partial saturation, high soil permeability and low in situ confining stress allow rapid moisture draining, preventing pore pressure from having a significant effect.

It should be noted that the Bevameter shear velocity control in Figure 61 is not ideal and can use improvement. It was found that the rotational motor H-bridge controller, sourced from a golf cart drive unit, enforced a fixed 3-second 0-100% slew rate limit. This was unacceptably slow for the fast shear rate case; therefore, open-loop control with no velocity feedback was employed. However, it should be noted that the physical shaft speed does not fluctuate as severely as the data suggest. This is an artefact of sensor resolution, sensor alignment and derivation of displacement to get velocity.

5.6.2 Soil parameter estimation

As indicated in the experimental design in Table 11, no data was collected at different pressures for the shear velocity experiment. This was due to time constraints as well as conditions that changed in the outdoor soil bin with the onset of the rainy season. Therefore, the Mohr-Coulomb parameters cannot be determined. However, the maximum shear stress τ_{max} and stress-displacement parameters can still be estimated and compared. The model MAP from fitting equation (43) is indicated in Figure 62.

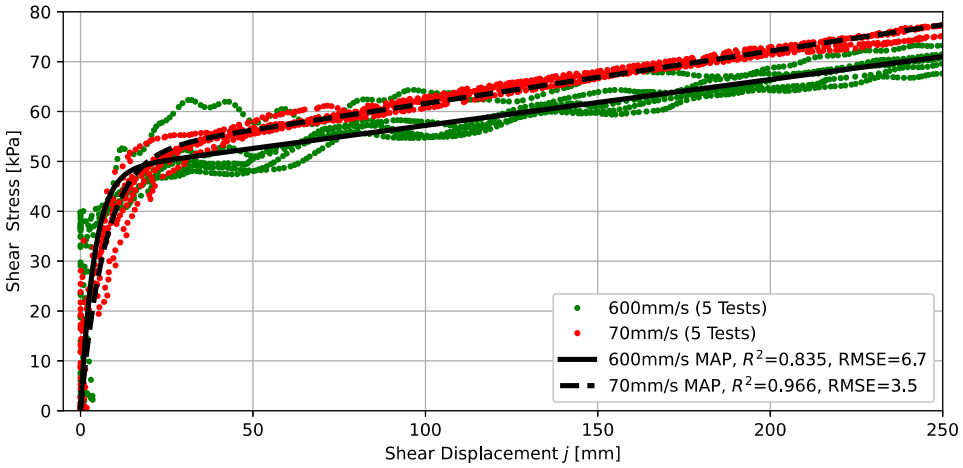

Figure 62-Regression model fit for different shear velocities (torsional shear, 93kPa normal pressure, 300cm² shear ring).

Figure 63 indicates the shear stress-displacement model parameter probability distributions.

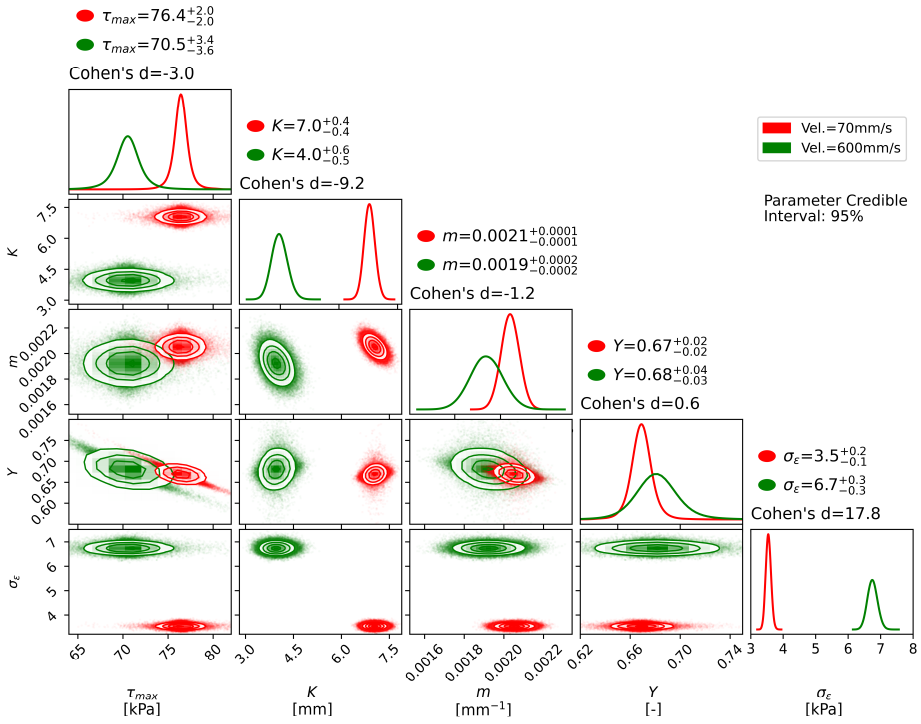

Figure 63-Posterior parameter distribution comparing the influence of shear velocity.

The maximum shear stress τ_{max} in Figure 63 indicates a clear separation between the probability distributions of the two shear velocities with 3.0 standard deviations of separation. The shear deformation modulus (indicative of the gradient at the origin) also indicates clear separation with a lower shear deformation modulus for the high-velocity case ($3.0^{+0.6}_{-0.5}$mm vs. $7.0^{+0.4}_{-0.4}$mm). The gradient m and scale parameter Y appear relatively equivalent, exhibiting partial credible interval overlap.

5.6.3 Formal hypothesis testing

Hypothesis tests for a difference in identified soil model parameters

Formal hypothesis tests for differences in identified parameters are indicated in Table 21. The results indicate that the two processes are different with a decisive level of evidence (largest BF_{10}>100). All the parameters exhibit a statistically significant difference due to shear rate except for the scale parameter Y (BF_{10}<3). The conclusions are supported by other observations, such as the clear separation of the 95% confidence intervals in the dataspace in Figure 61 and parameter distributions in Figure 63.

Table 21-Hypothesis testing for statistical significance of shear velocity.

Null hypothesis H_0	Effect size	BF_{10}	Evidence level	Accept or Reject H_0
$\hat{\tau}_{max,1}$=$\hat{\tau}_{max,2}$	-3.0	30.3	Very Strong	***Reject***
$\hat{K}_1$=$\hat{K}_2$	-9.2	>100	Decisive	***Reject***
$\hat{m}_1$=$\hat{m}_2$	-1.2	3.3	Substantial	***Reject***
$\hat{Y}_1$=$\hat{Y}_2$	0.6	1.4	Anecdotal	Accept
$\hat{\boldsymbol{\theta}}_1$=$\hat{\boldsymbol{\theta}}_2$	*NA*	*NA*	Decisive	***Reject***

Hypothesis test for the influence of extraneous variables

Figure 64 indicates the influence of moisture content on maximum shear stress. The MC is observed to be practically equivalent, with a maximum difference of 0.7% between all tests. The physical control of the MC is therefore considered adequate, and there is no need to perform formal hypothesis tests.

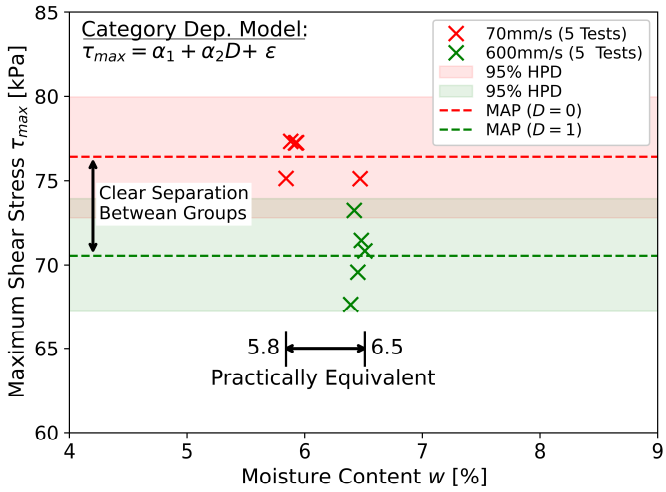

Figure 64-Influence of moisture on shear velocity experiment.

5.6.4 Summary of critical findings regarding the influence of shear rate

A) Formal hypothesis testing found the influence of shear velocity to have a statistically significant influence on shear stress with a decisive level of evidence (largest BF_{10}>100).

B) Although a statistically significant difference exists due to perturbing shear rate, the shear stress is not very sensitive to shear rate. An order of magnitude increase in shear rate resulted in a shear stress decrease of only 10%; therefore, the influence is not practically significant.

C) The findings are only valid for partially saturated fine sandy soils. Other soil types should be investigated for shear rate effects. High clay content soils are postulated to exhibit significant shear rate dependence. The shear rate may still be an important factor for Bevameter soil characterisation for these soils and requires further investigation.

5.7 Overview of soil parameters identified across independent variables

Sections 5.4 to 5.6 considered the independent variables III to V in isolation. For a holistic overview of shear stress-displacement parameters identified across the different independent variables and displacement cut-off selections, they are compared in Figure 65. The uncertainty is indicated using the Interquartile Range (IRQ) to emphasise where the central mass of the probability distributions lie.

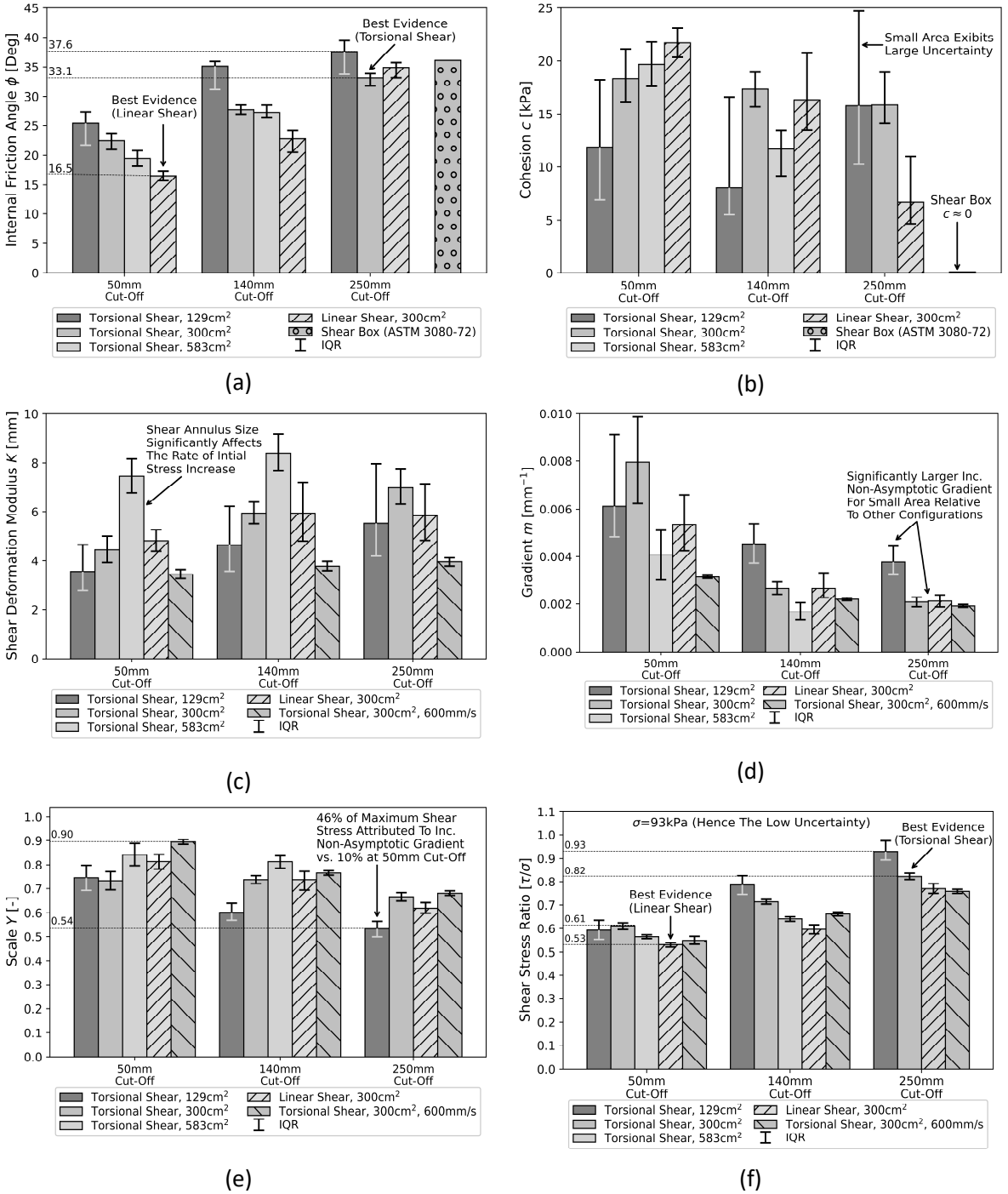

Figure 65-Effects of Bevamter test setup on identified soil parameters. (a) Internal friction angle. (b) Cohesion. (c) Shear deformation modulus. (d) Gradient.(e) Scale. (f) Shear stress ratio.

Figure 65 indicates that some parameters, like the internal friction angle, are significantly influenced by the displacement cut-off selection. Even more so than perturbing the test setup configuration. However, it should be noted that the test setup configuration is a factor that influences the cut-off

selection. By comparing the "best evidence" for cut-off selection for linear and torsional shear in Figure 65 (a), the friction angle estimate varies from 16.5° to 33.1°. This is considered a highly significant difference and exacerbates the already significant variation due to perturbing the independent variables at an equivalent cut-off (e.g. 16.5° to 25.0° at 50mm cut-off).

Other parameters, like shear deformation modulus and cohesion, are not significantly affected by displacement cut-off selection. Most notably, the deformation modulus in Figure 65 (c) indicates a similar difference irrespective of cut-off selection. Here the contact area was most influential, with a significantly slower initial onset of shear stress for larger areas (shear annulus size). Similarly, the cohesion parameter is also more influenced by the test setup than the displacement cut-off selection. Here, the parameter uncertainty is significantly influenced by the specific test setup configuration.

By comparing the soil parameters, it is not immediately clear which test configuration will likely lead to the most accurate vehicle traction prediction. Therefore Figure 65 (f) compares the shear stress ratio at a nominal vehicle ground pressure of 93kPa and 250mm displacement. The shear stress ratio is observed to range from 0.53 to 0.93. This is considered a significant difference. Literature indicated that Bevameter soil characterisation tends to over-predict the shear stress of vehicles; therefore, the configuration with the lowest shear stress ratio is likely to be the most representative. However, the friction angle (16.5°) associated with the lowest shear stress ratio is considered unrealistically low for sandy soil. Therefore, some test setup configurations lead to more realistic soil parameter estimates like friction angle (e.g. torsional shear, 300cm^2, 250mm cut-off), while other configurations lead to more reasonable shear stress ratios for traction prediction (e.g. linear shear, 300cm^2, 50mm cut-off).

Overall, Figure 65 highlights significant problems with the Bevameter soil characterisation technique. For the same soil condition (density, MC, etc.), significantly different soil shear stress-displacement parameters are identified depending on the test setup configuration and data processing decisions.

5.8 Limitations of this study

- The results of this study are only applicable to partially saturated fine sandy soil.
- The single-factor experimental design proved to be limiting. Regression analysis showed that extraneous variables did not significantly influence the results. However, if the extraneous variables indicated a more pronounced influence, it would require a more sophisticated experimental design. The solution would be to perform multi-factor experiments that purposely perturb the extraneous variables to quantify their influence over a broader range of values.
- The initial sample size for the SBF design was relatively low, with a minimum of five tests. Due to the large effect size, this was shown to be adequate to exceed the evidence threshold for data collection. However, a larger sample size would further strengthen the statistical conclusions.
- Only a limited number of soil density tests were performed, and no data was collected for soil preparation methods one and two. The relative density measurements also exhibited a large variance. Similarly, only a limited number of MC samples were collected (two samples per test day).
- The soil preparation method prepared a relatively small area of 500mm wide by 800mm long. For some tests, this was on the recommended boundary distance, or in case the 583cm^2 area, violated the "soft" boundary between prepared and unprepared soil. However, it should be noted the tests are still surrounded by a semi-infinite soil boundary.

CHAPTER 6

Conclusion and Recommendations

"We can only see a short distance ahead, but we can see plenty there that needs to be done."

-Alan Turning[6]

[6]AZ QUOTES (2022) *Alan Turning.* Available at: https://www.azquotes.com/quote/297979 (Accessed: 15 Aug 2022).

6. Conclusion and Recommendations

6.1 Conclusion

The overall aim of the study is to determine if, and to what extent, intrinsic experimental test setup factors influence Bevameter soil characterisation. In order to achieve the overall aim, the research set out to achieve the following specific research objectives: 1) to develop a new Bevameter and infrastructure for soil tests, 2) to investigate intrinsic experimental test setup factors that may affect Bevameter soil characterisation, and 3) use a probabilistic approach to estimate soil model parameters and determine if the factors under investigation in objective two are statistically significant.

The first objective was successfully achieved by designing, manufacturing, and performing extensive testing of a new Bevameter. A self-contained Bevameter was presented that is capable of performing linear shear tests, torsional shear tests and pressure-sinkage tests. The Bevameter is highly capable and can match the forces and shear areas of full-scale off-road vehicles. Furthermore, a new soil bin was commissioned to spearhead terramechanics research at the University of Pretoria.

In addressing the second objective, five factors that affect Bevameter tests were investigated. The first two factors investigated the influence of soil preparation on pressure-sinkage and shear stress. The soil preparation method (primarily a reflection of soil density) significantly influenced pressure-sinkage, with an order of magnitude difference observed in soil bearing capacity. The shear stress tests exhibited a notable but less significant response. The third factor investigated was the shear mechanism. Hypothesis testing found the influence of the shear mechanism to be statistically significant, with torsional shear tests exhibiting a maximum increase of 17.6% over linear shear tests. Considering literature indicates that Bevameter soil characterisation tends to over-predict drawbar pull, linear shear tests are believed to be the more applicable method for predicting vehicle traction. However, torsional shear exhibits closer agreement with laboratory methods for friction angle estimation. The fourth factor investigated was the shear contact area. The smallest contact area indicated a 20% increase in shear stress over the largest area. Shear tests at full tyre contact areas are recommended as it exhibits lower variance, shear stress and non-asymptotic behaviour than smaller areas. The fifth factor investigated was the shear rate. The influence of shear rate was statistically significant but relatively insensitive, with an order of magnitude increase indicating a shear stress decrease of 10.0%.

For all shear test configurations investigated, the soil exhibited increasing non-asymptotic behaviour. This was shown to be problematic in that the Mohr-Coulomb parameters are influenced by the shear displacement cut-off selection. Literature suggests the phenomenon is attributed to drag shear. However, experimental tests indicated that drag shear has a minor contribution. The behaviour is most prominent at high normal pressures (>93kPa) and low relative soil densities. Recent literature tends to conduct Bevameter tests at low normal pressures that are not considered representative of contact pressures of SUV-size vehicles, which may explain why the phenomenon has been rarely addressed. Existing stress-displacement models are not able to adequately capture the observed soil response. A new model was presented and shown to be superior for data of non-asymptotic form.

The third and final objective was also successfully addressed. Literature indicated soil behaviour is a stochastic process and has long indicated a need to move away from simple point parameter estimation methods and toward a probabilistic approach. A new method using the Bayesian MCMC approach was applied to estimate the soil model parameters. The proposed method is advocated for two reasons. First, the soil parameters exhibited peaky, tail heavy, and highly non-Gaussian probability

distributions. Alternative parameter estimation methods that make a Gaussian distribution assumption and perform linearisation around the point estimate are not recommended. Secondly, the current state of the art uses a hierarchical modelling approach, with the Mohr-Coulomb model serving as input to the shear stress-displacement model. Existing parameter estimation methods do not consider the uncertainty of the Mohr-Coulomb model when estimating the parameters of the stress-displacement model. A new method was presented to conditionally propagate uncertainty from the first to the second model. The propagation of uncertainty is critical for the parameter estimation of the shear-displacement model. Furthermore, a new regression-based hypothesis testing method was applied to determine the statistical significance of nonlinear data. This presents an improvement over previous Bevameter hypothesis testing methods that could only accommodate linear soil models.

Overall, the findings of this study make it clear that the experimental test setup configuration of the Bevameter technique significantly influences the identified soil parameters. It is hypothesized that the findings (differences of up to 20% in shear stress and soil parameters that vary significantly, most notably, the friction angle that ranged from 16.5 to 37.6) may have a profound effect on the Bekker-Wong terramechanics model that relies on the equilibrium of shear stress and normal stress to predict vehicle traction. Further investigation is required into the Bevameter soil characterisation method before sufficient confidence can be reached to use it to identify a definitive set of soil parameters.

6.2 Novel contributions

The novel contributions of this study are highlighted as follows:

(i) This study investigated novel factors that may influence Bevameter soil characterisation. To the best of the author's knowledge, this study presents the first study to:
- Compare the linear and torsional shear mechanisms at an equivalent contact area.
- Investigate the influence of shear contact area at equivalent shear annulus aspect ratios.
- Investigate the influence of shear velocity at realistic shear velocities expected for SUV-size vehicles and report the influence on the shear stress-displacement response.

(ii) Presented a rigorous framework for probabilistic data analysis for Bevameter soil characterisation.
- Presented a novel approach for estimating soil parameters using the Bayesian MCMC method. This presents the first approach that can determine the asymptotically exact soil parameter distribution as opposed to point estimate or approximate inference methods.
- Presented a method to conditionally propagate uncertainty from the Mohr-Coulomb model to the shear-displacement model. This is a critically important aspect for uncertainty quantification of the shear-displacement model that has not been addressed previously.
- Presented a novel method to perform formal hypothesis tests for factors affecting Bevameter tests for data of nonlinear form. Previous hypothesis test methods used in literature for Bevameter tests could only accommodate linear soil models.

(iii) Presented a novel empirical model for shear data of increasing non-asymptotic form. Existing model recommendations are not representative of the observed physical soil behaviour.

(iv) Other less significant contributions of this study include:
- Presented novel Bevameter hardware. The Bevameter device developed for this study presents a single device that is capable of linear shear, torsional shear and pressure-sinkage.
- Presented a novel method to determine soil density and the full 3D soil displacement for Bevameter tests using the photogrammetry method.

6.3 Recommendations for future work

The hardware developed for this study opened a number of new research opportunities. Furthermore, insight was gained on possibilities for future work. The recommendations for future work are:

Research questions emanating from this study directly related to Bevameter tests

- The difference between the shear mechanism of an actual wheel and that from Bevameter tests should be investigated. A half-round soil engagement tool or tyre can be mounted to the Bevameter and translational shear tests performed. It is hypothesised that the shear-displacement curve will differ significantly from standard Bevameter tests due to the different physical shear mechanisms.
- Investigate the size and shape of the linear shear soil engagement tool. A longer tool will allow more displacement to take place before the centre shaft engages the soil. The bulldozing force of the first grouser is also expected to decrease, but the lateral grouser drag is expected to increase.
- Investigate if numerical and analytical methods can replicate the experimental results from this study. Numerical and analytical modelling methods can be validated on in situ Bevameter data before moving on to the more complex tyre-soil interaction problem.
- Perform a detailed investigation of the drag shear phenomenon. By manufacturing special experimental equipment with force-sensing members in the grousers, the contribution of individual components, such as bulldozing, can be measured. Analytical and numerical analysis methods can also be used to quantify the individual contribution of each component of drag shear.
- Investigate more sophisticated shear stress-displacement models. Models in literature only take normal stress and shear displacement as input. A more general predictive model can be created by empirically incorporating soil density, moisture content and soil type and training the model with data from experimental Bevameter tests, such as the data already collected in this study.
- Only five factors that affect Bevameter soil characterisation were investigated in this study. A large number of test setup factors may still influence Bevameter soil characterisation. There exists significant scope for further investigation of other factors, such as the effect of grouser size.

Other questions emanating from this study

- A prominent research question emanating from this study is to theoretically investigate the vehicle traction predicted by the Bekker-Wong soil-wheel interaction model using the experimental data from this study. Preliminary investigation indicated unrealistically high drawbar pull to normal load is predicted, with a significant positive drawbar pull predicted at zero slip.
- Experimentally verify the traction predicted by the Bekker-Wong model based on Bevameter soil characterisation using the target vehicle of the current study. Although extensive literature exists to predict vehicle traction theoretically, few studies verify this experimentally on full-size vehicles.

Improvements to the current study

- The main improvement recommended for the current study is to improve the experiment design. The experiment design implemented single-factor experiments. With a full factorial experimental design, multiple factors can be taken into account simultaneously. This will allow extraneous variables like MC to be quantified more accurately compared to the single-factor design.

- Although the SBF experimental design indicated that the sample size is adequate, given the large effect size, increasing the sample size will further strengthen the statistical conclusions.
- Improve the soil density measurement by using more sophisticated methods (e.g. using a nuclear soil density gauge). Additionally, cone penetrometer measurements are also recommended.
- Collect more MC samples (ideally one for every test) instead of only two samples per test day. Measure and report the MC variation across the soil bin and soil bin depth.

Improvements recommended to the Bevameter hardware and the soil bin

- The speed control of the Bevameter rotational axis requires improvement. Two improvements are recommended: 1) replace the H-bridge driver that exhibited the slew rate limit, and 2) increase the angular encoder resolution by using a belt drive to increase the total angular displacement.
- It is highly recommended to relocate the outdoor soil bin commissioned for this study to an indoor laboratory for better control of the environmental conditions.

Recommendation for standardisation of Bevameter tests

It is suggested that the ISTVS establish a focus group of experts to update the current ISTVS standards to incorporate standards for Bevameter soil characterisation (He *et al.*, 2020). The problem with a lack of a rigorous standard is that terramechanics researchers make subjective equipment and data analysis choices that lead to identifying different soil model parameters for the same soil state. The standards should make provision for various different physical soil responses, such as the increasing non-asymptotic shear-displacement behaviour observed in this and other studies. However, before a sensible standard can be established, further research is required to determine the nuances of the technique, such as the magnitude of factors that contribute to the increasing non-asymptotic form and to determine which test configuration is more representative for predicting off-road vehicle traction.

References

AASHTO (2002) 'AASHTO T 191-02: Density of Soil In-Place by the Sand-Cone Method'. Washington, USA: American Association of State Highway and Transportation Officials.

AASHTO (2011) 'AASHTO T 310-11: Standard Method of Test for In-Place Density and Moisture Content of Soil and Soil–Aggregate by Nuclear Methods (Shallow Depth)'. Washington, USA: American Association of State Highway and Transportation Officials.

Abdulazeez, A. (2017) 'Effects of Soil Texture on Vegetative and Root Growth of Senna obtusifolia seedlings indigenous to Bichi, Sudan savannah of Northern Nigeria, in Green House Conditions', *IOSR Journal of Agriculture and Veterinary Science*, 10(04), pp. 70–74. doi:10.9790/2380-1004027074.

Agius, D., Wallbrink, C. and Kourousis, K.I. (2017) 'Cyclic Elastoplastic Performance of Aluminum 7075-T6 Under Strain- and Stress-Controlled Loading', *Journal of Materials Engineering and Performance*, 26(12), pp. 5769–5780. doi:10.1007/s11665-017-3047-2.

Al-Khafaji, Amir Wadi; Andersland, O.B. (1992) 'Geotechnical Engineering and Soil Testing', in. Oxford, UK: Oxford University Press.

AMS (2018) *AS5600 12-Bit Programmable Contactless Potentiometer*. Available at: https://ams.com/documents/20143/36005/AS5600_DS000365_5-00.pdf/649ee61c-8f9a-20df-9e10-43173a3eb323 (Accessed: 6 August 2022).

Apfelbeck, M., Kuß, S., Rebele, B. and Schäfer, B. (2011) 'A systematic approach to reliably characterize soils based on Bevameter testing', *Journal of Terramechanics*, 48(5), pp. 360–371. doi:10.1016/j.jterra.2011.04.001.

Apfelbeck, M., Wedler, A., Gibbesch, A. and Rebele, B. (2009) 'A Novel Terramechanics Testbed Setup for Planetary Rover Wheel- Soil Interaction Testbed Setup', in *11th European Regional Conference of the International Society for Terrain-Vehicle Systems*. Bremen, pp. 1–8.

Archer, A. (2014) *Using small-strain stiffness to predict the settlement of shallow foundations on sand*. Masters Thesis, University of Pretoria. Available at: https://repository.up.ac.za/bitstream/handle/2263/43358/Archer_Using_2014.pdf?sequence=1&isAllowed=y (Accessed: 02 April 2022).

Archer, A. and Heymann, G. (2015) 'Using small-strain stiffness to predict the load-settlement behaviour of shallow foundations on sand', *Journal of the South African Institution of Civil Engineering*, 57(2), pp. 28–35. doi:10.17159/2309-8775/2015/v57n2a4.

ASTM (1972) 'ASTM D3080-72: Standard Test Method for Direct Shear Test of Soils Under Consolidated Drained Conditions'. West Conshocken, USA: ASTM International.

ASTM (1991) 'ASTM D4254-91: Standard Test Methods for Minimum Index Density and Unit Weight of Soils and Calculation of Relative Density'. West Conshohocken, USA: ASTM International.

ASTM (1993a) 'ASTM D4253-93: Standard Test Methods for Maximum Index Density and Unit Weight of Soils Using a Vibratory Table'. West Conshohocken, USA: ASTM International.

ASTM (1993b) 'ASTM D4643-93: Determination of Water (Moisture) Content of Soil by the Microwave Oven Method'. Philadelphia, USA: ASTM International.

ASTM (1994) 'ASTM D2167-94: Standard Test Method for Density and Unit Weight of Soil in Place by the Rubber Balloon Method'. West Conshohocken, USA: ASTM International.

ASTM (2006) 'ASTM D 2487-06: Standard Practice for Classification of Soils for Engineering Purposes (Unified Soil Classification System)'. West Conshohocken, USA: ASTM International.

ASTM (2017) 'ASTM D6913-17: Standard Test Methods for Particle-Size Distribution (Gradation) of Soils Using Sieve Analysis'. West Conshohocken, USA: ASTM International.

Azevedo-Filho, A. and Shachter, R.D. (1994) 'Laplace's Method Approximations for Probabilistic Inference in Belief Networks with Continuous Variables', in *Tenth Conference on Uncertainty in Artificial Intelligence*, pp. 28–36. doi:10.1016/b978-1-55860-332-5.50009-2.

Baladi, G.Y. (1987) 'Terrain evaluation for off-road mobility', *Journal of Terramechanics*, 24(2), pp. 127–140. doi:10.1016/0022-4898(87)90003-6.

Basir, S. and Senocak, I. (2022) 'Critical Investigation of Failure Modes in Physics-informed Neural Networks', *AIAA Science and Technology Forum and Exposition, AIAA SciTech Forum 2022* [Preprint]. doi:10.2514/6.2022-2353.

Basu, S. and Bresler, Y. (2000) 'The stability of nonlinear least squares problems and the cramér-rao bound', *IEEE Transactions on Signal Processing*, 48(12), pp. 3426–3436. doi:10.1109/78.887032.

Becker, C.M. (2022) *Parameterisation of Tyres with Large Lugs*. Ph.D. Dissertation, University of Pretoria.

Becker, C.M. and Els, P.S. (2022) 'Effect of surface roughness on tyre characteristics', *Journal of Terramechanics*, 102, pp. 27–48. doi:10.1016/j.jterra.2022.04.003.

Bekker, M.G. (1956) *Theory of Land Locomotion: The Mechanics of Vehicle Mobility*. Ann Arbor, USA: University of Michigan Press.

Bekker, M.G. (1960) *Off-the-road Locomotion: Research and Development in Terramechanics.* Ann Arbor, USA: University of Michigan Press.

Bekker, M.G. (1964) 'Mechanics of Locomotion and Lunar Surface Vehicle Concepts', in *SAE Transactions*, pp. 549–569. doi:10.4271/640049.

Bekker, M.G. (1969) *Introduction to Terrain Vehicle Systems*. Ann Arbor, USA: University of Michigan Press.

Berney, E.S., Ganesh, N.B. and Pratt, T.C. (2018) *A Photogrammetric Method for Obtaining Soil Density*. Washington: United States Army Corps of Engineers. Available at: https://apps.dtic.mil/sti/pdfs/AD1057055.pdf (Accessed: 29 August 2022).

Bilanski, W.K. and L'Esperance, A.L. (1990) 'An investigation of the Bevameter soil physical measurements in the prediction of soil tool draft', *Journal of Terramechanics*, 27(1), pp. 41–50. doi:10.1016/0022-4898(90)90022-E.

Bishop, A.W. (1966) 'The Strength of Soils as Engineering Materials', *Géotechnique*, 16(2), pp. 91–130. doi:10.1680/geot.1966.16.2.91.

Bishop, C.M. (2006) *Pattern Recognition and machine learning*. New York, USA: Springer.

Van Breukelen, G.J.P. (2006) 'ANCOVA versus change from baseline had more power in randomized studies and more bias in nonrandomized studies', *Journal of Clinical Epidemiology*, 59(9), pp. 920–925. doi:10.1016/j.jclinepi.2006.02.007.

Carter, M. and Bentley, S.P. (2016) *Soil Properties and their Correlations*. 2nd Editio. Cardiff, Wales: John Wiley & Sons.

Casella, G. and George, E.I. (1992) 'Explaining the Gibbs Sampler', *The American Statistician*, 46(3), p. 167. doi:10.2307/2685208.

Chang, B.S. and Baker, W.J. (1973) 'Soil parameters to predict the performance of off-road vehicles', *Journal of Terramechanics*, 9(2), pp. 13–31. doi:10.1016/0022-4898(73)90195-X.

Chao, L.-P. and Chen, K.-T. (1997) 'Shape optimal design and force sensitivity evaluation of six-axis force sensors', *Sensors and Actuators A: Physical*, 63(2), pp. 105–112. doi:10.1016/S0924-4247(97)01534-3.

TE Connectivity (2015) *SP1 Compact String Potentiometer*. Available at: https://www.te.com/commerce/DocumentDelivery/DDEController?Action=srchrtrv&DocNm=SP1&DocType=Data+Sheet&DocLang=English (Accessed: 6 August 2022).

Craig, R.F. (2002) *Soil Mechanics*. Sixth Edit. London, UK: Spon Press.

Dagum, P. and Luby, M. (1993) 'Approximating probabilistic inference in Bayesian belief networks is NP-hard', *Artificial Intelligence*, 60(1), pp. 141–153. doi:10.1016/0004-3702(93)90036-B.

Dantan, J.Y., Gayton, N., Qureshi, A.J., Lemaire, M. and Etienne, A. (2013) 'Tolerance Analysis Approach based on the Classification of Uncertainty (Aleatory/Epistemic)', in *12th CIRP Conference on Computer Aided Tolerancing*. Huddersfield, England: Elsevier, pp. 287–293. doi:10.1016/j.procir.2013.08.044.

Dechao, Z. and Yusu, Y. (1991) 'Investigation on the relationship between soil shear strength and shear rate', *Journal of Terramechanics*, 28(1), pp. 1–10. doi:10.1016/0022-4898(91)90002-N.

Ding, L., Gao, H., Deng, Z., Li, Y. and Liu, G. (2014) 'New perspective on characterizing pressure-sinkage relationship of terrains for estimating interaction mechanics', *Journal of Terramechanics*, 52(1), pp. 57–76. doi:10.1016/j.jterra.2014.03.001.

Dowling, N.E. (2013) *Mechanical Behavior of Materials*. Fourth Edi. Edinburgh, UK: Pearson Education.

Dunstan, D.J., Crowne, J. and Drew, A.J. (2022) 'Easy computation of the Bayes factor to fully quantify Occam's razor in least-squares fitting and to guide actions', *Scientific Reports*, 12(1), pp. 1–10. doi:10.1038/s41598-021-04694-7.

Edwards, M.B., Dewoolkar, M.M., Huston, D.R. and Creager, C. (2017) 'Bevameter testing on simulant Fillite for planetary rover mobility applications', *Journal of Terramechanics*, 70, pp. 13–26. doi:10.1016/j.jterra.2016.10.004.

EN (2007) 'EN 1991-1-1(2007) Design of aluminium structures Part 1-1 : General structural rules'. Rue de Stassart, Belgium: European Union Standard.

Expressive Systems (2021) *ESP32 Technical Reference Manual*. Available at: https://www.espressif.com/sites/default/files/documentation/esp32_technical_reference_manual_en.pdf (Accessed: 17 June 2022).

Fisher, R.A. (1922) 'On the Mathematical Foundations of Theoretical Statistics', *Philosophical Transactions of the Royal Society of London*, 222, pp. 309–368.

Fitzmaurice, G., Davidian, M., Verbeke, G. and Molenberghs, G. (2008) *Longitudinal Data Analysis*. New York, USA: Chapman and Hall/CRC Press.

Fong, E. and Holmes, C.C. (2020) 'On the marginal likelihood and cross-validation', *Biometrika*, 107(2), pp. 489–496. doi:10.1093/biomet/asz077.

Foreman-Mackey, D., Hogg, D.W., Lang, D. and Goodman, J. (2013) 'emcee : The MCMC Hammer ', *Publications of the Astronomical Society of the Pacific*, 125(925), pp. 306–312. doi:10.1086/670067.

Gallina, A., Krenn, R. and Schäfer, B. (2016) 'On the treatment of soft soil parameter uncertainties in planetary rover mobility simulations', *Journal of Terramechanics*, 63, pp. 33–47. doi:10.1016/j.jterra.2015.08.002.

Gallina, A., Krenn, R., Scharringhausen, M., Uh, T. and Schäfer, B. (2014) 'Parameter Identification of a Planetary Rover Wheel-Soil Contact Model via a Bayesian Approach', *Journal of Field Robotics*, 33(1), pp. 1–17. doi:10.1002/rob.

Gelman, A., Carlin, J.B., Stern, H.S., Dunson, D.B., Vehtari, A. and Rubin, D.B. (2013) *Bayesian Data Analysis*, *Bayesian Data Analysis*. doi:10.1201/b16018.

Gelman, A., Hill, J. and Yajima, M. (2012) 'Why We (Usually) Don't Have to Worry About Multiple Comparisons', *Journal of Research on Educational Effectiveness*, 5(2), pp. 189–211. doi:10.1080/19345747.2011.618213.

Godwin, R.J., Brighton, J.L., Blackburn, K., Richards, T.E., Ansorge, D. and Wheeler, P.. . (2006) 'Off-Road Dynamics Research at Cranfield University at Silsoe', in *2006 Portland, Oregon, July 9-12, 2006*. St. Joseph, MI: American Society of Agricultural and Biological Engineers. doi:10.13031/2013.20633.

Godwin, R.J., Spoor, G. and Kilgour, J. (1980) 'The design and operation of a simple low cost soil bin', *Journal of Agricultural Engineering Research*, 25(1), pp. 99–104. doi:10.1016/0021-8634(80)90051-7.

Golob, T.B. (1981) 'Development of a terrain strength measuring system', *Journal of Terramechanics*, 18(2), pp. 109–118. doi:10.1016/0022-4898(81)90004-5.

Goodman, J. and Weare, J. (2010) 'Ensemble samplers with affine invariance', *Communications in Applied Mathematics and Computational Science*, 5(1), pp. 65–80. doi:10.2140/camcos.2010.5.65.

Harnisch, C., Lach, B., Jakobs, R. and Troulis, M. (2011) 'A new tyre – soil interaction model for vehicle simulation on deformable ground A new tyre – soil interaction model for vehicle simulation on deformable ground', 3114. doi:10.1080/00423110500139981.

Harris, C.R., Millman, K.J., van der Walt, S.J., Gommers, R., Virtanen, P., Cournapeau, D., Wieser, E., Taylor, J., Berg, S., Smith, N.J., Kern, R., Picus, M., Hoyer, S., van Kerkwijk, M.H., Brett, M., Haldane, A., del Río, J.F., Wiebe, M., Peterson, P., Gérard-Marchant, P., Sheppard, K., Reddy, T., Weckesser, W., Abbasi, H., Gohlke, C. and Oliphant, T.E. (2020) 'Array programming with NumPy', *Nature*, 585(7825), pp. 357–362. doi:10.1038/s41586-020-2649-2.

He, C., You, Y., Wang, D. and Wu, H. (2018) 'Estimating soil failure due to torsion via vane shear test by varying vane diameter and soil properties', *Soil and Tillage Research*, 177, pp. 68–78. doi:10.1016/j.still.2017.12.004.

He, J., Wang, W., Huang, M., Wang, S. and Guan, X. (2021) 'Bayesian inference under small sample sizes using general noninformative priors', *Mathematics*, 9(21), pp. 1–20. doi:10.3390/math9212810.

He, R., Sandu, C., Khan, A.K., Guthrie, A.G., Els, P.S. and Hamersma, H.A. (2019a) 'Review of terramechanics models and their applicability to real-time applications', *Journal of Terramechanics*, 81, pp. 3–22. doi:10.1016/j.jterra.2018.04.003.

He, R., Sandu, C., Mousavi, H., Shenvi, M.N., Braun, K., Kruger, R. and Els, P.S. (2020) 'Updated standards of the international society for terrain-vehicle systems', *Journal of Terramechanics*, 91, pp. 185–231. doi:10.1016/j.jterra.2020.06.007.

He, R., Sandu, C. and Osorio, J.E. (2019b) 'Systematic tests for study of tire tractive performance on soft soil: Part 1 - Experimental data collection', *Journal of Terramechanics*, 85, pp. 59–76. doi:10.1016/j.jterra.2019.07.004.

Hougaard, P. (1988) 'The Asymptotic Distribution of Nonlinear Regression Parameter Estimates: Improving the Approximation', *International Statistical Review / Revue Internationale de Statistique*, 56(3), p. 221. doi:10.2307/1403350.

Intergovernmental Panel on Climate Change (2015) *Climate Change 2014: Mitigation of Climate Change: Contribution of Working Group III to the Fifth Assessment Report*. Cambridge, UK: Cambridge University Press.

Janosi, Z. and Hanamoto, B. (1961) 'The analytical determination of drawbar pull as a function of slip for tracked vehicles in deformable soils', in *Proceedings of the 1st International Conference on the Mechanics of Soil Vehicle System*. Torino, Italy.

Jefferies, M.G. (1993) 'Nor-Sand: A simple critical state model for sand', *Geotechnique*, 43(1), pp. 91–103. doi:10.1680/geot.1993.43.1.91.

Jeffreys, H. (1961) *Theory of Probability*. Oxford, UK: Oxford University Press.

Jiang, Y., Wang, G. and Kamai, T. (2017) 'Fast shear behavior of granular materials in ring-shear tests and implications for rapid landslides', *Acta Geotechnica*, 12(3), pp. 645–655. doi:10.1007/s11440-016-0508-y.

Kaniraj, S.R. (1988) 'Design Aids in Soil Mechanics and Foundation Engineering'. New Deli, India: Tata McGraw-Hill Publishing Company Limited.

Karstunen, M. and Amavasai, A. (2017) *Soft soil modelling and parameter determination*. Gothenburg, Sweden : Chamlers University Of Technology. Available at: https://research.chalmers.se/publication/522789/file/522789_Fulltext.pdf (Accessed: 29 August 2022).

Kelter, R. (2020) 'Analysis of Bayesian posterior significance and effect size indices for the two-sample t-test to support reproducible medical research', *BMC Research Notes*, 13(1), pp. 1–18. doi:10.1186/s13104-020-05291-z.

Kim, J.T., Im, D., Park, J.H., Choi, H.J., Oh, J.W., Cho, S.J. and Park, Y.J. (2022) 'Experimental analysis of mechanical properties of coastal terrain via bevameter tests', *Journal of Terramechanics*, 100, pp. 39–50. doi:10.1016/j.jterra.2021.12.001.

Kim, J.T., Im, D.U., Choi, H.J., Oh, J.W. and Park, Y.J. (2021) 'Development and Performance Evaluation of a Bevameter for Measuring Soil Strength', *Sensors*, 21(4), p. 1541. doi:10.3390/s21041541.

Kruschke, J.K. (2013) 'Bayesian estimation supersedes the t test', *Journal of Experimental Psychology: General*, 142(2), pp. 573–603. doi:10.1037/a0029146.

Kruschke, J.K., Aguinis, H. and Joo, H. (2012) 'The Time Has Come', *Organizational Research Methods*, 15(4), pp. 722–752. doi:10.1177/1094428112457829.

Kruschke, J.K. and Liddell, T.M. (2018) 'The Bayesian New Statistics: Hypothesis testing, estimation, meta-analysis, and power analysis from a Bayesian perspective', *Psychonomic Bulletin & Review*, 25(1), pp. 178–206. doi:10.3758/s13423-016-1221-4.

Kumar, S., Noori, M.T. and Pandey, K.P. (2019) 'Performance characteristics of mode of ballast on energy efficiency indices of agricultural tyre in different terrain condition in controlled soil bin environment', *Energy*, 182, pp. 48–56. doi:10.1016/j.energy.2019.06.043.

Lanthaler, S., Mishra, S. and Weber, F. (2022) 'On Bayesian data assimilation for PDEs with ill-posed forward problems', *Inverse Problems*, 38(8), pp. 1–43. doi:10.1088/1361-6420/ac7acd.

Latz, J. (2020) 'On the well-posedness of Bayesian inverse problems', *SIAM-ASA Journal on Uncertainty Quantification*, 8(1), pp. 451–482. doi:doi.org/10.1137/19M1247176.

Li, D., Yin, K., Glade, T. and Leo, C. (2017) 'Effect of over-consolidation and shear rate on the residual strength of soils of silty sand in the Three Gorges Reservoir', *Scientific Reports*, 7(1), pp. 1–11. doi:10.1038/s41598-017-05749-4.

Lin, H.-M., Wu, J.-H. and Sunarya, E. (2018) 'Consolidated and Undrained Ring Shear Tests on the Sliding Surface of the Hsien-du-shan Landslide in Taiwan', *Geofluids*, 2018, pp. 1–12. doi:10.1155/2018/9410890.

Lin, Z., Zou, Q., Ward, E.S. and Ober, R.J. (2005) 'Cramer-Rao lower bound for parameter estimation in nonlinear systems', *IEEE Signal Processing Letters*, 12(12), pp. 855–858. doi:10.1109/LSP.2005.859498.

Lisowski, A., Świętochowski, A., Dąbrowska, M., Klonowski, J., Nowakowski, T., Chlebowski, J., Tryskuć, P., Parys, T., Ferré, S. and Roberge, M. (2022) 'Effect of Stone Impacts on Various Ground Engaging Tools (Flexible/Stiff Tines and Coulter): Part I', *Materials*, 15(4). doi:10.3390/ma15041568.

Liu, S.A. and Tzo, H.L. (2002) 'A novel six-component force sensor of good measurement isotropy and sensitivities', *Sensors and Actuators, A: Physical*, 100(2–3), pp. 223–230. doi:10.1016/S0924-4247(02)00135-8.

Lyasko, M. (2010a) 'How to calculate the effect of soil conditions on tractive performance', *Journal of Terramechanics*, 47(6), pp. 423–445. doi:10.1016/j.jterra.2010.04.003.

Lyasko, M. (2010b) 'Multi-pass effect on off-road vehicle tractive performance', *Journal of Terramechanics*, 47(5), pp. 275–294. doi:10.1016/j.jterra.2010.05.006.

Lynas, M., Houlton, B.Z. and Perry, S. (2021) 'Greater than 99% consensus on human caused climate change in the peer-reviewed scientific literature', *Environmental Research Letters*, 16(11). doi:10.1088/1748-9326/ac2966.

Mähönen, J., Lintzén, N. and Casselgren, J. (2021) 'Portable bevameter for measuring snow properties in field', *Cold Regions Science and Technology*, 182(May 2020). doi:10.1016/j.coldregions.2020.103195.

Makowski, D., Ben-Shachar, M.S., Chen, S.H.A. and Lüdecke, D. (2019) 'Indices of Effect Existence and Significance in the Bayesian Framework', *Frontiers in Psychology*, 10(December), pp. 1–14. doi:10.3389/fpsyg.2019.02767.

Marin, J.-M. and Robert, C.P. (2009) *Importance sampling methods for Bayesian discrimination between embedded models*, *ArXiv preprint*. Available at: http://arxiv.org/abs/0910.2325 (Accessed 30 September 2022).

Massah, J. and Noorolahi, S. (2010) 'Design, development and performance evaluation of a tractor-mounted bevameter', *Soil and Tillage Research*, 110(1), pp. 161–166. doi:10.1016/j.still.2010.07.002.

Mavin (2020) *Mavin Load Cell*. Available at: https://www.mavin.cn/uploadfile/downloads/Mavin catalog.pdf (Accessed: 6 August 2022).

MeshRoom (2021) *CameraInit*, *meshroom-manual*. Available at: https://readthedocs.org/projects/meshroom-manual/downloads/pdf/latest/ (Accessed: 5 October 2021).

Montgomery, D.C. and Runger, G.. (2014) *Applied Statistics and Probability for engineers*. 6th Editio. Hoboken, USA: John Wiley and Sons.

Muro, T. and O'Brien, J. (2005) *Terramechanics-Land Locomotion Mechanics*. Tokyo, Japan: A.A. Balkema Publishers.

Naranjo, S.D., Sandu, C., Taheri, Saied and Taheri, Shahyar (2014) 'Experimental testing of an off-road instrumented tire on soft soil', *Journal of Terramechanics*, 56, pp. 119–137. doi:10.1016/j.jterra.2014.09.003.

NATO (2021) *AMSP-06 Guidance for Standards Applicable To the Development of Next Generation Nato Reference Mobility Models (NG-NRMM)*. Available at: https://nso.nato.int/nso/nsdd/main/standards?search=AMSP-06 (Accesed: 02 April 2022).

Nemeth, C. and Fearnhead, P. (2019) 'Stochastic Gradient Markov Chain Monte Carlo', *Journal of the American Statistical Association*, 116(533), pp. 433–450. doi:10.1080/01621459.2020.1847120.

Okello, A. (1991) 'A review of soil strength measurement techniques for prediction of terrain vehicle performance', *Journal of Agricultural Engineering Research*, 50(C), pp. 129–155. doi:10.1016/S0021-8634(05)80010-1.

Omega (n.d.) *Strain Gauge Installation: How to Position Strain Gauges to Monitor Bending, Axial, Shear, and Torsional Loads*. Available at: https://www.omega.co.uk/techref/pdf/Strain-gauge-application-info/how-to-position-strain-gauges.pdf (Accessed: 15 June 2022).

Osinenko, P. V., Geissler, M. and Herlitzius, T. (2015) 'A method of optimal traction control for farm tractors with feedback of drive torque', *Biosystems Engineering*, 129, pp. 20–33. doi:10.1016/j.biosystemseng.2014.09.009.

Pinto, E. (2012) *A three dimensional discretized tire model for soft soil applications*. Masters Thesis, Virginia Polytechnic Institute and State University. Available at: https://vtechworks.lib.vt.edu/bitstream/handle/10919/41335/Pinto_EJ_T_2012.pdf?sequence=2&isAllowed=y (Accesed: 02 April 2022).

Raper, R.L., Bailey, A.C., Burt, E.C., Way, T.R. and Liberati, P. (1995) 'Inflation pressure and dynamic load effects on soil deformation and soil-tire interface stresses', *Transactions - American Society of Agricultural Engineers*, 38(3), pp. 685–689. doi:10.13031/2013.27881.

Van Ravenzwaaij, D., Monden, R., Tendeiro, J.N. and Ioannidis, J.P.A. (2019) 'Bayes factors for superiority, non-inferiority, and equivalence designs', *BMC Medical Research Methodology*, 19(1), pp. 1–12. doi:10.1186/s12874-019-0699-7.

Reece, A.R. (1964) *Problems of Soil-Vehicle Mechanics*. Warren, US: United States Army Land Locomotion Laboratory. Available at: https://apps.dtic.mil/sti/pdfs/AD0450151.pdf (Accessed 30 September 2022).

Reece, A.R. (1981) 'An assessment of the value of cone penetrometer in mobility prediction', in *7th ISTVS International Conference*. Calgary, Canada.

Reece, S. and Nicholson, D. (2007) 'Tighter alternatives to the cramér-rao lower bound for discretetime filtering', *Bayesian Bounds for Parameter Estimation and Nonlinear Filtering/Tracking*, pp. 717–722. doi:10.1109/9780470544198.ch72.

Rouder, J.N., Speckman, P.L., Sun, D., Morey, R.D. and Iverson, G. (2009) 'Bayesian t-tests for accepting and rejecting the null hypothesis', *Psychonomic Bulletin and Review*, 16(2), pp. 225–237. doi:10.3758/PBR.16.2.225.

Rupp, A.A., Dey, D.K. and Zumbo, B.D. (2004) 'To bayes or not to bayes, from whether to when: Applications of Bayesian methodology to modeling', *Structural Equation Modeling*, 11(3), pp. 424–451. doi:10.1207/s15328007sem1103_7.

SAE (1967) 'SAE J939 Off-Road Vehicle Mobility Evaluation'. New York, USA: Society of Automotive Engineers.

Sakata, S.I., Ashida, F. and Zako, M. (2008) 'Approximate structural optimization using kriging method and digital modeling technique considering noise in sampling data', *Computers and Structures*, 86(13–14), pp. 1477–1485. doi:10.1016/j.compstruc.2007.05.007.

Salman, N.D., Pillinger, G., Hanon, M.M. and Kiss, P. (2020) 'Design and performance evaluation of bevameter equipment', *Journal of Advanced Mechanical Design, Systems and Manufacturing*, 14(6), pp. 1–9. doi:10.1299/JAMDSM.2020JAMDSM0084.

Sandu, C., Taheri, S, Taheri, Sh and Gorsich, D. (2019a) 'Hybrid Soft Soil Tire Model (HSSTM). Part I : Tire material and structure modeling', *Journal of Terramechanics*, 86, pp. 1–13. doi:10.1016/j.jterra.2019.08.002.

Sandu, C., Taheri, Sh, Taheri, S and Gorsich, D. (2019b) 'Hybrid Soft Soil Tire Model (HSSTM). Part II: Tire-terrain interaction', *Journal of Terramechanics*, 86, pp. 15–29. doi:10.1016/j.jterra.2019.08.004.

SANS (2006) 'SANS 5845:2006 Bulk Densities and Void Content of Aggregates'. Pretoria, South Africa: South African National Standards.

SANS (2014) 'SANS 3001-GR3:2014 Civil engineering test methods-Part GR3: Particle size analysis of material smaller than 2 mm (hydrometer method)'. Pretoria, South Africa: South African National Standards.

SANS (2015) 'SANS 3001-GR30:2015 Determination of the Maximum Dry Density and Optimum Moisture Content'. Pretoria, South Africa: South African National Standards.

Sawicki, J., Łoś, M., Smołka, M., Schaefer, R. and Álvarez-Aramberri, J. (2018) 'Approximating landscape insensitivity regions in solving ill-conditioned inverse problems', *Memetic Computing*, 10(3), pp. 279–289. doi:10.1007/s12293-018-0258-5.

Scaringi, G., Hu, W., Xu, Q. and Huang, R. (2018) 'Shear-Rate-Dependent Behavior of Clayey Bimaterial Interfaces at Landslide Stress Levels', *Geophysical Research Letters*, 45(2), pp. 766–777. doi:10.1002/2017GL076214.

Schönbrodt, F.D., Wagenmakers, E., Zehetleitner, M. and Perugini, M. (2017) 'Sequential hypothesis testing with Bayes factors: Efficiently testing mean differences.', *Psychological Methods*, 22(2), pp. 322–339. doi:10.1037/met0000061.

Schönbrodt, F.D. and Wagenmakers, E.J. (2018) 'Bayes factor design analysis: Planning for compelling evidence', *Psychonomic Bulletin and Review*, 25(1), pp. 128–142. doi:10.3758/s13423-017-1230-y.

Scott, D.W. (1979) 'On optimal and data-based histograms', *Biometrika*, 66(3), pp. 605–610. doi:10.2307/2335182.

Seber, G.A.F. and Wild, C.J. (2003) *Nonlinear Regression*. Auckland, New Zealand: John Wiley & Sons.

Senatore, C. and Sandu, C. (2011) 'Off-road tire modeling and the multi-pass effect for vehicle dynamics simulation', *Journal of Terramechanics*, 48(4), pp. 265–276. doi:10.1016/j.jterra.2011.06.006.

Seyedan, S. and Sołowski, W.T. (2019) 'Enhancing Constitutive Models for Soils: Adding the Capability to Model Nonlinear Small Strain in Shear', *Advances in Civil Engineering*, 2019. doi:10.1155/2019/6016350.

Shamrao, Padmanabhan, C., Gupta, S. and Mylswamy, A. (2018) 'Estimation of terramechanics parameters of wheel-soil interaction model using particle filtering', *Journal of Terramechanics*, 79, pp. 79–95. doi:10.1016/j.jterra.2018.07.003.

Shoop, S.A. (1993a) *Terrain Characterization for Trafficability*. Springfield, USA. Available at: https://erdc-library.erdc.dren.mil/jspui/bitstream/11681/9158/1/CRREL-93-6.pdf (Accessed: 15 August 2022).

Shoop, S.A. (1993b) 'Thawing soil strength measurements for predicting vehicle performance', *Journal of Terramechanics*, 30(6), pp. 405–418. doi:10.1016/0022-4898(93)90034-U.

Söhne, W. (1968) 'Four-wheel drive or rear-wheel drive for high power farm tractors', *Journal of Terramechanics*, 5(3), pp. 9–28. doi:10.1016/0022-4898(68)90078-5.

Stafford, J. V. and Tanner, D.W. (1982) 'The 9th conference of the international soil tillage research organization (ISTRO)', in *Soil and Tillage Research*, pp. 656–661.

Stocker, T.F., Qin, D., Plattner, G.-K., Tignor, M., Allen, S.K., Boschung, J., Nauels, A., Xia, Y., And, V.B. and Midgley, P.M. (2013) *Technical Summary. In: Climate Change 2013: The Physical Science Basis. Contribution of Working Group I to the Fifth Assessment Report of the Intergovernmental Panel on Climate Change*, *Climate Change 2013 - The Physical Science Basis*. Cambridge. doi:10.1017/cbo9781107415324.005.

Taheri, Sh, Sandu, C., Taheri, S., Pinto, E. and Gorsich, D. (2015a) 'A technical survey on Terramechanics models for tire-terrain interaction used in modeling and simulation of wheeled vehicles', *Journal of Terramechanics*, 57, pp. 1–22. doi:10.1016/j.jterra.2014.08.003.

Taheri, Sh, Sandu, C., Taheri, S., Pinto, E. and Gorsich, D. (2015b) 'A technical survey on Terramechanics models for tire-terrain interaction used in modeling and simulation of wheeled vehicles', *Journal of Terramechanics*, 57(1), pp. 1–22. doi:10.1016/j.jterra.2014.08.003.

Tekscan (2022) *Pressure Mapping Sensor 8001*, *Tekscan*. Available at: https://tekscan.com/sites/default/files/resources/IDL-Pressure-Mapping-Sensor-8001-Datasheet.pdf (Accessed: 9 April 2022).

Trelleborg (2021) *Technical Data*. Available at: https://www.trelleborg.com/wheels/-/media/tires-aft/datatsheet/brochure/trelleborg-pressure-table_eng.pdf?rev=55d7697697ba4c09bf83a9dcde9fdc4c&hash=3B2858BF0455AC1BE310DFD58CCF52E0 (Accessed: 5 September 2021).

Tsitouridis, G. (2019) *Terramechanics and Soil-Wheel Interactions for Road Vehicle Applications*. Ph.D dissertation, Loughborough University. Available at: https://repository.lboro.ac.uk/ndownloader/files/21813933/1 (Accessed: 02 April 2022).

Upadhyaya, S.K., Chancellor, W.J., Perumpral, J. V., Schafer, R.L., Gill, W.R. and VandenBerg, G.E. (1994) *Advances in Soil Dynamics*. Vol. 1. St. Joseph, USA: American Society of Agricultural and Biological Engineers.

Upadhyaya, S.K., Perumpral, J. V, Wulfsohn, D. and Way, T.R. (2009) *Advances in Soil Dynamics*. Vol. 2. St. Joseph, USA: American Society of Agricultural and Biological Engineers.

Upadhyaya, S.K., Wulfsohn, D. and Jubbal, G. (1989) 'Traction prediction equations for radial ply tyres', *Journal of Terramechanics*, 26(2), pp. 149–175. doi:10.1016/0022-4898(89)90004-9.

Upadhyaya, S.K., Wulfsohn, D. and Mehlschau, J. (1993) 'An instrumented device to obtain traction related parameters', *Journal of Terramechanics*, 30(1), pp. 1–20. doi:10.1016/0022-4898(93)90027-U.

USDA (1987) *United States Department of Agriculture*, *Soil Mechanics Level I Module 3 - USDA Textural Soil Classification Study Guide*. Available at: https://www.nrcs.usda.gov/Internet/FSE_DOCUMENTS/stelprdb1044818.pdf.

Van, N.N., Matsuo, T., Koumoto, T. and Inaba, S. (2008) *Experimental Device for Measuring Sandy Soil Sinkage Parameters*, *Bulletin Faculty Agriculture, Saga University*. Available at: https://core.ac.uk/download/pdf/59165296.pdf (Accessed 30 August 2022).

Wagenmakers, E., Love, J., Marsman, M., Jamil, T. and Ly, A. (2018) 'Bayesian inference for psychology . Part II : Example applications', 25(1), pp. 58–76. doi:10.3758/s13423-017-1323-7.

Wagenmakers, E.J., Lodewyckx, T., Kuriyal, H. and Grasman, R. (2010) 'Bayesian hypothesis testing for psychologists: A tutorial on the Savage-Dickey method', *Cognitive Psychology*, 60(3), pp. 158–189. doi:10.1016/j.cogpsych.2009.12.001.

Wang, G., Suemine, A. and Schulz, W.H. (2010) 'Shear-rate-dependent strength control on the dynamics of rainfall-triggered landslides, Tokushima Prefecture, Japan', *Earth Surface Processes and Landforms*, 35(4), pp. 407–416. doi:10.1002/esp.1937.

Wang, Y. and Cong, L. (2019) 'Effects of Water Content and Shearing Rate on Residual Shear Stress', *Arabian Journal for Science and Engineering*, 44(10), pp. 8915–8929. doi:10.1007/s13369-019-03922-7.

Wells, L.G. and Treesuwan, O. (1978) 'Response of Various Soil Strength Indices To Changing Water Content and Bulk Density', *Transactions of the American Society of Agricultural Engineers*, 21(5), pp. 854–861. doi:10.13031/2013.35401.

Wong, J.Y. (1984) 'An introduction to terramechanics', *Journal of Terramechanics*, 21(1), pp. 5–17. doi:10.1016/0022-4898(84)90004-1.

Wong, J.Y. (1989) *Terramechanics and Off-Road Vehicles*. Amsterdam, Netherlands: Elsevier.

Wong, J.Y. (2010) *Terramechanics and Off-Road Vehicle Engineering (Second Edition)*. Oxford, UK: Butterworth-Heinemann.

Wong, J.Y., Garber, M., Radforth, J.R. and Dowell, J.T. (1979) 'Characterization of the mechanical properties of muskeg with special reference to vehicle mobility', *Journal of Terramechanics*, 16(4), pp. 163–180. doi:10.1016/0022-4898(79)90026-0.

Wong, J.Y. and Reece, A.R. (1967) 'Prediction of rigid wheel performance based on the analysis of soil-wheel stresses. Part II. Performance of towed rigid wheels', *Journal of Terramechanics*, 4(2), pp. 7–25. doi:10.1016/0022-4898(67)90047-X.

Appendices

Appendix A-Data used for estimating Bevameter shear loads

Table A-1: Internal friction angle and shear stress ratio for a range of soils (predominantly cohesionless soils).

Soil Description	**Friction Angle ϕ**	**Stress Ratio (τ/σ)**	**Reference**
Sandy gravel-dense	50	1.19	(Carter and Bentley, 2016)
Well-graded sand, angular grains- dense	45	1.00	(Carter and Bentley, 2016)
Very dense sand-unconsolidated	41-43	0.86-0.93	(Carter and Bentley, 2016)
Dense sand-unconsolidated	36-43	0.72-0.86	(Bishop, 1966)
Silty sand & gravel	40	0.83	(Bishop, 1966)
Sand	38	0.78	(Bishop, 1966)
Rock fill	36	0.72	(Bishop, 1966)
Sandy gravel-loose	35	0.70	(Carter and Bentley, 2016)
Glacial till	35	0.70	(Bishop, 1966)
Medium dense sand-unconsolidated	30-36	0.58-0.72	(Carter and Bentley, 2016)
Uniform sand, round grains-dense	34	0.67	(Carter and Bentley, 2016)
Inorganic silt-dense	30-35	0.58-0.70	(Carter and Bentley, 2016)
Silty sand-dense	30-34	0.58-0.67	(Carter and Bentley, 2016)
Well-graded sand, angular grains-loose	33	0.65	(Carter and Bentley, 2016)
Silty sand-Loose	27-33	0.51-0.67	(Carter and Bentley, 2016)
Canyonville silt	32	0.62	(Bishop, 1966)
Chattahoochee river sand	32	0.62	(Bishop, 1966)
Loose sand- unconsolidated	28-30	0.53-0.58	(Carter and Bentley, 2016)
Very Loose sand- unconsolidated	26-28	0.49-0.53	(Carter and Bentley, 2016)
Inorganic silt-loose	27-30	0.51-0.57	(Carter and Bentley, 2016)
Avonmouth clay	28	0.53	(Bishop, 1966)
Uniform sand- round grains-loose	27	0.51	(Carter and Bentley, 2016)
London clay-undisturbed	20	0.36	(Bishop, 1966)
London clay	16	0.28	(Bishop, 1966)
Mean	**33.4**	**0.67**	
SD	**6.9**	**0.21**	

Appendix B-Four degree of freedom load cell modelling and shape optimization

Strain gauge configuration

The load cell strain gauge configuration is indicated in Figure B-1. The load cell employs four full Wheatstone bridges with individual strain gauges labelled R1 to R16. Also indicated are the critical dimensions (D1-D9) determined by numeric optimization. Note D2 (top shaft length) is not indicated.

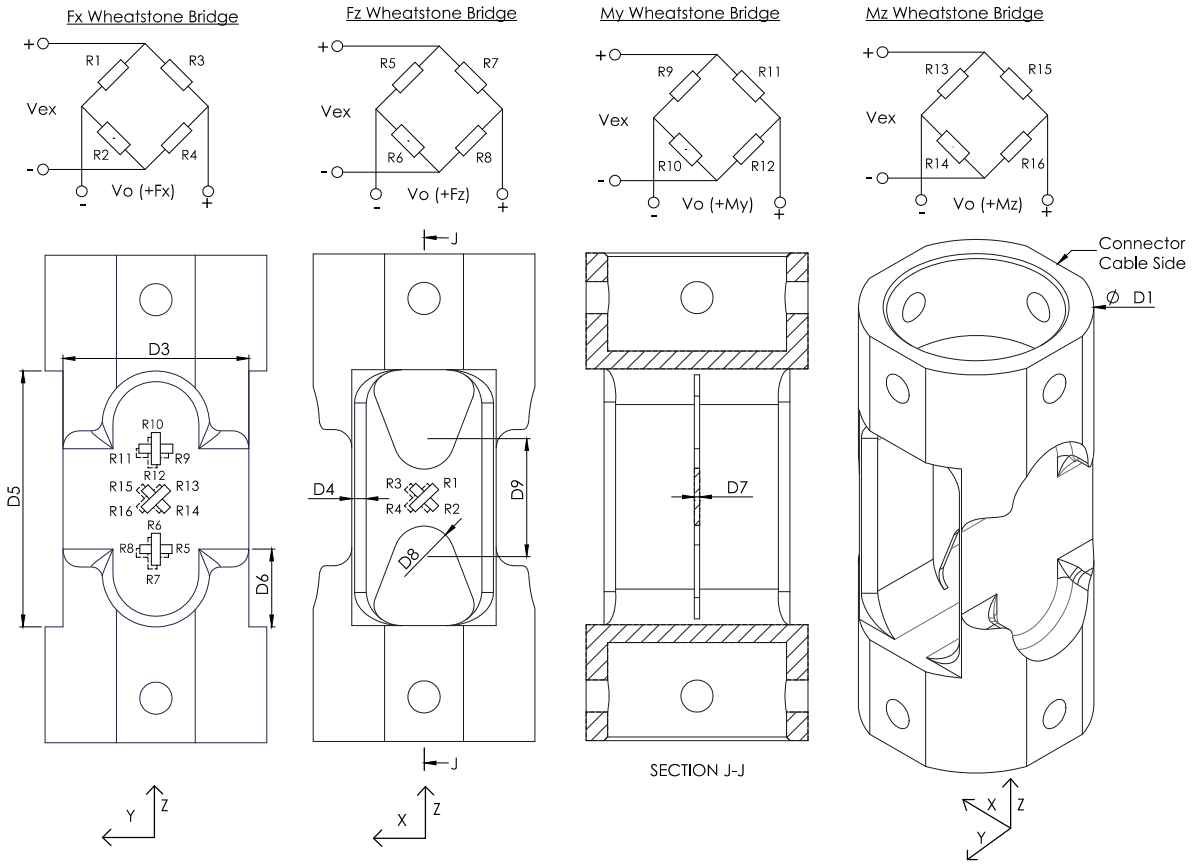

Figure B-1: 4 DOF load cell strain gauge configuration and critical dimensions.

Table B-1 indicates which Wheatstone bridges are theoretically compensated for superimposed strain from loading in other directions. See the technical report by Omega (n.d.) for detail on how this can be determined. All channels except M_y exhibit no theoretical cross-coupling. Channel M_y exhibits cross-coupling due to an unavoidable bending moment around the M_y axis when loaded in the F_x direction.

Table B-1: 4 DOF load cell superimposed strain compensation matrix.

Wheatstone Bridge / Loading Direction	F_x	F_y	F_z	M_x	M_y	M_z
F_x **Bridge**	-	Yes	Yes	Yes	Yes	Yes
F_z **Bridge**	Yes	-	Yes	Yes	Yes	Yes
M_y **Bridge**	**No**	Yes	Yes	Yes	-	Yes
M_z **Bridge**	Yes	Yes	Yes	Yes	Yes	-

Load cell material

The transducer is made of 7075-T6 aluminium. This specific alloy is a common material choice for force transducers due to its high strength (500MPa), low modulus of elasticity E (71GPa) and linear stress-strain curve up to the yield point (Chao and Chen, 1997; Liu and Tzo, 2002; Agius *et al.*, 2017).

Determining the maximum allowable transducer stress

The maximum transducer stress was determined using a fatigue life approach. Realistically, only a few hundred Bevameter tests will ever be performed; therefore, a fatigue life of 1000 cycles was specified. A strain life approach was employed as it is a more rational approach that considers local stress concentrations, as opposed to nominal stresses for the stress life approach (Dowling, 2013).

For the strain life approach, the strain amplitude ϵ_a is expressed by the Ramberg-Osgood equation,

$$\epsilon_a = \frac{\sigma_a}{E} + \left(\frac{\sigma_a}{H'E}\right)^{1/n} \tag{45}$$

Where σ_a is the stress amplitude, H' is the strength coefficient, and n is the strain hardening coefficient. The coefficients for 7075-T6 alloy, and all other material coefficients used for the strain life calculation, can be found in Table 14.1 in Dowling (2013). The Coffin-Manson equation then relates strain amplitude ϵ_a to the number of cycles to failure N_f,

$$\epsilon_a = \frac{\sigma_f{}'}{E}(2N_f)^b + \epsilon_f{}'(2N_f)^c \tag{46}$$

Where quantities $\sigma_f', b, \epsilon_f{}'$ and c are material properties describing the strain life behaviour. Setting Equation (45) equal to equation (46) results in an implicit relation for stress amplitude.

In this application, the load cell will always only be used in one direction, therefore inducing mean stress. Dowling (2013) recommends using Smith Weston and Topper (SWT) mean stress correction for aluminium alloys. Equation (46) with the SWT mean stress compensation incorporated is given as,

$$\sigma_{max}\epsilon_a = \sigma_f{}'(2N_f)^b\left[\frac{\sigma_f{}'}{E}(2N_f)^b + \epsilon_f{}'^{(2N_f)^c}\right] \tag{47}$$

Where,

$$\begin{aligned}\sigma_{max} &= 2\sigma_a + \sigma_{min} \\ &= 2f(\epsilon_a) + \sigma_{min}\end{aligned} \tag{48}$$

The stress amplitude $\sigma_a = f(\epsilon_a)$ indicates the stress amplitude from equation (45) as an implicit function of strain amplitude ϵ_a, which is solved numerically. In this application $\sigma_{min} = 0$.

Equation (47) requires further correction for environmental factors. However, at a low number of cycles, the fatigue life is not highly sensitive to environmental factors. The only reduction factors recommended are size effects and surface finish (Dowling, 2013). However, size effects are not available for complex shapes, therefore omitted. For a machined surface, b is reduced to b_s,

$$b_s = b + \frac{\log(4.51\sigma_u^{-0.265})}{\log(2N_e)} \tag{49}$$

Where σ_u is the ultimate tensile stress and N_e is the endurance limit (taken as 10^8 for aluminium).

A final reduction factor is included for material property and load case uncertainty. The EN 199-1-3:2007 (EN, 2007) standard recommends a safety factor of $\gamma_{Ff} = 1$ for consequence class CC2 (low), and design approach DTD-II (damage tolerant design). Since $\gamma_{Ff} = 1$, no further reduction is required.

Substituting the correction factor b_s into equation (47), equation (47) is solved numerically for strain amplitude. The Python $scipy.optimize.fsolve$ numeric solver was utilised for this task.

The fatigue life calculation results are indicated in Figure B-2. The maximum allowed strain is 5447$\mu\epsilon$ and the maximum allowed stress is 378MPa. This corresponds to a yield safety factor of 1.33.

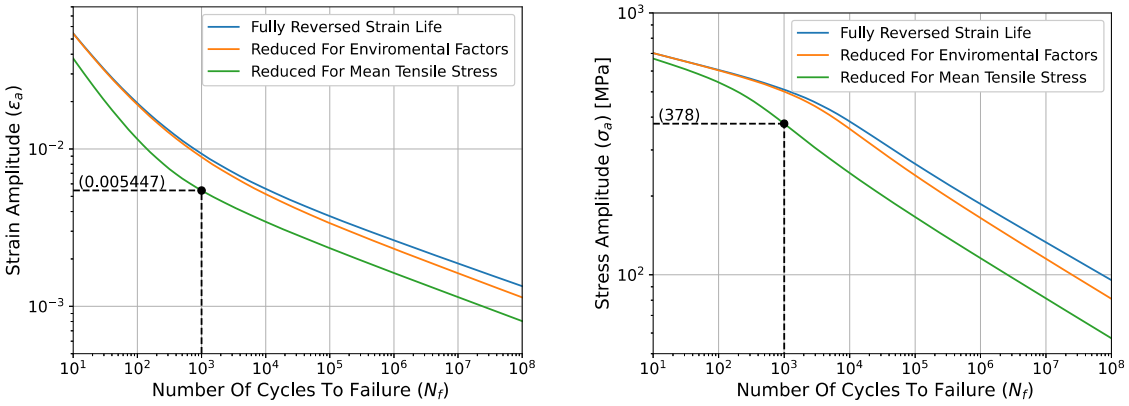

(a) (b)

Figure B-2: Load cell fatigue life. (a) Strain life curve. (b) Stress life curve.

Finite element modelling and transducer shape optimization

The technology stack used to implement FEM modelling and shape optimization is indicated below,

- FEM package: Solidworks Simulate
- Interface layer: Visual Basic with Solidworks API plugin
- Numeric optimization: Python $scipy.optimise$ library

At each iteration step, the numeric optimization package passes input parameters (D1-D9) from Figure B-1 to the interface layer, which instructs the FEM package to update the CAD geometry, mesh the solid body and runs two linear FEM analyses, each applying the design load. Once each iteration is finished, the overall maximum stress and individual strains of the strain gauges are measured.

The objective function Φ maximised by the optimization is indicated in equation (50),

$$\Phi(\epsilon_{1-16}) = 0.75(\frac{\epsilon_1 - \epsilon_2 - \epsilon_3 + \epsilon_4}{4}) + 0.25(\frac{\epsilon_{13} - \epsilon_{14} - \epsilon_{15} + \epsilon_{16}}{4}) \quad (50)$$

Where ϵ_{1-16} is the measured strain that corresponds with strain gauge R1-16. The objective function placed more weight on the shear bridge as it exhibited lower strain than the torsional bridge. The load cell was only optimized for linear and torsional shear. The cross-sectional area required to withstand the required torque and shear loads leads to a large cross-sectional area that results in small strains in the vertical direction. For vertical force measurement, the S-type load cells from Figure 15 is utilised.

The optimization algorithm employed was Constrained Optimization By Linear Approximation (COBYLA). This method was used because gradient-based methods are known to struggle with FEM shape optimization (Sakata *et al.*, 2008). The solution space was constrained by 17 inequality constraints, as indicated in Table B-2. The results of the optimization are also indicated in Table B-2.

Table B-2: FEM model parameter constraints and optimisation results.

Parameter	Description	Lower Bound	Upper Bound	Initial Value	Optimised Value
D1	Outside diameter [mm]	50	70	70	65.8
D2	Top shaft length [mm]	-	-	-	173 (Fixed)
D3	Width (as ratio of D1) [mm]	0.5	0.9	0.5	0.614
D4	Flange thickness [mm]	4	10	4	4
D5	Height [mm]	65	85	65	71.8
D6	Side extrude [mm]	5	22	10	16.8
D7	Web thickness [mm]	1.5	5	1.5	1.5
D8	Cut diameter[mm]	8	40	8	17.1
D9	Cut spacing [mm]	8	20	8	8
-	Maximum stress [MPa]	-	375	-	374

The evolution of objective function and primary constraint (maximum stress) is indicated in Figure B-3. The COBYLA method quickly converged to an optimum value, after which it oscillated near the optimum value as it attempted to satisfy the maximum stress constraint indicated in Figure B-3 (b).

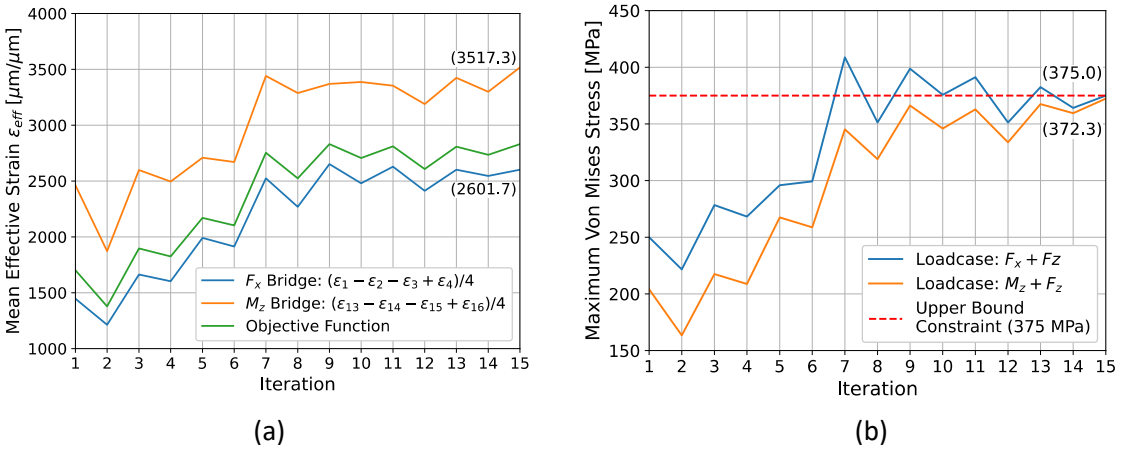

Figure B-3: Load cell optimization performance metrics. (a) Objective function. (b) Primary constraint.

The stress and strain fields of the optimised load cell are indicated in Figure B-4. Also indicated is the mesh, which consists of 1mm quadratic tetrahedral elements and 0.5mm elements in areas of high stress. Further mesh refinement did not significantly affect the results, indicating the FEM converged.

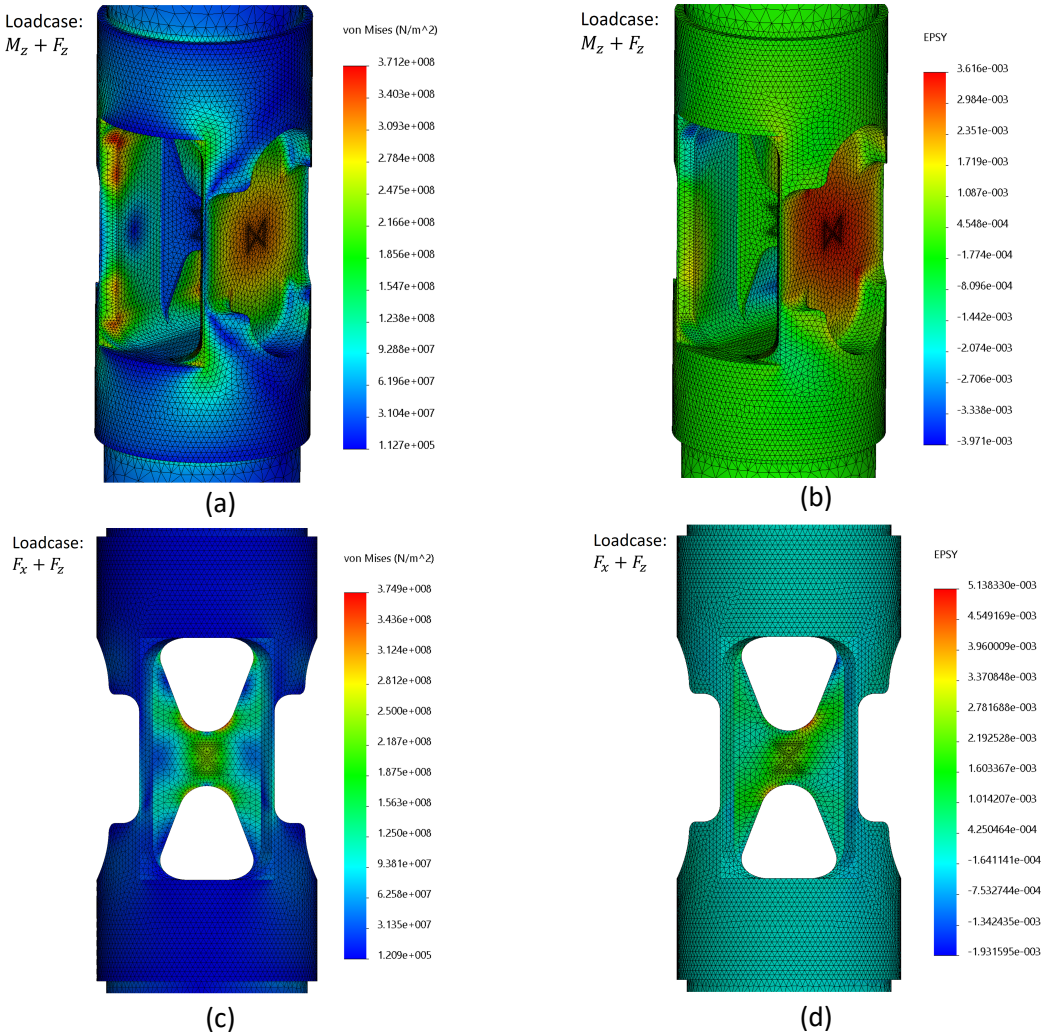

Figure B-4: FEM model stress and strain distribution. (a) Von Mises stress for torsion load case. (b) Strain in the direction of R13 for torsion load case. (c) Von Misses stress for shear load case. (d) Strain in the direction of R1 for shear load case.

Appendix C-Additional control system details

The Bevameter control system hardware is indicated in Figure C-1. Figure C-1 (a) indicates the low power circuit based around the 40-pin ESP32 dual-core Wi-Fi-enabled chip (Expressive Systems, 2021). Figure C-1 (b) indicates the high power circuit based around the 48V and 12V H-Bridge motor drivers.

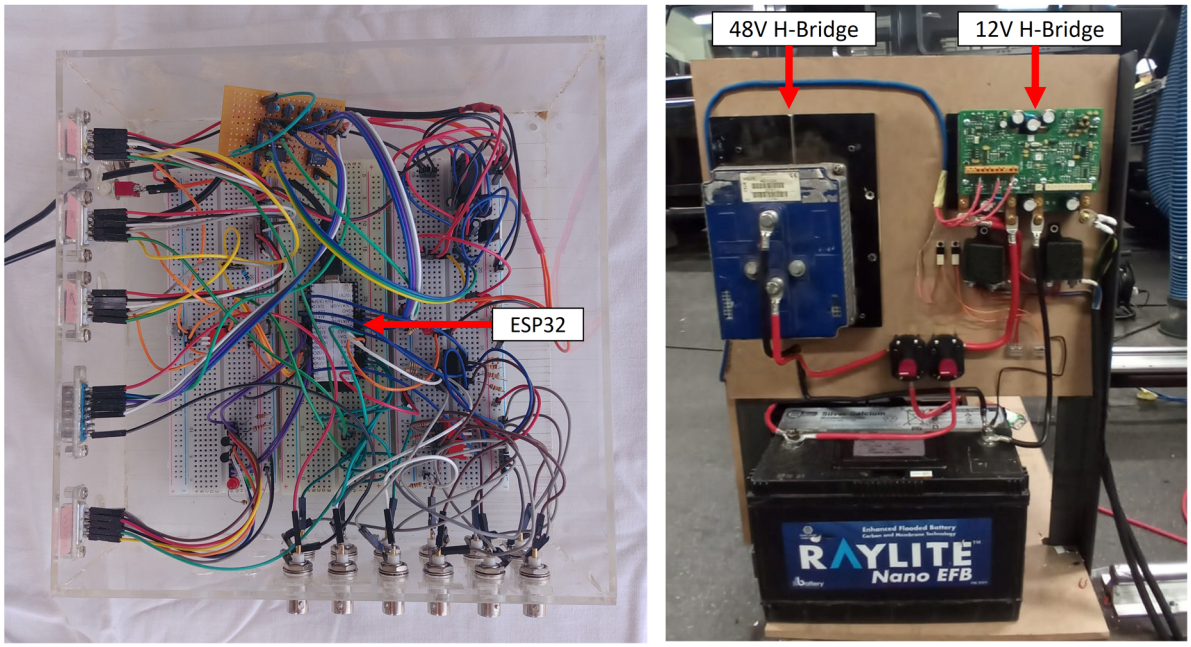

(a) (b)

Figure C-1: Control system hardware. (a) Embedded control unit. (b) Motor H-Bridge drivers and high power circuit.

Figure C-2 indicates the Graphical User Interface developed to control the Bevameter from any Wi-Fi-enabled Personal Computer (PC). The GUI allows the user to control the Bevameter's movement in three (3) axes', set the speed for each axis and set the closed-loop PI controller tuning terms in real-time.

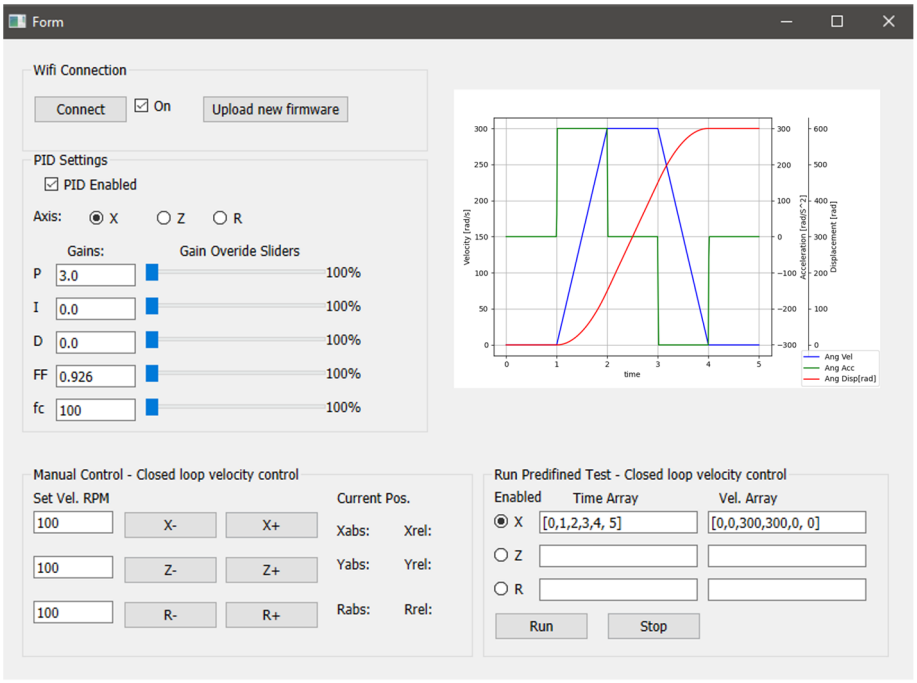

Figure C-2: Bevameter graphical user interface.

Appendix D-Additional calibration results and unit conversions

S-Type load cell calibration

The calibration of the two S-type load cells was performed with the application of calibrated weights. The results of the calibration are indicated in Figure D-1. The linear regression model exhibits an excellent fit for both load cells with low residual errors and a coefficient of determination of 1.0000.

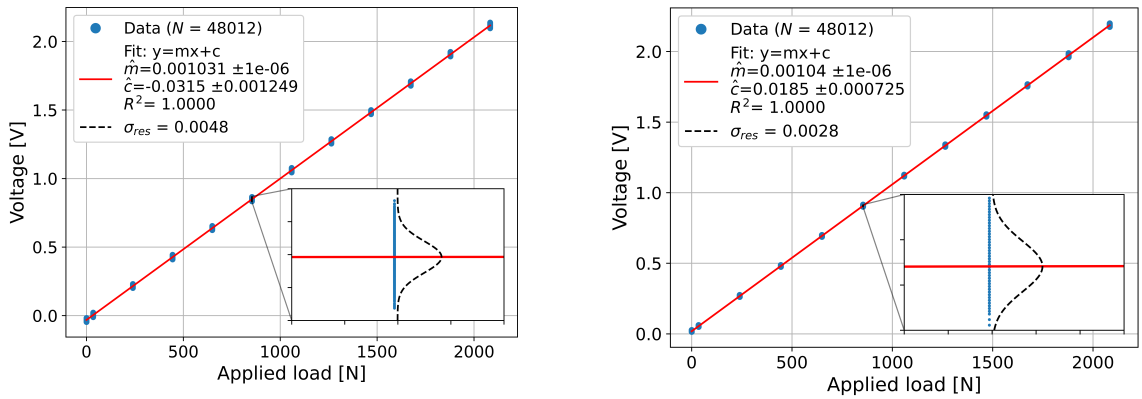

Figure D-1: Calibration of S-Type load cells. (a) Load cell one. (b) Load cell two.

Unit conversion for the 4 DOF load cell calibration matrix

The regression model in equation (17) is expressed in units of force and voltage, while the FEM model from Appendix B is expressed in force and strain. In order to be able to compare the experimental calibration to a FEM model requires the voltage data to be converted to mean effective strain ϵ_{eff} or vice versa. Using Wheatstone bridge theory, the bridge voltage can be related to effective strain,

$$\frac{V_o}{V_{ex}} = \frac{K_s(\epsilon_1 - \epsilon_2 - \epsilon_3 + \epsilon_4)}{4} = k\epsilon_{eff} \tag{51}$$

Where:

V_o – Output voltage[mV]
V_{ex} – Excitation voltage[mV]
K_s – Gauge factor
ϵ_{1-4} – Individual strain gauge strains
ϵ_{eff} – Mean effective strain

Rearranging equation (51) for mean effective strain, including amplifier gain G_a and extending the scalar solutions to multiple channels, the effective strains are expressed in terms of voltages $[O']$,

$$[\epsilon_{eff}] = [O']V_{ex}K_s\{G_a\} \tag{52}$$

Similarly, the calibration matrix $[C]$ can be expressed in terms of strains and is called the strain compliance matrix $[C']$ (Chao and Chen, 1997),

$$[C'] = [C]V_{ex}K_s\{G_a\} \tag{53}$$

Where the units of $[C]$ are transformed from volts per unit load to strain per unit load for $[C']$. The values for the constants in equation (53) are: $K_s = 2.1$, $V_{ex} = 5$V and $\{G_a\} = \{166, 991, 496, 111\}$.

Appendix E-Additional laboratory soil tests results

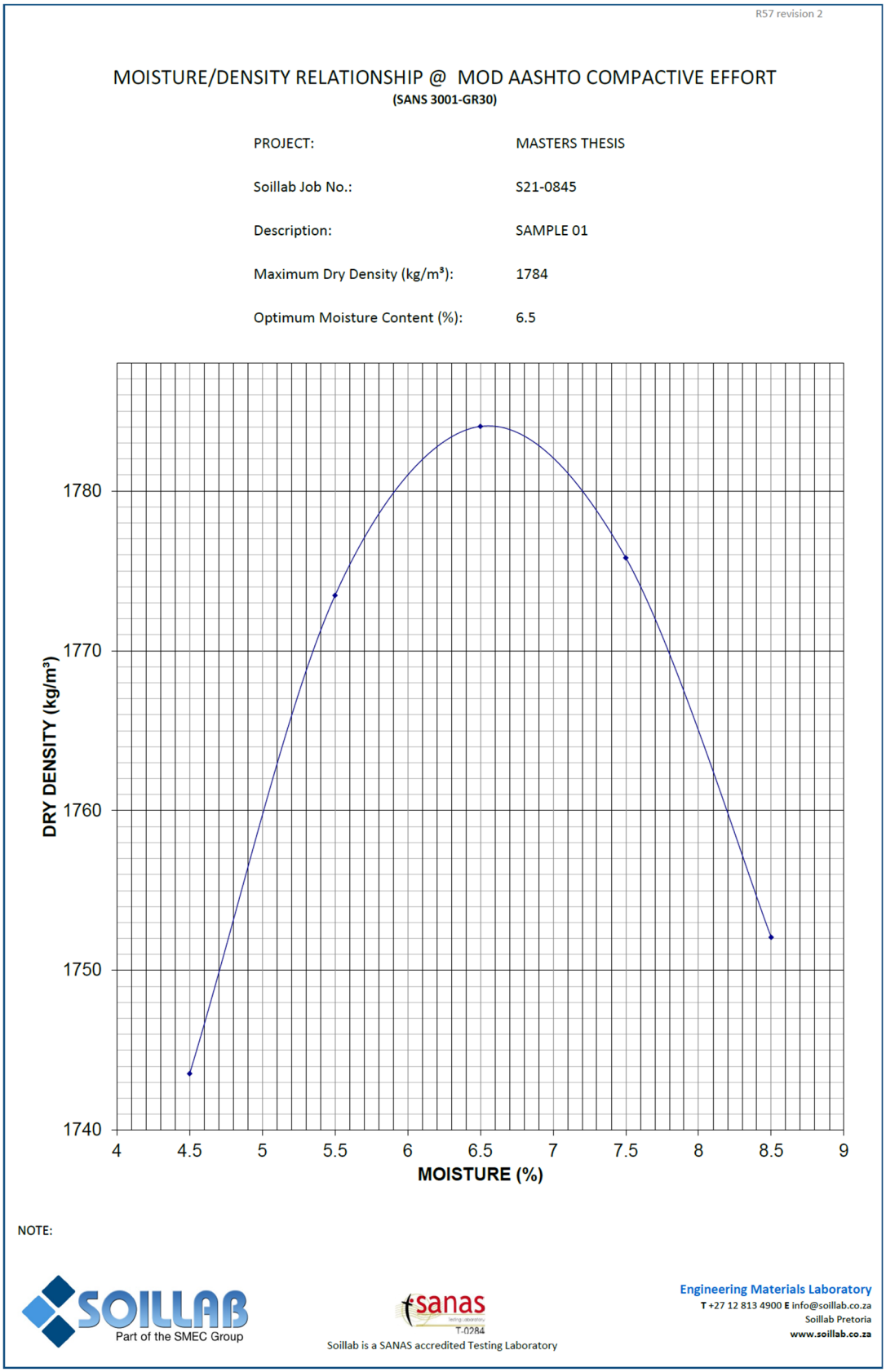

Figure E-1: Modified Procter soil compaction test results.

Shearbox

Project:	Masters Thesis
Client:	Ray Kruger
Geolab Job Nr:	S21-895
Test Method:	ASTM 3080-72

Sample Nr:	Sample01
Sample Depth:	-
Date:	2021/10/08

Results		
ϕ' =	36.1	°
c' =	0.0	kPa

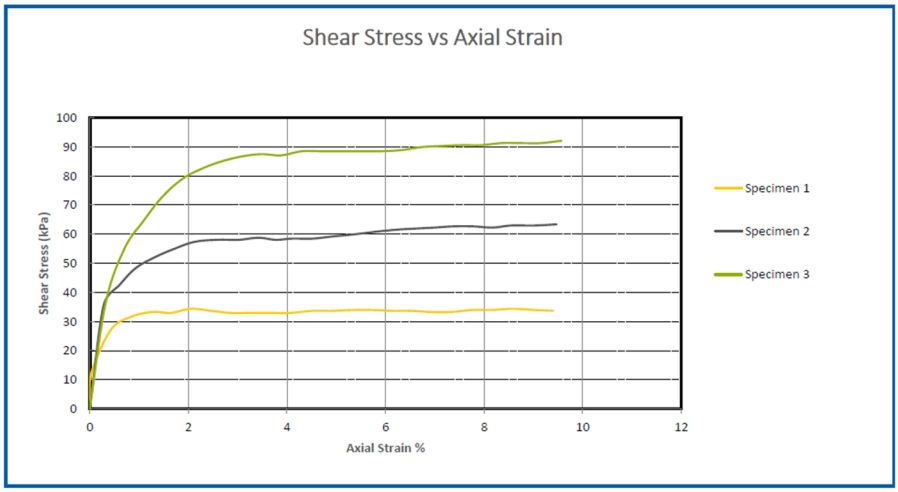

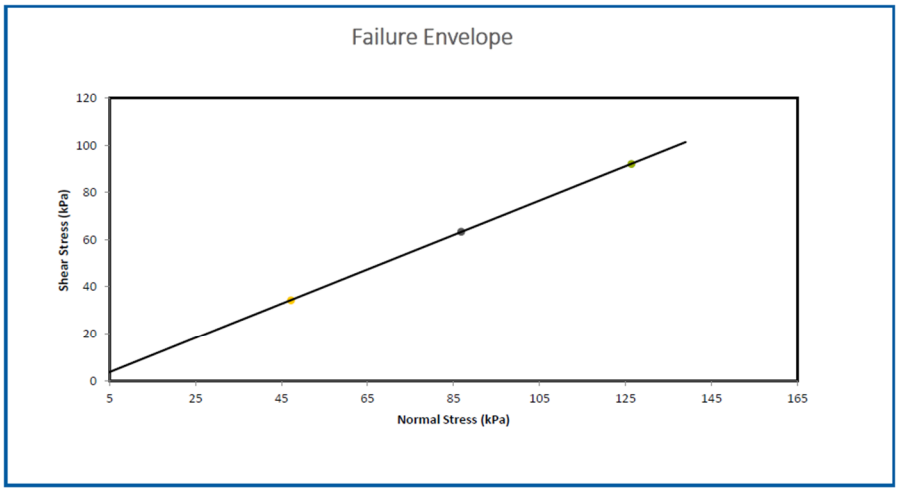

GEOLAB
Part of the SMEC Group

Geotechnical Laboratory
T +27 12 813 4936
E geolab@soillab.co.za
Geolab
www.soillab.co.za

GF46 Rev2

Figure E-2: Shear box test results.

Appendix F-Detail of numerical methods used for Bayesian parameter estimation

Determining the maximum a posterior $\widehat{\boldsymbol{\theta}}_{MAP}$

The maximum a posterior is the point estimate of the most probable parameter vector and is defined as,

$$\widehat{\boldsymbol{\theta}}_{MAP} = argmax_{\theta}\{p(\boldsymbol{\theta}|\boldsymbol{D},\mathcal{M})\} \tag{54}$$

Where $p(\boldsymbol{\theta}|\boldsymbol{D},\mathcal{M})$ is the posterior distribution given by Bayes rule in equation (20). Since the denominator on the right-hand side of equation (20) is simply a scaling factor, it can be neglected when determining the MAP. The MAP can then be determined from the log of the un-normalised posterior,

$$\widehat{\boldsymbol{\theta}}_{MAP} = argmax_{\theta}\{\ln p(\boldsymbol{D}|\boldsymbol{\theta},\mathcal{M}) + \ln p(\boldsymbol{\theta})\} \tag{55}$$

The maximum of equation (55) is found by numeric optimization. A global optimization strategy using basin hopping and the L-BFGS-B method from the Python $scipy.optimise$ library is implemented.

Determining the parameter credible intervals

Closed-form solutions for the parameter credible intervals are not available for nonlinear Bayesian parameter estimation. In order to determine the parameter credible intervals requires integration of the posterior distribution $p(\boldsymbol{\theta}|\boldsymbol{D},\mathcal{M})$ to find the continuous density interval that is equal to the desired Highest Probable Density (HPD) for each individual parameter θ_i,

$$\mathrm{p}(\mathrm{a} \leq \theta_i \leq \mathrm{b}) = \int_a^b \mathrm{p}(\theta_i|\boldsymbol{D},\mathcal{M})d\theta_{\mathrm{i}} = 1-\alpha \tag{56}$$

The integral bounds a and b need to be found so that the HPD evaluates to $1-\alpha$, where α is the desired significance level. For the MCMC approach, this is done by finding the Empirical Continuous Distribution Function (ECDF), inverting the ECDF and evaluating the resulting function at the desired bounds. Practically this is done using the Python $numpy.percentiles$ library (Harris *et al.*, 2020).

Determining the confidence intervals in the dataspace

In order to determine the uncertainty in the dataspace requires evaluating the Posterior Predictive Distribution (PPD) (Bishop, 2006). Formally the PPD is determined by the integral,

$$\mathrm{p}(\widetilde{\boldsymbol{D}}|\boldsymbol{D},\mathcal{M},\boldsymbol{\theta}) = \int p(\widetilde{\boldsymbol{D}}|\boldsymbol{\theta},\mathcal{M})p(\boldsymbol{\theta}|\mathcal{M},\boldsymbol{D})d\boldsymbol{\theta} \tag{57}$$

Where $\widetilde{\boldsymbol{D}}$ is the new unobserved data combination where the uncertainty is to be evaluated, $p(\widetilde{\boldsymbol{D}}|\boldsymbol{\theta},\mathcal{M})$ is the likelihood of the new data, and $p(\boldsymbol{\theta}|\mathcal{M},\mathbf{D})$ is the posterior of the training data $\boldsymbol{D}$. The integral in equation (57) can be evaluated using standard Monte Carlo integration,

$$\mathrm{p}(\widetilde{\boldsymbol{D}}|\mathbf{D},\mathcal{M},\boldsymbol{\theta}) \approx \frac{1}{\mathrm{n}}\sum_i^N p(\widetilde{\boldsymbol{D}}|\boldsymbol{\theta}^s,\mathcal{M}) \text{ where } \boldsymbol{\theta}^s \sim p(\boldsymbol{D}|\boldsymbol{\theta},\mathcal{M})p(\boldsymbol{\theta}) \tag{58}$$

Note that $\mathrm{p}(\widetilde{\boldsymbol{D}}|\boldsymbol{D},\mathcal{M},\boldsymbol{\theta})$ is a singular scaler value. To determine the HPD region in the dataspace, the PPD is evaluated over a grid of $\widetilde{\boldsymbol{D}}$ values and the values where $p(\widetilde{\boldsymbol{D}}|\boldsymbol{D},\mathcal{M},\boldsymbol{\theta}) > \frac{\alpha}{2}$ are determined. Where α is the desired confidence level of the HPD region.

Appendix G-Visualisation of the model fits for the soil preparation investigation

The model fits corresponding to the estimated pressure-sinkage and shear stress-displacement model parameters from Table 16 are indicated in Figure G-1 and Figure G-2, respectively.

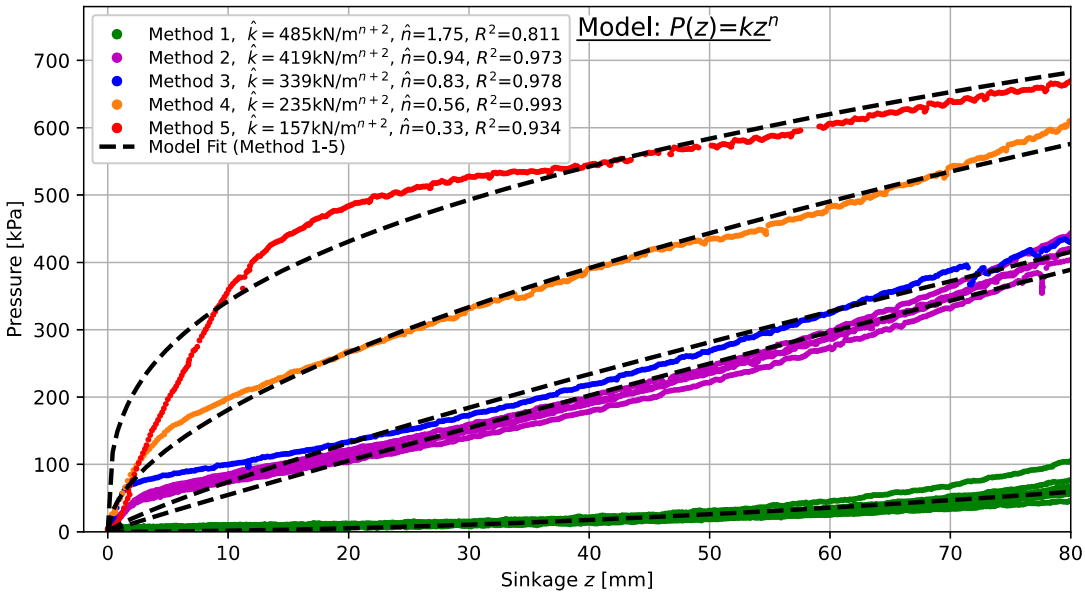

Figure G-1: Pressure-sinkage model fit (Bernstein model, 150mm diameter circular plate).

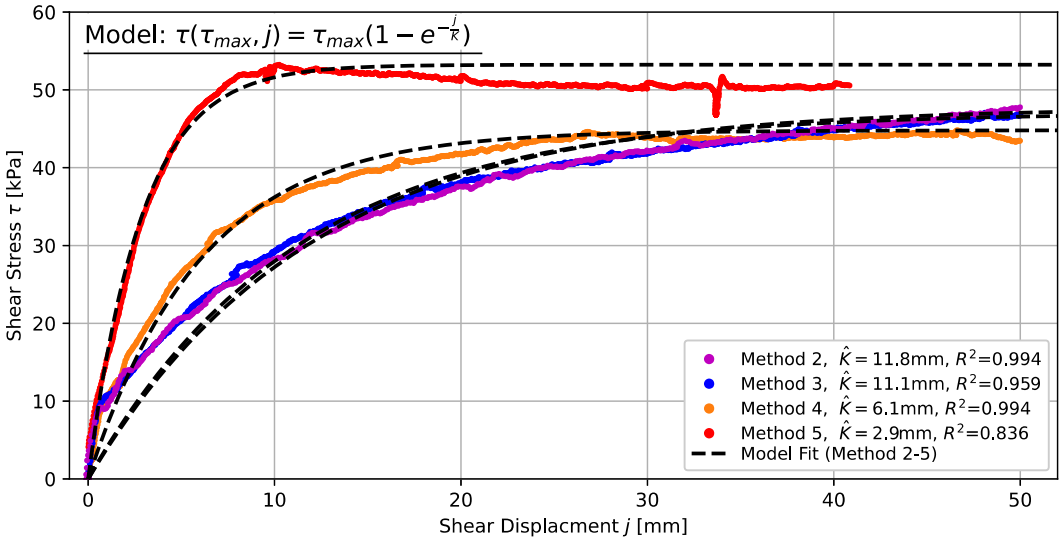

Figure G-2: Shear stress-displacement model fit (Janosi-Hanamoto model, 93kPa normal pressure, 50mm cut-off).

From Figure G-1 it is observed that the Bernstein model captures the range of soil responses well if only higher sinkages are considered. However, substantial errors occur at low sinkages (<30mm). Wong (1989) and Apfelbeck *et al.* (2011) advocate placing more weight on high pressures for parameter estimation; however, arguably equal or more weight should be placed on low pressures since this corresponds with the vehicle ground pressure of 100kPa and is the range where the most significant errors occur.

From Figure G-2 it is observed that at a 50mm cut-off, the Janosi-Hanamoto model describes the shear response well. Although better models exist for the humped type curve of method five (5), the purpose of the current comparison is to illustrate the effect of the soil preparation method (primarily a reflection of soil density) on the identified shear deformation modulus K.

Appendix H-Normal pressures used by literature for Bevameter shear tests

Table H-1: Normal pressures used by literature for Bevameter shear tests.

Study	Normal Pressure [kPa]	Target Vehicle
(Kim *et al.,* 2022)	15-27	Large agricultural vehicle
(Kim *et al.*, 2021)	13-26	Large agricultural vehicle
(Mähönen *et al.,* 2021)	2.7-3.8	Snow mobile
(Tsitouridis, 2019)	17.8-37	SUV size vehicle
(Edwards *et al.*, 2017)	3-15	Planetary rover
(Apfelbeck *et al.*, 2010)	1-3	Planetary rover
(Shoop, 1993b)	5-36	SUV size vehicle
(Upadhyaya et al., 1993)	**40-240** [a]	Large agricultural vehicle
(Bilanski and L'Esperance, 1990)	**250-700** [a]	Large agricultural vehicle
(Stafford & Tanner, 1982)	80	Not indicated
(Wong *et al.*, 1979)	4-26	Large tracked vehicle
(Wells & Treesuwan, 1978)	15-75	SUV size vehicle
(Chang & Baker, 1973)	**20-125**[a]	Armoured tank
(Bekker, 1969)	7-48	Not indicated
(Reece, 1964)	3-43	Small-scale tracked vehicle

Note: [a] Studies that performed shear tests at 100kPa and above.